Methods in Molecular Biology 2258

Springer Protocols

Mo R. Ebrahimkhani
Joshua Hislop *Editors*

Programmed Morphogenesis

Methods and Protocols

Humana Press

METHODS IN MOLECULAR BIOLOGY

Series Editor
John M. Walker
School of Life and Medical Sciences
University of Hertfordshire
Hatfield, Hertfordshire, UK

For further volumes:
http://www.springer.com/series/7651

For over 35 years, biological scientists have come to rely on the research protocols and methodologies in the critically acclaimed *Methods in Molecular Biology* series. The series was the first to introduce the step-by-step protocols approach that has become the standard in all biomedical protocol publishing. Each protocol is provided in readily-reproducible step-by-step fashion, opening with an introductory overview, a list of the materials and reagents needed to complete the experiment, and followed by a detailed procedure that is supported with a helpful notes section offering tips and tricks of the trade as well as troubleshooting advice. These hallmark features were introduced by series editor Dr. John Walker and constitute the key ingredient in each and every volume of the *Methods in Molecular Biology* series. Tested and trusted, comprehensive and reliable, all protocols from the series are indexed in PubMed.

Programmed Morphogenesis

Methods and Protocols

Edited by

Mo R. Ebrahimkhani

Department of Pathology, Division of Experimental Pathology,School of Medicine, University of Pittsburgh, Pittsburgh, PA, USA; Pittsburgh Liver Research Center, University of Pittsburgh, Pittsburgh, PA, USA; Department of Bioengineering, Swanson School of Engineering, University of Pittsburgh, Pittsburgh, PA, USA; McGowan Institute for Regenerative Medicine, University of Pittsburgh, Pittsburgh, PA, USA

Joshua Hislop

Department of Bioengineering, Swanson School of Engineering, University of Pittsburgh, Pittsburgh, PA, USA; Pittsburgh Liver Research Center, University of Pittsburgh, Pittsburgh, PA, USA; Department of Pathology, Division of Experimental Pathology,School of Medicine, University of Pittsburgh, Pittsburgh, PA, USA

Humana Press

Editors
Mo R. Ebrahimkhani
Department of Pathology
Division of Experimental Pathology
School of Medicine
University of Pittsburgh
Pittsburgh, PA, USA

Pittsburgh Liver Research Center
University of Pittsburgh
Pittsburgh, PA, USA

Department of Bioengineering
Swanson School of Engineering
University of Pittsburgh
Pittsburgh, PA, USA

McGowan Institute for Regenerative Medicine
University of Pittsburgh
Pittsburgh, PA, USA

Joshua Hislop
Department of Bioengineering
Swanson School of Engineering
University of Pittsburgh
Pittsburgh, PA, USA

Pittsburgh Liver Research Center
University of Pittsburgh
Pittsburgh, PA, USA

Department of Pathology
Division of Experimental Pathology
School of Medicine
University of Pittsburgh
Pittsburgh, PA, USA

ISSN 1064-3745 ISSN 1940-6029 (electronic)
Methods in Molecular Biology
ISBN 978-1-0716-1173-9 ISBN 978-1-0716-1174-6 (eBook)
https://doi.org/10.1007/978-1-0716-1174-6

Preface

Cells in the tissue of every organism have undergone a robust process of fate acquisition, positioning, and maturation. These processes, controlled by a variety of natural morphogenetic cues, including genetic, mechanical, and electrical signals, are responsible for the formation of various aspects of the body plan, from cell-to-cell interactions to higher-level structures. The application of these cues in natural cellular systems results in highly ordered, highly specialized functional structures such as the eye, the lung, and the liver. There is an immense interest in decoding programs that naturally control and drive formation of tissues and organs. Understanding and engineering such programs open powerful opportunities to produce physiologically relevant tissue of interest, generate models to study human disease, and set the path for manufacturing of advanced tissue and organs.

The first chapters presented in this volume are focused on understanding signaling events and patterns in morphogenetic systems. Walczak et al. describe the TASBE image analytics pipeline, which integrates several different algorithms in order to process multichannel time lapse microscopy data. Carter et al. present a quantitative method to study the impact of a cell's local environment in the acquisition of lineage characteristics, and Ulyanchenko and Guiu cover an approach to understand gut morphogenesis in a mouse model through engineered lineage tracing.

Following these methods to understand morphogenesis, the next chapters focus on programming signaling events and patterns to drive morphogenesis. Kim et al. demonstrate how to engineer cell-intrinsic signaling gradients for the secreted morphogenetic factor sonic hedgehog, and investigate those gradients using a complementary sonic hedgehog receiver cell line. Rexius-Hall et al. present a method for fabricating patterned polyacrylamide hydrogels, with the goal of creating microgels that are capable of supporting geometrically controlled microtissues. Richardson et al. demonstrate how to change and assay the properties of alginate substrates to create environments of specific stiffnesses to aid in the engineering of different cell types. Nanos and Levin detail a method for rewiring bioelectric circuits in Xenopus, leveraging a Cas9 system to change the bioelectric environment and investigate its impact on cell state and fate. And Libby et al. engineer mosaicism in an engineered PSC cell population, using CRISPR-based gene knockdown to generate changes within subpopulations of human iPSCs, allowing for control over organization and analysis of emergent behaviors.

Cellular systems engineered to model early development are presented by Britton et al. and Anlas et al. Britton et al. generate patterned hESC colonies for the purpose of investigating tissue development at the point of gastrulation and neural differentiation. Anlas et al. present a protocol for gastruloid differentiation; however, this protocol focuses on creating 3D gastruloids out of aggregates of a PSC of interest.

A variety of techniques for engineering organoids, tissue barriers, and disease models are also covered. von Maydell and Jorfi present a method to build uniform brain spheroids to investigate morphology, pathophysiology, or for drug screening. Selfa et al. present a human kidney organoid differentiation protocol, where PSCs are driven to develop into complex kidney tissue containing renal vesicles and nephron-like structure. Aghayee and Ashton describe how to direct hPSC-derived neural tissue to model the architecture of a transverse slice of the neural tube, generating forebrain, hindbrain, and spinal cord rosettes on

micropatterned culture. Campisi et al. present a protocol for creation of a blood–brain barrier on a chip, combining in vitro and ex vivo using iPSCs, astrocytes, and pericytes to model the creation of blood–brain barrier-like microvasculature. Clark focuses on the use of an organ-on-a-chip system to model the metastatic niche of the liver in cancer development, and Siani and Nikkhah also investigate cancer, but do so in the context of how cancer-associated fibroblasts aid in tumor invasion and migration in a hydrogel model.

Finally, two methods that have applicability in vivo are presented. Emerson et al. present a methodology for preparation of loading vasculogenic hydrogels with cells of interest, followed by transplantation of these hydrogels in vivo into mice to allow investigation of vascularization of these tissues, and Persson et al. demonstrate how to create platelet-like cells from a megakaryoblast cell line.

The methods contained within this book showcase some of the most cutting-edge techniques in the field of programmed morphogenesis. The goal of the presentation of these methods is not only to communicate knowledge but also to inspire approaches to new challenges, and to empower readers with the capability to approach those challenges.

Pittsburgh, PA, USA *Mo R. Ebrahimkhani*
Joshua Hislop

Contents

Contributors

Alireza Aghayee • *Wisconsin Institute for Discovery, University of Wisconsin–Madison, Madison, WI, USA; Department of Material Science and Engineering, University of Wisconsin–Madison, Madison, WI, USA*

Kerim Anlas • *European Molecular Biology Laboratory (EMBL), Barcelona, Barcelona, Spain; EMBL Heidelberg, Developmental Biology Unit, Heidelberg, Germany*

Krisztina Arató • *European Molecular Biology Laboratory (EMBL), Barcelona, Barcelona, Spain*

Nethika R. Ariyasinghe • *Laboratory for Living Systems Engineering, Department of Biomedical Engineering, USC Viterbi School of Engineering, University of Southern California, Los Angeles, CA, USA; Smidt Heart Institute, Cedars-Sinai Medical Center, Los Angeles, CA, USA*

Randolph Ashton • *Wisconsin Institute for Discovery, University of Wisconsin–Madison, Madison, WI, USA; Department of Material Science and Engineering, University of Wisconsin–Madison, Madison, WI, USA; Department of Biomedical Engineering, University of Wisconsin–Madison, Madison, WI, USA*

Peter Baillie-Benson • *Formerly Wellcome—MRC Cambridge Stem Cell Institute, Department of Genetics, University of Cambridge, Cambridge, UK*

Ipsita Banerjee • *Department of Chemical and Petroleum Engineering, University of Pittsburgh, Pittsburgh, PA, USA; McGowan Institute for Regenerative Medicine, University of Pittsburgh School of Medicine, Pittsburgh, PA, USA*

Jacob Beal • *Raytheon BBN Technologies, Cambridge, MA, USA*

George Britton • *Systems, Synthetic, and Physical Biology Graduate Program, Department of Biosciences, Department of Bioengineering, Rice University, Houston, TX, USA*

Lucas M. Bush • *Department of Biomedical Engineering, University of Utah, Salt Lake City, UT, USA*

Marco Campisi • *Department of Mechanical and Aerospace Engineering, Politecnico di Torino, Turin, Italy; Interuniversity Center for the Promotion of the 3Rs Principles in Teaching and Research, Pisa, Italy*

Joseph Candiello • *Department of Bioengineering, University of Pittsburgh, Pittsburgh, PA, USA; RoosterBio, Frederick, MD, USA*

Shay Carter • *School of Biological and Health Systems Engineering, Fulton School of Engineering, Arizona State University, Tempe, AZ, USA*

Shaylina R. Carter • *School of Biological and Health Systems Engineering, Fulton School of Engineering, Arizona State University, Tempe, AZ, USA*

Sapna Chhabra • *Systems, Synthetic, and Physical Biology Graduate Program, Department of Biosciences, Department of Bioengineering, Rice University, Houston, TX, USA*

Valeria Chiono • *Department of Mechanical and Aerospace Engineering, Politecnico di Torino, Turin, Italy; Interuniversity Center for the Promotion of the 3Rs Principles in Teaching and Research, Pisa, Italy*

Amanda M. Clark • *Department of Pathology and UPMC Hillman Cancer Center, University of Pittsburgh, Pittsburgh, PA, USA*

Tara L. Deans • *Department of Biomedical Engineering, University of Utah, Salt Lake City, UT, USA*

Mo R. Ebrahimkhani • *Department of Pathology, Division of Experimental Pathology, School of Medicine, University of Pittsburgh, Pittsburgh, PA, USA; Pittsburgh Liver Research Center, University of Pittsburgh, Pittsburgh, PA, USA; Department of Bioengineering, Swanson School of Engineering, University of Pittsburgh, Pittsburgh, PA, USA; McGowan Institute for Regenerative Medicine, University of Pittsburgh, Pittsburgh, PA, USA*

Amy E. Emerson • *School of Biological and Health Systems Engineering, Arizona State University, Tempe, AZ, USA*

Maria Gallo • *Pluripotency for Organ Regeneration, Institute for Bioengineering of Catalonia (IBEC), The Barcelona Institute of Science and Technology (BIST), Barcelona, Spain*

Elena Garreta • *Pluripotency for Organ Regeneration, Institute for Bioengineering of Catalonia (IBEC), The Barcelona Institute of Science and Technology (BIST), Barcelona, Spain*

Jordi Guiu • *Biotech Research and Innovation Centre (BRIC), University of Copenhagen, Copenhagen, Denmark; Cell Plasticity and Regeneration Group, Regenerative Medicine Program, Institut d'Investigació Biomèdica de Bellvitge—IDIBELL, L'Hospitalet de Llobregat, Spain; Program for Advancing the Clinical Translation of Regenerative Medicine of Catalonia, P-CMR[C], L'Hospitalet de Llobregat, Spain*

Joshua Hislop • *Department of Bioengineering, Swanson School of Engineering, University of Pittsburgh, Pittsburgh, PA, USA; Pittsburgh Liver Research Center, University of Pittsburgh, Pittsburgh, PA, USA; Department of Pathology, Division of Experimental Pathology, School of Medicine, University of Pittsburgh, Pittsburgh, PA, USA*

Joshua Hsu • *School of Biological and Health Systems Engineering, Fulton School of Engineering, Arizona State University, Tempe, AZ, USA*

Mehdi Jorfi • *Center for Engineering in Medicine, Massachusetts General Hospital, Harvard Medical School, Charlestown, MA, USA*

David A. Joy • *Gladstone Institute of Cardiovascular Disease, Gladstone Institutes, San Francisco, CA, USA; UC Berkeley-UC San Francisco Graduate Program in Bioengineering, San Francisco, CA, USA*

Roger Dale Kamm • *Department of Biological Engineering, Massachusetts Institute of Technology, Cambridge, MA, USA*

Julia S. Kim • *Whitehead Institute for Biomedical Research, Cambridge, MA, USA*

Pauline V. Kneller • *Department of Biomedical Engineering, University of Utah, Salt Lake City, UT, USA*

Michael Levin • *Department of Biology, and Allen Discovery Center, Tufts University, Medford, MA, USA*

Ashley R. G. Libby • *Developmental and Stem Cell Biology PhD Program, University of California, San Francisco, CA, USA; Gladstone Institute of Cardiovascular Disease, Gladstone Institutes, San Francisco, CA, USA*

Sei Hien Lim • *AIM Biotech, Singapore, Singapore*

Pulin Li • *Whitehead Institute for Biomedical Research, Cambridge, MA, USA; Department of Biology, Massachusetts Institute of Technology, Cambridge, MA, USA*

Mark W. Livingston • *Department of Biomedical Engineering, University of Utah, Salt Lake City, UT, USA*

Joseph Massey • *Department of Biosciences, Rice University, Houston, TX, USA*

Shibin Mathew • *Department of Chemical and Petroleum Engineering, University of Pittsburgh, Pittsburgh, PA, USA; Pfiezer, Boston, MA, USA*

Megan L. McCain • *Laboratory for Living Systems Engineering, Department of Biomedical Engineering, USC Viterbi School of Engineering, University of Southern California, Los Angeles, CA, USA; Department of Stem Cell Biology and Regenerative Medicine, Keck School of Medicine of USC, University of Southern California, Los Angeles, CA, USA*

Todd C. McDevitt • *Gladstone Institute of Cardiovascular Disease, Gladstone Institutes, San Francisco, CA, USA; Department of Bioengineering and Therapeutic Sciences, University of California, San Francisco, CA, USA*

Nuria Montserrat • *Pluripotency for Organ Regeneration, Institute for Bioengineering of Catalonia (IBEC), The Barcelona Institute of Science and Technology (BIST), Barcelona, Spain; Centro de Investigación Biomédica en Red en Bioingeniería, Biomateriales y Nanomedicina, Madrid, Spain; Catalan Institution for Research and Advanced Studies (ICREA), Barcelona, Spain*

Vasilios Nanos • *Department of Biology, and Allen Discovery Center, Tufts University, Medford, MA, USA*

Mehdi Nikkhah • *Harrington Department of Bioengineering, School of Biological and Health Systems Engineering (SBHSE), Arizona State University, Tempe, AZ, USA; Center for Personalized Diagnostics (CPD), Biodesign Institute, Arizona State University, Tempe, AZ, USA*

Kylie M. Persson • *Department of Biomedical Engineering, University of Utah, Salt Lake City, UT, USA*

Kevin Pietz • *Department of Bioengineering, University of Pittsburgh, Pittsburgh, PA, USA*

Michael Pineda • *Whitehead Institute for Biomedical Research, Cambridge, MA, USA*

K. Ravikumar • *Department of Chemical and Petroleum Engineering, University of Pittsburgh, Pittsburgh, PA, USA*

Megan L. Rexius-Hall • *Laboratory for Living Systems Engineering, Department of Biomedical Engineering, USC Viterbi School of Engineering, University of Southern California, Los Angeles, CA, USA*

Thomas Richardson • *Department of Chemical and Petroleum Engineering, University of Pittsburgh, Pittsburgh, PA, USA; Lonza, Houston, Texas, PA, USA*

Harpinder Saini • *Harrington Department of Bioengineering, School of Biological and Health Systems Engineering (SBHSE), Arizona State University, Tempe, AZ, USA*

Idoia Lucía Selfa • *Pluripotency for Organ Regeneration, Institute for Bioengineering of Catalonia (IBEC), The Barcelona Institute of Science and Technology (BIST), Barcelona, Spain*

Emily M. Slaby • *School of Biological and Health Systems Engineering, Arizona State University, Tempe, AZ, USA*

Jesse Tordoff • *Massachusetts Institute of Technology, Cambridge, MA, USA*

Vikas Trivedi • *European Molecular Biology Laboratory (EMBL), Barcelona, Barcelona, Spain*

David A. Turner • *Institute of Life Course and Medical Sciences, University of Liverpool, Liverpool, UK*

Svetlana Ulyanchenko • *Biotech Research and Innovation Centre (BRIC), University of Copenhagen, Copenhagen, Denmark*

Jeremy J. Velazquez • *School of Biological and Health Systems Engineering, Fulton School of Engineering, Arizona State University, Tempe, AZ, USA; Pittsburgh Liver Research Center, University of Pittsburgh School of Medicine, Pittsburgh, PA, USA; Division of Experimental Pathology, Department of Pathology, University of Pittsburgh School of*

Medicine, Pittsburgh, PA, USA; McGowan Institute for Regenerative Medicine, University of Pittsburgh School of Medicine, Pittsburgh, PA, USA

Djuna von Maydell • *Center for Engineering in Medicine, Massachusetts General Hospital, Harvard Medical School, Charlestown, MA, USA*

Nicholas Walczak • *Raytheon BBN Technologies, Cambridge, MA, USA*

Aryeh Warmflash • *Department of Biosciences, Rice University, Houston, TX, USA; Department of Bioengineering, Rice University, Houston, TX, USA*

Jessica D. Weaver • *School of Biological and Health Systems Engineering, Arizona State University, Tempe, AZ, USA*

Ron Weiss • *Massachusetts Institute of Technology, Cambridge, MA, USA*

Connor Wiegand • *Department of Chemical and Petroleum Engineering, University of Pittsburgh, Pittsburgh, PA, USA*

Part I

Understanding Signaling Events and Patterns

Chapter 1

TASBE Image Analytics: A Processing Pipeline for Quantifying Cell Organization from Fluorescent Microscopy

Nicholas Walczak, Jacob Beal, Jesse Tordoff, and Ron Weiss

Abstract

Laboratory automation now commonly allows high-throughput sample preparation, culturing, and acquisition of microscopy images, but quantitative image analysis is often still a painstaking and subjective process. This is a problem especially significant for work on programmed morphogenesis, where the spatial organization of cells and cell types is of paramount importance. To address the challenges of quantitative analysis for such experiments, we have developed TASBE Image Analytics, a software pipeline for automatically segmenting collections of cells using the fluorescence channels of microscopy images. With TASBE Image Analytics, collections of cells can be grouped into spatially disjoint segments, the movement or development of these segments tracked over time, and rich statistical data output in a standardized format for analysis. Processing is readily configurable, rapid, and produces results that closely match hand annotation by humans for all but the smallest and dimmest segments. TASBE Image Analytics can thus provide the analysis necessary to complete the design-build-test-learn cycle for high-throughput experiments in programmed morphogenesis, as validated by our application of this pipeline to process experiments on shape formation with engineered CHO and HEK293 cells.

Key words Image processing, Cell quantification, Fluorescence microscopy, Programmed morphogenesis, Software tools

1 Introduction

Fluorescence microscopy is one of the most commonly used assay tools of synthetic biology, making use of fluorescent proteins or dyes to deliver rich information about both the state and structure of individual cells and also about the spatial organization of cells, colonies, and tissues. As both protocols and laboratory automation have improved, an increasing number of synthetic biology projects involve high-throughput sample preparation, culturing, and acquisition of microscopy images. With potentially large numbers of wells observed at many different time points, the volume of

Mo R. Ebrahimkhani and Joshua Hislop (eds.), *Programmed Morphogenesis: Methods and Protocols*, Methods in Molecular Biology, vol. 2258, https://doi.org/10.1007/978-1-0716-1174-6_1,

fluorescent image data can rapidly become quite large, easily going into the tens or hundreds of gigabytes. This is especially true in the case of work on programmed morphogenesis, where fluorescence images are often used to image the shape of cell cultures and distribution of cell types over time, repeated across a number of different experimental parameters. Yet much of the analysis of image datasets—even quite large ones—is still done qualitatively or by hand. Such analysis is thus typically a time-consuming and painstaking process, as well as subject to a high degree of variability based on observer interpretation. Automation of quantitative analysis using image processing and computer vision techniques can provide great benefits in the use of such data, as well as greatly enhancing the repeatability of these types of experiments.

A number of different image analysis software packages that are specialized to cell biology already exist to aid in this process, such as CellProfiler [1], ImageJ [2, 3], and WIPP [4]. These tools are designed to be broadly applicable to a wide variety of work flows, but require expert crafting by the user to apply them to any particular class of experiments. This makes it difficult for these highly general tools to be applied by researchers who do not simultaneously also have expertise in both software engineering and in developing computer image processing pipelines. Complementarily, a number of specialized packages exist, which are effective but highly tailored for specific purposes, such as SuperSegger [5] (optimized for rod-shaped bacterial cells), NICE [6] (colony counting), or FogBank [7] (overlapping cell segmentation). No such tool, however, had previously been developed for quantifying the shapes of cell populations, as is typically needed for experiments on programmed morphogenesis.

We thusdeveloped this image analysis pipeline to support research in programmed morphogenesis, in the form of a highly configurable pipeline for segmentation and quantification of a broad class of experiments regarding the organization of fluorescent cells in space. We now present the resulting software package, TASBE Image Analytics, distributed under a free and open license at https://github.com/TASBE/TASBEImageAnalytics. Our implementation is a processing pipeline developed using the general ImageJ framework, which segments cells and regions of cells in fluorescence microscopy images using a thresholding process, then tracks the evolution of those segments over time. We first describe the architecture and operation of this processing pipeline, then describe its validation by comparison with human annotation, and finally provide an example of its operation in the context of shape formation experiments with engineered CHO and HEK293 cells.

2 Materials

The experiments performed for this work were done in Ubuntu Linux 18.04 using Java 8 and Jython 2.7. The version of ImageJ was 1.52p used from Fiji. The version of TrackMate used was 4.0.1. The data used for experiments presented in this work was captured with a Leica TCS SP5 II Confocal Laser Scanning Microscope. Data generated by a BioTek Cytation5 was also analyzed with this software pipeline. It is our intent that the software could be used with any version of Java and Jython that are compatible with ImageJ although other configurations have not been tested.

3 Methodology

Figure 1 shows the architecture of the TASBE Image Analytics image processing pipeline (named for its relationship with prior automation projects [8, 9]), which is implemented as a set of Jython scripts utilizing ImageJ plugins, proceeding in five stages. First, data and metadata are marshaled to configure the processing. Second, cells and regions of cells are segmented in each microscopy image based on intensity. Third, the binary segment images are filtered to remove artifacts and clustered to identify connected components. Fourth, per-frame statistics are computed for each identified component. Finally, these components can also be tracked through time from one microscopy frame to another.

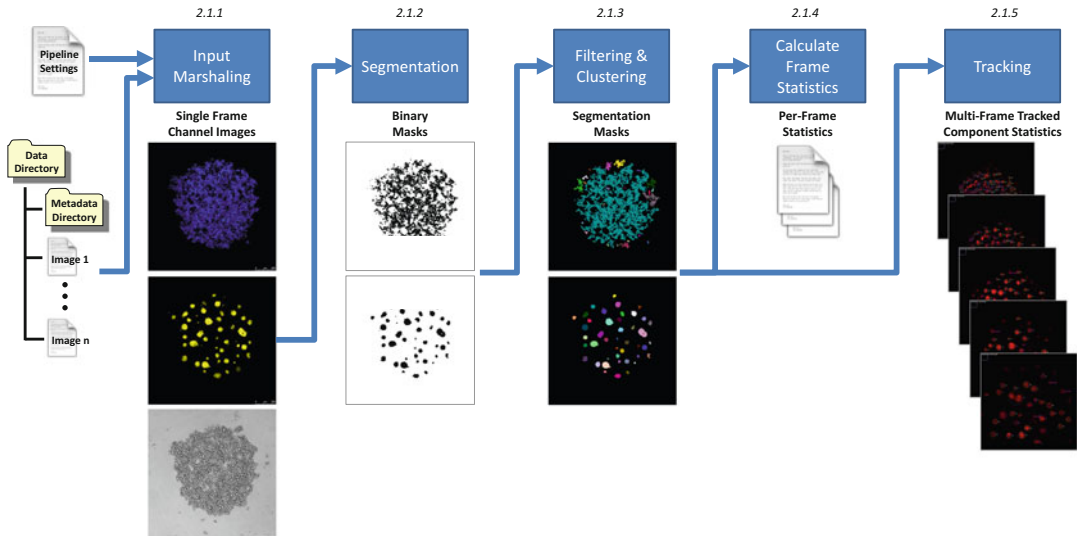

Fig. 1 The TASBE Image Analytics pipeline executes in five stages: (*1*) marshaling microscopy data, metadata, and other configuration settings, (*2*) processing each frame into binary masks, (*3*) filtering and clustering to segment the image, (*4*) calculation of cell cluster statistics, and (*5*) tracking of clusters across timesteps

The steps outlined here represent a common approach to solving this problem. However, this work aims to create a pipeline that is readily available and can work on a wide variety of fluorescence microscopy datasets with a minimum amount of reconfiguration. The nature of the design-build-test-learn cycle, combined with high-throughput sample preparation, means that a large amount of data can be generated in a short period of time, so facilitating quick analysis of the microscopy experiments can allow the cycle times to be shortened. Jython scripts (one of the standard options for scripting ImageJ) were chosen to facilitate this, as they can be run on a directory of microscopy images by just specifying a few parameters in a configuration file.

3.1 Step-by-Step Procedure

3.1.1 Input Marshaling

The first step in the processing pipeline is defining and reading in the data, including metadata that describes information about the input microscopy images. The TASBE Image Analytics pipeline is also highly configurable, with a number of different parameters (intensity threshold parameters, threshold computation algorithm, filtering thresholds, etc.) that can be adjusted by a pipeline settings configuration file. The scripts are also designed to handle directories of microscopy images, as high-throughput microscopes can generally be configured to output files into a structured pattern of directories and filenames for each well in a plate examined by the microscope. Further information about relevant configuration parameters can be found in Subheading 4.2. At present, two instrument-specific classes of metadata are supported: for Leica microscopes, the properties of XML files can be parsed to determine things like number of channels, number of time steps, and number of Z slices, as well as the dimensions of the images in pixels and physical units. Similarly, for BioTek Cytation microscopes, the TIFF tags in the input images can be read to pull out available metadata. For other microscopes, these parameters can be defined manually in the configuration file.

3.1.2 Segmentation

Once the settings and images have been marshaled for processing, the next step is to segment out the foreground of the image from the background. This is done by computing a threshold on the image and only keeping the pixels that meet the threshold. Foreground will be above the threshold for fluorescent images, but for brightfield images an upper threshold is computed as well and only pixels between the two thresholds are kept. Morphological closing [10] is applied to the resulting binary masks, which helps to fill in holes. ImageJ supports numerous different methods for computing the threshold values (default, Otsu, max entropy, and many others, as well as adaptive methods), and these different methods can be specified in the configuration, if desired. Further information about relevant configuration parameters can be found in Subheading 4.3.

3.1.3 Filtering and Clustering

Once the foreground mask is created, the resulting pixels must be grouped together into objects. A common approach to this is connected component analysis, which combines pixels that are touching based on four-connectedness or eight-connectedness [11]. An advanced version of this approach is performed with ImageJ's ParticleAnalyzer tool, which also allows the resulting objects to be filtered based on several parameters, such as circularity. Further information about relevant configuration parameters can be found in Subheading 4.4.

3.1.4 Calculation of Frame Statistics

A set of statistics is then output for each object detected in each frame, including centroid, height, width, perimeter, area (in pixels^2), area (in microns^2), and many other standard image component statistics. Images of the segmentation masks at each stage are also produced in order to help debug processing.

3.1.5 Tracking

Once cell clusters have been identified at each timestep, their identities need to be associated across time such that the progression of each cell is tracked. There are several tracking plugins available for ImageJ, of which we have selected TrackMate [12], a recent addition that offers a powerful and flexible interface. We combine TrackMate with the previously described threshold-based detection mechanism to implement multi-frame tracking. The result is another set of statistics, summarizing all tracking information for all of the components in each frame.

Once configured, the execution of the complete processing pipeline is quite fast, even on substantial high-throughput datasets. Because TASBE Image Analytics is built as an application of mature image processing tools, it is able to operate quickly and efficiently. We benchmarked performance by processing 1024×1024 images with three channels on an Intel i7 equipped laptop, finding that each image took an average of only 2.2 s to process.

3.2 Validation

We validated the performance of TASBE Image Analytics against hand-labeled ground truth by comparison of detections for a collection of 60 microscopy images. Hand-labeling was done with an interactive labeling script created in Python using the GrabCut [13] implementation in OpenCV [14], allowing a human to draw a rectangle around a region of interest and then mark some background and foreground pixels to generate a segmentation mask.

Human and machine labeling are compared with a standard widely used metric [15]: bounding boxes B_h and B_m, determined by human and machine, respectively, are compared using intersection over union (IOU):

$$\mathrm{IOU}(B_h, B_m) = \frac{\mathrm{Area}(B_h \cap B_m)}{\mathrm{Area}(B_h \cup B_m)}, \quad (1)$$

judging two components sufficiently equivalent when IOU is greater than or equal to 50%. This allows performance to be judged in terms of true positives (TP, equivalent components), false negatives (FN, human segment with no machine equivalent), and false positives (FP, machine segment with no human equivalent), from which we compute standard [16] performance metrics precision, recall, and F_1 score:

$$\text{Precision} = \text{TP}/(\text{TP} + \text{FP}), \tag{2}$$

$$\text{Recall} = \text{TP}/(\text{TP} + \text{FN}), \tag{3}$$

$$F_1 = 2\text{TP}/(2\text{TP} + \text{FN} + \text{FP}). \tag{4}$$

Our evaluation used 60 images (1110 labeled components) from a CHO and HEK293 coculture experiment, ignoring any component with an area less than 350 microns^2. Overall performance was satisfactory, with a total recall of 82.3%, total precision of 97.1%, and a total F_1 of 89.1%. More importantly, nearly all errors involved small components (statistics by area range are presented in Fig. 2a), which tend to have weaker fluorescent returns and hence can sometimes dip below the automatically computed thresholds, as well as being more sensitive to small differences in edge location. In many cases, these issues can also be mitigated by choosing a different threshold computation algorithm or specifying a default threshold to fall back on if the automated threshold is problematic. TASBE Image Analytics may thus be expected to provide human-level performance in segmenting microscopy images.

3.3 Example Results

To illustrate the use of this method, we show an example of how the TASBE Image Analytics pipeline has been applied experimentally to quantification of microscopy data from shape-formation experiments. These experiments considered mixtures of CHO and HEK293 cells, genetically modified to express different fluorescent proteins and using differential levels of cadherin expression to sort into various spatial patterns (full details of this work may be found in [17]). Figure 2b–d shows samples of results produced using TASBE Image Analytics from an experiment in which mixtures of HEK293 and CHO were imaged every 20 min over the course of 66 hours, with one 68-min gap around hour 13.

The rich collection of statistics generated from the TASBE Image Analytics image processing pipeline can be plotted and used in various ways to draw conclusions about the experiment. For example, in the case of these CHO/HEK293 adhesion experiments, it was predicted that low concentrations of HEK293 cells would result in the formation of a multiple cluster pattern. By plotting the areas of components over time at different concentrations, we were able to visually validate this hypothesis (Fig. 2b), as well as quantitatively validate the hypotheses through analysis of the statistics produced from those images.

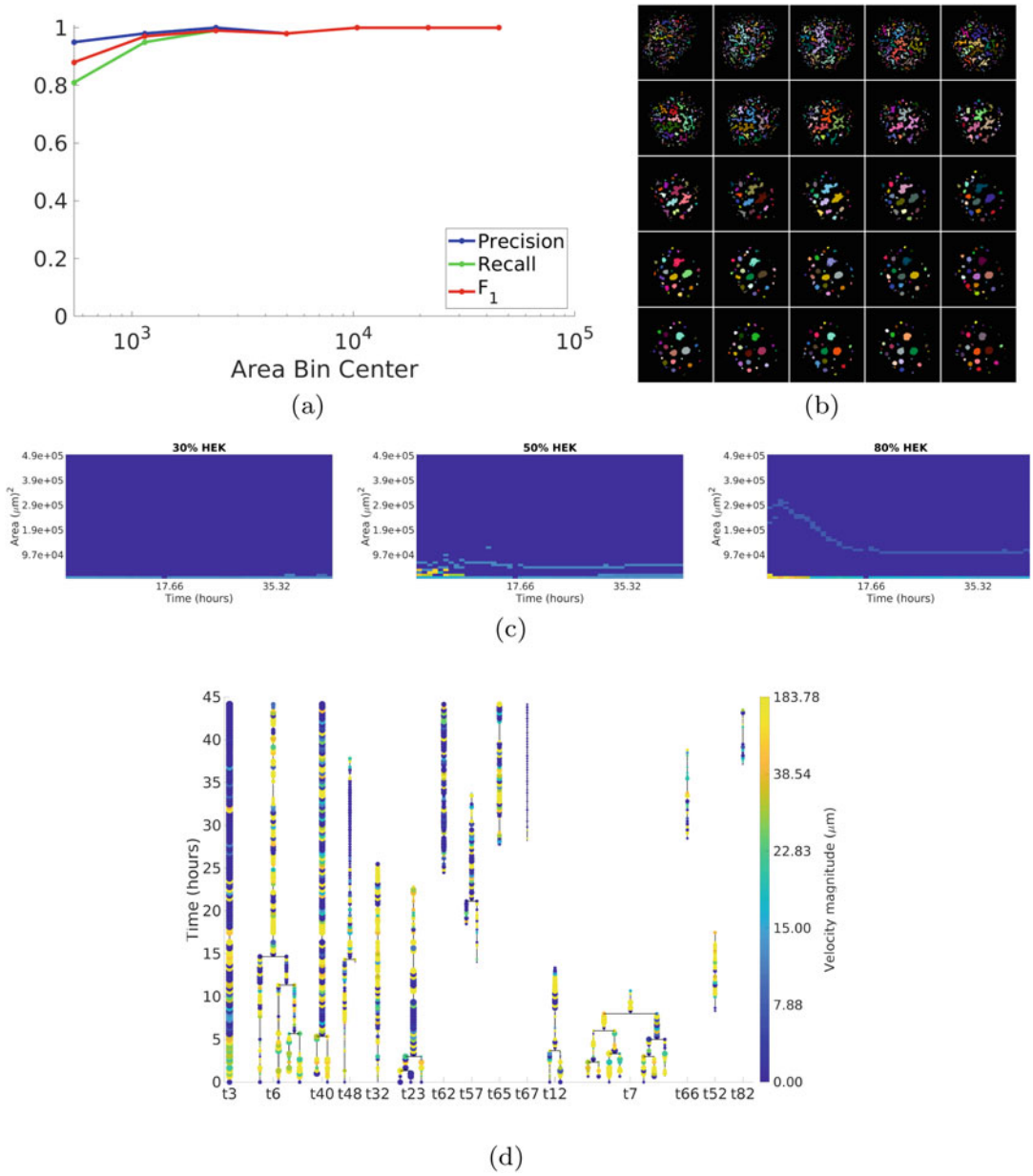

Fig. 2 Validation and experimental results: (**a**) Processing images with TASBE Image Analytics provides results closely equivalent to hand processing by humans, particularly for larger components. (**b**) Segmentation showing formation of a "polka dot" pattern in a mixture of HEK and CHO cells over time (time progresses left to right then top to bottom). (**c**) Heat maps of component size vs. time showing a transition from small fast-moving components at 30% HEK to a single large slow-moving component at 80% HEK (warmer colors are faster, dark blue means no components have that area at that time). (**d**) Tracking "phylogeny tree" showing how smaller components combine to form larger components over time

Figure 2c shows another example of a result computed from statistics over time. Here, the color of each cell in the heat map corresponds to the mean velocity of all components within an area range and time period. From this plot, we can see that at 30% HEK293, there are only small components, however around 50% a phase transition begins, where some larger components form, and by 80% there is a large component that forms (condensing to a smaller area) and then grows over time. In addition, we can see that smaller components move faster than large components in this data. Figure 2d shows one more example of the use of tracking, in this case a "phylogeny" tree graph that shows how smaller components combine to form larger components over time, as well as the area (dot size) and velocity (color) of these components.

These examples are by no means exhaustive: they merely illustrate a few of the many ways in which TASBE Image Analytics can be applied to data from real programmed morphogenesis experiments in order to provide insight and quantification.

4 Notes

4.1 Software Setup

The code necessary to run our pipeline can be found in the TASBE organization on GitHub: https://github.com/tasbe. There are three related repositories: TASBEImageAnalytics, TASBEImageAnalytics-Tutorial, and TASBEImageAnalytics-Data. The first repository houses the source code including Jython scripts for running the processing pipeline, Java code to create a thresholding-based detector for TrackMate, and C++ programs for creating point clouds from z-stacks generated by a confocal microscope (an aspect not covered in the main methods description above). The tutorial repository contains some shell scripts that illustrate how to execute the image analysis pipeline, and which can be used as a template for configuration of the pipeline for new experiments. The data repository, in turn, contains example image data used by the tutorial repository scripts.

In order to use the pipeline, one must download the source code and install ImageJ. For all of our processing, we used the ImageJ distribution FIJI (https://fiji.sc/). The scripts in the tutorials repository give a way to use the processing pipeline, and the data in the data repository show a common layout for the microscopy experiments we have worked with.

4.2 Parameter Configuration

Tables 1, 2, and 3 define all of the parameters recognized in the configuration file. These parameters are split into three groups: control of filename parsing, configuration of dataset properties, and configuration for processing. The filename parsing is important so that all of the files are properly marshaled. Data is grouped together by well on the plate, and across the possible channels, timesteps, and Z slices. Frequently, this information is encoded in

Table 1
Table of configuration parameters recognized in the configuration .ini file

Filename parsing options		
Parameter	**Name in File**	**Description**
Directory of microscopy images	inputDir	Directory that contains all of the microscopy images to process.
Location of results/output	outputDir	Directory where all outputs will be stored.
Well Index	wellIdx	Index of the well name in the filename when split on "_". Can be a comma separated list of values. Required.
Channel Index	cIdx	Index of the channel specifier in the filename when split on "_". Can be detected if the token has "ch" in it.
Z Index	zIdx	Index of the Z slice specifier in the filename when split on "_". Can be detected if the token has "z" in it.
Time Index	tIdx	Index of the timestep specifier in the filename when split on "_". Can be detected if the token has "t" in it.
Specify wells to process	wellNames	If specified, only wells in the comma separated list will be processed.
Specify wells to ignore	excludeWellNames	If specified, any wells in the comma separated list will be skipped.

This section contains options that determine how the filenames are parsed

the filename, and the script is able to extract this information when the tokens are separated by underscores ("_"). Well names generally need to be specified, but channel, timestep, and Z slice can be found automatically if their tokens contain "ch," "t," and "z" selectively, as are often used in microscopy filenames. Most of the dataset parameters can be found in microscope property files. For Leica confocal microscopes, these are contained in a metadata directory as an xml file. All of the data parsed from the properties files can be specified manually, but utilizing the xml files cuts down on the amount of configuration that is necessary.

4.3 Threshold Parameters

The last set of parameters, the processing parameters, are the ones that have the most effect on the outputs. If the computed threshold is too low, it can lead to a lot of background noise being considered and generally yields a poor result. To counter this, the maximum and minimum thresholds computed by ImageJ are compared: if the difference is too high, then the computed threshold is replaced by the default threshold. This is controlled by the maxThreshRange and defaultThreshold parameters. The FIJI distribution of ImageJ contains over a dozen different methods for computing an intensity threshold, and different algorithms can yield different results. The

Table 2
Table of configuration parameters recognized in the configuration .ini file

Dataset property options		
Parameter	**Name in File**	**Description**
Number of Channels	numChannels	Specifies number of channels in input. Read from microscope properties or set manually.
Number of Z slices	numZ	Specifies number of z slices in input. Read from microscope properties or set manually.
Number of timesteps	numT	Specifies number of timesteps in input. Read from microscope properties or set manually.
The first timestep	minT	Specifies the first timestep to start on. Defaults to 0.
No Z in Filename	noZInFile	Flag that indicates filenames do not contain Z slice specifiers.
No T in Filename	noTInFile	Flag that indicates filenames do not contain timestep specifiers.
Labels for channels	chanLabel	Comma separated list to label channels. Default is [Skip, Yellow, Blue, Gray].
Channels to skip	chansToSkip	List of channel labels for channels that should be ignored/skip. A channel labeled Skip will also be skipped.
Physical size of pixels	pixelHeight	Defines physical height of each pixel. Read from microscope properties. If not specified then areas will be in the value of pixels.
Physical depth of pixel	pixelDepth	Defines physical depth of each pixel. Read from microscope properties. If not specified then areas will be in the value of pixels.
Physical width of pixel	pixelWidth	Defines physical width of each pixel. Read from microscope properties. If not specified then areas will be in the value of pixels.
Debug mode flag	debugOutput	If specified additional output will be created to help with debugging. Optional.
Lower right exclusion X	lowerRightExclusionX	X coord for box to exclude in the lower right, where scale bars commonly appear. Optional.
Lower right exclusion Y	lowerRightExclusionY	Y coord for box to exclude in the lower right, where scale bars commonly appear. Optional.
Upper left exclusion X	upperLeftExclusionX	X coord for box to exclude in the upper left, where timestamps commonly appear. Optional.
Upper left exclusion Y	upperLeftExclusionY	Y coord for box to exclude in the upper left, where timestamps commonly appear. Optional.

This section contains options that specify properties of the dataset, most of which can be read from microscope property files

Table 3
Table of configuration parameters recognized in the configuration .ini file

Processing options		
Parameter	**Name in File**	**Description**
Max threshold range	maxThreshRange	Used to define a maximum range between the computed upper and lower thresholds. If exceeded the image is ignored or a default threshold is used.
Default threshold	defaultThreshold	Controls what happens if maximum threshold range is exceeded. If not set, image is ignored otherwise the set value is used as the threshold.
Thresholding method	thresholdMethod	Defines which method will be used to compute the image threshold.
Threshold from whole range	thresholdFromWholeRange	Only works for tracking, if true image threshold will be computed from all images instead of each frame.
Area threshold—% of max	areaMaxPercentThreshold	A threshold on area to remove unwanted cell clusters, defined as a percentage of the maximum area found in the current frame.
Area threshold—absolute	areaAbsoluteThreshold	A threshold on area to remove unwanted cell clusters, defined as an absolute area value.
Create segmentation masks	createSegMask	If specified, the outputs will include segmentation mask images where pixel values denote blob membership. This option does increase runtime.
LUT Path	lutPath	Specify a file to use as the LUT for segmentation masks. Controls the colors used for each detected cell cluster.

This section contains options that affect the output of processing

method that is used can be specified by the thresholdMethod parameter, although the default value works for many cases. FIJI has a good way to see the results of all available thresholding algorithms on a single image by using Image>Adjust>Auto Threshold... If the Try All method is used, FIJI will display the results for each image in a single collage. Finally, the default is to compute a threshold for each image independently of the other images. In some cases, it can be better to compute a single threshold to use on all images from the image data contained in all of the images. This can be enabled using the thresholdFromWholeRange option, though this option currently only works for the cellStatsTracking script.

4.4 Cluster Parameters

In some cases, some of the detected cell clusters are too small to include in data analysis. There are two parameters provided that can help to remove some of the smaller and more transient detections. The first one, areaAbsoluteThreshold, can be used to remove any

cell cluster with an area smaller than a defined threshold. The second parameter, areaMaxPercentThreshold, attempts to scale the threshold parameter by thresholding on a percentage of the largest cluster in the current frame.

4.5 Debugging Parameters

The createSegMask parameter can be useful for debugging results, and can also be used to apply the cell cluster segmentation in other contexts. When true, segmentation mask images will be created where each pixel in the output image will identify which cluster the pixel belongs to. Each cluster will be uniquely colored, and the color used is defined by a look-up table (LUT), which is defined by the lutPath parameter (FIJI comes with several different LUT options).

By adjusting these parameters, a large number of different situations can be covered. We have demonstrated that TASBE Image Analytics provides a high-throughput processing pipeline to segment cells and regions of cells in microscopy images and to track them over time. This processing pipeline has been validated against hand-labeled data and its utility has been demonstrated in quantifying experiments on shape formation with engineered CHO and HEK293 cells. We have made this system available under a permissive open-source license in the hopes that it will prove useful for a broad range of experiments involving fluorescent cells. Future development is anticipated to be incremental maintenance, refinement, and generalization as driven by the evolving needs of additional users and applications.

Acknowledgments

This work has been supported by the Defense Advanced Research Projects Agency under Contract No. W911NF-17-2-0098. The views, opinions, and/or findings expressed are of the author (s) and should not be interpreted as representing official views or policies of the Department of Defense or the U.S. Government. This document does not contain technology or technical data controlled under either U.S. International Traffic in Arms Regulation or U.S. Export Administration Regulations.

References

1. Lamprecht MR, Sabatini DM, Carpenter AE (2007) Cellprofiler: free, versatile software for automated biological image analysis. BioTechniques 42(1):71–75
2. Rasband W (2012) Imagej: image processing and analysis in java. Astrophys Sour Code Lib 1:06013
3. Schindelin J, Rueden CT, Hiner MC, Eliceiri KW (2015) The imagej ecosystem: an open platform for biomedical image analysis. Mol Reprod Dev 82(7-8):518–529
4. Bajcsy P, Chalfoun J, Simon MH (2018) Web microanalysis of big image data. Springer International Publishing, New York
5. Stylianidou S, Brennan C, Nissen SB, Kuwada NJ, Wiggins PA (2016) Supersegger: robust image segmentation, analysis and lineage

tracking of bacterial cells. Mol Microbiol 102 (4):690–700

6. Clarke ML, Burton RL, Hill AN, Litorja M, Nahm MH, Hwang J (2010) Low-cost, high-throughput, automated counting of bacterial colonies. Cytom Part A 77(8):790–797
7. Chalfoun J, Majurski M, Dima A, Stuelten C, Peskin A, Brady M (2014) Fogbank: a single cell segmentation across multiple cell lines and image modalities. BMC Bioinformatics 15 (1):431
8. Beal J, Weiss R, Densmore D, Adler A, Appleton E, Babb J, Bhatia S, Davidsohn N, Haddock T, Loyall J, Schantz R, Vasilev V, Yaman F (2012) An end-to-end workflow for engineering of biological networks from high-level specifications. ACS Synth Biol 1 (8):317–331
9. Beal J, Overney C, Adler A, Yaman F, Tiberio L, Samineni M (2019) Tasbe flow analytics: a package for calibrated flow cytometry analysis. ACS Synth Biol 8(7):1524–1529
10. Efford N (2000) Digital image processing: a practical introduction using java (with CD-ROM), 1st edn. Addison-Wesley Longman Publishing Co., Inc., Boston, MA, USA
11. Forsyth DA, Ponce J (2002) Computer vision: a modern approach. Professional Technical Reference, Prentice Hall
12. Tinevez JY, Perry N, Schindelin J, Hoopes GM, Reynolds GD, Laplantine E, Bednarek SY, Shorte SL, Eliceiri KW (2017) Trackmate: an open and extensible platform for single-particle tracking. Methods 115:80–90
13. Rother C, Kolmogorov V, Blake A (2004) Grabcut: interactive foreground extraction using iterated graph cuts. ACM Trans Graph 23:309–314
14. Bradski G (2000) The openCV library. Dr Dobb's J Softw Tools 120:122–125
15. Everingham M, Van Gool L, Williams CKI, Winn J, Zisserman A (2010) The pascal visual object classes (voc) challenge. Int J Comput Vis 88(2):303–338
16. Tan PN, Steinbach M, Kumar V (2005) Introduction to data mining, 1st edn. Addison-Wesley Longman Publishing Co., Inc., Boston, MA, USA
17. Tordoff J, Krajnc M, Walczak N, Lima M, Beal J, Shvartsman S, Weiss R (2020) Incomplete cell sorting creates engineerable structures with long term stability. Cell Reports Physical Science

Chapter 2

Neighborhood Impact Factor to Study Cell-Fate Decision-Making in Cellular Communities

Shaylina R. Carter, Joshua Hislop, Joshua Hsu, Jeremy J. Velazquez, and Mo R. Ebrahimkhani

Abstract

Cell-fate determination is a function of cell-intrinsic and -extrinsic signaling cues. Understanding the design principles governing fate control in multicellular systems remains difficult to understand and analyze. To address the current challenges of spatial analysis of potential signaling events, we have developed a pipeline for assessment of the neighboring cells at defined areas in the vicinity of target cells using a newly defined concept of Neighborhood Impact Factor. We have used our pipeline to interrogate cellular decision-making in a genetically derived multi-lineage liver organoid from induced pluripotent stem cells. We examined endothelial versus hepatocyte fate determination for cells with similar expression level of an engineered driver gene circuit. Our analysis suggests that the relative level of gene expression to the neighbor population can control the final fate choice in our engineered liver multicellular system.

Key words Cell fate, Cell state, Neighborhood impact factor, Organoids, Multicellular, Gene regulatory network

1 Introduction

Gene regulatory networks (GRNs) drive cellular fates, whereby the internal network is continuously affected by external environmental cues. Through the interaction of cell-intrinsic regulatory elements and cell-extrinsic signaling, individual cells constantly iterate their genetic state toward a final fate. Understanding the fate that individual cells have achieved is traditionally based on the absolute levels of gene expression as compared across the entire population of cells within a tissue.

To establish the right composition of cell types in a given tissue, integration of contextual signals from the multicellular environment in cellular decision-making is instrumental. As cell state progresses through the differentiation landscape, the GRNs will frequently become poised to specify along multiple lineages

Mo R. Ebrahimkhani and Joshua Hislop (eds.), *Programmed Morphogenesis: Methods and Protocols*, Methods in Molecular Biology, vol. 2258, https://doi.org/10.1007/978-1-0716-1174-6_2,

depending on environmental cues. Building tools for evaluation of these contextual signals can aid with decoding the design principles underlying tissue morphogenesis.

The concept of Impact Factor in the context of cell signaling attempts to integrate overlapping layers of local signals that influence a cell's GRN into a simplified quantitative form. The radius at which a local signaling element influences the cell fate in the microenvironment is referred to here as a cell's "neighborhood." Neighborhood Impact Factor (NIF) is the quantitative assessment of a given signaling element within a certain neighborhood radius around a target cell.

Other software tools have been developed to spatially assess gene expression in the form of mRNA or protein in a population of imaged cells. Open-source softwares such as Icy [1], BioImageXD [2], FluoRender [3], and many other tools [4] have been developed to aid analysis of multichannel fluorescence images. The procedure described here makes use of several of these open-source tools. To this end, we integrated CellProfiler [5], CellProfiler Analyst [6], and ImageJ [7] with customized Java code to develop the NIF analysis pipeline. Our developed program analyzes local gene expression in cellular microenvironments for many cells of a multilineage tissue. This code has been deposited at the following link: https://github.com/FeatherQuill/Neighborhood-Impact-Factor.

2 Materials

1. CellProfiler version 2.2.0.
2. CellProfiler Analyst version 2.2.1.
3. ImageJ version 1.50i.
4. Java version 1.8.
5. R version 3.32.

3 Methods

3.1 Image Preparation

1. Images should be captured at a sufficient resolution that both the cell population and the intracellular stain of interest can be resolved. These individual images should be stitched together to provide one image for an entire 8 mm immunostained coverslip (*see* **Note 1**).
2. From the stitched coverslip image, 1.6 mm × 1.6 mm regions of interest should be cropped for individual analysis. Grayscale images from each channel are needed for quantitative assessment, and a color composite is also recommended for

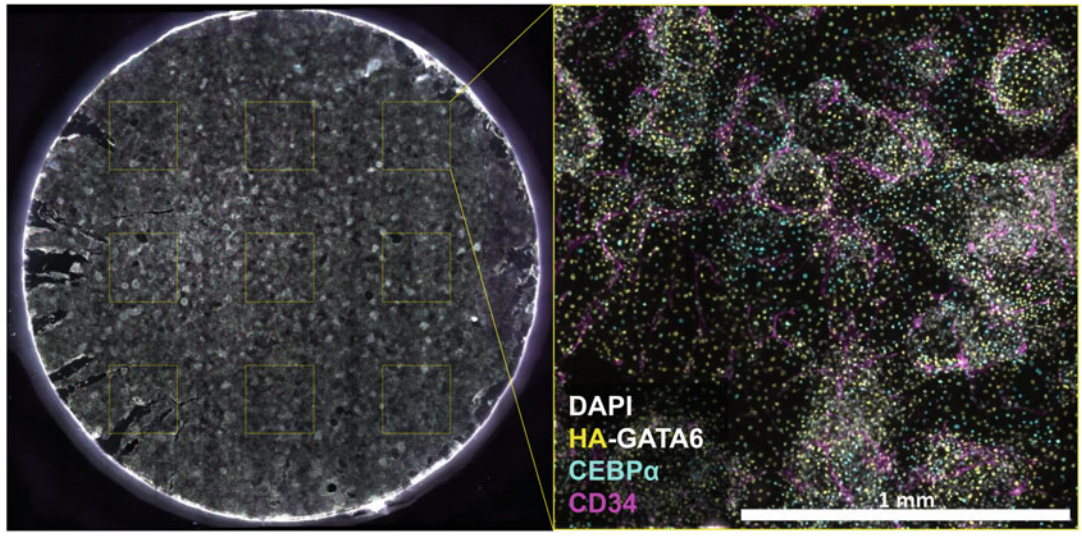

Fig. 1 A representative coverslip image demonstrating nine cropped areas for NIF analysis. The zoomed image shows the expression patterns of exogenous GATA6 (detected via an HA tag), CEBPα, and CD34

qualitative confirmation (*see* **Note 2**). An example of this type of cropping can be seen in a fetal liver organoid culture in Fig. 1.

3. If processing a large number of cropped images in series, consistent file names and storage locations should be established (*see* **Note 3**).

3.2 CellProfiler Processing Pipeline

This step of the NIF is implemented in CellProfiler, a cell image analysis software [5]. The CellProfiler pipeline is implemented as a sequential series of operations that are applied to individual images of an image set of interest. The following steps define the exact meanings and optimization for each step within the pipeline.

1. The *IdentifyPrimaryObjects* component of the CellProfiler program is first run on a nuclear stain in order to identify all cells. By identifying these objects first, areas of marker expression identified by the subsequent analysis steps can be associated properly to their parent cell. An example of the expected output for nuclei can be found in Fig. 2a (*see* **Note 4**).
2. For identifying other stains after the cell nucleus has been identified, the *IdentifyPrimaryObjects* function is used again; however, instead of initializing using an adaptive thresholding method, the "per object" method should be used to limit the search of expression to the previously identified locations from the nuclear stain. This can be useful for identification of secondary cytoplasmic markers, such as AAT (Fig. 2b).

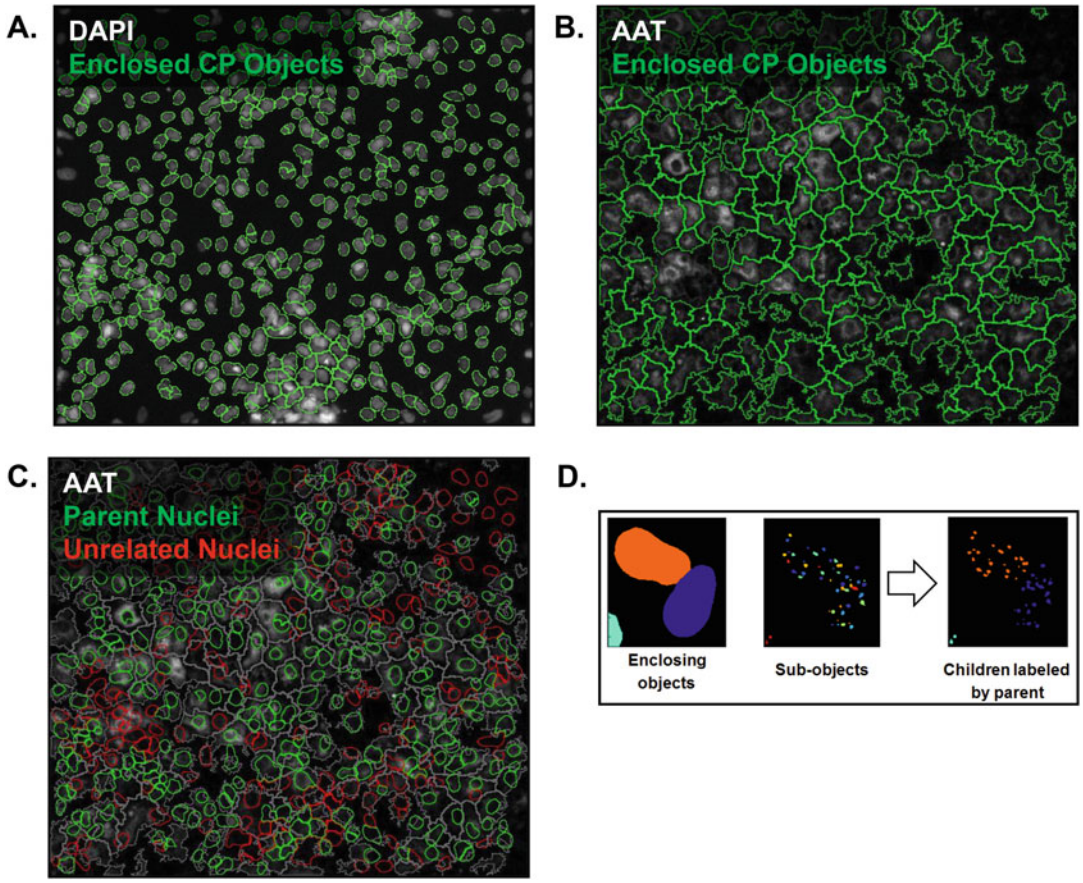

Fig. 2 Intermediate results from the CellProfiler pipeline for automated cell marker segmentation. (**a**) Day 14 fetal liver organoid nuclei segmented via the Otsu three-class method using the *IdentifyPrimaryObjects* function that meet input parameters have been identified in green. (**b**) Day 14 fetal liver organoid stained for AAT and segmented via the *IdentifyPrimaryObjects* function. The search for objects was limited to areas identified in the nuclear segmentation in (**a**). (**c**) The result from the RelateObjects module is shown here. Previously identified AAT objects have outlines drawn in gray, and the outlines of nuclei are drawn in green and red; the green outlines represent the objects that have been identified as "parents" to the "child" AAT objects, while the red outlines represent objects have not been related to an AAT object. (**d**) The use of the *RelateObjects* module is to relate all stains (whether nuclear or surface) back to a parent nucleus, so that all stains can be measured within context of the same nuclear object

3. The *MeasureObjectIntensity* function is used to measure and record the intensities of marker expression for each image channel of interest.
4. The *RelateObjects* function is used to associate the "child" marker expression object identified from each of the "parent" nuclei to its respective nucleus for downstream analysis. Cytoplasmic markers such as AAT are associated with the nucleus that most overlaps their expression area (Fig. 2c), and nuclear

markers with speckled expression patterns can be associated with the nucleus that encloses them (Fig. 2d).

5. The *CalculateMath* function is used to normalize the expression levels of each of the marker expression stains of interest against the nuclear stain intensity.
6. The *ExportToDatabase* function is used to export an SQLite database of the recorded information for downstream processing.
7. The *ExportToSpreadsheet* function can be used to export the recorded cell location and expression level information for downstream applications.

3.3 Import SQLite Database and Produce NIF Data

The SQLite database file now contains information for each individual cell object identified in all the images run through CellProfiler, and can be queried for population statistics. Two Java programs were written to access this file and create output products, and CellProfiler Analyst takes this database file as an input to run also (*see* **Note 5**).

The first Java program uses the database file to gather statistics about the stained populations and compare those populations with one another. These statistics are produced as a text file that can be easily compared between various experiments. This Java program also connects with the R statistical language to run a non-paired *t*-test on the mean expression levels of two populations of interest to check for a statistically significant difference (*see* **Note 6**).

The second Java program to work with the database file was designed to analyze the NIF of a biological signal (i.e., fluorescent stain associated with a gene of interest). It does so by creating a "cell" object consisting of a cell's x and y location within the image, values for the intensity of input biological signal, and the image number associated with the cell. The program then produces a detailed output for the NIF values of a given radius (set before running), or can compute the average NIF values for a range of radii to determine the optimal neighborhood radius based on the highest p value (significance of observations). It will output files as CSVs containing information about the radius, average Impact Factor values for the input biological signal, the percent differences between these Impact Factors, and the p value associated with that difference.

3.4 Produce Spatial Plot of Cell Expression

A subsequent script written in R produces a "spatial plot" of the cells based on their gene expression. The R program uses the CSV output from the CellProfiler pipeline which contains information about each parent nucleus. The R program takes all the nucleus objects for a given image, uses their x and y values to draw their location on a plot, and uses their marker expression signal intensity

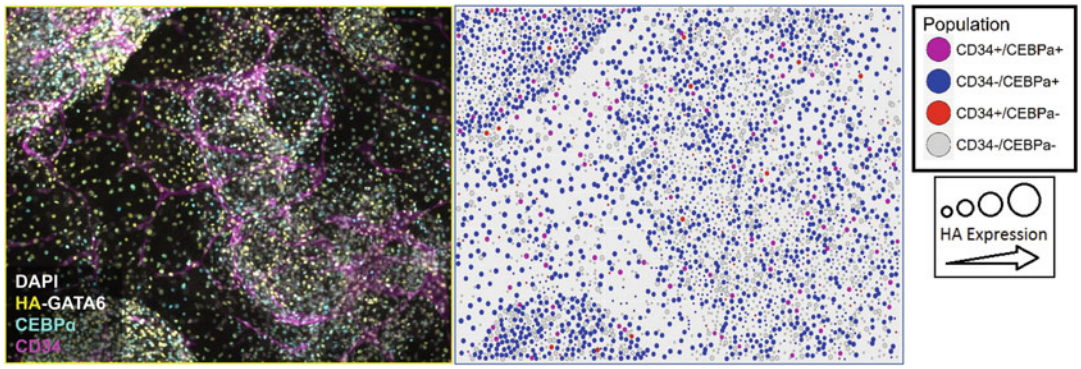

Fig. 3 A spatial plot derived from information from a sub-cropped section of the day 14 fetal liver organoid that has been stained for CEBPα (a hepatocyte marker), CD34 (an endothelial cell marker), and HA (GATA6, a cell-fate driver). The *x* and *y* axis represent pixel values within the cropped image. Each circle represents a detected cell, and the circles are colored based on CD34 and CEBPα expression. The radius of the circle for each image is determined by the measured HA intensity. The higher the HA intensity, the larger the circle representing the cell

to colorize and size circles that correspond to each cell location (Fig. 3, additional context and example in Subheading 3.6).

3.5 Analysis of NIF Results

We have proposed three ways to define the NIF, which we have termed "Total Expression," "Local Density," and "Distance Adjusted." However, the models of neighborhood expression should be tailored for the analysis of the system of interest, depending on a proposed or expected expression pattern.

3.5.1 Total Expression Impact Factor

Here a biological marker is shown as a gene of interest (GOI). The impact factor of the Total Expression method is defined as follows:

$$\mathrm{NIF}_{\text{Total expression}} = \frac{\sum(\text{GOI expression within optimal radius})}{\text{GOI in cell of interest}}$$

This method simply calculates the sum of the expression levels of all cells expressing a GOI within the neighborhood by finding all the cells within the neighborhood radius and adding up their GOI expression levels as quantified by intensity. This expression level is then normalized to the gene expression of the cell for which the neighborhood is being analyzed (Fig. 4a).

3.5.2 Local Density Impact Factor

The Local Density method defines impact factor as follows:

$$\mathrm{NIF}_{\text{Local density}} = \frac{\sum\left(\frac{\text{GOI expression within optimal radius}}{\text{Number of cells within optimal radius}}\right)}{\text{GOI in cell of interest}}$$

This method takes the sum of the expression of a given GOI within the neighborhood divided by all the cells in the neighborhood to produce an average expression per cell. This method can be useful to check if a density of nearby cells expressing a GOI, not just

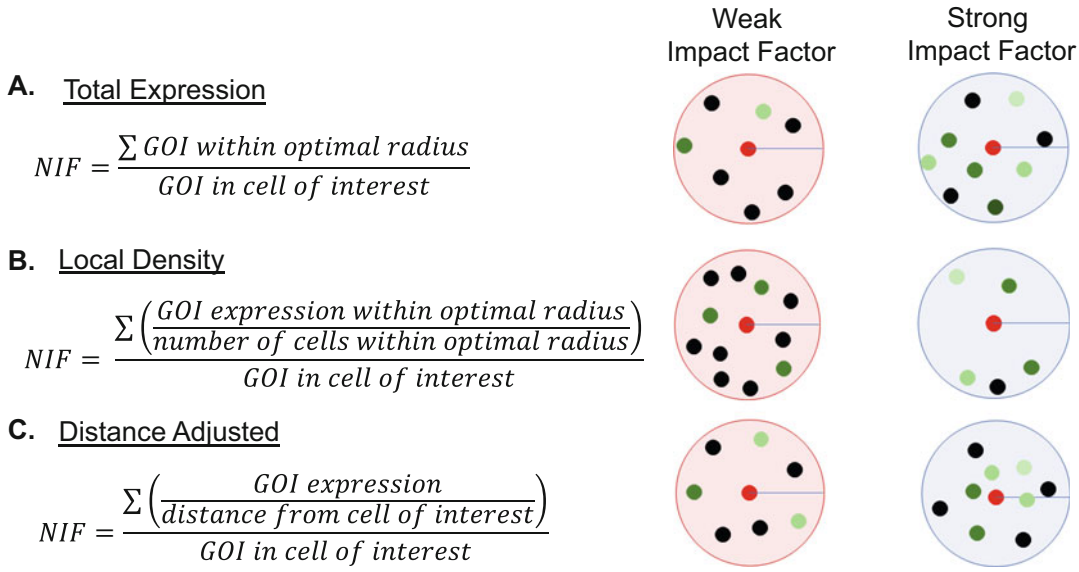

Fig. 4 Schematics demonstrating example cell distributions corresponding to strong or weak impact factors. The red and blue background circles represent the radius from the cell of interest. Every cell is depicted as a smaller circle. Red dots are the cells of interest; surrounding green dots represent neighborhood cells that are strongly (dark green) or weakly (light green) positive for a marker of interest. Black dots represent cells that are negative for the marker. (**a**) Total Expression Impact Factor measures the total expression of a biological marker (here defined as a GOI) in the population in the neighborhood radius of a cell of interest without consideration of distance or cell density. (**b**) Local Density Impact Factor measures the total expression of a GOI normalized to the total number of cells within the neighborhood radius. A high density of cells, of which only a few are positive, will result in a weaker Local Density Impact Factor than a population with fewer but more proportionally positive cells. (**c**) Distance Adjusted Impact Factor measures the intensity of expression of cells positive for a GOI normalized to the distance away from a cell of interest. A density of cells positive for a GOI close to a cell of interest will result in a higher Distance Adjusted impact factor

a threshold of local expression, is a key determining factor in driving the biological events associated with the cell neighborhood (Fig. 4b).

3.5.3 Distance Adjusted Impact Factor

The Distance Adjusted method defines impact factor as follows:

$$\mathrm{NIF}_{\text{Distance adjusted}} = \frac{\sum\left(\frac{\text{GOI expression}}{\text{GOI cell distance}}\right)}{\text{GOI in cell of interest}}$$

This method quantifies the neighborhood with the assumption that the neighborhood cells expressing a GOI farther away from the cell of interest have reduced influence on that cell. Therefore, the distance away from the central cell of interest is inversely proportional to the impact of that cell on the NIF (Fig. 4c).

The best NIF for representation of signaling effects within a given system should be iteratively optimized through modeling and

experimentation to fit the experimental parameters of that system (*see* **Notes 7** and **8**).

3.6 Example of NIF Processing and Output in Human Fetal Liver Organoid

NIF, in this case, is used to assess how cells that express similar levels of a fate-driving gene circuit, and at one point were genetically similar or identical, may have been driven toward divergent fates because of differences in local environmental contexts and signaling. The premise behind the NIF in this application is that perhaps the absolute expression of the fate-driving circuit is not necessarily the sole defining factor for producing the final cell fate. One alternative is that the cell fate is determined by "relative" circuit gene expression as compared to the cellular neighbors. To illustrate the NIF analysis process, below is the NIF pipeline as applied to a population of genetically engineered iPSCs coaxed to form a multicellular liver organoid described previously by Guye et al. [8]. These cells are engineered with an inducible GATA6 gene circuit. Upon induction by addition of doxycycline, iPSCs differentiate to endoderm and mesoderm progenitors [8]. In brief, iPSCs are treated with doxycycline first for 5 days in mTeSR media [8]. After day 5, doxycycline is removed, and cells are left to differentiate in basal media for additional 9 days. Here, by virtue of the circuit design, GATA6 contains an HA tag that allows interrogation of the GATA6 protein level produced by the engineered circuit via staining. It is assumed that doxycycline-induced GATA6 level is correlated to the initial GATA6 copy number per cell. We assumed, based on our past experience, there is minimal transgene silencing in the engineered cells. Therefore, a short pulse of doxycycline at any given time during the life of the organoid can provide indirect information about the initial copy number of the gene circuit.

Following a short pulse of doxycycline on day 14, we stained for the HA tag, as well as for markers of cell fates (hepatocyte vs. endothelial) and assessed current cell state as well as GATA6 levels in the cell and its neighborhood to determine what role local differences in initial GATA6 expression level may have had on final cell fate. The hepatocyte marker CEBPα, endothelial marker CD34, and the HA tag for initial GATA6 levels are used for NIF analysis. Full 8 mm coverslips stained for these markers were imaged at 10× magnification, and then nine 1.6 × 1.6 mm regions of interest were cropped for analysis (Fig. 1).

The *IdentifyPrimaryObjects* module was used to identify cell nuclei from the nuclear stain channel, as well as expression areas of each of the factors of interest from the individual stain channels. The best method for distinguishing nuclei was to use an adaptive strategy (as opposed to global), and to use Otsu's method with three classes, with the two classes of greater intensity assigned as "foreground." The identified nuclei objects were then used as the

Table 1
Statistics for the day 14 liver organoid experiment

Metric	Value
Mean HA expression	0.31338
Mean CD34+ HA expression	0.14102
Mean CEBPα+ HA expression	0.22924
P value for mean difference	4.40 E-161

Statistics are, from top to bottom, average HA expression across all cells, average HA expression for the entire CD34 positive population, average HA expression for the entire CEBPα-positive population, *P* value for the difference between those two means

starting points for identifying the child stains for each cell. Based on this, an output file was created that defined relative cell locations as well as expression levels for each of the markers of interest. This information was exported to an SQLite database file using the *ExportToDatabase* function of CellProfiler. This SQLite database was then used with the Java program to run NIF analysis.

A summary of marker expression was output by CellProfiler. Mean expression levels for each investigated marker can be found in Table 1. We identified that for cells expressing with high initial GATA6 expression levels, there was a bias toward hepatic fates, while among cells with low initial expression levels there was a bias toward endothelial fates. To assess the impact of GATA6 expression level in neighbor cells on the target cell fate, we selected cells expressing a medium level of GATA6 (within the mean level ±2.5% of the maximum intensity measurement for GATA6) for NIF assessment. We measured NIF in this subpopulation using the Total Expression, Local Density, and Distance Adjusted methods detailed above. Next we compared NIF values between CEBPα (hepatocyte-like) vs. CD34 (endothelial-like) fates. This analysis resulted in statistically significant findings for the Total Expression and Distance Adjusted IF methods (Fig. 5). The optimal neighborhood size was determined to be 20 μm for the Total Expression method, and 30 μm for the Distance Adjusted method. This resulted in approximately 6–8 cells in the cellular neighborhoods. CD34-expressing cells were found to have a 21–29% difference in impact factor value as compared to CEBPα-expressing cells. Collectively, cells with the same absolute GATA6 expression level were found to take on two different fates, depending on their local neighborhood; cells with a mean level of exogenous GATA6 in high GATA6 neighborhoods became CD34+, while cells with that same mean GATA6 expression in lower GATA6 neighborhoods became CEBPα+. This supports the idea that relative gene expression is an important player in determining whether a GATA6-expressing cell will acquire endothelial- or hepatic-like

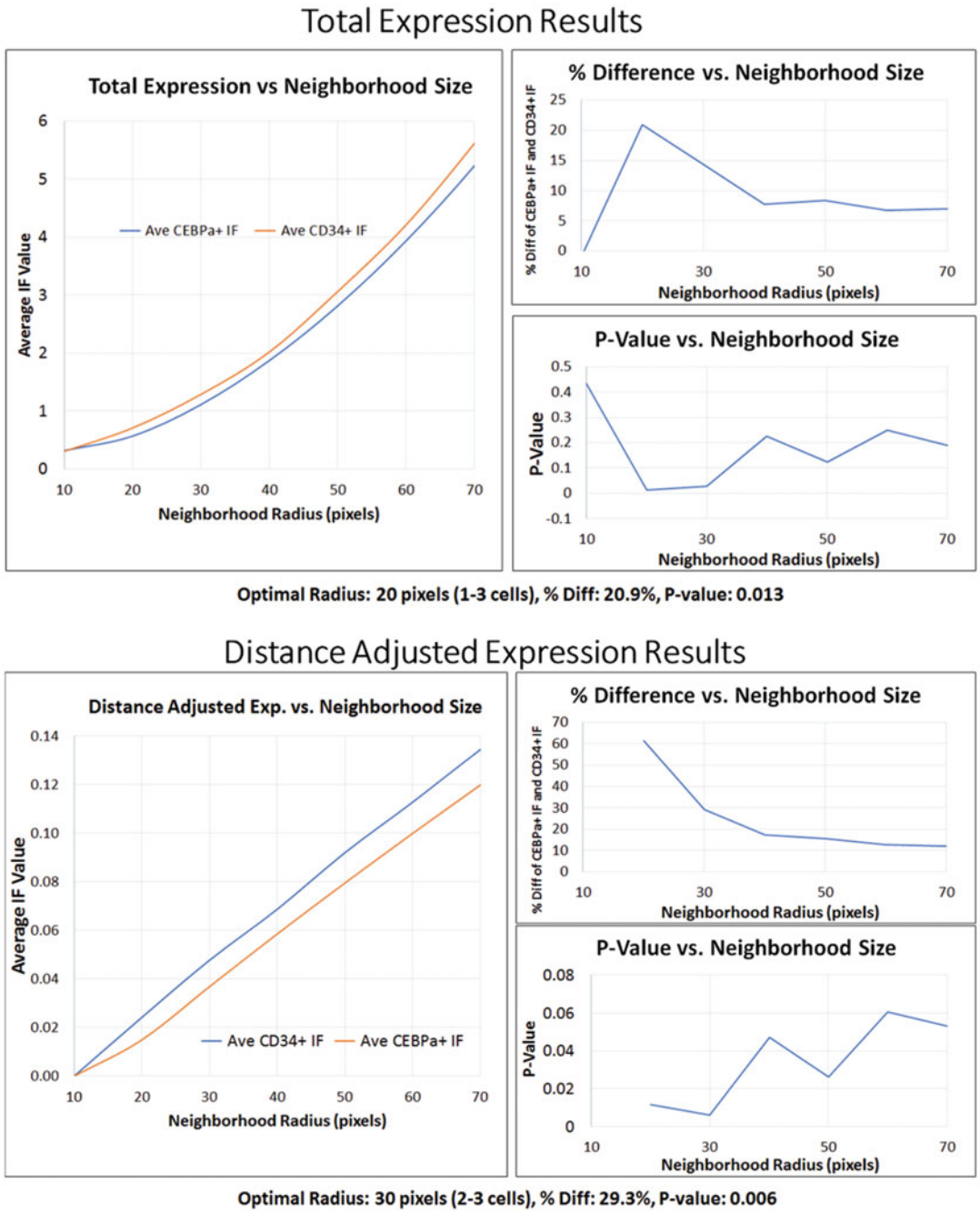

Fig. 5 Plots detailing the results of the Total Expression NIF method and the Distance Adjusted Expression NIF method applied to the day 14 liver organoid cultures. The left plot of each section shows the average IF values for the two populations (CEBPα+ and CD34+, represented in blue and orange respectively on the left graph and orange and blue respectively on the right graph) against the neighborhood radius. The upper right plot for each section has the corresponding percent impact factor difference for the two populations vs. the neighborhood radius, and the lower right shows the *p* values for those differences. The bottom line of each section shows the optimal radius (in pixels), its percent difference, and its *p* value. 30 pixels is equal to approximately 30 μm, or 2–3 cells

fates. This new form of quantification and analysis of gene expression in a spatial context can provide useful information to describe and explain cell fate when developing multicellular systems such as organoids.

4 Notes

1. We have found the optimal magnification parameters to be 10× magnification on a widefield microscope. This has allowed capture of abundant immunostained markers across a wide field of view, as seen in Fig. 1.
2. A full color composite is helpful as a final screening step to ensure that debris or artifacts are not within the cropped area of the image, to prevent their consideration for analysis.
3. CellProfiler can load batches of images and process them sequentially as long as a consistent naming scheme is applied to individual grayscale channel images of similar stains. Many microscope software packages will do this automatically when exporting images into different formats, but it should be ensured that file name conventions remain consistent across all datasets of interest.
4. It may be helpful, depending on the image and nuclear stains used, to apply an additional despeckle step before analysis of the nuclei. This may be accomplished in external programs, or through CellProfiler directly by the use of the *EnhanceOrSuppressFeatures* module added at the beginning of the pipeline. Parameters should be optimized to your image when using this function.
5. CellProfiler Analyst is useful for creating scatter and density plots based on the measurements from the image set. CellProfiler Analyst also has the capability to gate certain populations from a plot and view them individually in subareas of the color composite image to check for abnormalities or other factors that might be easier to spot visually.
6. In addition to the Java programs that were written, further analysis can be performed in CellProfiler Analyst using the query interface, which allows database queries to be run against the SQLite database. This allows the flexibility of investigating other relationships or phenomena without the need to re-perform any of the initial analysis.
7. If you define a limited expression intensity range for a biological marker in a given population for which you are comparing NIF, depending on the extent of difference in neighborhood expression, it might not be necessary to divide

the NIF result by the expression level of the biological marker in the cell of interest, as indicated in Fig. 4.

8. NIF equations should be refined based on observations and data gathered from the system until a best model for analysis of cellular neighbors is reached through iterative cycles of experimentation and new analyses.

Acknowledgements

This work was supported by an R01 from National Institute of Biomedical Imaging and Bioengineering (EB028532), an R01 from the National Heart, Lung, and Blood Institute (HL141805), the New Investigator Award from Arizona Biomedical Research Council (ADHS16-162402), as well as support from the Pittsburgh Liver Research Center (NIH-NIDDK P30DK120531).

References

1. de Chaumont F, Dallongeville S, Chenouard N, Herve N, Pop S, Provoost T, Meas-Yedid V, Pankajakshan P, Lecomte T, Le Montagner Y, Lagache T, Dufour A, Olivo-Marin JC (2012) Icy: an open bioimage informatics platform for extended reproducible research. Nat Methods 9 (7):690–696. https://doi.org/10.1038/nmeth.2075
2. Kankaanpaa P, Paavolainen L, Tiitta S, Karjalainen M, Paivarinne J, Nieminen J, Marjomaki V, Heino J, White DJ (2012) BioImageXD: an open, general-purpose and high-throughput image-processing platform. Nat Methods 9(7):683–689. https://doi.org/10.1038/nmeth.2047
3. Wan Y, Otsuna H, Chien CB, Hansen C (2012) FluoRender: an application of 2D image space methods for 3D and 4D confocal microscopy data visualization in neurobiology research. IEEE Pac Vis Symp 2012:201–208. https://doi.org/10.1109/pacificvis.2012.6183592
4. Eliceiri KW, Berthold MR, Goldberg IG, Ibanez L, Manjunath BS, Martone ME, Murphy RF, Peng H, Plant AL, Roysam B, Stuurman N, Swedlow JR, Tomancak P, Carpenter AE (2012) Biological imaging software tools. Nat Methods 9(7):697–710. https://doi.org/10.1038/nmeth.2084
5. Kamentsky L, Jones TR, Fraser A, Bray MA, Logan DJ, Madden KL, Ljosa V, Rueden C, Eliceiri KW, Carpenter AE (2011) Improved structure, function and compatibility for CellProfiler: modular high-throughput image analysis software. Bioinformatics 27(8):1179–1180. https://doi.org/10.1093/bioinformatics/btr095
6. Jones TR, Kang IH, Wheeler DB, Lindquist RA, Papallo A, Sabatini DM, Golland P, Carpenter AE (2008) CellProfiler Analyst: data exploration and analysis software for complex image-based screens. BMC Bioinformatics 9:482. https://doi.org/10.1186/1471-2105-9-482
7. Schneider CA, Rasband WS, Eliceiri KW (2012) NIH Image to ImageJ: 25 years of image analysis. Nat Methods 9(7):671–675. https://doi.org/10.1038/nmeth.2089
8. Guye P, Ebrahimkhani MR, Kipniss N, Velazquez JJ, Schoenfeld E, Kiani S, Griffith LG, Weiss R (2016) Genetically engineering self-organization of human pluripotent stem cells into a liver bud-like tissue using Gata6. Nat Commun 7:10243. https://doi.org/10.1038/ncomms10243

Chapter 3

A Quantitative Lineage-Tracing Approach to Understand Morphogenesis in Gut

Svetlana Ulyanchenko and Jordi Guiu

Abstract

Lineage-tracing experiments aim to identify and track the progeny and/or fate of cells. The use of inducible recombinases and fluorescent reporters has been instrumental in defining cellular hierarchies and allowing for the identification of stem cells in an unperturbed in vivo setting. The refinement of these approaches, labeling single cells, and the subsequent quantitative analysis of the clonal dynamics have allowed the comparison of different stem cell populations as well as establishing different mechanisms of cellular replenishment during steady-state homeostasis as well as during morphogenesis and disease. Utilizing this approach, it is now possible to establish the cellular hierarchy in a given tissue and the frequency of cell fate decisions on a population basis, thus providing a comprehensive analysis of cellular behavior in vivo. Although in this chapter we describe a protocol for lineage tracing of cells from fetal intestinal epithelium to the adult intestine, this approach can be widely applied to quantitatively assess the cell fate of any fetal cell during morphogenesis.

Key words Fetal intestine, Lineage tracing, Intestinal stem cells, Intestine, C-section

1 Introduction

Lineage tracing is a powerful tool that allows for the identification of the progeny of specific cells, thus allowing the establishment of the cellular hierarchy responsible for maintaining functional organs. The first pioneering lineage-tracing works were performed by direct observation at the beginning of the nineteenth century (reviewed in [1]), while later on the implementation of radioactive labeling and cellular dyes allowed for limited cell tracing. These indirect methods were particularly relevant in the study of the intestine when Cheng and Leblond proposed that cells located at the bottom of the crypts were intestinal stem cells [2], which was later validated and expanded in Dr. Hans Clevers' lab using genetic lineage-tracing models [3].

Mo R. Ebrahimkhani and Joshua Hislop (eds.), *Programmed Morphogenesis: Methods and Protocols*, Methods in Molecular Biology, vol. 2258, https://doi.org/10.1007/978-1-0716-1174-6_3,

The use of genetic models in which an inducible cre recombinase is combined with fluorescent reporters allows labeling of potentially any cell in the organism (Fig. 1a). Moreover, if labeling is performed at low density it allows following the fate of the progeny of single labeled cells over time (clones) in adult tissues and during morphogenesis (Fig. 1b–c). The qualitative analysis of the cellular composition of the resulting clones will allow to infer the cellular hierarchy of the tissue, importantly when clones are quantitatively analyzed it is even possible to elucidate the frequency of a particular cell fate decision. The addition of quantitative analysis to lineage-tracing data has been instrumental in revealing several mechanisms in epithelial tissues: neutral competition of intestinal stem cells [4–6], fetal origin of adult intestinal stem cells [7], skin epithelial stem cells specification [8–10], stomach stem cell behavior [11], and mammary gland epithelial stem cell origin [12], to name a few.

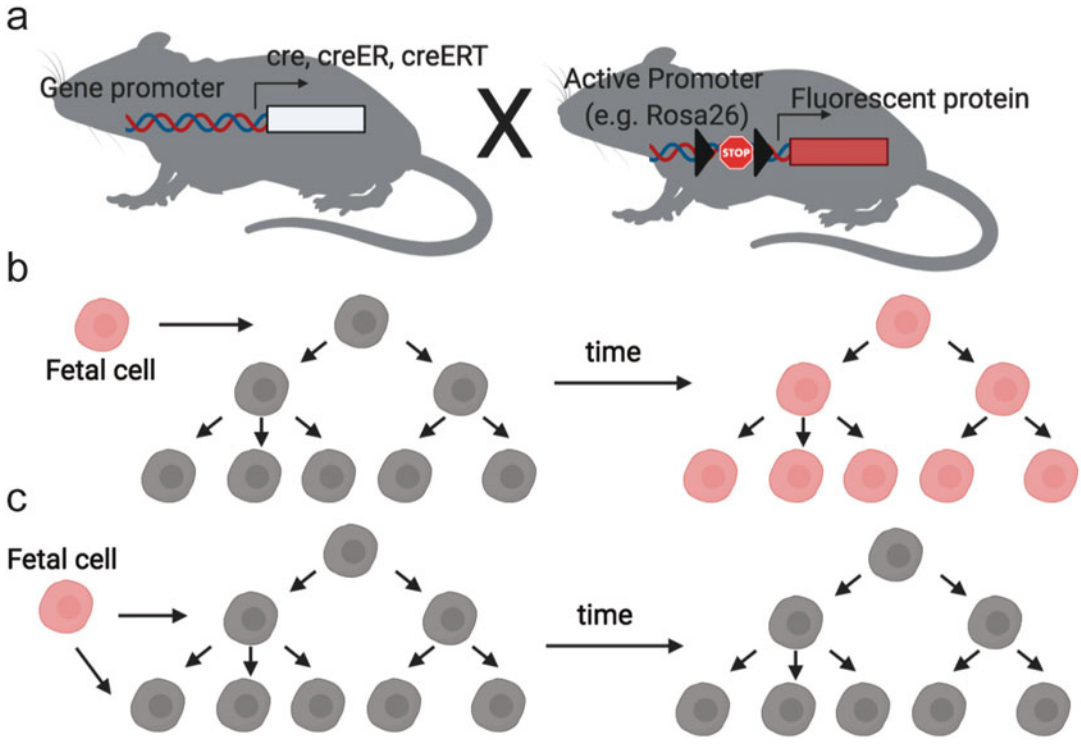

Fig. 1 Lineage tracing during morphogenesis. Cross a male carrying a cre recombinase with a reporter female (**a**). If the fetal-labeled cells are precursors of an adult stem cell, they will generate clones that will persist over time up to adulthood (although some of them are lost due to competition among stem cells) giving rise to clones that will include differentiated cells (**b**). In contrast, if the labeled fetal cells are precursors of adult progenitors or differentiated cells, they will generate clones that will be lost (**c**)

The small intestine is the tissue responsible for the digestion and absorption of nutrients. In the proximal part, it is connected to the stomach and pancreas and in the distal to the caecum and colon. The intestinal tube is composed of finger-like protrusions, which are comprised of postmitotic cells, and crypts that harbor the proliferative cells (Fig. 2a). Intestinal stem cells, characterized by *Lgr5* expression, are located at the bottom of the crypts [3]. Lineage-tracing experiments of *Lgr5*-positive cells have been instrumental to undoubtedly classify these columnar basal cells as the intestinal stem cells [3] in contrast to the villus cells which are not capable of contributing to long-term tissue maintenance [13] (Fig. 2b) during homeostasis. In the developing mouse embryo at E13.5, the intestinal epithelium is pseudostratified, while by E16.5 it becomes a folded simple epithelium composed of protruding villi and the interconnecting intervillus regions. Interestingly *Lgr5*-expressing cells are exclusively located in the intervillus regions (Fig. 2c). Using a quantitative lineage-tracing approach, that we describe in this chapter, we demonstrated that fetal *Lgr5*-positive cells alone

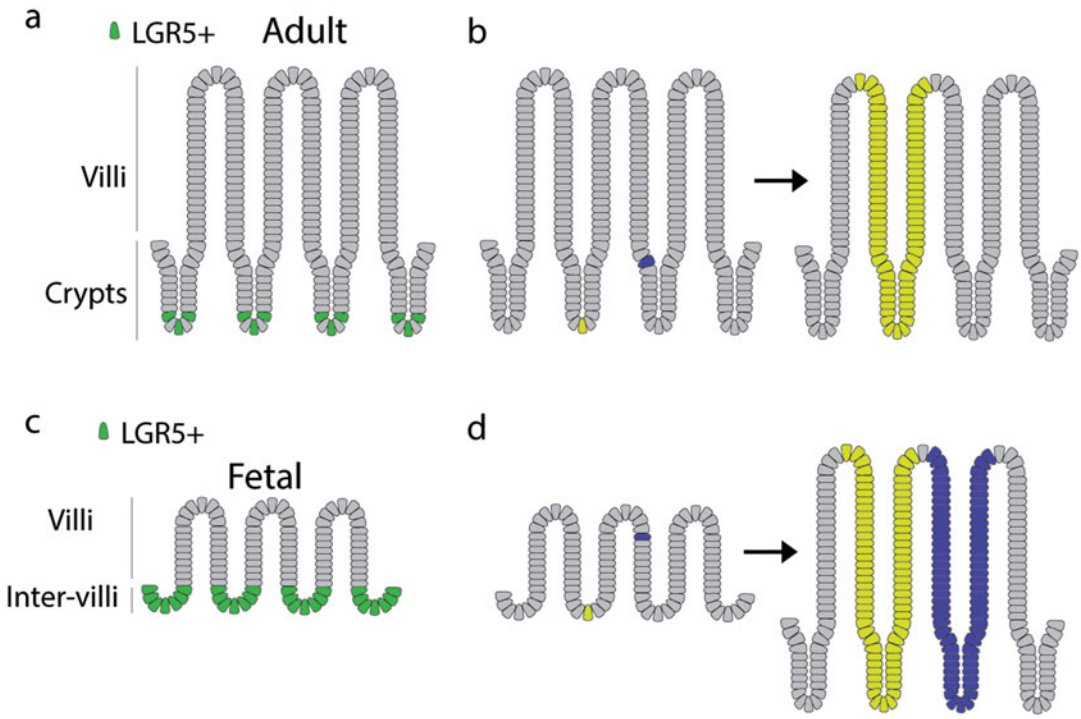

Fig. 2 Intestinal organization. The fetal intestine is organized in villi and intervillus regions and the adult intestine into villus and crypts. Intestinal stem cell markers including Lgr5 are expressed at the bottom of the crypt domains **(a)**. The adult intestine is hierarchically organized with the Lgr5 stem cells located in the apex of the hierarchy. During adult homeostasis lineage tracing of the adult intestine reveals that only cells located in the crypts give rise to long-term persisting clones **(b)**. Intestinal stem cell markers including Lgr5 are expressed at the bottom of the intervillus regions in the fetal intestine **(c)**. Lineage tracing of fetal intestinal cells reveals that it is composed by a layer of equipotent progenitors **(d)**

are not sufficient to sustain the expansion of the intestinal epithelium and that cells from the villus are capable of relocating to the intervillus regions through villus fission and contribute to the generation of the adult intestinal stem cell pool [7] (Fig. 2d).

In this chapter, we describe a protocol to label and lineage trace-specific cells from the fetal intestinal epithelium and assess their contribution to the adult intestinal epithelium. This protocol can be adapted to execute similar lineage-tracing studies in other fetal tissues. Moreover, we address and describe several challenges and potential caveats when utilizing this approach, including the cesarean section procedure, which is very often indispensable in these experiments due to the use of CreERT2 genetic systems that require the use of tamoxifen.

2 Materials

1. Mice.
2. 4-Hydroxytamoxifen (4OHT), dissolved in ethanol (stock concentration 20 mg/mL).
3. Absolute ethanol.
4. Syringe and needles.
5. Corn oil.
6. Scissors, Operating, 11.5 cm, straight, sharp/sharp.
7. Forceps.
8. Phosphate-buffered saline (PBS).
9. Paraformaldehyde (PFA) 4% dissolved in PBS.
10. Petri dish 14 × 90 mmØ.
11. Antibodies.
12. Methanol.
13. Triton X-100 Surfact-Amps, Detergent Solution dissolved in PBS.
14. Petri dish 14 × 90 mmØ.
15. Adult bovine serum diluted in PBS.
16. Optimal cutting temperature compound (OCT).
17. Paraffin.
18. Superfrost Ultra Microscope Slides.
19. Bovine Serum Albumin (BSA) diluted in PBS.
20. Blocking solution: 10% Adult bovine serum, 0.3% Triton X-100 in PBS.
21. Diamidino-2-phenylindole dihydrochloride (DAPI).
22. Hematoxylin.
23. Benzyl alcohol:benzyl benzoate (BABB) 1:2 proportion.

3 Methods

3.1 Plug Detection and Tamoxifen Injection

In order to obtain reliable lineage-tracing results from fetal cells, it is important to set up timed mattings. Females ranging from 2 to 4 months old are injected with the same amount of tamoxifen.

1. Put two females with a male in the same cage in the afternoon. In general, we recommend using females carrying the reporter (e.g., *Rosa26-Confetti, mT/mG*) and the male the cre recombinase alleles (*see* **Note 1**).
2. Check vaginal plug in the morning. If detected, place the plugged female into a different cage. The day of the plug detection is considered E0.5.
3. Inject 4OHT diluted in corn oil (Final volume 300 μL) intraperitoneally into a pregnant female at the desired time point. It is important to perform the intraperitoneal injection in the middle of the abdomen to avoid damage to the bicornuate uterus and the embryos/pups (Fig. 3a). The dose of tamoxifen used in order to obtain clonal labeling depends on the specific combination of "creERT2" and reporter mouse strains used, and therefore it has to be optimized. Performing a tamoxifen

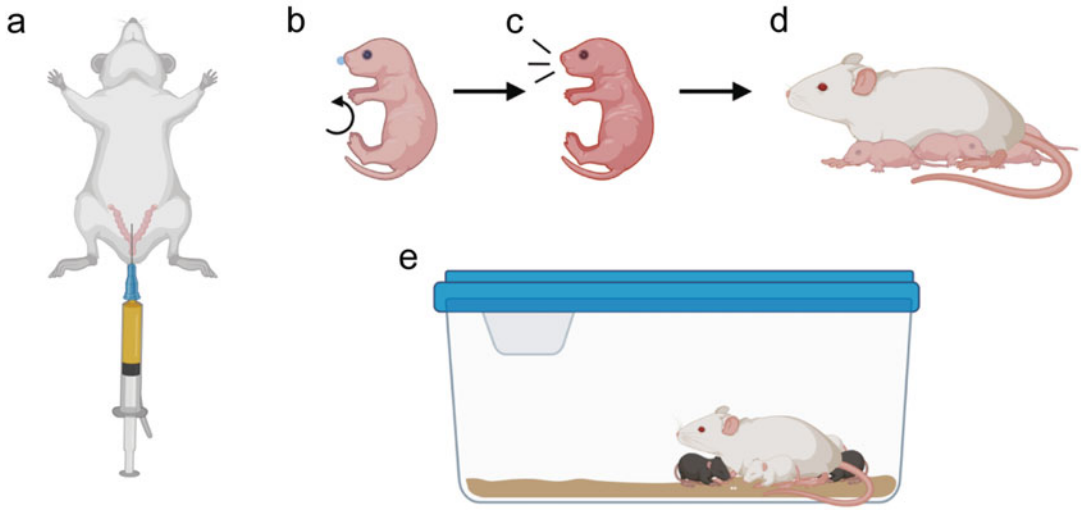

Fig. 3 Tamoxifen injection and c-section. In order to avoid injury to the pups, tamoxifen injections in pregnant females are performed in between the bicornuate uterus (**a**). Schematic representation of the c-section procedure. After the initial dissecting out of the uterus, pups have a pale appearance and do not move much, wipe away the amniotic fluid and massage the pup gently stimulating the remaining fluid to clear the airway (**b**), make sure the airway is clear by gently pinching the pup, if the airway is clear the pup will emit a soft squeak, leave the pup on the heating pad until it acquires a darker color and exhibits active movement (**c**). Place the pup with the foster mother mixing the pups with the foster mother's litter (**d**). Do not disturb the foster mother for at least 24 h. If using strains with different coat colors, it is easy to identify the foster pups by coat color (**e**)

titration experiment with a variety of doses ranging from 0.1 to 1 mg of 4OHT to establish the appropriate dose for single cell labeling is advised. Labeling can be performed even the day before the estimated birth date (usually E18.5) (*see* **Notes 2** and **3**).

3.2 Cesarean Section (Fig. 4) (See Note 4)

C-sections are performed at E18.5–E19.5 depending on the mouse strain (*see* **Notes 5** and **6**). To ensure the best survival rates of the pups, it is recommended to move quickly, therefore the following steps should be taken before the procedure begins.

1. Identify the cage with the foster female. Typically for this procedure it is recommended to use the CD1 strain. Place the foster mother in a different cage (alone) during the whole procedure. CD1 mice produce large litters; therefore, it is advisable to cull some of the pups to increase the amount of care the foster female can devote to the adopted pups.
2. Set up a heating pad or heating chamber.
3. Remove some of the dirty bedding from the foster female's cage and place it on the heating pad.
4. Rub some dirty bedding from the foster female cage on your gloves in order to impregnate them with the foster mother smell.
5. Prepare two surgical forceps, straight scissors, and highly absorbent tissues.

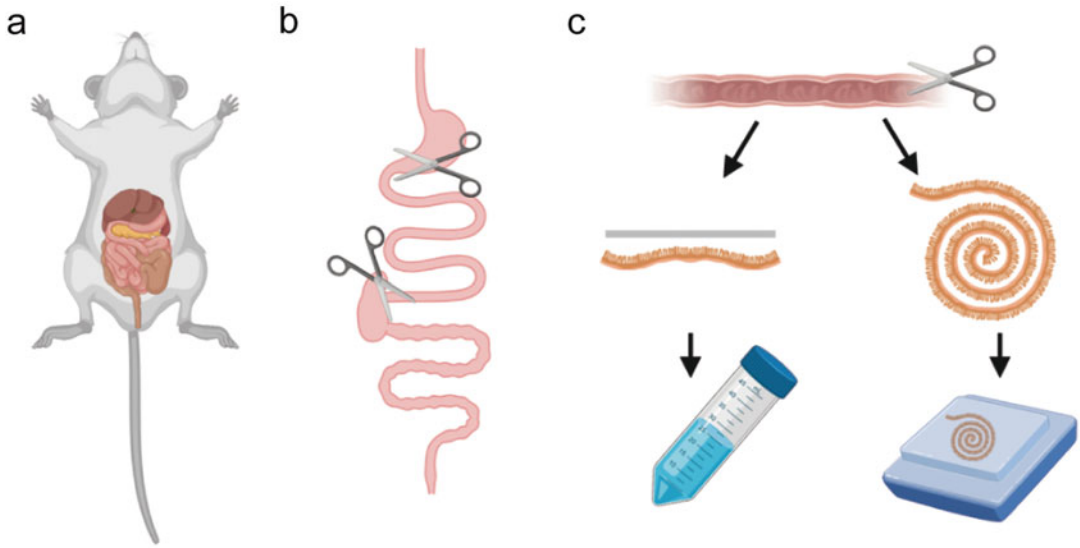

Fig. 4 Tissue isolation. The abdominal cavity of the mouse is opened (**a**); the intestine is dissected (**b**) flushed with PBS and opened longitudinally **(c)**, then it can be fixed with tissue on top (to keep it as flat as possible) and dehydrated in methanol to store it for whole-mount immunostaining; or fixed in a swiss role for embedding in OCT or paraffin to be analyzed in section

You are now ready to carry out the procedure.

1. Sacrifice the pregnant female using cervical dislocation. Do not use anesthetic drugs as this can impact the survival of the pups.
2. Turn the mouse on its back exposing the abdomen. Lifting the skin make an incision along the midline of the abdomen cutting through the skin and then muscle layer with surgical scissors, while being careful to avoid damaging the uterus.
3. Remove the uterus with blunt forceps and place it onto a highly absorbent tissue. Quickly yet carefully open the uterine wall using one sharp and one blunt forceps and dissect the pups out of the yolk sac and amnion (one pup at the time keeping the rest inside the uterus during the whole procedure **steps 3–5**). Note that care must be taken not to damage the pups as it is easy at this point to injure the pups with the sharp forceps. Use the scissors to severe the umbilical cord.
4. Using an absorbent tissue gently wipe the amniotic fluid from the pup. Further gently massage the pup's abdomen and rib cage, additional fluid might come out of the pup's nose and mouth, wipe this away carefully. This should facilitate a clear airway and independent breathing. To make sure the airway is clear gently pinch the pup's tail or leg, if the airway is clear the pup will make a soft squeaking noise. Transfer the pup to the bedding on the heat pad, and repeat this procedure for the rest of the litter.
5. Keep the pups on the heating pad and cover them in bedding until they acquire a pink coloration and exhibit active movement (1–5 min usually).
6. At this point transfer the pups to the foster mother's cage, and mix the pups with the foster female's litter. Transfer the foster mother back to the cage, place cage back on the rack, and do not disturb for at least 24 h.

3.3 Tissue Collection (Fig. 4) and Staining (Fig. 5)

1. Sacrifice the mice at the desired time; usually different time points after labelling are useful to quantitatively assess the clonal dynamics.
2. Open the abdominal cavity of the mouse and dissect the intact intestine.
3. Flush the intestine with PBS several times until feces are washed out.
4. Open the intestine longitudinally. In order to analyze the tissue in two-dimensions, perform a Swiss roll. In order to analyze the tissue in three-dimensions, flatten the intestine in a Petri dish and put a piece of tissue soaked in 4% PFA on top (this will allow to fix it in the right orientation and completely flat).
5. Fix tissue in 4% PFA at 4 °C for a minimum of 4 h or O/N.

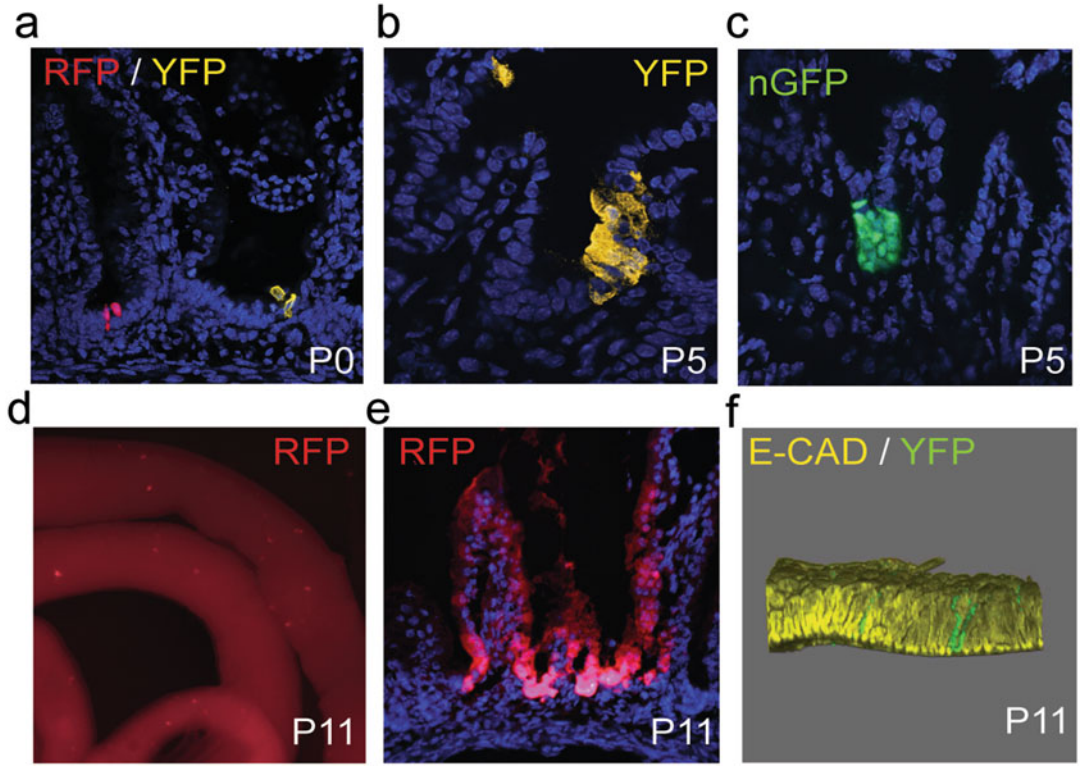

Fig. 5 Expected results. If the fetal-labeled cells are precursors of adult stem cells, those cells will generate clones that persist after birth. Fetal intestinal cells were labeled at E16.5 with Krt19-CreERT (ubiquitously expressed) and the presence of clones were analyzed at P0 (**a**), P5 (**b**, **c**), P11 (**d**, **e**), and adult (**f**). In (**a**, **b**, **c**, **e**), a two-dimensional immunostaining of the intestine is shown. In (**d**), a picture of the whole intestine at P11 is shown. In (**f**), a whole-mount immunostaining in the adult intestine is shown

6. Wash tissue and embed in OCT or paraffin, alternatively proceed to dehydration in ascending methanol solutions for whole mount immunostainings. Stain tissue using standard protocols for immunofluorescence or whole mount.
7. Immunofluorescence:
   (a) Section the OCT or paraffin blocks at 5 μm. For paraffin samples, dehydrate and perform antigen retrieval.
   (b) Block and permeabilize in 10% adult bovine serum, 0.3% Triton X-100 in PBS for at least 1 h at room temperature.
   (c) Incubated primary antibody O/N in blocking solution.
   (d) Wash and incubate secondary antibody 1–2 h at room temperature in 0.5% Bovine Serum Albumin. For immunofluorescence, diamidino-2-phenylindole dihydrochloride (DAPI; 1 μM) might be used to counterstain nuclei.
   (e) For the immunohistochemistry, develop secondary antibody using DAB and counterstain nuclei hematoxylin.

8. Whole mount immunostaining:
   (a) Rehydrate the samples in PBS. Block and permeabilize in 1% Bovine Serum Albumin and 0.5% Triton X-100 in PBS for 24 h.
   (b) Incubate primary antibody in 1% Bovine Serum Albumin, 0.5% Triton in PBS for 48 h.
   (c) Wash in 0.5% Triton in PBS overnight.
   (d) Incubate secondary antibody in 1% Bovine Serum Albumin, 0.5% Triton X-100 in PBS for 48 h and wash subsequently with 0.5% Triton X-100 in PBS. Diamidino-2-phenylindole dihydrochloride (DAPI; 1 μM; Sigma) might be used to counterstain nuclei.
   (e) Dehydrate samples in methanol and keep them at −20 °C.
   (f) Samples can be cleared using BABB and proceed to imaging.

3.4 Clonal Dynamics Quantification (Fig. 6)

Several parameters are crucial to quantitatively compare the contribution of specific fetal cells to the resulting adult mature tissues, which are described as follows:

% of cells: This parameter is the percentage of cells that express the fluorescent protein marker that is lineage traced.

Tissue expansion (*Tissue E*): it is the increase in number of cells or overall volume of the epithelium or other relevant cell type in a tissue from the time of the label initiation to the time of analysis. In lineage-tracing experiments during morphogenesis this parameter

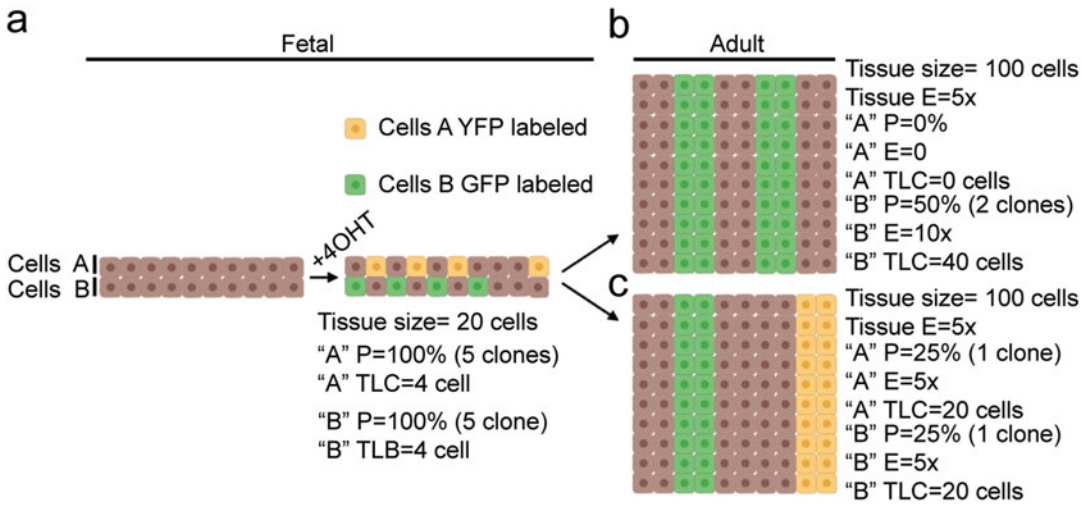

Fig. 6 Quantitative clonal analysis. Example of analysis of a putative lineage tracing experiment labeling cells in fetuses (**a**) and analyzing them in the adult homeostatic tissue (**b**), in which it is assumed that the tissue size is stable and the amount of proliferation is compensated by cell loss/apoptosis (*P* persistence, *TLC* total labeled cells, *E* expansion)

is particularly relevant as the tissues are rapidly growing during this time.

Total clonal expansion (*TCE*): total expansion of labeled cells measured by cell number or total volume during the course of the tracing experiment.

Persistence (*P*): the total number of clones detected at the different time points analyzed relative to the starting point. It provides information about the capacity of cells to survive/persist during time.

Using the measurements obtained above, it is now possible to perform modeling and infer which cells contribute to the development and expansion of the tissue.

In the theoretical example illustrated in Fig. 6, the percentage of "A" and "B" cells is 50% (10 out of 20) at the time of labeling. This parameter is useful to assess whether the expansion of a given population is enough to sustain fetal expansion. When labeling a precursor of a stem cell in a cell population, it is expected that the clones generated will expand proportionally to the tissue, if the labelled cells are the unique source capable of contributing to tissue growth in the tissue, it is expected that the resulting clones will overscale the overall tissue growth by a factor that can be calculated from the number of cells at the time of labeling and the number of labeled cells in clones at the end of the experiment compared to the overall tissue expansion. In the example depicted in Fig. 6a, a few cells in the population of "B" cells and the population of "A" cells are labeled. At the end point of the experiment, the tissue has expanded by a factor of 5. We can see that all cells labeled in the "A" population are lost (Persistence = 0), while for the "B" population we see a twofold reduction in the number of clones (Persistence = 50%). This indicates that cells in population "B" are able to contribute to tissue maintenance. In addition, we see that the number of labeled cells in population "B" has increased ten-fold overscaling the overall tissue expansion by a factor of 2. Taking into account that the "B" population of cells make up 50% of cells in the tissue at the initial labeling, this indicates that cells from this population are capable of producing all the necessary cells to contribute to the tissue expansion and so constitute the unique source of progenitor cells.

In contrast, in the example depicted in Fig. 6b, "B" cells again represent 50% of the tissue at the time of labeling; however, in this case the contribution to the adult mature epithelium is proportional to the tissue expansion (without overscaling), which means that "A" or "B" cells can only account for 50% of the tissue expansion respectively and therefore both populations are equal in their stem cell potential. Again, this is supported by the persistence data, showing that unlike in the previous example, cells from both "A" and "B" populations persist long term at similar rates and have the same probability to give rise to adult stem cells.

4 Notes

1. When using the Rosa26-Confetti reporter, it is important to keep in mind that there is a preference for the generation of YFP and RFP clones, with the GFP and CFP clones being less abundant. CFP clones are generally harder to identify as they are dimmer and seem to be preferentially lost over time, perhaps indicating a negative selection, therefore it is not recommended to analyze these clones for quantitative lineage tracing.
2. It is essential that the specific CreERT2 used in this analysis, as well as the reporter it is crossed to, is extensively validated. It is paramount to the analyses that there is no activation of label without exposure to tamoxifen (leakiness), and no nonspecific recombination as this will confound the interpretation of the lineage tracing.
3. When possible, use the same batch of 4OHT for all experiments including the initial titration experiments to establish the dosage needed for clonal labeling. This will prevent any discrepancies in labeling efficiency due to batch-to-batch variation in the drugs activity.
4. If the dosage of 4OHT required to initiate clonal labeling is 0.1 mg, females will only be capable of delivering the litter in roughly 50% of cases. If the dosage is above 0.1 mg, the delivery percentage will be drastically reduced. Performing a c-section and fostering is strongly advised.
5. When performing c-sections, it is advised to perform the procedure as late as possible on the date of estimated delivery. This greatly increases the chances of survival for the pups.
6. There is variation in the gestation time between strains of mice, and within strains it is not uncommon for a female to deliver a day before or after the estimated delivery date. This should be taken into account when setting up plugs for foster females.

Acknowledgments

We thank Dr. Kim B. Jensen and Jensen lab for his support, advice, and helpful discussion. We acknowledge Biorender.com as Figs. 1, 3, 4, and 6 were created with Biorender.com and exported under a paid subscription. This work was supported by MSCA-IF-2014-EF-656099. We thank CERCA Programme / Generalitat de Catalunya for institutional support.

References

1. Kretzschmar K, Watt FM (2012) Lineage tracing. Cell 148(1–2):33–45. https://doi.org/10.1016/j.cell.2012.01.002
2. Cheng H, Leblond CP (1974) Origin, differentiation and renewal of the four main epithelial cell types in the mouse small intestine. I. Columnar cell. Am J Anat 141 (4):461–479. https://doi.org/10.1002/aja.1001410403
3. Barker N, van Es JH, Kuipers J, Kujala P, van den Born M, Cozijnsen M, Haegebarth A, Korving J, Begthel H, Peters PJ, Clevers H (2007) Identification of stem cells in small intestine and colon by marker gene Lgr5. Nature 449(7165):1003–1007. https://doi.org/10.1038/nature06196
4. Lopez-Garcia C, Klein AM, Simons BD, Winton DJ (2010) Intestinal stem cell replacement follows a pattern of neutral drift. Science 330 (6005):822–825. https://doi.org/10.1126/science.1196236
5. Ritsma L, Ellenbroek SIJ, Zomer A, Snippert HJ, de Sauvage FJ, Simons BD, Clevers H, van Rheenen J (2014) Intestinal crypt homeostasis revealed at single-stem-cell level by in vivo live imaging. Nature 507(7492):362–365. https://doi.org/10.1038/nature12972
6. Snippert HJ, van der Flier LG, Sato T, van Es JH, van den Born M, Kroon-Veenboer C, Barker N, Klein AM, van Rheenen J, Simons BD, Clevers H (2010) Intestinal crypt homeostasis results from neutral competition between symmetrically dividing Lgr5 stem cells. Cell 143(1):134–144. https://doi.org/10.1016/j.cell.2010.09.016
7. Guiu J, Hannezo E, Yui S, Demharter S, Ulyanchenko S, Maimets M, Jorgensen A, Perlman S, Lundvall L, Mamsen LS, Larsen A, Olesen RH, Andersen CY, Thuesen LL, Hare KJ, Pers TH, Khodosevich K, Simons BD, Jensen KB (2019) Tracing the origin of adult intestinal stem cells. Nature 570 (7759):107–111. https://doi.org/10.1038/s41586-019-1212-5
8. Andersen MS, Hannezo E, Ulyanchenko S, Estrach S, Antoku Y, Pisano S, Boonekamp KE, Sendrup S, Maimets M, Pedersen MT, Johansen JV, Clement DL, Feral CC, Simons BD, Jensen KB (2019) Tracing the cellular dynamics of sebaceous gland development in normal and perturbed states. Nat Cell Biol 21 (8):924–932. https://doi.org/10.1038/s41556-019-0362-x
9. Clayton E, Doupe DP, Klein AM, Winton DJ, Simons BD, Jones PH (2007) A single type of progenitor cell maintains normal epidermis. Nature 446(7132):185–189. https://doi.org/10.1038/nature05574
10. Latil M, Nassar D, Beck B, Boumahdi S, Wang L, Brisebarre A, Dubois C, Nkusi E, Lenglez S, Checinska A, Vercauteren Drubbel A, Devos M, Declercq W, Yi R, Blanpain C (2017) Cell-type-specific chromatin states differentially prime squamous cell carcinoma tumor-initiating cells for epithelial to mesenchymal transition. Cell Stem Cell 20 (2):191–204. e195. https://doi.org/10.1016/j.stem.2016.10.018
11. Han S, Fink J, Jorg DJ, Lee E, Yum MK, Chatzeli L, Merker SR, Josserand M, Trendafilova T, Andersson-Rolf A, Dabrowska C, Kim H, Naumann R, Lee JH, Sasaki N, Mort RL, Basak O, Clevers H, Stange DE, Philpott A, Kim JK, Simons BD, Koo BK (2019) Defining the identity and dynamics of adult gastric isthmus stem cells. Cell Stem Cell 25(3):342–356. e347. https://doi.org/10.1016/j.stem.2019.07.008
12. Lilja AM, Rodilla V, Huyghe M, Hannezo E, Landragin C, Renaud O, Leroy O, Rulands S, Simons BD, Fre S (2018) Clonal analysis of Notch1-expressing cells reveals the existence of unipotent stem cells that retain long-term plasticity in the embryonic mammary gland. Nat Cell Biol 20(6):677–687. https://doi.org/10.1038/s41556-018-0108-1
13. Tetteh PW, Basak O, Farin HF, Wiebrands K, Kretzschmar K, Begthel H, van den Born M, Korving J, de Sauvage F, van Es JH, van Oudenaarden A, Clevers H (2016) Replacement of lost Lgr5-positive stem cells through plasticity of their enterocyte-lineage daughters. Cell Stem Cell 18(2):203–213. https://doi.org/10.1016/j.stem.2016.01.001

Part II

Programming Signaling Events and Patterns

Chapter 4

Reconstitution of Morphogen Signaling Gradients in Cultured Cells

Julia S. Kim, Michael Pineda, and Pulin Li

Abstract

Development of multicellular organisms depends on the proper establishment of signaling information in space and time. Secreted molecules called morphogens form concentration gradients in space and provide positional information to differentiating cells within the organism. Although the key molecular components of morphogen pathways have been identified, how the architectures and key parameters of morphogen pathways control the properties of signaling gradients, such as their size, speed, and robustness to perturbations, remains challenging to study in developing embryos. Reconstituting morphogen gradients in cell culture provides an alternative approach to address this question. Here we describe the methodology for reconstituting Sonic Hedgehog (SHH) signaling gradients in mouse fibroblast cells. The protocol includes the design of morphogen sending and receiving cell lines, the setup of radial and linear gradients, the quantitative time-lapse imaging, and the data analysis. Similar approaches could potentially be applied to other cell–cell communication pathways.

Key words Reconstitution, Morphogen gradients, Tissue patterning, Quantitative imaging

1 Introduction

Establishing precise patterns of gene expression in space and time is a key feature in the development of multicellular organisms. Such patterns are controlled in part by morphogen gradients. Morphogens are signaling molecules that emanate from a source and diffuse through space creating concentration gradients [1]. Morphogen ligand gradients then trigger graded signaling responses in the field of receiving cells, which differentiate into discrete cell types based on the quantitative signals. Features of the morphogen gradients, such as the amplitude, length scale, timescale, and robustness to environmental and genetic perturbations, provide the crucial information to allow for complex tissue patterning. These quantitative

Julia S. Kim and Michael Pineda authors contributed equally to this work.

Mo R. Ebrahimkhani and Joshua Hislop (eds.), *Programmed Morphogenesis: Methods and Protocols*, Methods in Molecular Biology, vol. 2258, https://doi.org/10.1007/978-1-0716-1174-6_4,

features are determined by the key biochemical parameters in the morphogen pathway, such as the diffusion and degradation rates of the morphogen, as well as the architecture of the pathway, such as the signal transduction logic and feedback loops [2–4]. Understanding how the extra- and intra-cellular contexts of cells regulate these features of morphogen gradients is important for revealing the principles underlying the spatial organization of tissues. Addressing this question requires direct visualization of the morphogen ligand or signaling gradients in space and time, as well as genetic manipulation of the extra- and intra-cellular environment in a spatiotemporally precise manner, both of which remain technically challenging in developing embryos.

Here, we describe a new approach for quantitatively studying morphogen signaling gradients outside an embryo, using the Hedgehog (HH) pathway as an example [5]. Within the HH pathway, mammalian Sonic Hedgehog (SHH) is the most studied ligand and a classic example of a long-range morphogen. During embryo development, SHH is responsible for patterning tissues such as the neural tube, limb, and the gut [6, 7]. In the absence of the ligand, the Patched (PTCH) receptor represses the intracellular signaling cascade [8, 9]. In this "signal-OFF" state, Glioma-associated Oncogene Homolog (GLI) transcription factors are processed from a full-length protein to a transcriptional repressor [10]. Binding of SHH to PTCH relieves the negative regulation and subsequently, GLI proteins are processed into transcription activator to induce gene expression. Using this pathway, we will demonstrate how morphogen signaling gradients can be reconstituted in a Petri dish, and how the spatiotemporal dynamics of the signaling gradient can be quantitatively analyzed.

1.1 General Method

In living organisms, specific cells secrete morphogens which other cells, or even themselves, respond to. Our synthetic system relies on the same principle; we created cell lines that either produce morphogen ligands ("sender cells") upon induction with a chemical or respond to the ligand ("receiver cells") by turning on a transcription-based fluorescent reporter. By coculturing senders and receivers in different spatial arrangements, signaling gradients of radial or linear geometries can be created in a Petri dish, to recapitulate some aspects of the patterning systems found in nature [11, 12].

1.2 Strengths

The reconstituted system provides several strengths. First, genetic manipulation in cultured cells can be achieved easily and precisely. For example, we were able to not only rewire the SHH pathway to eliminate or employ a key negative feedback loop but also tune the strength of the negative feedback, a key parameter that determines the gradient robustness to variations in the morphogen production rate [5]. Second, the effects of a gene on signal sending vs. receiving can be easily disentangled. This is because signaling senders and

receivers can be manipulated separately and patterned in defined spatial arrangements. Third, the signaling gradients can be quantitatively measured in space and time in the reconstituted system. Morphogens often exist at low concentrations, making it challenging to quantify the ligand directly. Instead, the reporter system is established on the capability of cells to detect low levels of morphogens and induce gene expression, which ultimately determines cell fates. Finally, this system allows for the isolation of morphogen signaling from other developmental processes that could occur simultaneously in a developing embryo and complicate the interpretation of mutant phenotypes. While simplified, this cell-based reconstituted system still relies on the complexities of cellular processes, such as protein degradation, ligand uptake, and extracellular matrix dynamics, and thus is suitable for studying morphogen-mediated intercellular communication.

1.3 Weaknesses

Reconstitution allows for precise control of the morphogen pathways and isolation of the gradient formation process, which is valuable and necessary in many cases. However, it does not recapitulate the entire spectrum of complexity that exists in a developing tissue. First, developing embryos may have quantitative or qualitative differences in the expression levels of morphogen pathway components, such as receptors or co-receptors. However, this is offset by the ease of genetic manipulation in cultured cells which enables the possibility of reconstituting the pathway complexity piece by piece and precisely tuning the level of gene expression. Second, cells within both the sender and receiver populations exhibit cell-to-cell variability, such as transgene expression levels, motility, and sensitivity to contact inhibition when the cultures reach confluency. Therefore, to deduce a biologically meaningful conclusion, it is crucial to take into account the cell-to-cell variability when designing cell lines and experiments, such as checking multiple clonal populations and averaging across multiple gradient measurements. Third, cell proliferation has been implicated to play a role in establishing gradients in certain contexts, but cell division is relatively limited under our current culture conditions [13]. Therefore, without further modification, it cannot be used to assess the contribution of cell division to patterning. However, we expect that incorporating these additional cellular behaviors into the reconstituted system is possible by choosing the right cell types and growth conditions.

2 Materials

2.1 Parental Cell Lines

Identifying a proper cell line that is able to recapitulate the signaling pathway is essential. For receivers, a cell type where all the necessary components of the pathway are or can be expressed, excluding the ligand, reduces the number of components that need to be

reconstituted. The chosen cell line also needs to have the structural or behavioral features relevant to the signaling pathway. In the case of the SHH pathway, the presence of cilia is needed for proper signaling activation in mammalian cells [14]. Additionally, while the sender and receiver cells do not necessarily have to be the same cell type, the cell lines must be able to be cocultured stably in the same condition. With these criteria, NIH3T3 cells, an immortalized mouse embryonic fibroblast cell line, were chosen for creating SHH sender and receiver cells [15]. NIH3T3 cells can respond to SHH without differentiation, and do not produce any HH ligands naturally. They are subject to contact inhibition and enter quiescence at high confluency, which promotes the formation of cilia and competency of activating the SHH signaling pathway [16]. We also observed that NIH3T3 cells can stay at 100% confluency for over 3 days without major cell death [5].

2.2 Cell Culture Materials

High-glucose DMEM (ThermoFisher 11960044) supplemented with the following at a final concentration of:

2.2.1 NIH3T3 Cell Culture Media

- 10% Cosmic Calf Serum (GE Healthcare SH30087.03).
- 1× Penicillin-Streptomycin-Glutamine (Gibco 10378016).
- 1 mM sodium pyruvate (Gibco 11360070).

2.2.2 NIH3T3 Imaging Media

FluoroBrite™ DMEM (ThermoFisher A1896701) supplemented with the following at a final concentration:

- 10% Cosmic Calf Serum (GE Healthcare SH30087.03).
- 1× Penicillin-Streptomycin-Glutamine (Gibco 10378016).
- 1 mM Sodium Pyruvate (Gibco 11360070).

2.2.3 General Tissue-Culture Supplies

- Trypsin-EDTA (0.05%) (Gibco 25300054).
- Dulbecco's phosphate-buffered saline (1× DPBS) without calcium or magnesium (Gibco 14190250).
- Corning® Costar® TC-Treated Multiple Well Plates.

2.2.4 Transfection Kit and Chemicals

- Lipofectamine LTX (ThermoFisher 15338030).
- Blasticidin S Solution (InvivoGen ant-bl-1).
- Hygromycin B Gold Solution (InvivoGen ant-hg-1).
- (Z)4-Hydroxytamoxifen (4-OHT) (Sigma H7904) dissolved in DMSO at a concentration of 500 μg/mL.

2.2.5 Fluorescent Dye Control

- Fluorescein Sodium Salt (Millipore Sigma F6377).

2.2.6 Materials for Establishing and Imaging Gradients

- Ibidi cell culture inserts (Ibidi 80209) for setting up linear gradients.
- 24-well imaging plates with glass-bottom or imaging-compatible polymer coverslip plates (e.g., Ibidi 82406).

2.3 Microscopy

This method is suited for quantitatively measuring the spatiotemporal dynamics of morphogen signaling gradients using time-lapse imaging. We recommend an inverted widefield microscope with multiple filter cubes for identifying senders and receivers separately and autofocus capability for long-term movies over 48 h. We use Nikon Ti2-E equipped with the Perfect Focus System and the OKO Labs environmental enclosure to keep cells at 37 °C with 5% CO_2 and proper humidity. 10× or 20× objectives provide sufficient resolution.

3 Methods

3.1 Morphogen-Producing and -Detecting Cell Lines

To create the SHH sender cells, an inducible gene expression system of two plasmids under the control of 4-OHT was used (Fig. 1a). One plasmid constitutively expresses a GAL4 transcription factor fused to a mutant estrogen receptor ERT2, and a blue fluorescent protein mTurquoise2 fused to histone H2B [17, 18]. The two coding sequences are separated by a viral 2A self-cleaving peptide (T2A) to produce separate protein products under the control of a single *PGK* (3-phosphoglycerate kinase) promoter [19]. In the absence of 4-OHT, the ERT2-GAL4 fusion protein is found in the cytoplasm where it is unable to induce gene expression. Once 4-OHT is introduced, GAL4 moves into the nucleus where it binds to an upstream activating sequence (*UAS*) that controls the expression of *Shh*. This enables a rapid induction of gene expression that is sensitive to dose and temporal control. In addition, the nuclear localization of mTurquoise2 allows for easy identification of sender cells.

Receiver cells lines are created through stable integration of a fluorescent reporter that is controlled by GLI proteins, which are transcription factors downstream of the SHH signaling pathway. The reporter was constructed based on the reporter designed by Balaskas et al. [20, 21]. Specifically, eight tandem copies of GLI-binding sites (GBS) taken from the enhancer of *FoxA2* gene, a natural target of SHH in the neural tube, was placed upstream of a minimal CMV promoter, and together they drive the expression of a yellow fluorescent protein mCitrine that is fused to H2B (H2B-mCitrine) (Fig. 1a) [20–22]. Increasing concentration of recombinant SHH induces increasing mean intensity of mCitrine within the receiver population [5].

Both sender and receiver cell lines were created using a piggyBac transposon system (System Biosciences) where plasmids

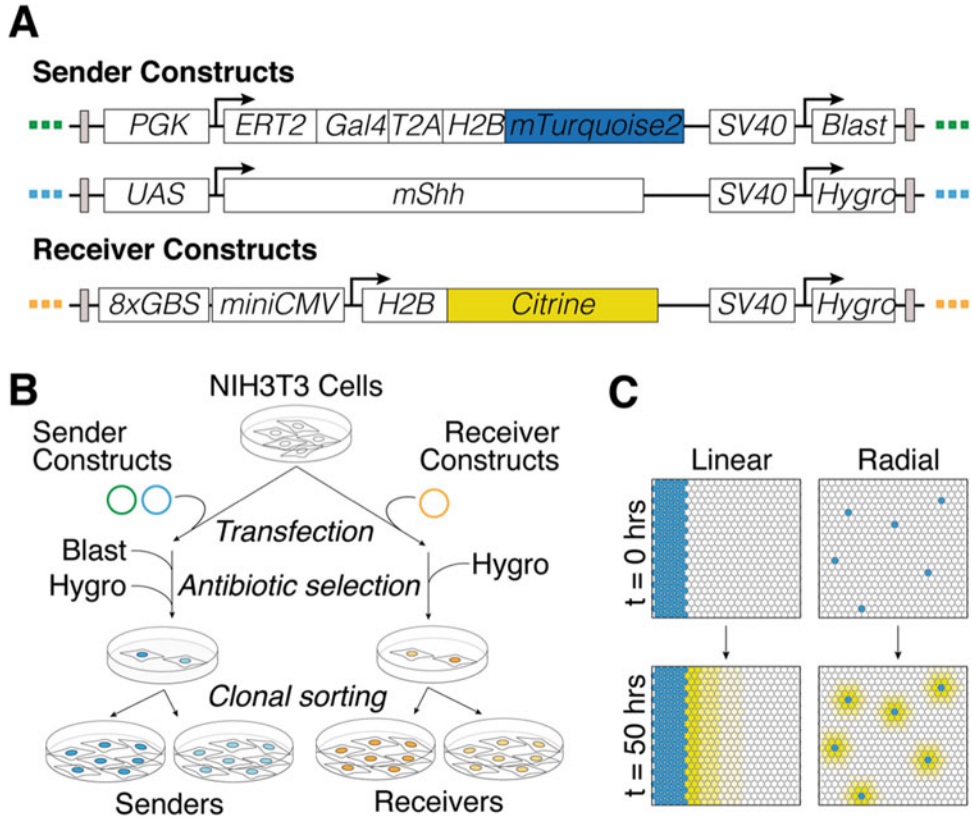

Fig. 1 Engineering stable clonal sender and receiver cell lines. (**a**) The constructs used for creating senders and receivers based on a piggyBac transposase system. (**b**) Procedures for transfecting constructs and selecting for clonal populations. Constructs are transfected into wild-type NIH3T3 cells together with a plasmid overexpressing piggyBac transposase. Cells stably integrated with the desired plasmids are selected with antibiotics. Clonal populations with desired features (e.g., high expression level of SHH) were further sorted. (**c**) Coculture of senders and receivers is used for producing radial or linear gradients that can be quantitatively imaged and analyzed

carrying genes of interest are co-transfected with a plasmid expressing piggyBac transposase (Fig. 1b). The piggyBac transposase recognizes inverted terminal repeats (ITRs) that flank the genes of interest, cut the ITRs and insert the genes into the genome at TTAA DNA sequences [23]. For reproducibility, cells with plasmids stably integrated were selected using antibiotics, and clonal cell lines were isolated and used throughout the study. To achieve stable integration, each plasmid carries a unique antibiotic resistance gene that can be selected for by treating the cells with the corresponding antibiotic 48 h after transfection. Because of the high efficiency of integration and the low false-positive rate of antibiotic selection in the piggyBac system, at least two constructs carrying different antibiotic resistance genes can be integrated into the genome of the same cell simultaneously, greatly shortening the

time required for cell line construction. In such cases, the cells are first treated with the "harsher" antibiotic (that cells are more sensitive to) for 2 days to eliminate the untransfected cells as quickly as possible (*see* **Note 1**), before being switched to the secondary antibiotic selection in fresh media for another 2 days, or until the negative control cells have been fully selected against. To select clonal cell population, either limiting dilution or fluorescence-activated cell sorting (FACS) can be used to ensure only one cell populates a single well in a 96-well plate. After about 2 weeks, healthy clones with desired properties can be selected through qPCR, immunofluorescence staining, flow cytometry, imaging, or whichever method best suited for the underlying biology (*see* **Note 2**).

3.2 Radial Gradients

This experimental setup is both versatile and simple to execute (Fig. 2a).

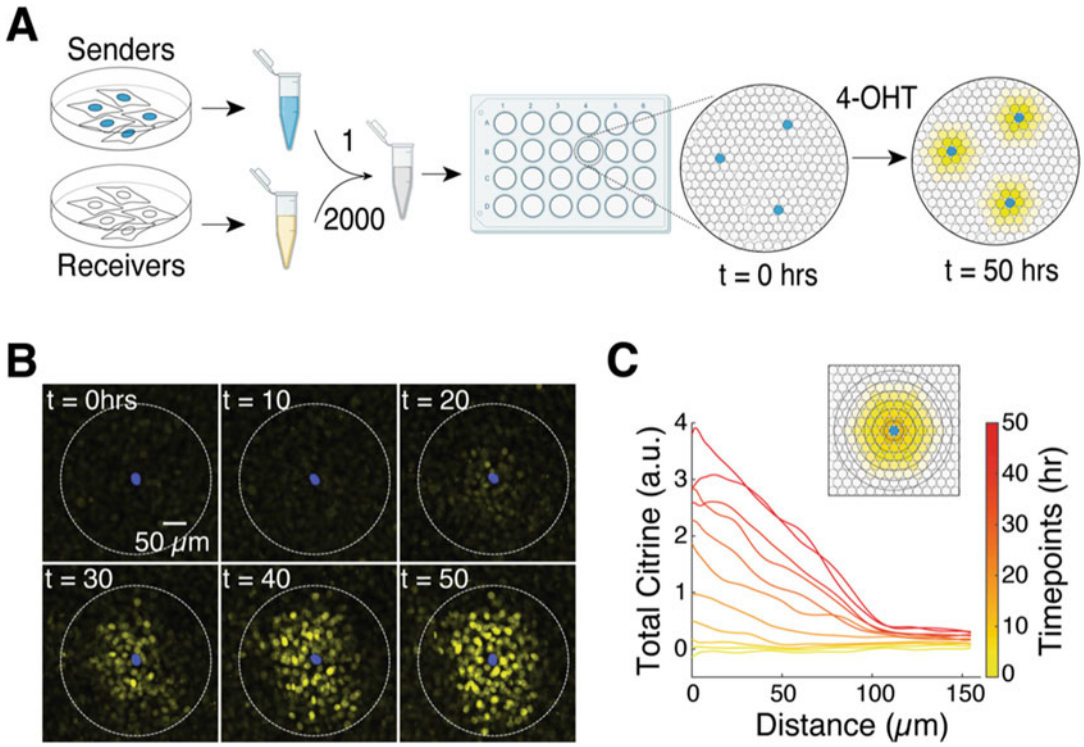

Fig. 2 Reconstituting and quantifying radial gradients. (**a**) Experimental setup. Sender and receiver cell lines are mixed at a 1:2000 ratio to establish the geometry in which a single sender is surrounded by receivers, and multiple gradients do not overlap. After induction of SHH expression with 4-OHT, signaling response in receiver cells can be measured based on mCitrine expression. (**b**) Representative time-lapse images of a radial gradient. Gradients begin to form at ~12 h and can reach distances of ~100 μm. (**c**) Quantification of radial gradients. Concentric circles around the sender are used to create bands of constant width, within which the average mCitrine fluorescence intensity is measured (*inset*). The spatiotemporal dynamics of signaling gradient formation is plotted as a function of distance from the sender (n = 9)

1. Grow sender and receiver cells to confluency in a 6-well plate (*see* **Note 3**).
2. Wash the wells with 500 μL 1× DPBS.
3. Add 200 μL Trypsin-EDTA (0.05%) to each well and incubate the cells for 10 min or until the cells detach from the plate.
4. Add 1 mL culture media to each well to neutralize the Trypsin-EDTA and gently pipet to dissociate the cells into single-cell suspension (*see* **Note 4**).
5. Spin down both sender and receiver populations at 500 × *g* for 5 min to pellet the cells and remove the Trypsin-EDTA.
6. Aspirate the supernatant and resuspend the cells in 1 mL culture media by gentle pipetting.
7. Count the sender and receiver populations (*see* **Note 5**).
8. Thoroughly mix senders and receivers at a ratio of 1:2000.
9. Dispense 500,000 cells into each well on a 24-well imaging plate with minimal disturbance as to keep the cells at an even density across the well. The cell number should ensure 100% confluency to minimize cell division after adherance (*see* **Note 6**).
10. Once the cells have attached (4–5 h to overnight), check the well to ensure single, isolated senders in a field of receivers.
11. Dilute 4-OHT to 100 ng/mL in fresh imaging media (*see* **Note 7**).
12. Aspirate the regular culture media and add 1 mL of the imaging media containing 4-OHT to induce SHH production in the senders.
13. Set up time-lapse imaging immediately or keep the plate in the incubator and take images at desired time points (e.g., ~50 h post 4-OHT addition).

3.3 Linear Gradients

To create gradients in which senders and receivers share a linear boundary, removable adhesive culture inserts are used to confine senders in a rectangular region (Fig. 3a).

1. Prepare sender and receiver cell populations following **steps 1–7** in the above radial gradient protocol.
2. Place the Ibidi insert in a 24-well plate well using forceps so that one of the chambers is centered in the middle of the well (the other chamber will not be used).
3. Rinse the centered chamber with 100 μL culture media to prime all surfaces for sender cell placement.
4. Seed 100,000 sender cells suspended in 100 μL culture media into the centered chamber and keep the plate in an incubator for 4–5 h.

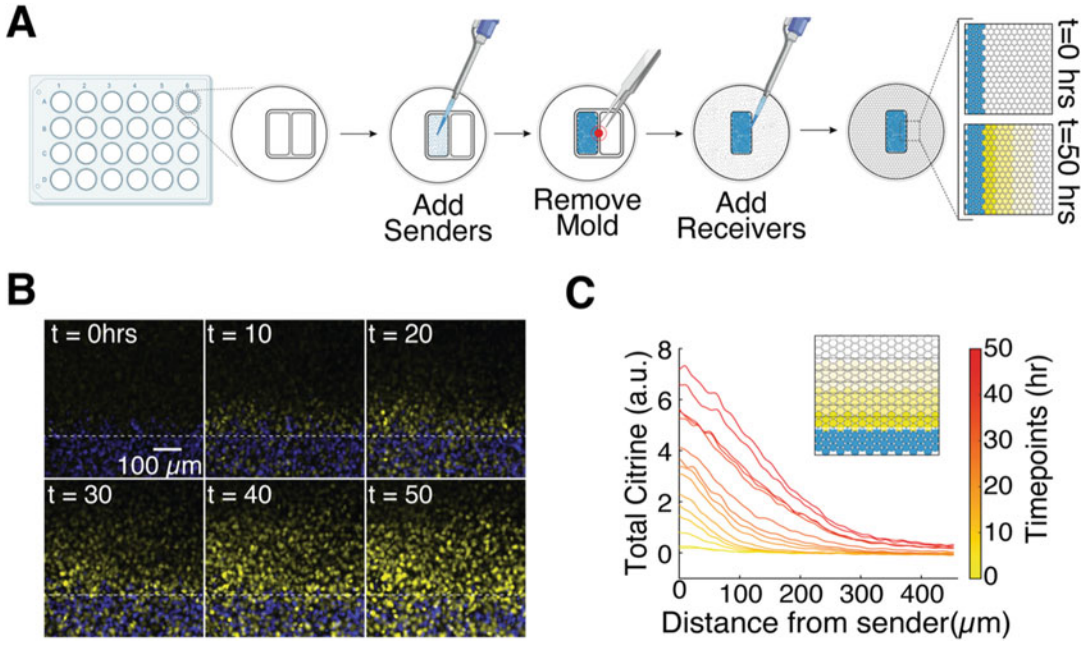

Fig. 3 Reconstituting and quantifying linear gradients. (**a**) Experimental setup. A culture insert is used to plate sender cells within a rectangular region, and receiver cells are then used to cover the remainder of the plate. Gradients can be analyzed starting from the sender–receiver boundary. (**b**) Representative time-lapse images of a linear gradient. Initial mCitrine expression begins at ~10 h and after 50 h the gradient extends further than 200 μm. White dashed line indicates the sender–receiver boundary. (**c**) Quantification of linear gradients. Slices of the gradient parallel to the sender–receiver boundary are analyzed, and the average mCitrine intensity within each slice across space and time is plotted (mean of seven gradients)

5. Once the cells have settled, rinse the Ibidi chamber with 100 μL culture media three times to remove unattached cells and prevent the formation of satellite gradients.
6. Remove the Ibidi insert carefully by pulling it perpendicular from the surface of the well to minimize boundary disturbance (*see* **Note 3**).
7. Wash the entire well with 500 μL culture media three times to get rid of any loosely attached cells.
8. Dispense 500,000 receiver cells into the well.
9. Incubate the plate overnight to give receiver cells sufficient time to form confluent layers and enter quiescence (*see* **Note 5**).
10. The following morning, replace the culture media with 4-OHT diluted to 100 ng/mL in fresh imaging media (*see* **Note 8**).
11. Setup time-lapse imaging immediately or keep the plate in the incubator and take images at desired time points (e.g., ~50 h post 4-OHT addition).

3.4 Time-lapse Imaging

To quantify the spatiotemporal dynamics of the signaling gradients, the plates were imaged on a Nikon Ti2 fluorescence microscope. The microscope is equipped with a fully enclosed environmental chamber that is kept at 37 °C, 5% CO_2, and the appropriate humidity. Images were collected using a 10× objective and filter cubes for mTurquoise2 (Ex436/Em480) and mCitrine (Ex500/Em535) in 30 min intervals over a 50 h period (Figs. 2b and 3b). SHH signaling gradients start to appear at ~12 h in the radial geometry and at ~10 h in the linear geometry (Figs. 2c and 3c).

3.5 Imaging Controls

Several factors, such as media autofluorescence and non-uniform illumination within the field of view, can confound the quantification of the true signal from the SHH reporter. Therefore, two types of controls were measured side by side with the gradient samples.

1. To measure the autofluorescence of the media, add 1 mL of fresh imaging media to an empty well in the same 24-well imaging plate.
2. To quantify the non-uniform illumination within the field of view, add 1 mL of fresh imaging media containing fluorescein at a final concentration of 10 nM to an empty well in the same 24-well imaging plate.
3. Image five random positions in each of the control wells using the same microscope settings as those used for the experiment and use the mean of the five images for the data analysis.

3.6 Image Analysis

We have developed customized MATLAB codes for analyzing both radial and linear gradients. In both cases, the raw data is preprocessed in two steps; first by subtracting the media-only background signal and second by dividing the mCitrine signals by the fluorescein control to account for nonuniform illumination. These preprocessed images were then analyzed as radial or linear gradients.

For radial gradients, single individual senders are segmented and tracked based on their nuclear-localized mTurquoise2, using a program developed by Bintu L [24]. From these clusters of identified points, the XY positions of the senders are extracted, which represents a single pixel in the center of the sender nucleus. The list of sender positions over time are used to center the analysis of radial gradients and account for cell migration. Radial gradients are analyzed by building concentric circles around the sender cell position at each time point (Fig. 2c, *inset*). The averaged signal intensity within each ring corresponds to the activation level of the signaling reporter. The actual gradient starts outside the sender cell boundary and is identified as the peak in the mCitrine signal. The peaks then can be used to align and compare the individual quantified gradients to each other. The 8 × GBS-CMV promoter drives a basal level of mCitrine expression, which is independent from signaling response. The level of the basal expression depends on the copy

number of the reporter integrated into the genome and their genomic locations, and thus the basal expression level often correlates with the maximum expression level induced by SHH. Therefore, we calculate the signaling activation based on the fold change in mCitrine intensity over the basal level of mCitrine intensity. Single gradients from the same experimental sample can be averaged together and plotted as a function of time and distance from the sender (Fig. 2c). An alternative method for image analysis is the Fiji Radial Profile plugin where a circle can be drawn encompassing the gradient and centered on the single sender cell. The intensity of the pixels is associated with the degree of receiver cell activation. However, the Fiji Radial Profile plugin only works for static images.

The analysis of the linear gradients depends on quantifying the receiver response in intervals from a defined linear boundary. To automatically detect the linear boundary between senders and receivers, all pixels in the mTurquoise2 channel are first binarized based on the background threshold, with pixels above the threshold identified as being associated with senders and assigned "1," and pixels below the threshold as "0." By adding up all the pixels within each column that runs parallel to the orientation of the sender–receiver boundary, a sender density profile can be calculated as a function of space, with $x = 1$ having the lowest sender density, and $x = 1024$ having the highest sender density (each image has 1024×1024 pixels) (*see* **Note 9**). The boundary can then be defined as where the sender density profile drops below 10% of its maximum value. The mCitrine intensity of pixels within each column parallel to the defined sender–receiver boundary was then averaged to quantify the gradient as a function of distance (Fig. 3c, *inset*). Similar to the radial gradients, the averaged mCitrine intensities were normalized to the basal level of expression. By applying this method to all timepoints, the spatiotemporal dynamics of signaling gradients can be reconstructed. These values again can be averaged across multiple gradients or displayed separately in respect to time and distance (Fig. 3c).

All the image analysis codes are archived and publicly available at https://doi.org/10.5281/zenodo.3772886.

4 Notes

1. Hygromycin is a stronger antibiotic than blastomycin for NIH3T3 cells, therefore, in making the sender cell line, the hygromycin selection will be done first to increase selection efficiency.
2. Flow cytometry or qPCR can also be used to sort clones based on their expression of the target protein. This step can ensure

comparable results between constructs, when quantifying gradients.

3. When many gradients are planned, we recommend growing cells using 10 cm dishes or 6-well plates. We also recommend checking cell lines for their respective markers (e.g., receivers are mCitrine positive and senders are mTurquoise2 positive) during selection, culturing, and after gradient plating to check the distribution, activity, and health of the cells. General cell culture health can be checked on a fluorescent microscope with long working-distance objectives compatible with the Corning® Costar® TC-Treated Multiple Well Plates.
4. Achieving single cell suspension is important to ensure accurate cell counting and to prevent formation of cell aggregates.
5. Cells should be accurately counted to ensure they are plated to confluency. Underplating cells results in sender cell division, extensive cell migration, and receiver cells without cilia. Conversely, over-plating results in cell death and cells peeling off from the culture plate.
6. For radial gradients, while the cells have to be plated at confluency, the proportion of senders to receiver cells can be adjusted to increase or decrease the distance between gradients. This adjustment is important in preventing gradients from overlapping or interacting with each other which would interfere with gradient quantification. Additionally, increasing the number of radial gradients can be achieved by using imaging plates with a larger well size.
7. 4-OHT sensitivity may vary between clones due to different expression levels of ERT2-Gal4. Thus, while 100 ng/mL 4-OHT was optimal for the sender cell line used in this experiment, 4-OHT concentrations should be carefully titrated for new cell lines.
8. In the linear gradients, where a high fraction of cells in the well are senders (~17% in a 24-well), the ligand released into the media can accumulate to a high concentration and activate all the receiver cells over time. To circumvent this issue, it is recommended to double the media volume in the well (e.g., 1 mL for a 24-well plate) and replace the media every 12 h. Additionally, the sender cells can be "diluted" with wild-type cells that do not produce SHH to reduce the amount of ligand being produced.
9. Due to the geometry of the coculture, sender cells can be located on any of the four edges on the image. The MATLAB code can automatically detect the location of the sender cells, and flip or rotate the images accordingly so that the sender cells will locate on the left edge in all images.

Acknowledgments

We thank the Michael Elowitz lab where the method was initially developed. We also thank Yaron Antebi for providing the single-cell segmentation/tracking program. This work was funded by NIH Pathway to Independence Career Award 1R00HD087532 and Mathers Foundation MF-1905-00336.

References

1. Rogers KW, Schier AF (2011) Morphogen gradients: from generation to interpretation. Annu Rev Cell Dev Biol 27:377–407
2. Wartlick O, Kicheva A, González-Gaitán M (2009) Morphogen gradient formation. Cold Spring Harb Perspect Biol 1:a001255
3. Perrimon N, McMahon AP (1999) Negative feedback mechanisms and their roles during pattern formation. Cell 97:13–16
4. Freeman M (2000) Feedback control of intercellular signalling in development. Nature 408:313–319
5. Li P, Markson JS, Wang S, Chen S, Vachharajani V, Elowitz MB (2018) Morphogen gradient reconstitution reveals Hedgehog pathway design principles. Science 360:543–548
6. Patten I, Placzek M (2000) The role of sonic hedgehog in neural tube patterning. Cell Mol Life Sci 57:1695–1708
7. Nüsslein-Volhard C, Wieschaus E (1980) Mutations affecting segment number and polarity in Drosophila. Nature 287:795–801
8. Nakano Y, Guerrero I, Hidalgo A, Taylor A, Whittle JR, Ingham PW (1989) A protein with several possible membrane-spanning domains encoded by the Drosophila segment polarity gene patched. Nature 341:508–513
9. Hooper JE, Scott MP (1989) The Drosophila patched gene encodes a putative membrane protein required for segmental patterning. Cell 59:751–765
10. Hui C-C, Angers S (2011) Gli proteins in development and disease. Annu Rev Cell Dev Biol 27:513–537
11. Chamberlain CE, Jeong J, Guo C, Allen BL, McMahon AP (2008) Notochord-derived Shh concentrates in close association with the apically positioned basal body in neural target cells and forms a dynamic gradient during neural patterning. Development 135:1097–1106
12. Dessaud E, Yang LL, Hill K, Cox B, Ulloa F, Ribeiro A, Mynett A, Novitch BG, Briscoe J (2007) Interpretation of the sonic hedgehog morphogen gradient by a temporal adaptation mechanism. Nature 450:717–720
13. Averbukh I, Ben-Zvi D, Mishra S, Barkai N (2014) Scaling morphogen gradients during tissue growth by a cell division rule. Development 141:2150–2156
14. Spassky N, Han Y-G, Aguilar A, Strehl L, Besse L, Laclef C, Ros MR, Garcia-Verdugo JM, Alvarez-Buylla A (2008) Primary cilia are required for cerebellar development and Shh-dependent expansion of progenitor pool. Dev Biol 317:246–259
15. Goodrich LV, Johnson RL, Milenkovic L, McMahon JA, Scott MP (1996) Conservation of the hedgehog/patched signaling pathway from flies to mice: induction of a mouse patched gene by Hedgehog. Genes Dev 10:301–312
16. Rohatgi R, Milenkovic L, Scott MP (2007) Patched1 regulates hedgehog signaling at the primary cilium. Science 317:372–376
17. Goedhart J, von Stetten D, Noirclerc-Savoye-M, Lelimousin M, Joosen L, Hink MA, van Weeren L, Gadella TWJ Jr, Royant A (2012) Structure-guided evolution of cyan fluorescent proteins towards a quantum yield of 93%. Nat Commun 3:751
18. Gerety SS, Breau MA, Sasai N, Xu Q, Briscoe J, Wilkinson DG (2013) An inducible transgene expression system for zebrafish and chick. Development 140:2235–2243
19. Szymczak AL, Workman CJ, Wang Y, Vignali KM, Dilioglou S, Vanin EF, Vignali DAA (2004) Correction of multi-gene deficiency in vivo using a single'self-cleaving'2A peptide—based retroviral vector. Nat Biotechnol 22:589–594
20. Balaskas N, Ribeiro A, Panovska J, Dessaud E, Sasai N, Page KM, Briscoe J, Ribes V (2012) Gene regulatory logic for reading the Sonic Hedgehog signaling gradient in the vertebrate neural tube. Cell 148:273–284
21. Li C, Hirsch M, Carter P, Asokan A, Zhou X, Wu Z, Samulski RJ (2009) A small regulatory

element from chromosome 19 enhances liver-specific gene expression. Gene Ther 16:43–51

22. Griesbeck O, Baird GS, Campbell RE, Zacharias DA, Tsien RY (2001) Reducing the environmental sensitivity of yellow fluorescent protein. Mechanism and applications. J Biol Chem 276:29188–29194
23. Ding S, Wu X, Li G, Han M, Zhuang Y, Xu T (2005) Efficient transposition of the piggyBac (PB) transposon in mammalian cells and mice. Cell 122:473–483
24. Bintu L, Yong J, Antebi YE, McCue K, Kazuki Y, Uno N, Oshimura M, Elowitz MB (2016) Dynamics of epigenetic regulation at the single-cell level. Science 351:720–724

Chapter 5

Engineering Shape-Controlled Microtissues on Compliant Hydrogels with Tunable Rigidity and Extracellular Matrix Ligands

Megan L. Rexius-Hall, Nethika R. Ariyasinghe, and Megan L. McCain

Abstract

In vitro models that recapitulate key aspects of native tissue architecture and the physical microenvironment are emerging systems for modeling development and disease. For example, the myocardium consists of layers of aligned and coupled cardiac myocytes that are interspersed with supporting cells and embedded in a compliant extracellular matrix (ECM). These cell–cell and cell–matrix interactions are known to be important regulators of tissue physiology and pathophysiology. In this protocol, we describe a method for mimicking the alignment, cell–cell interactions, and rigidity of the myocardium by engineering an array of square, aligned cardiac microtissues on polyacrylamide hydrogels. This entails three key methods: (1) fabricating elastomer stamps with a microtissue pattern; (2) preparing polyacrylamide hydrogel culture substrates with tunable elastic moduli; and (3) transferring ECM proteins onto the surface of the hydrogels using microcontact printing. These hydrogels can then be seeded with cardiac myocytes or mixtures of cardiac myocytes and fibroblasts to adjust cell–cell interactions. Overall, this approach is advantageous because shape-controlled microtissues encompass both cell–cell and cell–matrix adhesions in a form factor that is relatively reproducible and scalable. Furthermore, polyacrylamide hydrogels are compatible with the traction force microscopy assay for quantifying contractility, a critical function of the myocardium. Although cardiac microtissues are the example presented in this protocol, the techniques are relatively versatile and could have many applications in modeling other tissue systems.

Key words Cardiac myocytes, Microcontact printing, Photolithography, Polyacrylamide hydrogels

1 Introduction

Native myocardium consists of layers of aligned, rhythmically contracting cardiac myocytes that are mechanically and electrically coupled to each other and interspersed with supporting cells, such as fibroblasts, endothelial cells, and neurons. These cells are embedded in a compliant mesh of extracellular matrix (ECM) macromolecules that are a rich source of mechanical and biochemical signals [1]. Each of these cellular and extracellular features can

Mo R. Ebrahimkhani and Joshua Hislop (eds.), *Programmed Morphogenesis: Methods and Protocols*, Methods in Molecular Biology, vol. 2258, https://doi.org/10.1007/978-1-0716-1174-6_5,

impact the contractile performance of the myocardium and are often altered in many forms of heart disease. For example, after a myocardial infarction, fibrotic tissue forms at the site of injury, which causes local increases in tissue rigidity [2], disruptions in tissue alignment [3], and increased presence of myofibroblasts [4]. However, these tissue-level features are challenging, if not impossible, to precisely and independently control with in vivo or conventional in vitro models, limiting our understanding of disease progression and obstructing the development of effective therapies to mitigate ongoing pathological remodeling.

Recently, advances in biomaterials and microfabrication techniques have been leveraged to manufacture more sophisticated in vitro culture substrates that can provide tunable and independent control over tissue architecture and physical features in the cellular microenvironment [5]. For example, microcontact printing is a lithographic technique for transferring a pattern of proteins, peptides, or other bioactive molecules onto the surface of a substrate to prescribe geometric regions for cell adhesion [6]. This technique has been extensively applied to control the shape and distribution of cardiac myocytes in vitro, ranging from single cells [7–10] to confluent mm-scale tissues [11–15]. In our previous publication, we used microcontact printing to engineer shape-controlled cardiac microtissues, each of which comprises approximately 50 cells [16]. These engineered microtissues are advantageous for measuring tissue-level phenomena because they encompass both cell–ECM and cell–cell interactions in a relatively reproducible and scalable form factor.

Culture surfaces with tunable rigidity are also valuable tools for modeling changes in the mechanical properties of tissues due to fibrosis, which is especially relevant for the myocardium because fibrotic remodeling is prevalent in many forms of heart disease [17, 18]. Synthetic hydrogels are advantageous for modeling ECM remodeling because their mechanical properties are easily tunable by adjusting the concentrations of polymer and cross-linker [19]. Another advantage of synthetic hydrogels is that their surfaces are biologically inert and thus can be controllably functionalized with ECM proteins. These ECM proteins can be applied as a uniform layer [20, 21] or a user-defined pattern by leveraging microcontact printing [22–25]. For example, we previously used microcontact-printed polyacrylamide hydrogels to determine how ECM rigidity affects the phenotypes of shape-controlled single cardiac myocytes [9], cardiac myocyte pairs [26], and cardiac microtissues [16].

In this chapter, we describe how to engineer shape-controlled cardiac microtissues on polyacrylamide hydrogels with tunable rigidity and ECM ligand, similar to those described in our previous publication [16]. First, we describe how to fabricate stamps from polydimethylsiloxane (PDMS) with features that are an array of

squares, each of which is a series of lines. Next, we describe how to fabricate polyacrylamide hydrogels with tunable rigidity and use the PDMS stamps to microcontact print laminin or fibronectin onto their surface. These hydrogels can then be seeded with a single cell type, such as cardiac myocytes, or a mixture of cell types, such as cardiac myocytes and fibroblasts, which will self-assemble into shape-controlled microtissues dictated by the ECM pattern. Collectively, this approach offers multiple levels of modularity, as the elastic modulus of the hydrogel, type of ECM ligand, macro- and microscale geometry of the microtissues, and cell–cell interactions are each independently tunable. We have also shown in our previous publication that these substrates are compatible with traction force microscopy to quantify tissue-level contractility [16], which is a key functional readout. Although the cells used to develop this protocol were neonatal rat ventricular myocytes, these approaches are likely also compatible with human-induced pluripotent stem cell-derived cardiac myocytes [7, 23], which would be a useful model for determining how patient-specific genotypes affect cardiac myocyte phenotypes on the tissue level. Due to their versatility, these techniques can likely also be extended to a variety of other cell types as a relatively efficient and scalable approach for engineering tunable microtissues with many applications in disease modeling and drug testing.

2 Materials

2.1 Fabricating Silicon Wafer Masters

1. Computer-aided design software (e.g., AutoCAD).
2. Silicon wafer (3″ diameter recommended).
3. Photoresist (Microchem SU-8 2005 Negative Photoresist recommended).
4. Spin coater.
5. Aluminum foil.
6. Hot plate.
7. Wafer tweezers.
8. Mask aligner with UV light source (e.g., Karl Suss MJB3 Mask Aligner).
9. SU-8 developer (MicroChem) or propylene glycol monomethyl ether acetate (PGMEA).
10. Glass laboratory dishes (e.g., PYREX 100 mm × 50 mm).
11. Isopropanol.
12. Trichloro (1*H*, 1*H*, 2*H*, 2*H*-perfluorooctyl) silane.
13. Vacuum desiccator.

2.2 Fabricating PDMS Stamps

1. Dow Corning Sylgard 184 Silicone Elastomer Kit.
2. 150 mm Disposable Petri dishes.
3. Planetary centrifugal mixer with 100 mL disposable cups (Thinky).
4. Vacuum desiccator.
5. Benchtop oven.
6. Razor blade or blade knife.

2.3 Activating Coverslips

1. Round 25 mm diameter glass coverslips.
2. Coverslip rack and glass staining dish (Electron Microscopy Sciences large coverglass staining rack and staining dishes recommended).
3. Magnetic stir bar and stir plate.
4. Ultrapure water.
5. 1 M Sodium hydroxide solution.
6. 95% Ethanol.
7. (3-Aminopropyl) trimethoxysilane (APTMS).
8. 70% Glutaraldehyde solution.
9. Glass Pasteur pipette with rubber bulb.
10. Tweezers.
11. 150 mm Disposable Petri dishes.
12. Aluminum foil.
13. Benchtop incubator at 37 °C.
14. Parafilm.

2.4 Fabricating Polyacrylamide Hydrogels

1. Activated round 25 mm diameter glass coverslips.
2. Round 18 mm diameter glass coverslips.
3. 40% Acrylamide solution (Bio-Rad).
4. 2% *N*,*N*′-methylenebisacrylamide (Bis) (Sigma-Aldrich).
5. 10% Ammonium persulfate (APS): Prepare 10 μL aliquots and store at −20 °C.
6. *N*,*N*,*N*′,*N*′-Tetramethylethane-1,2-diamine (TEMED) (Thermo Fisher Scientific).
7. 10× Phosphate-buffered saline (PBS).
8. 1× Phosphate-buffered saline (PBS).
9. 2 mL Eppendorf tubes.
10. Streptavidin acrylamide (Invitrogen): Prepare 10 μL aliquots and store at −20 °C.
11. 6-Well cell culture plates.

2.5 Biotinylating Fibronectin or Laminin

1. Sodium carbonate.
2. Glass beakers, 500 mL and 1 L.
3. Ultrapure water.
4. pH meter.
5. 1 mg/mL Human fibronectin (BD Biosciences) and/or 1 mg/mL laminin (Sigma-Aldrich).
6. Sulfo-NHS-LC-Biotin (Thermo Fisher Scientific).
7. Platform rocker.
8. Dialysis Cartridge (Slide-A-Lyzer 10 K molecular weight cut-off, Thermo Fisher Scientific).

2.6 Microcontact Printing Polyacrylamide Hydrogels

1. 95% Ethanol.
2. 500 mL Glass beaker.
3. Sonicator.
4. Fabricated PDMS stamps.
5. Forceps.
6. Compressed air.
7. 1× Phosphate-buffered Saline (PBS).
8. Biotinylated fibronectin.
9. Pipette tips (1000 μL).
10. Delicate task wipes (e.g., Kimwipes).
11. Disposable plastic Petri dishes, 150 mm diameter.
12. Benchtop incubator at 37 °C.

3 Methods

An overview of the entire fabrication process described in this protocol is shown in Fig. 1.

3.1 Fabricating Silicon Wafer Masters

1. Use computer-aided design software to design a microtissue pattern. To engineer an aligned cardiac microtissue, a 200 μm × 200 μm square with an array of 15 μm-wide lines separated by 2 μm-wide gaps is recommended. Duplicate the microtissue pattern with appropriate spacing (such as 200 μm) to fill an area approximately 2.5 cm × 2.5 cm.
2. Duplicate this 2.5 cm × 2.5 cm square to fill the surface area of your wafer (for example, a 3″ diameter silicon wafer can fit four 2.5 cm × 2.5 cm arrays). Each of these 2.5 cm × 2.5 cm blocks will become one PDMS stamp.
3. Transfer your complete pattern to a chrome on glass photomask using e-beam lithography (*see* **Note 1**). This process can

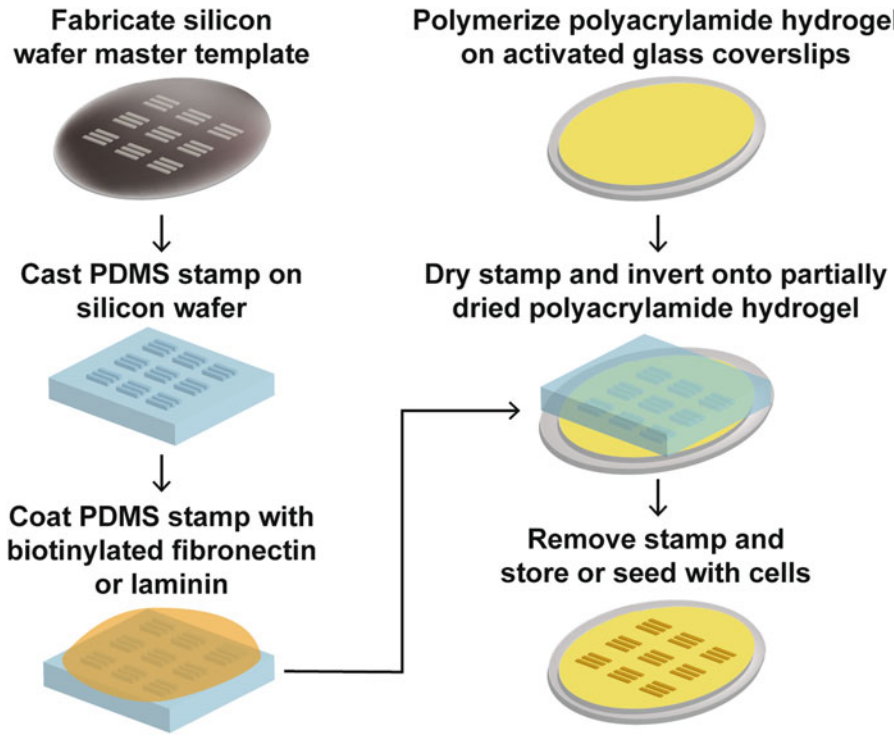

Fig. 1 Schematic of the fabrication process for engineering shape-controlled cardiac microtissues on microcontact-printed polyacrylamide hydrogels

be outsourced to a company that performs this service, such as Photoplot Store.

Steps 4–10 should be performed in a Class 100 cleanroom facility with the equipment listed in Subheading 2.1.

4. Fabricate the silicon wafer master using standard photolithography techniques [6]. Briefly, handle the wafer at its edges using wafer tweezers and clean the surface using compressed air or nitrogen.
5. Spin-coat the wafer with SU-8 2005 photoresist using spin speeds adjusted for a thickness of 5 μm, according to manufacturer's instructions.
6. Bake the wafer on a hot plate according to manufacturer's instructions (*see* **Note 2**).
7. Mount the spin-coated wafer and photomask on the mask aligner and carefully bring the wafer into contact with the photomask.
8. Expose the wafer to UV light and then bake again based on instructions from the manufacturer.
9. Develop the wafer by submerging it in SU-8 developer or PGMEA inside a glass dish with gentle agitation.

10. After several minutes, remove the wafer, rinse it with isopropanol, and carefully dry it with compressed air or nitrogen.
11. Silanize the wafer to passivate the surface and ensure release of PDMS after the casting and curing process. Place approximately 30 μL of trichloro (1*H*, 1*H*, 2*H*, 2*H*-perfluorooctyl) silane in a small cap formed from aluminum foil and place it in a desiccator, along with a wafer or multiple wafers (*see* **Note 3**). Seal the desiccator, apply vacuum, and incubate for at least 1 h or ideally overnight.
12. Store each wafer in a Petri dish inside a drawer or covered with aluminum foil to minimize light exposure.

3.2 Fabricating PDMS Stamps

1. Place a silanized silicon wafer master (Fig. 2a) in a Petri dish with the patterned side facing up.
2. Prepare PDMS prepolymer by measuring the base and curing agent of Sylgard 184 at a weight ratio of 10:1 into a 100-mL disposable Thinky cup. Mix and degas the PDMS for 2 min each in the planetary centrifugal Thinky mixer (*see* **Note 4**).

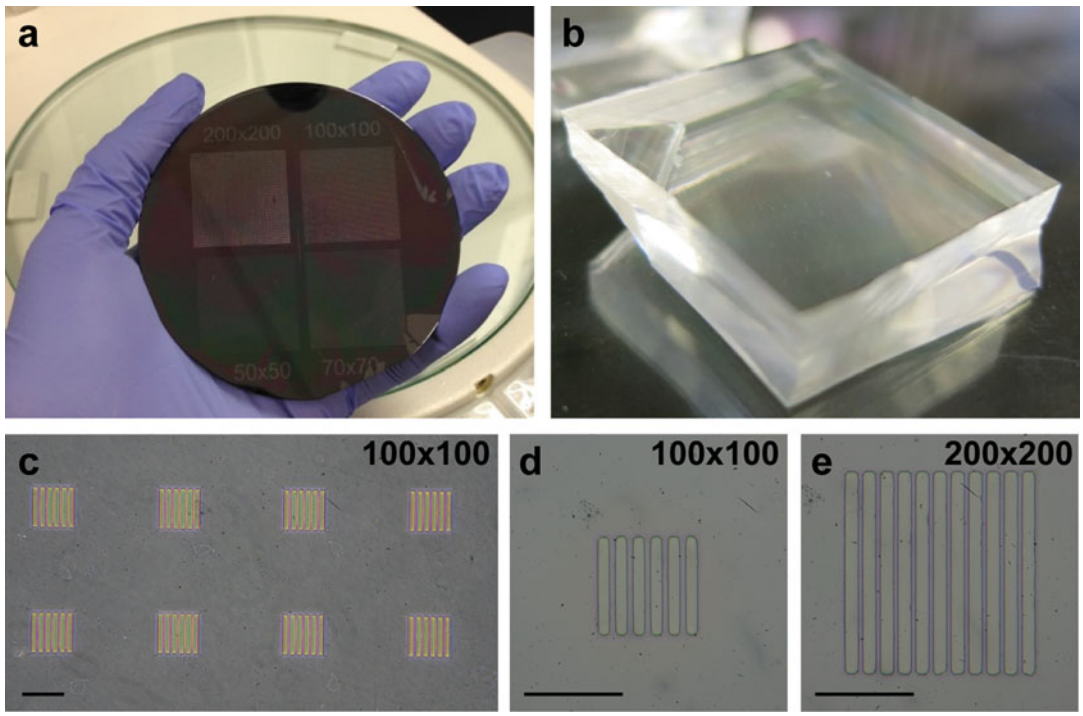

Fig. 2 Fabricating PDMS stamps for microcontact printing. (**a**) Silicon wafer master with patterned photoresist in four different 2.5 cm × 2.5 cm stamp designs. (**b**) A single PDMS stamp molded on the silicon wafer. (**c**) Microtissue features on a PDMS stamp. This stamp has an array of 100 μm × 100 μm squares that each consist of 15 μm-wide lines separated by 2 μm-wide gaps. The size of the microtissue can be tuned by adjusting the pattern design, as shown by the (**d**) 100 μm × 100 μm square and (**e**) 200 μm × 200 μm square. For (**c–e**), scale bar, 100 μm

3. Pour enough PDMS mixture over the silicon wafer master to form a layer at least 5 mm thick. Place the dish in a vacuum desiccator and degas until all bubbles are removed (*see* **Note 5**).
4. Place the dish in a 65 °C oven for at least 4 h to cure the PDMS.
5. Carefully cut the PDMS around the wafer using a razor blade or blade knife.
6. Carefully peel the cured PDMS slab from the wafer. The wafer can be reused for casting PDMS immediately or stored.
7. Use a razor blade to cut the slab of PDMS into square stamps approximately matching each 2.5 cm × 2.5 cm feature region (Fig. 2b). Cut the PDMS on a surface with features facing up (Fig. 2c–e) to avoid damage (*see* **Note 6**).

3.3 Preparing Polyacrylamide Hydrogel Culture Substrates

3.3.1 Activating Coverslips

1. Load two coverslip racks with 25 mm glass coverslips and place the racks in a square glass dish with a stir bar in the middle. Place the dish on a stir plate in a chemical fume hood.
2. Add 270 mL ultrapure water and 30 mL 1 M NaOH to the dish and stir for 5 min.
3. Carefully remove coverslip racks from the dish and dispose of the NaOH solution.
4. Replace the coverslip racks in the glass dish and add 300 mL of 95% ethanol.
5. Add approximately 1.5 mL of APTMS. Use a glass Pasteur pipette and a rubber bulb if possible, as APTMS can react with plastic. Stir for 5 min.
6. Carefully remove coverslip racks from the dish again and dispose of the APTMS solution.
7. Replace the coverslip racks in the glass dish, add 300 mL of 95% ethanol, and stir for 5 min. Remove racks and dispose of the ethanol. Repeat twice for a total of three ethanol rinses.
8. Replace the coverslip racks in the glass dish and add 300 mL ultrapure water and 2.16 mL of 70% glutaraldehyde. Stir for 30 min and dispose of the liquid. Repeat this process three times with 300 mL ultrapure water.
9. Line the bottom of 150 mm Petri dishes with wrinkled aluminum foil. Remove coverslips with forceps and place them on the foil in a single layer.
10. Place the dishes in a 37 °C oven with the lid tilted for 15–20 min until they are dry (*see* **Note 7**).
11. Use Parafilm to seal the Petri dishes and minimize dust contamination. Activated coverslips can be stored at room temperature for several months.

3.3.2 Fabricating Polyacrylamide Hydrogels

The elastic modulus of polyacrylamide hydrogels depends on the ratio of acrylamide to bis-acrylamide. To fabricate hydrogels with 13 kPa or 90 kPa, follow the formulations in Table 1. Other formulations have also been reported [19].

1. Transfer the desired number of activated coverslips to a new Petri dish without aluminum foil.
2. Make polyacrylamide stock solutions by mixing acrylamide, bis-acrylamide, and water at the indicated ratios (Table 1). Stock solutions can be stored at 4 °C for several months.
3. Mix TEMED and water according to Table 1. Make this solution fresh and keep the solution covered because TEMED is light-sensitive.
4. Mix together the components of the working solution as listed in Table 1 in a 2-mL Eppendorf tube and vortex briefly (*see* **Note 8**).
5. At this point, move quickly as the gels will begin to polymerize. Transfer 50 μL of the working solution to a 10-μL tube of streptavidin acrylamide for a total of 60 μL. Pipette the solution up and down to mix.
6. Add a 20-μL drop of the solution from **step 5** to each activated coverslip (Fig. 3a).
7. Carefully drop an 18-mm glass coverslip on top of the solution to flatten the hydrogel as it polymerizes (Fig. 3b). Incubate for 15 min (*see* **Note 9**).
8. Transfer the coverslips with hydrogels to a cell culture hood.

Table 1
Formulations for fabricating polyacrylamide hydrogels with the indicated elastic modulus

		13 kPa	90 kPa
Stock solution	40% Acrylamide	2.344 mL	2.500 mL
	2% Bis	1.875 mL	2.500 mL
	Water	781 μL	—
TEMED solution	TEMED	9 μL	9 μL
	Water	1.901 mL	701 μL
Working solution	Stock solution	240 μL	360 μL
	10× PBS	60 μL	60 μL
	Water	6 μL	6 μL
	TEMED/water solution	191 μL	71 μL
	10% APS	3 μL	3 μL

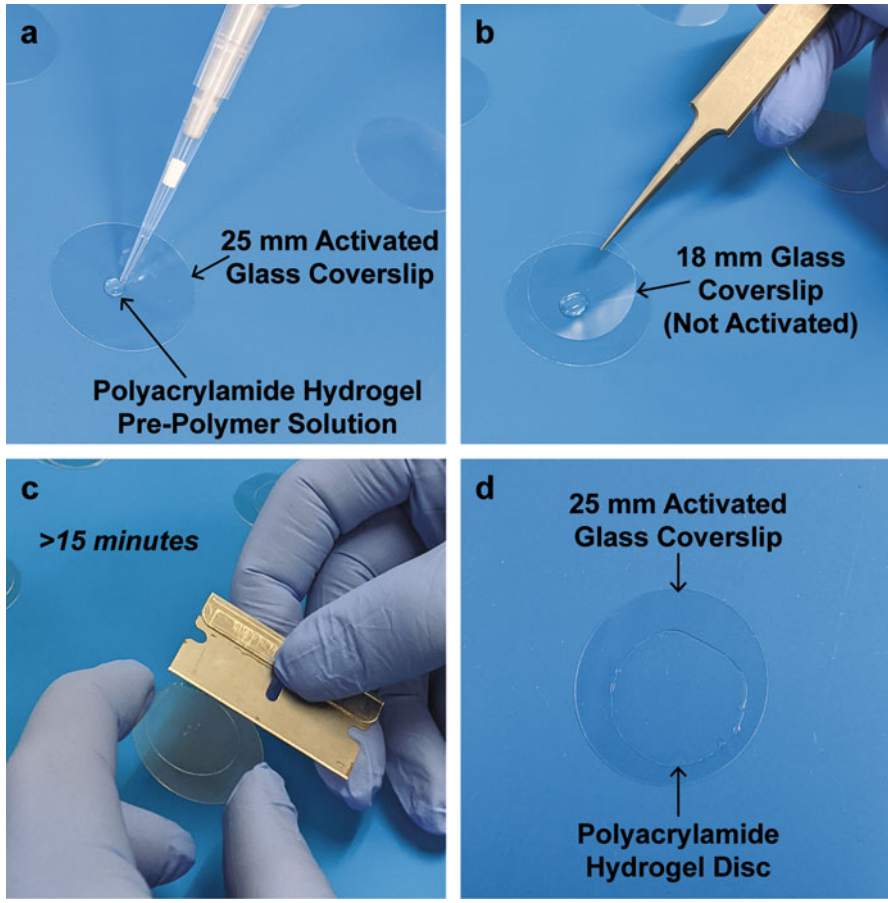

Fig. 3 Fabricating polyacrylamide hydrogels on activated glass coverslips. (**a**) Pipette a 20-μL drop of the hydrogel solution onto the center of the 25 mm activated glass coverslip. (**b**) Slowly drop an 18 mm glass coverslip onto the droplet. (**c**) Use a razor blade to separate the 18 mm glass coverslip from the polymerized polyacrylamide hydrogel. (**d**) Store or directly use the polymerized polyacrylamide hydrogel substrates for microcontact printing

9. Use a razor blade to carefully remove the top 18 mm coverslip with one hand while holding the 25 mm coverslip in the other hand (Fig. 3c). Use the razor blade as a lever to carefully separate the 18 mm coverslip from the hydrogel in one movement (*see* **Note 10**). Avoid rotating or sliding the coverslip as this will introduce defects into the hydrogel (Fig. 3d).
10. Place each 25 mm coverslip into the well of a 6-well plate and rinse three times with PBS.
11. Store the coverslips in PBS at 4 °C or immediately microcontact print their surface. Hydrogels should be used within 1 week.

3.4 Microcontact Printing of Biotinylated ECM Proteins on Polyacrylamide Gels

3.4.1 Biotinylating Fibronectin or Laminin

1. In a glass beaker, dissolve 5.3 g of sodium carbonate (Na_2CO_3) into 500 mL of ultrapure water. Adjust the pH to 8.5 (*see* **Note 11**).
2. Slowly add 5 mL of the solution from **step 1** to a 5-mg bottle of fibronectin for a final concentration of 1 mg/mL (*see* **Note 12**). Do not vortex.
3. Prepare a 10-mM solution of Sulfo-NHS-LC-Biotin by dissolving 2 mg in 360 μL ultrapure water.
4. Add 230 μL of the 10 mM Sulfo-NHS-LC-Biotin solution to the 5 mL fibronectin solution and incubate overnight on a rocker at 4 °C.
5. Remove nonreacted Sulfo-NHS-LC-Biotin solution by injecting the solution into a dialysis cartridge with a molecular weight cutoff of 10 K.
6. Float the dialysis cartridge in a 1-L beaker filled with PBS and a stir bar. Stir the solution for 2 h.
7. Dispose of the PBS, add fresh PBS, and stir the solution for another 2 h.
8. Extract the biotinylated fibronectin from the dialysis cartridge, aliquot to 200 μL, and store at 4 °C. Laminin can be biotinylated using a similar protocol (*see* **Note 13**).

3.4.2 Microcontact Printing

The procedure described below for biotinylated fibronectin could similarly be done with biotinylated laminin.

1. Submerge the PDMS stamps with features facing up in a glass beaker with 95% ethanol and sonicate in an ultrasonic bath for 30 min at room temperature.
2. Transfer the beaker to a sterile biosafety cabinet. Using forceps, carefully remove the PDMS stamps from the ethanol without contacting the features.
3. Dry the stamps with compressed air and place them in a Petri dish with features facing up.
4. Add 800 μL of PBS to a 200-μL aliquot of biotinylated fibronectin for a final concentration of fibronectin of 200 μg/mL. Mix gently with the pipette.
5. Pipet a 200–300 μL drop of fibronectin onto each stamp. Use the pipet tip to carefully spread the fibronectin drop until it fully covers the surface, taking care not to touch the patterned features with the tip (*see* **Note 14**).
6. Place the lid on the Petri dish and incubate the fibronectin solution on the stamp for at least 1 h.
7. With tweezers, remove a hydrogel coverslip from the 6-well plate and carefully blot the excess PBS using a KimWipe. Avoid

touching the hydrogel itself with the tweezers or Kimwipe. Place the blotted hydrogel coverslip in a 150-mm Petri dish and repeat for the desired number of coverslips.

8. Transfer the Petri dish with the coverslips to a 37 °C benchtop incubator with the lid tilted for approximately 10 min, until the hydrogel is sufficiently dry (*see* **Note 15**).
9. Transfer the dried hydrogel coverslips to the biological safety cabinet.
10. After the 1-h incubation period for biotinylated fibronectin on PDMS stamps, carefully pipette excess fibronectin off the stamps and collect it into the Eppendorf tube. The fibronectin can be stored at 4 °C and recycled for up to 2 months although bioactivity will decline with time.
11. Pick up a stamp with forceps, dry it with compressed air, and invert it onto the surface of the hydrogel.
12. Use forceps to apply slight pressure (*see* **Note 16**). Incubate the stamps for at least 5 min to ensure protein transfer.
13. Carefully remove the stamp from the hydrogel by using tweezers in one hand to hold down the coverslip and forceps in the other hand to remove the stamp. Transfer the coverslip to the well of a 6-well plate prefilled with PBS.
14. Repeat **steps 11–13** for the desired number of coverslips. Rinse all wells three times with PBS and store at 4 °C until cell seeding. Ensure that all coverslips are submerged in the PBS (i.e., not floating).
15. To sterilize the hydrogels, leave the plate in the biological safety cabinet with the lid off and turn on the UV light for at least 10 min to sterilize the hydrogels prior to cell seeding.
16. Seed coverslips with desired cell type(s). For primary neonatal rat cardiac myocytes, seed with 1.1×10^5 cells/cm^2 per coverslip to generate confluent microtissues with minimal fibroblasts after 3 days (Fig. 4). Fibroblasts are naturally present in suspensions of primary cardiac myocytes. Because fibroblasts are proliferative but cardiac myocytes are not, simply reduce the cell density (such as 5.5×10^4 cells/cm^2) to increase the presence of fibroblasts in microtissues. Fibroblasts or other supporting cell types could also be added separately.

4 Notes

1. For the design described in this protocol, a chrome on glass photomask is needed due to the resolution of the features (2 μm). However, lower-cost photomasks printed on polyester-based transparency films can also be used if the desired resolution is >10 μm.

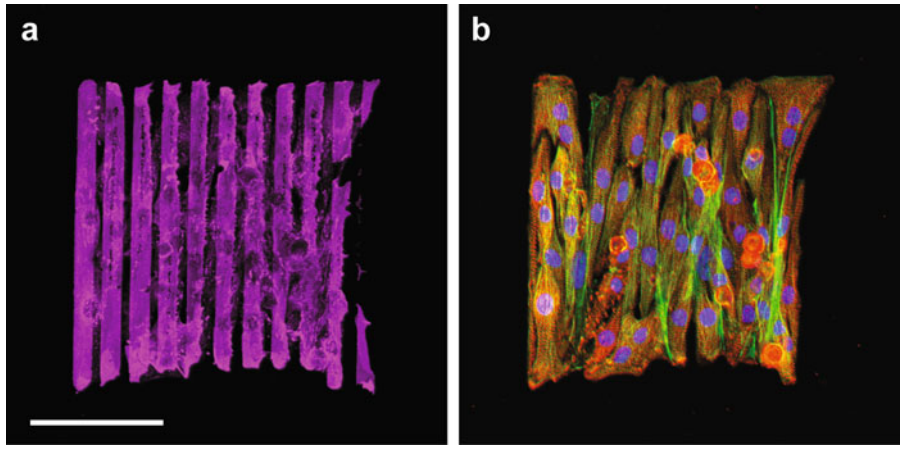

Fig. 4 Shape-controlled cardiac microtissue on a compliant hydrogel. Neonatal rat ventricular myocytes were seeded on a polyacrylamide hydrogel microcontact printed with laminin in the microtissue pattern. Immunostaining was used to visualize (**a**) laminin (magenta) and (**b**) sarcomeric α-actinin (red), actin (green), and nuclei (blue). Scale bar, 100 μm

2. Ramping temperatures up and down will prevent defects in the photoresist.
3. Use a wafer tray or Petri dishes to prop up the wafers and ensure that all surfaces will be coated with silane.
4. If a Thinky mixer is not available, mix the PDMS thoroughly with a transfer pipette or plastic fork for at least 5 min in any type of disposable plastic cup. Then, use a vacuum desiccator to de-gas the mixture.
5. If air bubbles are lingering, it can be helpful to periodically release and re-apply the vacuum and/or gently tap the dish on the benchtop.
6. Cutting a small, noticeable notch with a razor on the featureless side can be useful for quickly distinguishing the feature-containing side of the stamp. Alternatively, a line could be cut that represents the orientation of the features. For example, cutting a line that is parallel to lines on the stamp may be helpful for orienting the pattern on your substrate during microcontact printing.
7. The coverslips may have an orange tint or small aggregates of orange particles. This should not affect the performance of the coverslip.
8. To use these hydrogels with traction force microscopy (TFM), the 6 μL water in the working solution (Table 1) can be substituted for an equal volume of fluorescent microbeads, such as 0.2 μm FluoSpheres yellow-green 505/515 beads (Invitrogen).

9. The tube of leftover working solution should also cross-link into a hydrogel. You can use this tube to help you identify when cross-linking is complete. If the hydrogels do not polymerize within 30 min at room temperature, they can be placed in a 37 °C oven to accelerate the process.
10. If the coverslip does not easily separate, you may need to trace the edge of the 18 mm coverslip with the razor blade to detach any hydrogel that seeped onto the exposed surface of the 18 mm coverslip.
11. Because the solution will be very basic, it is recommended to start with approximately 300 mL of ultrapure water and adjust the pH of that solution to 8.5 using hydrochloric acid, which might be a relatively large volume depending on your stock concentration. Then, add enough ultrapure water so that the final volume is 500 mL and the final concentration of sodium carbonate is 100 mM. Re-check the pH and make additional adjustments as needed.
12. Slowly add the sodium carbonate solution dropwise to reconstitute the lyophilized fibronectin. If the solvent is added too quickly, the fibronectin may self-polymerize and form insoluble clumps. Avoid vortexing or excessive pipetting for the same reason.
13. Laminin can also be biotinylated using the same protocol as fibronectin. However, laminin is often shipped in a Tris-HCl solution and NaCl solution. Thus, laminin first must be dialyzed (using the same 10 K molecular weight cutoff cartridges) for 4 h in the 100 mM sodium carbonate solution to exchange the buffer.
14. If the fibronectin or laminin is not spreading easily, rest the pipet tip against the edge of the stamp and drag it along the edge. Add more fibronectin or laminin solution if needed.
15. After 10 min, check if the surface of the gel is dried. No large puddles of liquid should be visible, but some white residue from the PBS evaporating may be noticeable. If they are not yet dry, put them back into the oven for 2 min and check again. Repeat until they are dry. Under-drying will prevent fibronectin patterning and over-drying will cause the gels to crack.
16. It will likely take some trial-and-error to learn the amount of pressure that should be applied to the PDMS stamp when it is in contact with the PA gel. If there is too little pressure, the fibronectin will not transfer. If there is too much pressure, the PDMS stamp may buckle and fibronectin will also be transferred onto the featureless regions. When first learning this protocol, it can be useful to immunostain hydrogels for fibronectin or laminin (without cells) to determine the fidelity of your pattern and help troubleshoot the protocol.

References

1. Rienks M, Papageorgiou AP, Frangogiannis NG, Heymans S (2014) Myocardial extracellular matrix: an ever-changing and diverse entity. Circ Res 114(5):872–888
2. Berry MF, Engler AJ, Woo YJ, Pirolli TJ, Bish LT, Jayasankar V, Morine KJ, Gardner TJ, Discher DE, Sweeney HL (2006) Mesenchymal stem cell injection after myocardial infarction improves myocardial compliance. Am J Physiol Heart Circ Physiol 290(6):H2196–H2203
3. Reimer KA, Ideker RE (1987) Myocardial ischemia and infarction: anatomic and biochemical substrates for ischemic cell death and ventricular arrhythmias. Hum Pathol 18 (5):462–475
4. van den Borne SW, Diez J, Blankesteijn WM, Verjans J, Hofstra L, Narula J (2010) Myocardial remodeling after infarction: the role of myofibroblasts. Nat Rev Cardiol 7(1):30–37
5. Ariyasinghe NR, Lyra-Leite DM, McCain ML (2018) Engineering cardiac microphysiological systems to model pathological extracellular matrix remodeling. Am J Physiol Heart Circ Physiol 315(4):H771–H789
6. Qin D, Xia Y, Whitesides GM (2010) Soft lithography for micro- and nanoscale patterning. Nat Protoc 5(3):491–502
7. Ribeiro AJ, Ang YS, Fu JD, Rivas RN, Mohamed TM, Higgs GC, Srivastava D, Pruitt BL (2015) Contractility of single cardiomyocytes differentiated from pluripotent stem cells depends on physiological shape and substrate stiffness. Proc Natl Acad Sci U S A 112 (41):12705–12710
8. Wheelwright M, Win Z, Mikkila JL, Amen KY, Alford PW, Metzger JM (2018) Investigation of human iPSC-derived cardiac myocyte functional maturation by single cell traction force microscopy. PLoS One 13(4):e0194909
9. McCain ML, Yuan H, Pasqualini FS, Campbell PH, Parker KK (2014) Matrix elasticity regulates the optimal cardiac myocyte shape for contractility. Am J Physiol Heart Circ Physiol 306(11):H1525–H1539
10. Bray MA, Sheehy SP, Parker KK (2008) Sarcomere alignment is regulated by myocyte shape. Cell Motil Cytoskeleton 65(8):641–651
11. Knight MB, Drew NK, McCarthy LA, Grosberg A (2016) Emergent global contractile force in cardiac tissues. Biophys J 110 (7):1615–1624
12. Feinberg AW, Alford PW, Jin H, Ripplinger CM, Werdich AA, Sheehy SP, Grosberg A, Parker KK (2012) Controlling the contractile strength of engineered cardiac muscle by hierarchal tissue architecture. Biomaterials 33 (23):5732–5741
13. Grosberg A, Alford PW, McCain ML, Parker KK (2011) Ensembles of engineered cardiac tissues for physiological and pharmacological study: heart on a chip. Lab Chip 11 (24):4165–4173
14. Lyra-Leite DM, Andres AM, Petersen AP, Ariyasinghe NR, Cho N, Lee JA, Gottlieb RA, McCain ML (2017) Mitochondrial function in engineered cardiac tissues is regulated by extracellular matrix elasticity and tissue alignment. Am J Physiol Heart Circ Physiol 313(4): H757–H767
15. Petersen AP, Lyra-Leite DM, Ariyasinghe NR, Cho N, Goodwin CM, Kim JY, McCain ML (2018) Microenvironmental modulation of calcium wave propagation velocity in engineered cardiac tissues. Cell Mol Bioeng 11 (5):337–352
16. Ariyasinghe NR, Reck CH, Viscio AA, Petersen AP, Lyra-Leite DM, Cho N, McCain ML (2017) Engineering micromyocardium to delineate cellular and extracellular regulation of myocardial tissue contractility. Integr Biol (Camb) 9(9):730–741
17. Berk BC, Fujiwara K, Lehoux S (2007) ECM remodeling in hypertensive heart disease. J Clin Invest 117(3):568–575
18. Ho CY, Lopez B, Coelho-Filho OR, Lakdawala NK, Cirino AL, Jarolim P, Kwong R, Gonzalez A, Colan SD, Seidman JG, Diez J, Seidman CE (2010) Myocardial fibrosis as an early manifestation of hypertrophic cardiomyopathy. N Engl J Med 363(6):552–563
19. Aratyn-Schaus Y, Oakes PW, Stricker J, Winter SP, Gardel ML (2010) Preparation of complaint matrices for quantifying cellular contraction. J Vis Exp 46:2173
20. Engler AJ, Carag-Krieger C, Johnson CP, Raab M, Tang HY, Speicher DW, Sanger JW, Sanger JM, Discher DE (2008) Embryonic cardiomyocytes beat best on a matrix with heart-like elasticity: scar-like rigidity inhibits beating. J Cell Sci 121(Pt 22):3794–3802
21. Jacot JG, Kita-Matsuo H, Wei KA, Chen HS, Omens JH, Mercola M, McCulloch AD (2010) Cardiac myocyte force development during differentiation and maturation. Ann N Y Acad Sci 1188:121–127
22. Engler AJ, Griffin MA, Sen S, Bonnemann CG, Sweeney HL, Discher DE (2004) Myotubes differentiate optimally on substrates with tissue-like stiffness: pathological implications

for soft or stiff microenvironments. J Cell Biol 166(6):877–887

23. Hazeltine LB, Simmons CS, Salick MR, Lian X, Badur MG, Han W, Delgado SM, Wakatsuki T, Crone WC, Pruitt BL, Palecek SP (2012) Effects of substrate mechanics on contractility of cardiomyocytes generated from human pluripotent stem cells. Int J Cell Biol 2012:508294
24. Aratyn-Schaus Y, Pasqualini FS, Yuan H, McCain ML, Ye GJ, Sheehy SP, Campbell PH, Parker KK (2016) Coupling primary and stem cell-derived cardiomyocytes in an in vitro model of cardiac cell therapy. J Cell Biol 212 (4):389–397
25. Pasqualini FS, Agarwal A, O'Connor BB, Liu Q, Sheehy SP, Parker KK (2018) Traction force microscopy of engineered cardiac tissues. PLoS One 13(3):e0194706
26. McCain ML, Lee H, Aratyn-Schaus Y, Kleber AG, Parker KK (2012) Cooperative coupling of cell-matrix and cell-cell adhesions in cardiac muscle. Proc Natl Acad Sci U S A 109 (25):9881–9886

Chapter 6

Engineering Biophysical Cues for Controlled 3D Differentiation of Endoderm Derivatives

Thomas Richardson, Shibin Mathew, Connor Wiegand, Kevin Pietz, Joseph Candiello, K. Ravikumar, and Ipsita Banerjee

Abstract

Biophysical cues synergize with biochemical cues to drive differentiation of pluripotent stem cells through specific phenotypic trajectory. Tools to manipulate the cell biophysical environment and identify the influence of specific environment perturbation in the presence of combinatorial inputs will be critical to control the development trajectory. Here we describe the procedure to perturb biophysical environment of pluripotent stem cells while maintaining them in 3D culture configuration. We also discuss a high-throughput platform for combinatorial perturbation of the cell microenvironment, and detail a statistical procedure to extract dominant environmental influences.

Key words Biophysical cues, Alginate encapsulation, hPSC differentiation, 3D Cell culture, Alginate stiffness

1 Introduction

Human pluripotent stem cells (hPSCs) have enormous potential in tissue engineering and cell therapy applications [1]. These cells have two distinct characteristics which make them highly attractive: they can become any cell type in the body and can self-renew indefinitely. Over the last two decades, there has been concentrated effort to derive functional organ-specific cells from hPSCs, which include, but are not limited to, cardiac cells [2–4], neurons [5, 6], hepatocytes [7–9], and pancreatic beta cells [10–13]. Self-renewal and lineage commitment of pluripotent stem cells are known to be influenced by environmental cues, which have been employed extensively to induce the cells through the desired phenotypic trajectory.

Predominant environmental cues can be broadly categorized as biochemical cues and biophysical cues. Biochemical signals are

Mo R. Ebrahimkhani and Joshua Hislop (eds.), *Programmed Morphogenesis: Methods and Protocols*, Methods in Molecular Biology, vol. 2258, https://doi.org/10.1007/978-1-0716-1174-6_6,

typically provided by soluble bioactive agents, autocrine and paracrine signaling pathways, along with the extracellular matrix proteins. In parallel, there is clear evidence that stem cell fate can be modulated by biophysical cues. Such biophysical cue can constitute the elasticity of the substrate, the surface topography of the culture scaffold, geometric configuration of the substrate, extracellular forces applied to the cells [1–4], to cite few examples. While biophysical cues have been reported to synergize with biochemical cues, there is evidence of biophysical cues directing stem cell fate even in the absence of biochemical factors [5, 6].

One of the commonly studied biophysical cues is the stiffness of the extracellular substrate the cells are exposed to. Multipotent mesenchymal stem cells (MSCs) can modulate their own stiffness to match that of the substrate, thereby differentiating into cell phenotype that correspond to the mechanical properties of the underlying substrate [7, 8]. Similarly, ESCs are also highly sensitive to its biophysical environment. In the context of endoderm-specific differentiation, our group has demonstrated the feasibility of driving early germ layer differentiation of mESCs by modifying the properties of alginate and fibrin substrates, in the absence of chemical inducers [9–12]. More recently, we modulated cellular biophysical environment while maintaining them in the 3D culture configuration, by encapsulating hPSC into alginate capsule and synergistically inducing differentiation using chemical cues [13]; we further modulated alginate substrate properties and identified the range of biophysical parameters supportive of pancreatic maturation [14]. Another important insoluble cue which can influence hPSC differentiation is cell–cell contact, especially in 3D cellular aggregates. This was successfully demonstrated by Lee et al., in a study where controlling hPSC colony size enabled control over germ layer specification [15].

The sensitivity of stem cells to various environmental factors has imbibed the development of various technologies to characterize and control cell fate. Adherent culture platforms were developed to screen the effect of physical stimuli such as substrate stiffness, ECM protein [16, 17], and surface topography [18] on stem cell fate. The effect of combinatorial perturbations to the microenvironment was explored with microengineered hydrogel microarray, to simultaneously probe the effect of substrate stiffness and signaling proteins on MSCs [18] and mESCs [19]. We have developed methods to maintain the hPSCs in 3D culture with combinatorial modulation of cell microenvironment. hPSCs cultured in this array configuration could be maintained under long-term culture and successfully differentiated in the array. Cell fate was characterized using a sensitive quantitative imaging platform, and a statistical model was developed to subsequently analyze cell response to the multiparametric modulation.

2 Materials

2.1 General Reagents

1. mTeSR1 (StemCell Technologies).
2. Single Cell Growth Media: composed of mTeSR1 with 3.2026 mg/L Y-27632 (ROCK Inhibitor-RI, Millipore) filtered with a 0.22-μm pore size PES membrane.
3. Alginate solution: 1.1 wt% low viscosity alginate (Sigma-Aldrich) and 0.2 vol% gelatin (Sigma-Aldrich) mixed in DMEM/F12 (Gibco) filtered with a 0.22-μm pore size PES membrane.
4. Calcium Chloride Solution: 11.095 g/L Calcium Chloride (Sigma-Aldrich) and 2.383 g/L HEPES (Sigma-Aldrich) filtered with a 0.22-μm pore size PES membrane.
5. $BaCl_2$ (Sigma-Aldrich).
6. Ba-PLL Solutions: 2.0823, 3.12345, 4.1646, 10.4115, and 20.823 g/L $BaCl_2$ dissolved in poly-(L-lysine) (PLL).
7. EDTA solution: 37.224 g/L EDTA (OmniPur) balanced to a 7.6 pH.
8. Nitrocellulose (Fisher).
9. Paraformaldehyde (PFA) powder (Sigma-Aldrich).
10. Phosphate Buffer Saline (PBS), (Lonza).
11. Permeabilizing agents—Saponin, Tween-20, and Triton X-100 (Sigma-Aldrich).
12. Bovine Serum Albumin (BSA, Sigma-Aldrich).
13. BCA total protein assay (Thermo Scientific).
14. Citrate Buffer, Antigen Retriever (Sigma-Aldrich).
15. Blocking Buffer: 3% BSA, 0.25% DMSO and 0.1% Saponin in PBS.
16. Donkey Serum (Sigma-Aldrich).
17. Paraffin Wax for Histology (Sigma-Aldrich).
18. Dissociation Reagents—Accutase (StemPro) and TrypLE (Gibco).
19. Matrigel (BD Bioscience).
20. Nucelospin RNA II kit (Machery-Nagel).
21. Improm II Reverse Transcription kit (Promega).
22. SYBER Green Master Mix (Agilent).

2.2 Differentiation Media

1. Stage 1 (Definitive Endoderm) Base Media: 0.44 g/L D-Glucose (Gibco), 2.46 g/L $NaHCO_3$ (Sigma-Aldrich), 2% FAF-BSA (Fisher Scientific), 2 mM Glutamax (Gibco), 1% Pen/Strep (Lonza), 0.044 g/L Vitamin C (Sigma-Aldrich), 1:50 ITS-X (Gibco), MCDB131 media (Corning).

2. Stage 2 (Primitive Gut Tube) Base Media: 0.44 g/L D-Glucose (Gibco), 1.23 g/L $NaHCO_3$ (Sigma-Aldrich), 2% FAF-BSA (Fisher Scientific), 2 mM Glutamax (Gibco), 1% Pen/Strep (Lonza), 0.044 g/L Vitamin C (Sigma-Aldrich), 1:50 ITS-X (Gibco), MCDB131 media (Corning).
3. Stage 3 (Pancreatic Progenitors 1 and 2) Base Media: 0.44 g/L D-Glucose (Gibco), 1.23 g/L $NaHCO_3$ (Sigma-Aldrich), 2% FAF-BSA (Fisher Scientific), 2 mM Glutamax (Gibco), 1% Pen/Strep (Lonza), 0.044 g/L Vitamin C (Sigma-Aldrich), 1:200 ITS-X (Gibco), MCDB131 media (Corning).
4. Stage 4 (Endocrine Progenitor) Base Media: 3.6 g/L D-Glucose (Gibco), 1.75 g/L $NaHCO_3$ (Sigma-Aldrich), 2% FAF-BSA (Fisher Scientific), 2 mM Glutamax (Gibco), 1% Pen/Strep (Lonza), 0.044 g/L Vitamin C (Sigma-Aldrich), 1:200 ITS-X (Gibco), MCDB131 media (Corning).
5. Stage 5 (Maturation) Base Media: 0.44 g/L D-Glucose (Gibco), 1.23 g/L $NaHCO_3$ (Sigma-Aldrich), 2% FAF-BSA (Fisher Scientific), 2 mM Glutamax (Gibco), 1% Pen/Strep (Lonza), 0.044 g/L Vitamin C (Sigma-Aldrich), 1:200 ITS-X (Gibco), MCDB131 media (Corning).
6. Growth Factors:
   (a) Activin A (R&D Systems).
   (b) Chir99021 (Sigma-Aldrich).
   (c) KGF (Peprotech).
   (d) Sant 1 (Sigma-Aldrich).
   (e) Retinoic Acid (Sigma-Aldrich).
   (f) LDN193189 (Sigma-Aldrich).
   (g) PdBU (EMD Millipore).
   (h) Y-27632 (R&D Systems).
   (i) XXI (EMD Millipore).
   (j) Alk5i II (Axxora).
   (k) T3 (EMD Millipore).
   (l) Betacellulin (R&D Systems).
   (m) Heparin (Sigma-Aldrich).

2.3 Equipment

1. Light Microscope.
2. Hemocytometer.
3. Stir Plate.
4. 200 mL Beaker
5. 10 mL Syringe
6. 22-Gauge needle

7. 500 mL Beaker
8. Microplate Reader.
9. Microtome.
10. Atomic Force Microscope (AFM).
11. Centrifuge.
12. V-bottom Ultralow Adherent (ULA) Plates.
13. LICOR Odyssey.

3 Methods

3.1 hPSC Preparation for Encapsulation

Normal culturing of the hPSCs is done in a 6-well tissue culture-treated plate with mTeSR1 as the normal culture medium. Once the cultures reach confluence, the cells are dissociated into single cells for encapsulation according to the following steps:

1. Under a microscope, mark regions where differentiation or overgrowth has occurred in the hPSC cultures and remove the marked areas (*see* **Note 1**).
2. 2 h prior to dissociating the hPSC cells, aspirate the culture media and add 1 mL single cell growth media to the desired adherent cell cultures (*see* **Note 2**).
3. 20 min before dissociating the cells, transfer a sufficient amount of Accutase to a 15-mL falcon tube to have 1 mL per well of hPSC culture being used for encapsulation and place it in a 37 °C water bath.
4. To dissociate the hPSCs, add 1 mL of the warmed Accutase to each well of the hPSC and incubate for 5–7 min (*see* **Note 3**).
5. Harvest hPSC from wells by gently pipetting Accutase directly onto the cell colonies on the well plate.
6. Transfer the harvested cell–Accutase solution from each well to a 15-mL falcon tube and add 1–2 mL of single cell growth media to the tube.
7. Spin down hPSC single cell suspension at 220–240 rcf for 4 min.
8. Aspirate the supernatant and resuspend in 3 mL of single cell growth media.
9. Make a 1:10 of single cell suspension of hPSC and count using the hemocytometer.

3.2 Encapsulation of hPSCs in Alginate Capsules

1. Use 70% ethanol to sterilize a stir plate, a 200-mL beaker, a 500-mL beaker, a stir bar, and a metal spatula and place them into the biohazard safety cabinet. Further sterilize with the safety cabinet UV lamp for 30 min.

2. Add sufficient volume of alginate solution to make a 500,000 cell per milliliter alginate solution into a 50-mL tube and place it into a 37 °C water bath 20 min before encapsulating the cells.
3. Add the desired cell suspension volume to a 50-mL falcon tube and centrifuge at 220–240 rcf for 4 min.
4. Aspirate supernatant and resuspend cells in the desired volume of alginate solution to achieve a seeding density of 500,000 cells/mL (*see* **Note 4**).
5. Add 100 mL of the calcium chloride solution to the 200 mL beaker, add the stir bar to the beaker, and place it on the stir plate. Increase the stir bar speed until a small vortex forms in the solution.
6. Using a 10-mL syringe, remove the cell–alginate solution from the 50 mL falcon tube and attach a 22-gauge needle to the syringe (*see* **Note 5**).
7. Add cell–alginate solution dropwise to the calcium chloride solution from approximately 3 cm above the liquid surface and away from the middle of the vortex.
8. Allow the alginate capsules to stir in the solution for 6–8 min.
9. Turn off stir bar and decant the calcium chloride solution into the 500 mL beaker.
10. Add resulting capsules to a 100-mm Petri dish with the metal spatula.
11. Wash the alginate capsules with phosphate-buffered saline (PBS) three times with volume of PBS equaling the volume of alginate being washed.
12. Aspirate the final PBS wash and distribute the alginate capsules into a 6-well plate with one million encapsulated cells per well.
13. Add 3 mL single cell growth media to each well of the encapsulated cells and place into the incubator set to 37 °C and 5% CO_2.

3.3 Modifying Biophysical Cues by Modification of Alginate Substrate Properties

The physical properties of alginate capsules can be modulated by changing the alginate (M/G ratio) and/or cation (Ca, Ba, Sr) type and concentration [20, 21]. As a general rule of thumb, increasing cation concentration will increase the stiffness of the resulting capsule by higher crosslinking of G residues; these effects are further enhanced by cations such as barium which have higher binding affinity [21, 22]. For example, depending on the concentration of Ba^{2+} ions, the Youngs modulus (a measure of stiffness) of the bead can range from approximately 5 kPa (for 2.0823 g/L $BaCl_2$) to 100 kPa (for 20.823 g/L $BaCl_2$) for 1.1 wt.% alginate. The stiffness of the alginate beads also varies with the amount of alginate in the gel. All of these can affect the fate and response of encapsulated cells [23–25].

3.3.1 Alginate Surface Roughness and Stiffness Characterization

1. On a 1.5-cm diameter mold, dispense 5–10 μL of 1.1 wt% of alginate solution to get a disk-shaped alginate.
2. Polymerize the disks by using different concentrations of $BaCl_2$ ranging from 2.0823 to 20.823 g/L.
3. Add $BaCl_2$ dropwise to the alginate disks to polymerize them and incubate at room temperature for 6–8 min to form Ba–alginate.
4. Wash the Ba–Alginate in saline to remove excess $BaCl_2$.
5. To probe the surface of the Ba–Alginate drops with an AFM, using a silica microsphere of radius 3.4 μm attached to a Si_3N_4 nitride cantilever with a calibrated force constant of ~0.4–1 N/m.
6. Place the array of Ba–Alginate drops in PBS to ensure sufficient hydration during the tests.
7. Engage the AFM probe in contact mode to indent the surface of the drops while measuring the corresponding force applied by the cantilever to generate a force vs. deflection curve.
8. Repeat the measurement at different locations in a 4 × 4 grid (for each Ba–Alginate drop in the array and for at least three drops per condition) (*see* **Note 6**).
9. Use a Hertzian model to fit the force v/s indentation depth data to obtain the stiffness of each drop in the array [14].

3.3.2 Diffusivity of Alginate Capsule

1. Prepare 1.1 wt.% alginate solution in water and add 2 mg of BSA per ml of alginate solution.
2. Form capsules of BSA-loaded alginate in $BaCl_2$ bath.
3. Vary the concentration of $BaCl_2$ in the bath between 2.0823 and 20.823 g/L to obtain alginate capsules containing BSA with different degrees of crosslinking.
4. Suspend the capsules in 2 mL of saline solution containing 9 g/L of NaCl.
5. Sample the saline supernatant regularly over a period of 24 h.
6. Measure the amount of BSA in the sampled supernatant using the BCA total protein assay and a microplate reader.
7. Estimate the diffusivity(D) by measuring the rate of change ($\partial C/\partial t$) of the amount of BSA in the supernatant leached out by the alginate capsule approximating the bead to be a spherically symmetric system.

$$\frac{\partial C}{\partial t} = \frac{1}{r}\frac{\partial}{\partial r}\left(rD\frac{\partial C}{\partial r}\right).$$

3.4 hPSC Differentiation into Pancreatic Islet Endocrine Cells

The hPSC differentiation is a 35-day process that is six major phases starting with induction into the definitive endoderm phase and ending with glucose-responsive pancreatic islet endocrine cells. Cells should be fed on specified days. The following outlines the six phases of differentiation and the supplements to be added to the differentiation base media. Growth factors should be reconstituted at higher concentrations and stored for long-term stability.

1. Day 1 will be supplemented further with 100 ng/mL activin A and 1.4 μg/mL Chir99021. Days 2–3 will be supplemented with 100 ng/mL activin A.
2. Days 4 and 6 will have 50 ng/mL KGF.
3. In Days 7 and 8, differentiation base media should be supplemented with 50 ng/mL KGF, 0.25 μM Sant 1, 2 μM Retinoic Acid, 200 nM LDN193189 (Day 7 only), 500 nM PdBU, 10 μM Y-27632.
4. Days 9, 11, and 13 supplements to the differentiation base media are 50 ng/mL KGF, 0.25 μM Sant 1, 0.1 μM Retinoic Acid, 10 μM Y-27632, 5 ng/mL Activin A.
5. For days 14 and 16, supplement the media with 0.25 μM Sant1, 0.1 μM Retinoic Acid, 1 μM XXI, 10 μM ALk5i II, 1 μM T3, 20 ng/mL Betacellulin, 10 μg/mL Heparin. For days 18 and 20, supplement the media with 0.025 μM Retinoic Acid, 1 μM XXI, 10 μM ALk5i II, 1 μM T3, 20 ng/mL Betacellulin, 10 μg/mL Heparin.
6. Maturation: Dissociate the cell colonies using a TrypLE for 20–25 min followed by mechanical disruption with a 1000-μL pipette (*see* **Note 7**). Dilute the TrypLE with differentiation base media supplemented with 10 μM Y-27632 and centrifuge cells at 100 rcf for 2 min. Suspend in differentiation base media supplemented with 10 μM Y-27632. Vitamin Count using a hemocytometer and distribute cells into V-bottom ultralow adherent plates with 10,000 cells per well. Refresh media every other day.

3.5 Characterization of hPSC Aggregates

3.5.1 Immunostaining of hPSC Aggregates

Sectioning and Imaging

1. Wash encapsulated cells in PBS three times, with each wash spanning at least 5 min.
2. In order to retrieve the aggregates in the capsule, add 37.224 g/L EDTA solution (pH ≈ 7.6) and incubate at room temperature for 1–2 min with gentle agitation. The EDTA removes the Ca^{2+} ions from the alginate structure thereby breaking down the capsule.
3. Wash the freshly decapsulated aggregates with PBS to remove any traces of EDTA.
4. Add freshly prepared 4% paraformaldehyde to the aggregates and incubate at room temperature for 30 min.

5. Once the cells are fixed, use a graded series of ethanol (20%, 30%, 50%, 70%, 90%, 100%) to displace the water by dehydrating the cells.
6. Infiltrate the dehydrated aggregates by adding hot paraffin wax (heated to slightly above its melting point) in a mold with the aggregates and allow it to cool for 30 min to obtain wax blocks with embedded aggregates.
7. Section the wax blocks using a microtome to the desired thickness (usually between 5 and 20 μm) to prepare them for imaging.
8. Add citrate buffer to the slides and heat the slides (usually in an oven or a microwave) in order to expose the antigen sites and to allow the antibodies to bind (antigen retrieval) (*see* **Note 8**).
9. Wash the sections with PBS three times.
10. Permeabilize the cut sections with 0.1% Triton X-100 in PBS for 5 min to allow for the penetration of the antibodies.
11. Use a blocking buffer with 10% donkey serum for 1 h to minimize nonspecific binding of antibodies (*see* **Note 9**) or.
12. Add the primary antibodies diluted 1:200 in the blocking buffer and incubate overnight at 4 °C.
13. Wash the sections with PBS three times to remove unbound antibodies.
14. Add the appropriate secondary antibodies diluted (1:500) in the blocking buffer and incubate for 45 min at room temperature.
15. Wash the sections with PBS three times.
16. Use a mounting medium containing DAPI (such as Vectashield, Vector laboratories or Prolong Gold anti-fade, ThermoFisher) and cover the sections with a cover slip before imaging (*see* **Note 10**).

Whole-Mount Imaging

The **steps 1–4** are the same as that of Sectioning and Imaging starting from alginate encapsulated aggregates.

5. Wash the fixed cells with PBS three times.
6. Permeabilize the aggregates and block for nonspecific binding with 1% Triton X-100, 5% Serum in PBS for 2–4 h at room temperature.
7. Wash with PBS three times.
8. Add primary antibodies diluted 1:100 in the blocking buffer (used in **step 6**) and incubate at 4 °C overnight (*see* **Note 11**).
9. Wash with PBS (3×).
10. Add appropriate secondary antibodies diluted 1:500 in the blocking buffer and incubate either at room temperature for 2–4 h or overnight at 4 °C.

11. Wash with PBS three times and mount on depression slide using Vectashield or Prolong Gold antifade with a coverslip for imaging.

3.5.2 Flow Cytometry

1. Decapsulate the cells in alginate capsule by adding 37.224 g/L EDTA at room temperature for 1–2 min with gentle agitation.
2. Harvest the cells from aggregates by incubating them with Accutase for 5–10 min in the CO_2 incubator at 37 °C with gentle agitation to dissociate them and obtain a single cell suspension.
3. Centrifuge to obtain cell pellet and wash with PBS (3×).
4. Fix the cells using freshly prepared 4% paraformaldehyde in PBS for 30 min at room temperature.
5. Permeabilize the cells using 0.1% saponin with 0.5% BSA in PBS for 60 min at room temperature (*see* **Note 12**).
6. Wash the cells with PBS three times.
7. Incubate the cells with a Blocking Buffer for 60 min at room temperature to minimize nonspecific binding.
8. Wash the cells with PBS three times.
9. Add primary antibodies diluted 1:500 in the blocking buffer and incubate overnight at 4 °C.
10. Wash the cells with PBS three times.
11. Add the appropriate secondary antibodies diluted (1:1000) in the blocking buffer and incubate at room temperature for 1–2 h (*see* **Note 13**).
12. Wash the cells with PBS three times before running them in a flow cytometer (*see* **Note 14**).

3.5.3 RT-qPCR

1. Aspirate the cell media and transfer the alginate capsules to a 15-mL tube using a sterile metal spatula.
2. Decapsulate cells by adding EDTA solution equivalent to the volume of alginate and allow the capsules to dissolve for 2–3 min if polymerized with the calcium chloride solution and 10–12 min if the Ba-PLL solution was used.
3. Spin down the cell solution at 220–240 rcf for 4 min.
4. Aspirate supernatant and wash the cells two times with PBS.
5. Isolate the mRNA using a Nucelospin RNA II kit.
6. Determine the mRNA concentration and quality using a spectrophotometer. A 260/280 nm value above 1.6 signifies a good mRNA solution.
7. Use an Improm II Reverse Transcription kit to form the cDNA.

8. In each well of a 96-well qPCR plate, add 5 μL SYBER Green Master Mix, 2 μL nuclease-free H_2O, 2 μL primer, and 1 μL cDNA (*see* **Note 15**).
9. The cycles used in the qRT-PCR are denaturing for 10 s at 95 °C, then annealing at 53 °C for 20 s, and extension at 72 °C for 15 s for 50 cycles followed by a final step with a 30 s denaturing at 95 °C, 30 s annealing at 53 °C, and 30 s elongation 95 °C.
10. Normalize samples to a housekeeping gene, such as GAPDH, by subtracting a sample's average GAPDH Ct value from the other genes' Ct values for the same sample.

Overall, it was observed that synergizing biophysical induction with chemical induction, in particularly under 3D culture configuration, significantly enhanced the efficiency of differentiation. Further, the efficiency of chemical induction was largely dependent on the properties of encapsulating substrate, even though diffusion was never restrictive within the capsules. Cell growth was observed to be favorable under the low stiffness regime, and was highly suppressed under high stiffness conditions. Interestingly, the effect of differentiation was more complex and differed based on stage of differentiation, possibly due to the complexity of the interaction of physical cues with nonlinear signaling pathways. Increased alginate capsule stiffness appeared to promote TGFβ signaling during the definitive endoderm (DE) stage, which enhanced DE differentiation (Fig. 1). However, increased substrate stiffness also promoted sonic hedgehog signaling at the pancreatic progenitor (PP) stage, which suppressed PP differentiation. Overall, cell growth and hESC-PP differentiation was found to be favorable in the stiffness range of approximately 4–7 kPa.

3.6 Alginate Array Fabrication for Quantifying Effects of Combinatorial Perturbations

In order to enable simultaneous, multiparametric modification to the cell microenvironment, we developed an alginate array platform with capabilities of quantitative imaging to effectively measure the resulting cell fate [26]. Analysis of the data using a linear statistical model allowed decoupling of the complex interactions between the stem cells and the effect of their microenvironment. Thus, in combination with statistical modeling, the developed platform enabled the identification of the sensitivity of stem cell proliferation and pancreatic differentiation to multiparametric modulation. Figure 2 presents a schematic of the overall workflow.

1. Coat the culture surface with nitrocellulose.
2. In a well of a 6-well plate, spot 0.5–5 μL of the Ba-PLL solution in a square array with five microspots per $BaCl_2$ condition using a repeater pipette and allow the spots to dry overnight in biohazard safety cabinet (*see* **Note 16**).

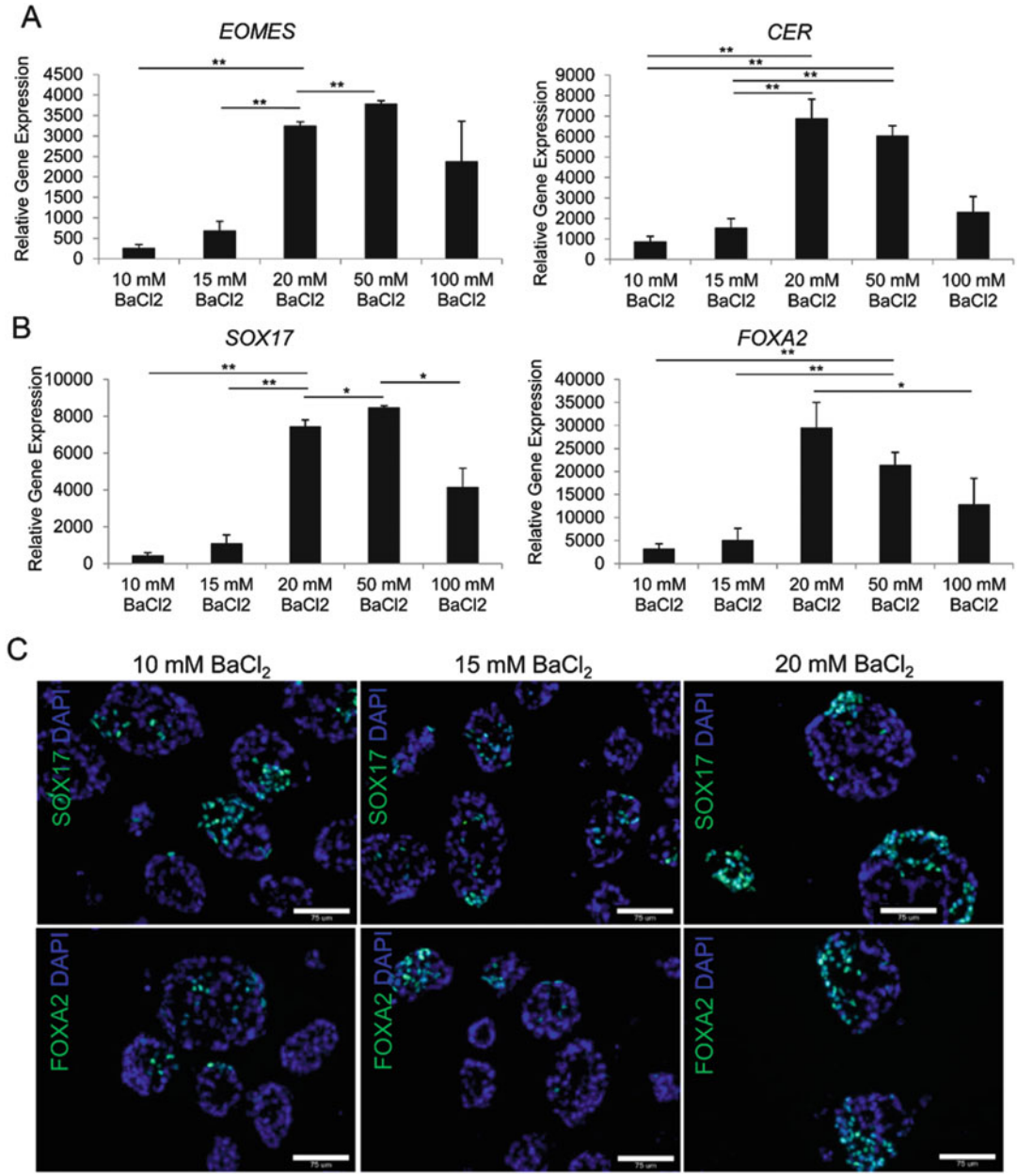

Fig. 1 Increased substrate stiffness enhances DE stage differentiation. (**a**) Relative gene expression of the mesendodermal genes EOMES and CER for each barium alginate condition at the DE stage, relative to undifferentiated hESC. (**b**) Relative gene expression of the definitive endoderm genes SOX17 and FOXA2 for each barium alginate condition at the DE stage, relative to undifferentiated hESCs. (**c**) Immunostaining of hESCs encapsulated with 10, 15, and 20 mM $BaCl_2$ at the DE stage, for SOX17 and FOXA2. Scale bar is 75 μm. (Adapted from [14])

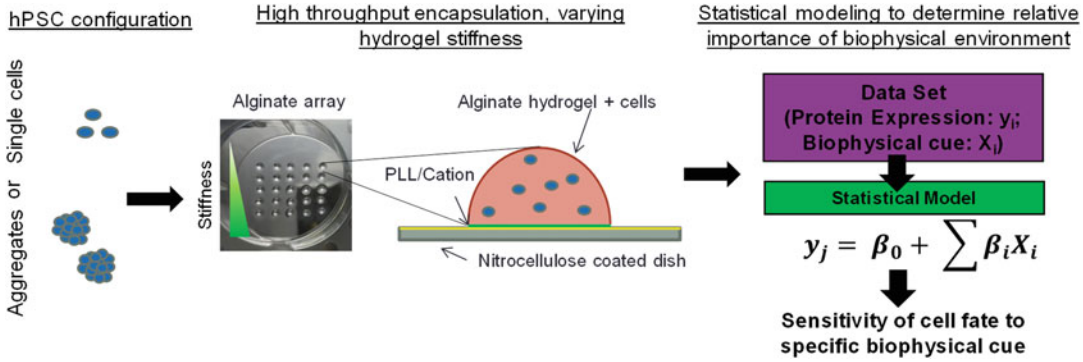

Fig. 2 Workflow for the 3D alginate array platform that allows for multiple combinatorial perturbations of insoluble differentiation cues on human pluripotent stem cells (hPSCs), namely hydrogel stiffness and cell–cell contact, during pancreatic differentiation. Our results indicated that while stiffness did influence proliferation and pancreatic differentiation, the effect of cell–cell contact was more significant. In combination with statistical modeling, the tools developed in this study allowed us to identify the sensitivity of hESC proliferation and fate to multiparametric modulation. (Adapted from [26])

3. For encapsulating single-cell hPSCs, prepare the cells on the day of encapsulation using the same steps from Subheading 3.1. For encapsulating hPSC aggregates, preparation must be done 2 days before encapsulation. To form the aggregates, obtain single cells using Subheading 3.1 steps and add 1×10^6 cells to a low adherent 30 mm dish with a final volume of 2 mL single cell culture media per dish. Culture the cells in a 37 °C and 5% CO_2 incubator on a plate shaker set to 55 rpm for 2 days.
4. Add a sufficient volume of alginate solution to make a 5×10^6 cell per mL alginate solution (single cell encapsulation) or 1 mL alginate solution per dish of aggregates (aggregate encapsulation) into a 50 mL tube and place it into a 37 °C water bath for 20 min before encapsulating the cells.
5. Add the desired number of single cells or aggregate cultures to a 15-mL falcon tube and centrifuge at 220–240 rcf for 4 min.
6. Aspirate supernatant and resuspend cells in the desired volume of alginate solution to achieve a seeding density of 5×10^5 cells/mL. Pipette the solution up and down with a 1000-μL pipette to create a homogenous single cell suspension, while avoiding introducing air bubbles to the solution.
7. The cell–alginate solution should be spotted onto the dried Ba-PLL arrays using the repeater pipette with the same volume used for the Ba-PLL solution and allow the alginate to polymerize for 5 min before washing with PBS (3×).
8. After last PBS wash, incubate cells in 1 mL mTeSR1.

9. Continue culturing cells in 1 mL mTeSR1 for 2 days after encapsulating before starting the differentiation mentioned in Subheading 3.4.
10. Analyze aggregates using LICOR (Subheading 3.7) at the desired stages of differentiation.

3.7 Imaging 3D Aggregates in the Array using LICOR

The LICOR system is capable of fast and high-throughput imaging of specimens tagged with the near-IR fluorescent dyes such as IR dye 680 LT and IR dye 800 CW. It has a wide linear dynamic range, which implies that fluorescence intensity is proportional to concentration over a wider range that results in easily detectable contrast and allows for accurate quantitative analysis of protein expression. The use of near-IR Laser and dyes eliminates the interference of auto-fluorescence signals that are usually observed in biological samples imaged with visible light imaging systems. In addition, the narrow wavelength band of the IR lasers ensures reduced background signals leading to superior signal-to-noise ratio, which is favorable for quantification and analysis. The following steps describe the use of LICOR system to image 3D aggregates encapsulated in an alginate array (described in Subheading 3.6) and quantify the protein expression from the intensity of fluorescence signal.

1. Wash the alginate array containing aggregates in PBS three times.
2. Fix the aggregates in the alginate capsule with 4% paraformaldehyde for 30 min at room temperature.
3. Wash the alginate array in PBS three times to remove traces of the fixative.
4. Permeabilize the aggregates in the alginate array with 0.1% Triton X-100 for 15 min and use the Odyssey blocking buffer (LICOR Biosciences) for 1 h at room temperature.
5. Wash in PBS three times.
6. Add the primary antibodies diluted 1:200 in the blocking buffer and incubate at 4 °C overnight. Generally, the antibodies are diluted to half their suggested concentration as the combination of near-IR dyes and sensitive scanner in LICOR can detect signals much better than conventional imaging.
7. Wash in PBS three times.
8. Add the appropriate secondary antibodies which are tagged with near-IR dyes diluted (1:800) in the blocking buffer and incubate them for 1 h at room temperature and counterstain with DRAQ 5 (1:10,000).
9. Wash in PBS three times before imaging with LICOR.

10. Image the aggregate array using appropriate wavelengths and sensitivity. Use appropriate negative controls to obtain the background intensity values (*see* **Note 17**).
11. Normalize the intensities of target antibody signals with the fluorescence signal of DARQ5 which is directly related to the DNA content/cell number in the capsule.

3.8 Statistical Modeling to Decouple the Effect of Multiparametric Perturbation

Cation concentrations and seeding configurations are the two externally modulated input parameters, which affect the measured outcomes, namely degree of differentiation and proliferation. To evaluate the relative importance of these input parameters in controlling the outcome, a regression analysis was performed. Linear regression analysis (which implies that overall equation is linear with respect to the proportionality coefficients to the dependent variables) is suitable for this analysis; however, we need to consider the different nature of the input variables. For example, cation concentration is a continuous variable, while configuration is a categorical variable.

3.8.1 Evaluating Importance of Cation Concentration

1. As a first step, only cation concentration was considered. The regression equation for this case becomes,

$$\Upsilon = \alpha + \sum_{i=1}^{3} \beta_i C^i \tag{1}$$

where Υ is the outcome marker (protein content in sample normalized to the DNA content), for example, Ki67/DNA and SOX17/DNA. C is the concentration of the cation and here we allow a third-order polynomial relationship. Each term in the RHS of Eq. (1) is a predictor. The intercept α and coefficients β_i are the unknown parameters to be estimated using the training dataset. For each culture configuration and marker, the parameters are determined separately.

2. The statistical model (Eq. 1) was encoded as a symbolic function and parameters (α, β_i) estimated using the *fitlm* function in MATLAB (R2017b). This function outputs the estimates of the coefficient, their standard errors, t-statistic for each coefficient (which tests the null hypothesis for each coefficient being zero vs. it being non-zero both in the presence of other predictors) and the corresponding p-value for the t-statistic.
3. A least squares objective function was chosen which minimizes the sum of squares of residuals between the model (Eq. 1) and observed data.
4. To evaluate statistical significance of the model, given the underlying uncertainty in the observations (from biological replicates), a bootstrapping approach was used [27]. Using random sampling with replacement technique, surrogate datasets were generated from the individual biological replicates,

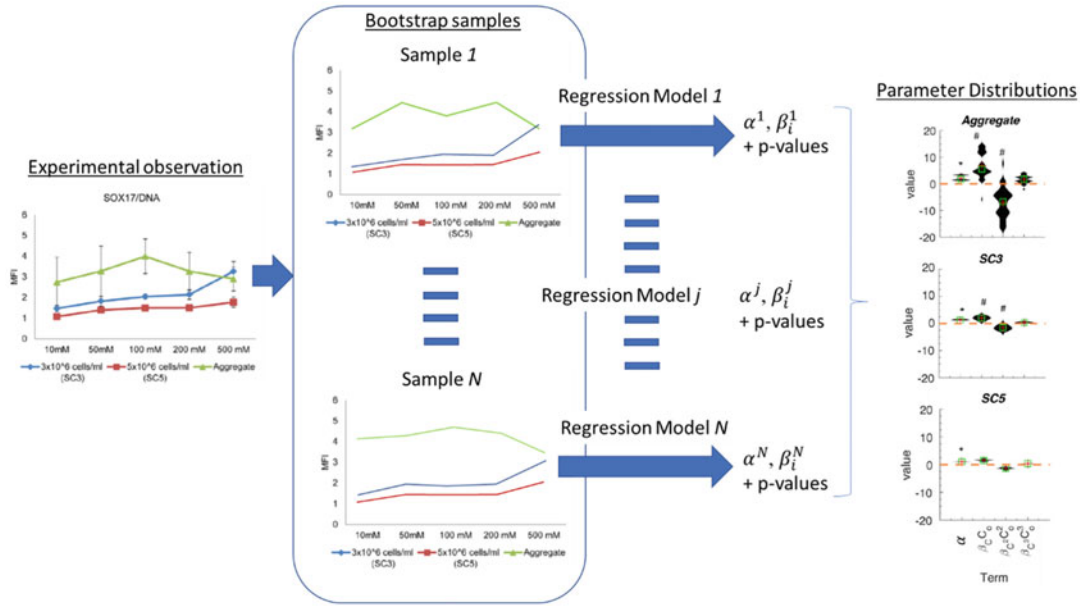

Fig. 3 Workflow for statistical analysis to identify the sensitivity of hESC proliferation and fate to multi-parametric modulation. From left to right: Experimental dataset for SOX17/DNA for five cation concentrations and three configurations, with multiple biological replicates. Bootstrap samples are generated from this dataset and regression is performed on each dataset separately, giving rise to parameter distributions. Parameter distributions of each linear and nonlinear term of Eq. (1) are shown as violin plots. Overall, cation concentration (hence, substrate properties) influence the differentiation outcome in the aggregate configuration, with relatively minor effects in the other configurations. (Adapted from [26])

and it was ensured that each such surrogate dataset contained the same number of cation concentrations (total 5) and configuration types (total 3). Regression was performed on each such surrogate dataset separately. *See* Fig. 3 for a summary of the entire workflow.

5. This gives rise to a distribution of p-values and of the coefficients (violin plots in Fig. 3). These distributions were monitored for convergence to find optimal number of bootstrap samples. A total of 1000 bootstrap samples were sufficient to make reliable conclusions for the current dataset.
6. The R^2 statistic was also monitored, and most bootstrap samples had values between 0.5 and 0.95, with median values being closer to the upper end.
7. Violin plots in Fig. 3 shows the coefficients for SOX17/DNA for the three configurations, with each higher order term brought to the same units using an average concentration, $C_0 = 255$ mM. The conclusions are insensitive to the value of this factor within the concentration range tested in this study.

8. Overall, it was seen that the cation concentration (hence, substrate properties) influence the differentiation outcome in the aggregate configuration, with relatively minor effects for the other configurations. The p-values lie in the range $(0.01, 1)$ for the aggregate condition.

3.8.2 Evaluating Combined Importance of Cation Concentration and Culture Configuration

1. To introduce configuration, which is categorical, Eq. (1) was expanded as follows:

$$\Upsilon = \alpha + \sum_{i=1}^{3} \beta_i C^i + \sum_{i=2}^{3} \beta_{\text{config\_}i} \text{Config\_}i + \sum_{i=2}^{3} \beta_{C\times\text{config\_}i} C \times \text{Config\_}i \quad (2)$$

   Here, the terms are similar as Eq. (1), with the difference being the incorporation of the configuration term, Config_i, which takes binary values. To simplify the analysis (without loss of accuracy), only configurations 2 (SC3) and 3 (SC5) appear in the equation. These are coded such that Config_2/Config_3 take on values 1/0 and 0/1 to indicate SC3 and SC5 and 0/0 for the aggregate condition. Therefore, the terms where Config_2/Config_3 appears capture the influence of SC3 and SC5 relative to the aggregate configuration. Concentration term in Eq. (2) appears as a third-order polynomial by itself or as a bilinear term with configuration.

2. The coefficients for these equations are obtained in the same manner as Subheading 3.8.1, but it was seen that comparatively larger number of bootstrap replicates were necessary for convergence of some parameters (minimum of 5000).

3. The mean coefficients for each term and the differentiation markers are shown in Fig. 4. From the current analysis, we can conclude that the configuration terms are relatively more important than the concentration terms (which are important for selected markers, but not as a bilinear term with configurations 2 and 3).

4 Notes

1. Differentiation will appear more segmented than surrounding smooth cell growth. Overgrowth will be darker and bulging than surrounding cells.
2. Media should be added along the side of the well and not directly onto the cells and place the cells in a 37 °C and 5% CO_2 incubator.
3. Check periodically for the cell colonies to begin lifting off the plate.

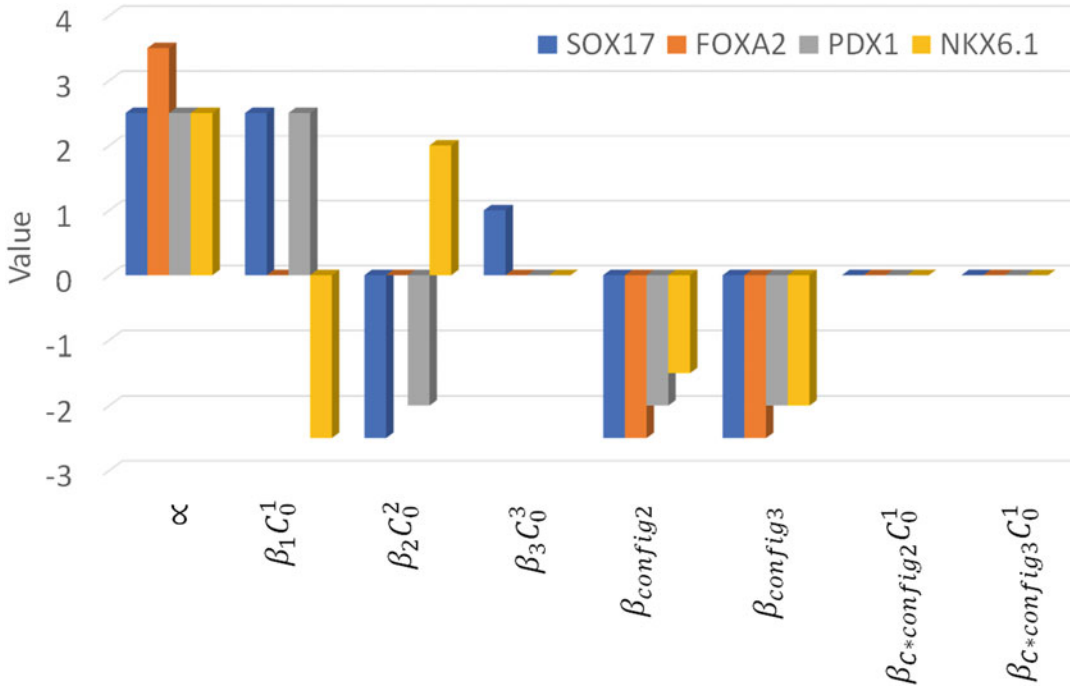

Fig. 4 Mean regression coefficients for DE and PP markers. For most markers, we see that the configuration terms are important to set the mean expression and concentration terms fine tunes the expression around the mean value

4. Pipette the solution up and down with a 1000-μL pipette to create a homogenous single cell suspension, while avoiding introducing air bubbles to the solution.
5. Draw the alginate into the syringe by pinching the falcon tube to allow the syringe to fully fit inside the tube and more easily transfer the alginate while avoiding forming bubbles.
6. Ensure that the successive indents are sufficiently spaced apart so that they do not interfere with each other. Usually, the space between indents should be at least 4× the size of the indent.
7. Slowly pipette the aggregates and only pipette 5–10 times. If the aggregates do not begin breaking apart immediately, put back in incubator for 3 more min to allow enzyme to work longer.
8. Antigen retrieval process is specific to the target antibody; different antibodies may respond better to other retrieval buffers.
9. Permeabilization and blocking steps can be combined into a single step for larger samples/thicker sections.
10. It is always advisable to image immediately after the antibody labeling procedure is complete. However, if necessary, the samples can be stored at 4 °C after mounting with Vectashield/Gold Antifade for up to 2 weeks.

11. While imaging aggregates, antibody penetration is generally an issue when the aggregates are larger than 200 μm. Hence, it is suggested to incubate primary and secondary antibodies overnight at 4 °C.
12. Saponin is a milder permeabilizing agent compared to Tween-20 and Triton X-100. Stronger permeabilizing agents can sometimes break down the cell membrane when used with single cell suspensions.
13. The concentration and time of incubation for the primary and secondary antibodies need to be optimized individually. Here we have suggested a good starting point.
14. Appropriate negative (secondary only) controls need to be run through the flow cytometer to eliminate false positives.
15. Add the cDNA to the very bottom of the well while avoiding the sides of the well before adding the other components. Make a premade mix of the Master Mix, H_2O, and primers and add them to the sides of the well, while avoiding touching the bottom where the cDNA is located.
16. Place the plate toward the back of the cabinet to let the airflow to ensure the liquid is evaporated.
17. Since quantitative analysis is done on images obtained from LICOR, it is generally suggested to use black-sided well plates for imaging to minimize scattering artifacts from interfering with the data collection.

References

1. Discher DE, Mooney DJ, Zandstra PW (2009) Growth factors, matrices, and forces combine and control stem cells. Science 324 (5935):1673–1677
2. Discher DE, Janmey P, Wang YL (2005) Tissue cells feel and respond to the stiffness of their substrate. Science 310(5751):1139–1143
3. Christopherson GT, Song H, Mao HQ (2009) The influence of fiber diameter of electrospun substrates on neural stem cell differentiation and proliferation. Biomaterials 30(4):556–564
4. Guilak F et al (2009) Control of stem cell fate by physical interactions with the extracellular matrix. Cell Stem Cell 5(1):17–26
5. Lee DA et al (2011) Stem cell mechanobiology. J Cell Biochem 112(1):1–9
6. Reilly GC, Engler AJ (2010) Intrinsic extracellular matrix properties regulate stem cell differentiation. J Biomech 43(1):55–62
7. Gasiorowski JZ, Murphy CJ, Nealey PF (2013) Biophysical cues and cell behavior: the big impact of little things. Annu Rev Biomed Eng 15:155–176
8. Engler AJ et al (2006) Matrix elasticity directs stem cell lineage specification. Cell 126 (4):677–689
9. Candiello J et al (2013) Early differentiation patterning of mouse embryonic stem cells in response to variations in alginate substrate stiffness. J Biol Eng 7(1):9
10. Jaramillo M et al (2015) Inducing endoderm differentiation by modulating mechanical properties of soft substrates. J Tissue Eng Regen Med 9(1):1–12
11. Task K et al (2014) Systems level approach reveals the correlation of endoderm differentiation of mouse embryonic stem cells with specific microstructural cues of fibrin gels. J R Soc Interface 11(95):20140009
12. Zhang XN et al (2012) Analysis of regulatory network involved in mechanical induction of embryonic stem cell differentiation. PLoS One 7(4):e35700

13. Richardson T, Kumta PN, Banerjee I (2014) Alginate encapsulation of human embryonic stem cells to enhance directed differentiation to pancreatic islet-like cells. Tissue Eng Part A 20(23–24):3198–3211
14. Richardson T et al (2016) Capsule stiffness regulates the efficiency of pancreatic differentiation of human embryonic stem cells. Acta Biomater 35:153–165
15. Lee LH et al (2009) Micropatterning of human embryonic stem cells dissects the mesoderm and endoderm lineages. Stem Cell Res 2 (2):155–162
16. Flaim CJ, Chien S, Bhatia SN (2005) An extracellular matrix microarray for probing cellular differentiation. Nat Methods 2(2):119–125
17. Derda R et al (2010) High-throughput discovery of synthetic surfaces that support proliferation of pluripotent cells. J Am Chem Soc 132 (4):1289–1295
18. Ankam S et al (2013) Substrate topography and size determine the fate of human embryonic stem cells to neuronal or glial lineage. Acta Biomater 9(1):4535–4545
19. Ranga A et al (2014) 3D niche microarrays for systems-level analyses of cell fate. Nat Commun 5:4324
20. Huang X et al (2012) Microenvironment of alginate-based microcapsules for cell culture and tissue engineering. J Biosci Bioeng 114 (1):1–8
21. Morch YA et al (2006) Effect of Ca2+, Ba2+, and Sr2+ on alginate microbeads. Biomacromolecules 7(5):1471–1480
22. Chan ES et al (2011) Effect of formulation of alginate beads on their mechanical behavior and stiffness. Particuology 9(3):228–234
23. Lee BH, Li B, Guelcher SA (2012) Gel microstructure regulates proliferation and differentiation of MC3T3-E1 cells encapsulated in alginate beads. Acta Biomater 8(5):1693–1702
24. Banerjee A et al (2009) The influence of hydrogel modulus on the proliferation and differentiation of encapsulated neural stem cells. Biomaterials 30(27):4695–4699
25. Musah S et al (2012) Glycosaminoglycan-binding hydrogels enable mechanical control of human pluripotent stem cell self-renewal. ACS Nano 6(11):10168–10177
26. Richardson TC et al (2018) Development of an alginate array platform to decouple the effect of multiparametric perturbations on human pluripotent stem cells during pancreatic differentiation. Biotechnol J 13(2):1700099
27. Mathew S et al (2012) Analysis of alternative signaling pathways of endoderm induction of human embryonic stem cells identifies context specific differences. BMC Syst Biol 6:154

Chapter 7

Rewiring Endogenous Bioelectric Circuits in the *Xenopus laevis* Embryo Model

Vasilios Nanos and Michael Levin

Abstract

Embryogenesis, as well as regeneration, is increasingly recognized to be orchestrated by an interplay of transcriptional and bioelectric networks. Spatiotemporal patterns of resting potentials direct the size, shape, and locations of numerous organ primordia during patterning. These bioelectrical properties are established by the function of ion channels and pumps that set voltage potentials of individual cells, and gap junctions (electrical synapses) that enable physiological states to propagate across tissue networks. Functional experiments to probe the roles of bioelectrical states can be carried out by targeting endogenous ion channels during development. Here, we describe protocols, optimized for the highly tractable *Xenopus laevis* embryo, for molecular genetic targeting of ion channels and connexins based on CRISPR, and monitoring of resting potential states using voltage-sensing fluorescent dye. Similar strategies can be adapted to other model species.

Key words Bioelectricity, Ion channel, CRISPR, Frog embryo

1 Introduction

In addition to biochemical and gene regulatory networks, ion channel-mediated slow changes of resting membrane potentials V_{mem} are pivotal for developmental processes such as cell differentiation [1], proliferation [2], and migration [3]. Bioelectric signaling has been shown to contribute essentially to the complex process of morphogenesis, where tissues exploit endogenous physiological signals passing between all cells (not only neurons) to coordinate cell growth with large-scale patterning of the developing embryo [4]. Through spatiotemporal gradients of resting membrane potentials, bioelectric signals provide long-range instructive cues to coordinate large-scale tissue patterning [5], growth control, and regeneration [6, 7] by means of cell-to-cell communication implemented by electrical synapses known as gap junctions [8].

Mo R. Ebrahimkhani and Joshua Hislop (eds.), *Programmed Morphogenesis: Methods and Protocols*, Methods in Molecular Biology, vol. 2258, https://doi.org/10.1007/978-1-0716-1174-6_7,

Endogenous bioelectric prepatterns are established by the function of a range of ion channel and pump proteins [9]. Two fundamental strategies are available to probe the functional role of bioelectric properties [10]: (a) gain-of-function, in which exogenous well-characterized channels are misexpressed in cells to depolarize or hyperpolarize them [11–14], and (b) loss-of-function, in which native ion fluxes are inhibited or upregulated by pharmacological or genetic methods. These means of manipulating ion channel activity enable functionally interfering with bioelectrical signaling pathways in order to probe their role in developmental or regenerative morphogenesis.

An easy and broadly used method to alter ion channel activity and to probe their effects on V_{mem} and developmental outcomes is the application of chemical ion channel modulators—pharmacological blockers or activators [15, 16].

These ion channel modulators can target several types of ion channels leading to de- or hyperpolarization of the resting membrane potential. However, the use of these inhibitors/activators is limited by several factors. First, for many ion channels there are no specific blockers available at all. Second, for ion channels that are broadly expressed in the whole body, it is very difficult to target specific locations and make spatially specific changes to the bioelectric prepattern. This can result in serious side effects such as long QT-Syndrome in heart or brain seizures, confounding both clinical application and phenotype analysis in basic studies in model systems. Finally, pharmacological experiments are best used as a screen, leveraging the ability of drugs to target families and subfamilies of channels, to focus attention on specific targets for subsequent genetic validation.

With the invent of CRISPR-Cas-based genome editing systems, it is now possible to create functional knockouts of specific genes. This allows to circumvent many of the above discussed off target effects induced by chemical ion channel modulators. These techniques enable the creation of models for known channelopathies [12, 17–25], as well the discovery of new roles for channel genes.

CRISPR also enables for the targeting of specific tissues and cell types (Fig. 1). This can be achieved by taking advantage of the fact that many functional ion channels are built of several subunit complexes, creating tissue-specific ion channel isoforms [26]. Moreover, instead of simply generating knockouts, it is now possible to interfere with the process of protein synthesis and the biophysical properties of the ion channels at various levels, generating gain- or loss-of-function mutations. For instance, the zebrafish another-long-fin (alf^{dty86}) mutant is a gain-of-function mutation of the kcnk5b potassium channel leading to increased K^+ conductance. This results in the hyperpolarization of the membrane potential of mesenchymal cells located at the distal tip of the fins, inducing

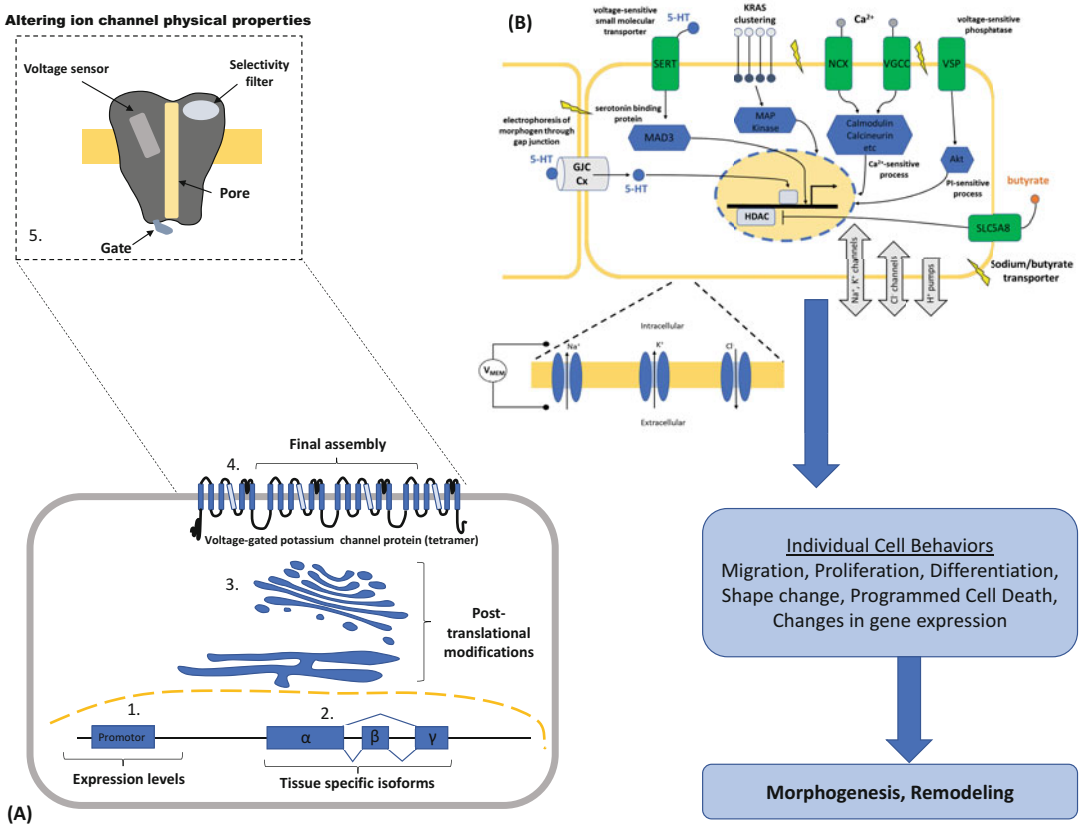

Fig. 1 Targeting ion channel functionality at different levels using CRISPR

higher cell proliferation rates and allometrically overgrown fins and barbels [27]. On the other hand, the short-of-fin missense mutant (sof^{J7e1}) of the Cx43 gene has been shown to reduce gap junction ionic conductance, resulting in disturbed cell-to-cell communication and shorter fins [28].

On the transcriptional level, gene expression can be manipulated using a nuclease-deactivated Cas9 (dCas9) targeted to the promotor sequence. dCas9 then functions as a transcriptional repressor by sterically blocking RNA polymerase from binding the promotor. Vice versa, it is also possible to convert dCas9 into a transcription factor by fusing it to an effector, subsequently resulting in higher expression of the ion channel [29]. On the posttranscriptional level, protein folding and trafficking can be targeted, affecting the final assembly of the protein. The biophysical properties of an ion channel can be altered by targeting several ion channel structures such as the voltage sensor (in the case of voltage-gated channels), the ion channel pore and gate, as well as the ion selectivity filter, resulting in aberrant ion channel conductance and altered functional linkage between ion channels and other cell components that regulate the channel function.

To investigate the molecular mechanisms by which bioelectric signaling regulates morphogenesis demands a model system that is established for biophysical and state-of-the-art molecular genetic techniques, in which outcomes from tissue structure, organ morphology, and functional physiology can be readily characterized. *Xenopus laevis* has been extensively used for studying cell and developmental biology [30–34], offering the advantage of large and easily accessible embryos throughout development, which makes these embryos highly suitable for manipulations such as microinjections and phenotypic screening of embryonic stages.

Here we describe how CRISPR-Cas9 can be used to study the role of ion channel-mediated signaling pathways involved in morphogenesis, using Xenopus as a model system. We show how to assay changes in resting membrane potentials using the voltage sensitive reporter dye DiBAC4(3) [35, 36], as well as changes in growth dynamics by morphometric measurements.

2 Materials

2.1 Guide RNA Design

Various online web tools are available for the design of gRNAs (e.g., https://chopchop.cbu.uib.no/).

2.2 CRISPR-Cas9 Microinjection

Composition and amount of Cas9 and sgRNA injection mixture depend on the Xenopus species being used and the actual cell stage. For easier injection use dyes such as phenol red since Cas9 and sgRNA solution is colorless.

It can be useful to label injected cells with mRNA expressing fluorescent proteins (e.g., GFP), for tracing injected cells and validation of injection efficiency.

2.3 Frog Handling and Obtaining Fertilized Eggs

2.3.1 Inducing Ovulation

1. Human chorionic gonadotropin (hCG). 500–800 units, depending on frog size.
2. Use a fine needle (26 gauge) attached to a 1-mL syringe for the injection.

2.3.2 Manual Egg Collection

1. Petri dish 80 mm.
2. 0.1 M $CaCl_2$ (11.1 g/L)
3. 10× MBS salts;
   880 mM NaCl.
   10 mM KCl.
   10 mM $MgSO_4$.
   50 mM HEPES (pH 7.8).
   25 mM $NaHCO_3$.
   Adjust solution to a final pH of 7.8 and autoclave.

4. High-salt MBS;
   7 mL 0.1 M $CaCl_2$.
   100 mL 10× MBS salts.
   4 mL 5 M NaCl.
   888 mL water.

2.3.3 Isolating Testes

1. 0.05% Benzocaine
2. Store testes in a solution of 80% calf serum, 20% 1× high-salt MBS (*see* Table 1) and antibiotic (0.05 mg/mL gentamycin).

2.3.4 Preparing Embryos for Microinjection

Marc's Modified Ringers (MMR);
0.1 M NaCl.
2.0 mM KCl.
1 mM $MgSO_4$.
2 mM $CaCl_2$.
5 mM HEPES (pH 7.8).
0.1 mM EDTA or adjust to pH 7.4.

2.3.5 Dejellying Embryos

1× MMR, or water, with 2% (w/v) cysteine adjusted to pH 8.0.

2.3.6 Microinjection and Embryo Handling

1. Variable temperature incubators.
2. Dissecting microscope with 50× magnification or higher.
3. Fluorescence microscope (for voltage dye measurements) plus filter.
4. Microinjector.
5. Micromanipulator (alternatively it is also possible to do free-handed microinjections).
6. Microscope micrometer calibration glass.
7. Needle puller.
8. Needle (1 mm × 10 cm microinjection capillaries).
9. Microfilament pipette tips for loading the needle.
10. Hair loop for moving embryos during microinjection.
11. Ficoll 400 (2–5% in 1/3 MMR).
12. 4 L plastic containers (for the frogs).

2.3.7 Bioelectric Measurements and Reagents

1. DiBAC4(3) (powder stored at 4 °C).
2. Prepare a DiBAC4(3) stock solution of 1 mg/mL (1.9 mM) in DMSO. Store at room temperature for up to 3 months.
3. Fluorescent microscope with FITC (GFP) cube.

Table 1
Composition and amount of Cas9 and sgRNA injection mixture

For *Xenopus tropicalis*	Volume	Final concentration	For 4 nL
For a 6-μL mix:			
2 mg/mL Cas9 protein	1.2 μL	0.4 ng/nL	1.6 ng
600–1200 ng/μL sgRNA	1 μL	100–200 pg/nL	400–800 pg
Fill to 6 μL with RNAse-free water, dye, or fluorescent mRNA			
Injection volume at 1 cell stage			4 nL
For *Xenopus laevis*	**Volume**	**Final concentration**	**for 10 nL**
For a 6-μL mix:			
2 mg/mL Cas9 protein	0.3 μL	0.1 ng/nL	1 ng
600–800 ng/μL sgRNA	0.5 μL	50–67 pg/nL	500–670 pg
Fill to 6 μL with RNAse-free water, dye, or fluorescent mRNA			
Injection volume at 1 cell stage			10 nL

Different injection volumes and final concentrations of Cas9 and sgRNA are recommended for *Xenopus laves* and *Xenopus tropicalis*

3 Methods

The choice of electrogenic target is made with respect to several considerations. Ideally, a specific channel or pump is already implicated by genetic studies, electrophysiology, or the outcome of a tiered drug screen [15, 16]. In the latter case, it may be a family whose members may need to be targeted individually and in combination. Combination knockout may be essential due to the high compensation and redundancy seen among channels within and across families (e.g., [37]). The effects of the knockdown of a specific type of conductance on V_{mem} is not always obvious, and it is possible to use physiology simulators such as BETSE to model the bioelectrical consequences of loss-of-function of specific channels, pumps, or connexins, at the single cell and tissue level [38, 39].

3.1 Isolating Testes and Sperm

1. Sacrifice a male frog by placing it into a plastic container filled with water, containing 0.05% benzocaine for 30–60 min (*see* **Note 1**).
2. Take out the frog and place it on a paper towel with the belly upside. Then remove the skin at the region of the lower belly using forceps and a scissor.
3. Cut on either side along the dorsal midline to expose the viscera.

4. Now it is possible to pull out the testes which are attached to the fat body. Remove the testis from the surrounding tissue with a scissor (*see* **Note 2**).
5. Removed testes can be stored for several days in 80% calf serum, 20% 1× high-salt MBS with 0.05 mg/mL of gentamycin at 4 °C (*see* **Note 3**).

3.2 Obtaining Fertilized Eggs

3.2.1 Inducing Ovulation

To induce ovulation, inject 500–800 units of human chorionic gonadotropin (hCG) into the dorsal lymph sac of a female frog (*see* **Note 4**).

3.2.2 Collecting the Eggs

1. Before egg collection females should be kept in water with 20 mM NaCl and 5 μg/mL gentamycin and a pH of 7.0. This procedure minimizes the risk of diseases.
2. Egg laying can be induced by holding the frogs with two hands and gently massaging the frog along the dorsal line. The frog should be hold over a clean Petri dish filled with 1× high-salt MBS. This process should not last longer than 3 min (*see* **Note 5**).
3. After egg laying, frogs should be kept in isolation for 12–24 h in water with 20 mM NaCl and 5 μg/mL gentamycin as previously described.

3.2.3 In Vitro Fertilization

1. Before fertilization, all buffer should be removed from the eggs using a pipette.
2. It is sufficient to use just a small piece of the testes, to fertilize thousands of eggs. Smash the piece of testes in high-salt MBS in a ration of approximately 1/20 and mix the sperm with the eggs. The remaining testes can be kept stored at 4 °C and used for later fertilizations.
3. Use a pair of forceps to separate eggs from each other and fill the dish with 0.1× MBS (*see* **Note 6**).

3.3 CRISPR Injections

3.3.1 Dejellying

1. Replace the old buffer by 1× MMR (or water) with 2% (w/v) cysteine at pH 8.0. Keep the embryos for approximately 4 min in the buffer and swirl regularly (*see* **Note 7**).
2. Remove the cysteine containing buffer and rinse 10 times for 10 min in 0.1× MBS (*see* **Note 8**).
3. Place embryos in a clean dish with 0.1× MBS. Remove dead embryos (*see* **Note 9**).

3.3.2 Micro Injection

1. Transfer dejellied embryos into clean injection dish containing a solution of Ficoll 2–5% in 1/3 MMR.
2. Prepare Cas9 protein, sgRNA, and tracer (optional) mixture dissolving in RNAse-free water as described (*see* Table 1).

3. Fill injection needle with the injection mixture and calibrate injection volume (*see* **Note 10**).
4. Embryos can be injected at a single or multicell stages (leads to mosaics). Injection can be performed using a micromanipulator or freehanded (with some practice this is easier and much faster), use a hair loop to position and hold embryos during the procedure. Embryos should be approached in an 45° angel with the injection needle.

3.4 Measuring Relative Resting Membrane Potentials

1. Dilute stock solution 1:1000 in water (or the medium in which the embryos are kept) (*see* **Note 11**).
2. Fill the Petri dish containing the embryos with the diluted DiBAC4(3) solution and incubate embryos for 20 min (*see* **Note 12**).
3. Take images of the embryos using a fluorescent microscope. Embryos should stay in the DiBAC solution during imaging **(***see* **Note 13)**.
4. Take a darkfield and a flatfield image (*see* **Note 14**).
5. Analyze darkfield–flatfield corrected images by measuring fluorescence intensities using image analysis software (e.g., ImageJ).

For more detailed experimental procedures, *see* [40, 41].

4 Notes

1. There should be no detectable heartbeat anymore. The animal should be decapitated using scissors to ensure death.
2. The testes are fairly easy to recognize. The fat body has a yellow color while the testes are white and covered with capillaries.
3. Sperm quality decreases after 48 h.
4. It is recommended to prime females which have never been induced to ovulate before, or the last induction is more than 6 months ago, with 50 units of hCG. This should be done at least 5 days before ovulation will be induced.
5. Eggs can be collected every hour for the first 2–3 h and thereafter with increasing time intervals. A maximum of six collections is possible throughout the day.
6. One can tell fertilized from unfertilized eggs by squeezing them with a hair loop or forceps. Successfully fertilized eggs are elastic and more resistant to pressure while unfertilized eggs are soft.

7. It is best not to start with dejellying during the first 30 min postfertilization since the vitelline membrane thickens during that time which is important for the protection of the sensitive embryos.
8. Embryos are sensitive to the cysteine treatment. It is important to avoid too long exposure and to rinse the embryos thoroughly to remove cysteine completely.
9. Keep embryos at low density (maximum. 100 embryos per 80-mm Petri dish). Dead embryos should be removed as early as possible and the buffer should be changed several times.
10. Calibration of injection volume: The first step in calibrating the injection volume is to backfill the injection needle using a pipette with a narrow tip. Mount the needle on the injector. Next, the tip of the needle needs to be broken creating an opening of approximately 10 μM, use forceps for breaking the tip.

    A microscope micrometer calibration glass mounted under a microscope can be used to estimate the injection volume by measuring the radius r of the droplet. Injection volume can be calculated using the equation $v = 4/3\pi r^3$. Volume can be further adjusted by manipulating injection pressure and injection time. Constant leaking or sucking in of liquid into the needle can be fixed by adjusting the balance. Each needle needs to be calibrated separately.
11. DiBAC4(3) is a negatively charged voltage-sensitive reporter dye. The more positive (depolarized) the resting membrane potential becomes the more DiBAC4(3) accumulates in the cell, resulting in an increasing fluorescent signal.
12. Tadpoles can be used as well but need to be anaesthetized before to avoid movements.
13. It is important to use the same exposure time for all images; otherwise, it will be impossible to make a quantitative analysis. It is also ideal to compare images from samples obtained on the same day, from the same batch of dye.
14. A darkfield image is an image taken while the shutter is closed. This is important to correct for the noise introduced by the camera. Correct your actual fluorescent images of the embryos by subtracting the darkfield image, as well as the Flatfield image. Take a Flatfield image of the medium with the DiBAC4(3). The picture should be out of focus as much as possible. This is important to detect uneven illumination. Each darkfield corrected image needs to be divided by the darkfield corrected flatfield image.

References

1. Sundelacruz S, Levin M, Kaplan DL (2008) Membrane potential controls adipogenic and osteogenic differentiation of mesenchymal stem cells. PLoS One 3:e3737
2. Sundelacruz S, Levin M, Kaplan DL (2009) Role of membrane potential in the regulation of cell proliferation and differentiation. Stem Cell Rev Rep 5:231–246
3. Funk RH (2015) Endogenous electric fields as guiding cue for cell migration. Front Physiol 6:143
4. Levin M, Martyniuk CJ (2018) The bioelectric code: an ancient computational medium for dynamic control of growth and form. Biosystems 164:76–93. https://doi.org/10.1016/j.biosystems.2017.08.009
5. Adams DS et al (2006) Early, H+-V-ATPase-dependent proton flux is necessary for consistent left-right patterning of non-mammalian vertebrates. Development 133:1657–1671
6. Levin M (2017) Seminars in cell & developmental biology. Elsevier, Amsterdam, pp 543–556
7. McLaughlin KA, Levin M (2017) Bioelectric signaling in regeneration: mechanisms of ionic controls of growth and form. Dev Biol 433 (2):177–189
8. Mathews J, Levin M (2017) Gap junctional signaling in pattern regulation: physiological network connectivity instructs growth and form. Dev Neurobiol 77:643–673. https://doi.org/10.1002/dneu.22405
9. Bates E (2015) Ion channels in development and cancer. Annu Rev Cell Dev Biol 31:231–247. https://doi.org/10.1146/annurev-cellbio-100814-125338
10. Adams DS, Levin M (2013) Endogenous voltage gradients as mediators of cell-cell communication: strategies for investigating bioelectrical signals during pattern formation. Cell Tissue Res 352:95–122. https://doi.org/10.1007/s00441-012-1329-4
11. Chernet BT, Adams DS, Lobikin M, Levin M (2016) Use of genetically encoded, light-gated ion translocators to control tumorigenesis. Oncotarget 7:19575–19588. https://doi.org/10.18632/oncotarget.8036
12. Adams DS et al (2016) Bioelectric signalling via potassium channels: a mechanism for craniofacial dysmorphogenesis in KCNJ2-associated Andersen-Tawil Syndrome. J Physiol 594:3245–3270. https://doi.org/10.1113/JP271930
13. Adams DS, Lemire JM, Kramer RH, Levin M (2014) Optogenetics in developmental biology: using light to control ion flux-dependent signals in Xenopus embryos. Int J Dev Biol 58:851–861. https://doi.org/10.1387/ijdb.140207ml
14. Adams DS, Tseng AS, Levin M (2013) Light-activation of the Archaerhodopsin H(+)-pump reverses age-dependent loss of vertebrate regeneration: sparking system-level controls in vivo. Biol Open 2:306–313. https://doi.org/10.1242/bio.20133665
15. Adams DS, Levin M (2006) Inverse drug screens: a rapid and inexpensive method for implicating molecular targets. Genesis 44:530–540
16. Sullivan KG, Levin M (2018) Inverse drug screening of bioelectric signaling and neurotransmitter roles: illustrated using a xenopus tail regeneration assay. Cold Spring Harb Protoc 2018:pdb.prot099937. https://doi.org/10.1101/pdb.prot099937
17. Belus MT et al (2018) Kir2.1 is important for efficient BMP signaling in mammalian face development. Dev Biol 444(Suppl 1): S297–S307. https://doi.org/10.1016/j.ydbio.2018.02.012
18. Ardissone A, Sansone V, Colleoni L, Bernasconi P, Moroni I (2017) Intrafamilial phenotypic variability in Andersen-Tawil syndrome: a diagnostic challenge in a potentially treatable condition. Neuromuscul Disord 27:294–297. https://doi.org/10.1016/j.nmd.2016.11.006
19. Dahal GR et al (2012) An inwardly rectifying K + channel is required for patterning. Development 139:3653–3664. https://doi.org/10.1242/dev.078592
20. Marrus SB, Cuculich PS, Wang W, Nerbonne JM (2011) Characterization of a novel, dominant negative KCNJ2 mutation associated with Andersen-Tawil syndrome. Channels (Austin) 5:500–509. https://doi.org/10.4161/chan.5.6.18524
21. George LF et al (2019) Ion channel contributions to wing development in Drosophila melanogaster. G3 (Bethesda) 9(4):999–1008. https://doi.org/10.1534/g3.119.400028
22. Smith RS et al (2018) Sodium channel SCN3A (NaV1.3) regulation of human cerebral cortical folding and oral motor development. Neuron 99:905–913 .e907. https://doi.org/10.1016/j.neuron.2018.07.052
23. Masotti A et al (2015) Keppen-Lubinsky syndrome is caused by mutations in the inwardly rectifying K(+) channel encoded by KCNJ6.

Am J Hum Genet 96:295–300. https://doi.org/10.1016/j.ajhg.2014.12.011

24. Kortum F et al (2015) Mutations in KCNH1 and ATP6V1B2 cause Zimmermann-Laband syndrome. Nat Genet 47(6):661–667. https://doi.org/10.1038/ng.3282
25. Veale EL, Hassan M, Walsh Y, Al-Moubarak E, Mathie A (2014) Recovery of current through mutated TASK3 potassium channels underlying Birk Barel syndrome. Mol Pharmacol 85:397–407. https://doi.org/10.1124/mol.113.090530
26. Curran J, Mohler PJ (2015) Alternative paradigms for ion channelopathies: disorders of ion channel membrane trafficking and posttranslational modification. Annu Rev Physiol 77:505–524
27. Perathoner S et al (2014) Bioelectric signaling regulates size in zebrafish fins. PLoS Genet e1004080:10
28. Hoptak-Solga AD, Klein KA, DeRosa AM, White TW, Iovine MK (2007) Zebrafish short fin mutations in connexin43 lead to aberrant gap junctional intercellular communication. FEBS Lett 581:3297–3302
29. La Russa MF, Qi LS (2015) The new state of the art: Cas9 for gene activation and repression. Mol Cell Biol 35:3800–3809
30. Beck CW, Slack JM (2001) An amphibian with ambition: a new role for Xenopus in the 21st century. Genome Biol 2:reviews1029
31. Blum M, Ott T (2018) Xenopus: an undervalued model organism to study and model human genetic disease. Cells Tissues Organs 205(5–6):303–313. https://doi.org/10.1159/000490898
32. Tseng AS (2017) Seeing the future: using Xenopus to understand eye regeneration. Genesis 55:1–2. https://doi.org/10.1002/dvg.23003
33. Getwan M, Lienkamp SS (2017) Toolbox in a tadpole: Xenopus for kidney research. Cell Tissue Res 369:143–157. https://doi.org/10.1007/s00441-017-2611-2
34. Dubey A, Saint-Jeannet JP (2017) Modeling human craniofacial disorders in Xenopus. Curr Pathobiol Rep 5:79–92. https://doi.org/10.1007/s40139-017-0128-8
35. Adams DS, Levin M (2012) Measuring resting membrane potential using the fluorescent voltage reporters DiBAC4(3) and CC2-DMPE. Cold Spring Harb Protoc 2012:459–464. https://doi.org/10.1101/pdb.prot067702
36. Adams DS, Levin M (2012) General principles for measuring resting membrane potential and ion concentration using fluorescent bioelectricity reporters. Cold Spring Harb Protoc 2012:385–397. https://doi.org/10.1101/pdb.top067710
37. Kim EZ, Vienne J, Rosbash M, Griffith LC (2017) Non-reciprocal homeostatic compensation in Drosophila potassium channel mutants. J Neurophysiol 117(6):2125–2136. https://doi.org/10.1152/jn.00002.2017
38. Pietak A, Levin M (2017) Bioelectric gene and reaction networks: computational modelling of genetic, biochemical and bioelectrical dynamics in pattern regulation. J R Soc Interface 14 (134):20170425. https://doi.org/10.1098/rsif.2017.0425
39. Pietak A, Levin M (2016) Exploring instructive physiological signaling with the bioelectric tissue simulation engine (BETSE). Front Bioeng Biotechnol 4:55. https://doi.org/10.3389/fbioe.2016.00055
40. Adams DS, Levin M (2012) Measuring resting membrane potential using the fluorescent voltage reporters DiBAC4 (3) and CC2-DMPE. Cold Spring Harb Protoc 2012:pdb.prot067702
41. Oviedo NJ, Nicolas CL, Adams DS, Levin M (2008) Live imaging of planarian membrane potential using DiBAC4 (3). Cold Spring Harb Protoc 2008:pdb.prot5055

Chapter 8

Engineering the Spatiotemporal Mosaic Self-Patterning of Pluripotent Stem Cells

Ashley R. G. Libby, David A. Joy, and Todd C. McDevitt

Abstract

Pluripotent stem cells (PSCs) possess the ability to self-organize into complex tissue-like structures; however, the genetic mechanisms and multicellular dynamics that direct such patterning are difficult to control. Here, we pair live imaging with controlled induction of gene knockdown by CRISPR interference (CRISPRi) to generate changes within subpopulations of human PSCs, allowing for control over organization and analysis of emergent behaviors. Specifically, we use forced aggregation of mixtures of cells with and without an inducible CRISPRi system to knockdown molecular regulators of tissue symmetry. We then track the resulting multicellular organization through fluorescence live imaging concurrent with the induction of knockdown. Overall, this technique allows for controlled initiation of symmetry breaking by CRISPRi to produce changes in cellular behavior that can be tracked over time within high-density pluripotent stem cell colonies.

Key words CRISPR interference, Forced aggregation, Pluripotent stem cells, Cell tracking, Live imaging, Morphogenesis

1 Introduction

The developing embryo undergoes a series of cellular rearrangements coordinated with cell fate specification to produce the complex tissues that comprise the body. In recent years, it has been demonstrated that pluripotent stem cells (PSCs) mimic such processes to create tissue-like structures outside the body [1–3], which show great potential for disease modeling, drug discovery, and eventually tissue replacement [4]. However, pluripotent differentiation to multiple cell types that mimic tissue structure, commonly referred to as "organoids," are often limited by lack of control over how multiple populations emerge over the course of the differentiation, leading to problems with reproducibility between batches and aggregates [4]. Here we demonstrate that a combination of forced aggregation and replating to monolayer coculture [5, 6],

Mo R. Ebrahimkhani and Joshua Hislop (eds.), *Programmed Morphogenesis: Methods and Protocols*, Methods in Molecular Biology, vol. 2258, https://doi.org/10.1007/978-1-0716-1174-6_8,

and inducible CRISPR interference (CRISPRi) [7, 8] can be used to program human induced PSC (hiPSC) morphogenesis in vitro, such that the emergence of different cellular populations can be modulated by varying cell mixing ratios and gene knockdown efficiency. Furthermore, the emergence of populations can be tracked over time using live imaging to quantitatively define changes in population behaviors resulting from transcriptional silencing.

Aggregation of PSCs into 3D spheroids has been traditionally used to induce embryoid body formation [9] at multiple scales, from culturing individual aggregates separately in small volumes [10] to large-scale suspension in dishes and bioreactors [11]. We demonstrated that forced aggregation [5, 6] can also be used to promote the mixture of different cell populations followed by replating in monolayer culture to produce "mosaic" 2D colonies (Fig. 1). We demonstrate that adherent mosaic colonies can be created at a range of sizes, from 25 to 500 cells, allowing for interrogation of mixed population colony dynamics by live imaging without relying on clonal expansion. This technique can be further extended using an inducible CRISPRi system where different guide RNAs establish distinct knockdown subpopulations within a single PSC colony. The inducible system allows PSC lines to be aggregated while still effectively homogeneous (i.e., prior to knockdown). Upon induction of knockdown, heterogenous loss of target gene expression, in this case the cell–cell adhesion molecule CDH1, robustly controls the emergence of two populations wherein CDH1(−) cells robustly segregate from CDH1(+) cells over the course of 5 days. Pairing the induction of knockdown with a fluorescent reporter allows live cell tracking through the gene knockdown time course to examine emergent behaviors as they occur (Fig. 2). Overall, we have established a platform that allows for robust induction of asymmetric population emergence and cell tracking to enable programmed control and quantification of multicellular organization in 2D human PSC colonies.

2 Materials

All solutions are stored at room temperature unless otherwise specified.

2.1 Cell Culture

1. mTeSR™1 (STEMCELL Technologies), store at 4 °C.
2. Growth Factor Reduced Matrigel (Corning), store at −20 °C.
3. Accutase (Sigma Aldrich), store at 4 °C.
4. ROCK inhibitor stock solution (Selleckchem): reconstitute ROCK inhibitor (Y-276932), in sterile water at 1000× (10 mM).

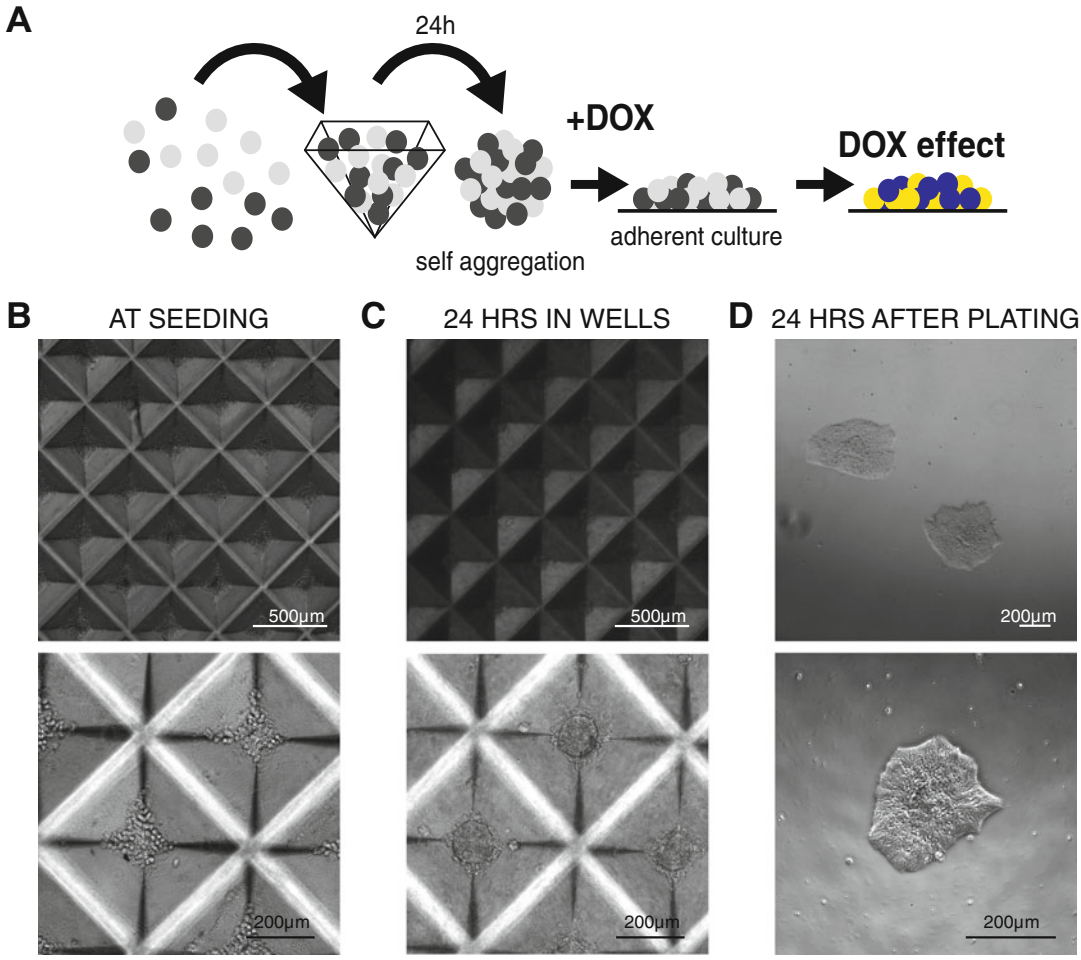

Fig. 1 Forced aggregation to create uniform size hiPSC colonies. (**a**) Schematic of the mixing populations, forced aggregation, and induction of CRIPSRi-based knockdown triggered by doxycycline addition. (**b**) Cells seeded into the microwells. (**c**) Cells after self-compaction into aggregates. (**d**) Aggregate after attachment and spreading, where the aggregate has expanded to form a typical compact 2D colony

5. Tissue culture incubator kept at 37 °C and 5% CO_2.
6. 96-Well optically clear flat-bottom plate, tissue culture-treated.

2.2 CRISPR Interference gRNA Creation and Line Generation

1. WTC hiPSC line, (Coriell Institute, #GM25256).
2. WTC CRISPRi Gen1C hiPSC line (Gladstone Stem Cell Core) (*see* **Note 1**).
3. pgRNA-CKB plasmid (Addgene), depositing lab Bruce Conklin.
4. BsmBI, purchase from New England Biolabs.
5. T4 Polynucleotide Kinase, purchase from New England Biolabs.

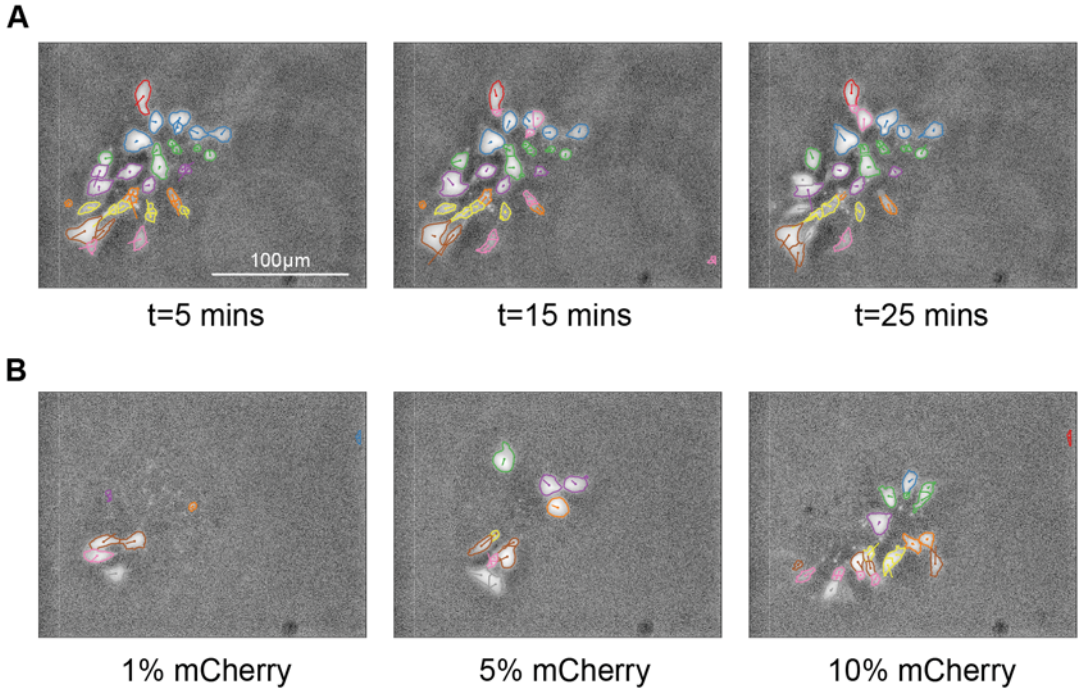

Fig. 2 Live image tracking of cells within mixed aggregates. (**a**) Every other sequential frame from a 25% mCherry-labeled colony demonstrating stable tracking of cells over time, where cell outline color represents the same cell over time. Arrows extend from the estimated cell center of mass in the instantaneous direction of travel estimated by differences in center of cell mass between frames. (**b**) Tracking in colonies labeled with different percentages of mCherry-positive cells. Colonies with fewer labeled cells are easier to stably track over time, although even sparsely labeled colonies demonstrate clonal pockets of labeled cells

6. T4 DNA Ligase, purchase from New England Biolabs.
7. NEB Turbo competent *E. coli*, purchase from New England Biolabs.
8. QIAGEN plasmid miniprep kit, purchase from QIAGEN.
9. Amaxa nucleofector 2b device (Lonza).
10. Human Stem Cell Nucleofector Kit 1 (Lonza), store as instructed by manufacturer.
11. 10 mg/mL Blasticidin 1000× stock solution (Millipore), and dissolve in sterile deionized water, store at 4 °C.
12. 2 mM Doxycycline 1000× stock solution (Sigma Aldrich), reconstitute in sterile deionized water, store at 4 °C.
13. RNeasy Mini Kit (QIAGEN).

2.3 Forced Aggregation

1. 400 μm diameter microwell plates, (STEMCELL Technologies, AggreWell™400).
2. Swinging rotor centrifuge with 6-well plate adaptors.

3. Sterile Gibco™ Dulbecco's phosphate buffered saline (DPBS) without calcium chloride or magnesium chloride (Fisher Scientific).
4. Widebore 1000 μm pipette tips (Rainin).

2.4 Live Imaging and Analysis

1. Zeiss Observer.Z1 with Incubator XL S1 system, 2 axis automatic stage, and Definite Focus module.
2. 20× LD Plan Achromat lens with NA correction collar.
3. 96-Well plate carrier adapter with spring clip.
4. Zen Blue v2.0.
5. Python 3.7.4.
6. Scikit-learn 0.20.2.
7. Scikit-image 0.15.0.

3 Methods

Carry out all procedures at room temperature in a tissue culture hood unless otherwise specified. All PSCs are cultured in humidified incubators at 37 °C and fed daily with mTeSR™ according to manufacturer's instructions, passaging cells 1:10 every 3–4 days or when 70% confluent.

3.1 Designing and Testing Guide RNAs for CRISPRi

1. Use Broad Institute gRNA designer website to generate guide sequences ensuring that the CRISPRi tab is selected, and using the SpyoCas9 (NGG) targeting the human genome (GRCh38): https://portals.broadinstitute.org/gpp/public/analysis-tools/sgrna-design-crisprai?mechanism=CRISPRi (*see* **Note 2**).
2. Clone guide sequences into pgRNA-CKB using BsmBI restriction enzyme strategy described in [7] and described in brief here.
3. Order single-strand DNA oligos of the forward and reverse sequence of the guide where the sequence TTGG is added to the 5′ end of the forward oligo and the sequence AAAC is added to the 5′ end of the reverse compliment (this will allow for insertion into plasmid via BsmBI).
   (a) Phosphorylate and anneal each pair of TTGG(20 N) and AAAC(20 N) guide oligos using T4 Polynucleotide Kinase as per manufacturer's instructions.
   (b) Dilute annealed oligo 1:100 in dH_2O.
   (c) Enzyme digest 1 μg of the pgRNA-CKB backbone plasmid using BsmBI for 1 h at 55 °C, run cut vector on an electrophoresis gel and gel extract cut band using QIAquick Gel Extraction Kit, eluting in dH_2O.

(d) Ligate the 1:100 diluted oligo into the cut backbone using T4 DNA Ligase as per manufacturer's instructions.

(e) Transform 20 μL of bacteria (NEB Turbo competent cells) with 5 μL of ligated product and plate on lysogeny broth (LB) plates containing ampicillin for selection overnight at 37 °C.

(f) After selection, pick colonies and grow in 5 mL of LB + ampicillin overnight at 37 °C on a shaker.

(g) Isolate vector DNA using QIAGEN plasmid miniprep kit and sequence plasmid for correct guide insertion.

4. Following manufacturer instructions, nucleofect pgRNA-CNKB into WTC CRISPRi Gen1C hiPSC line using an Amaxa Nucleofector 2b Device and Human Stem Cell Nucleofector Kit 1 with the pulse code EN135.
5. Prepare mTeSR with 10 μM ROCK inhibitor (add 1 μL ROCK inhibitor 1000× stock for every 1 mL mTeSR). Plate down nucleofected cells in serial dilutions into a 6-well plate in mTeSR & ROCK inhibitor. Allow to recover for 24 h.
6. After 24 h recovery, use blasticidin for 6 days to select cells that successfully took up the guide plasmid. Culture in mTeSR with blasticidin at 10 μg/mL (add 1 μL blasticidin 1000× stock for every 1 mL mTeSR) and ROCK inhibitor at 10 μM.
7. Pick colonies after blasticidin selection and expand. Verify knockdown by culturing in mTeSR with 2 μM doxycycline (add 1 μL doxycycline 1000× stock for every 1 mL mTeSR) for 4 days, then extract RNA using a Rneasy Mini kit and interrogate expression of target gene by quantitative PCR as described in [12].
8. Repeat for every desired knockdown population so that multiple types of knockdown can be combined in the next step to create mixed populations.

3.2 Creation of Mixed Aggregates

1. To create mixed aggregates (Fig. 1a), rinse desired knockdown populations of hiPSCs with DPBS (half of feeding volume) and then incubate at 37 °C in Accutase according to manufacturer instructions.
2. Once cells begin to detach from the plate, dilute Accutase with an equal volume of DPBS and transfer to 15 mL conical tube, pipetting vigorously at least five times to singularize cells.
3. Centrifuge at 100 rcf for 3 min to pellet cells and subsequently aspirate off diluted Accutase solution. Then resuspend single cells in mTeSR with 10 μM ROCK inhibitor and count cells.
4. Using PDMS microwell inserts [5] with 400 μm diameter where there are 5000 microwells per well of a 6-well (*see* **Note 3**), calculate total cell number needed to seed microwells

at desired aggregate size and ratio of multiple cell lines (*see* **Note 4**), add appropriate volume of cell suspension to mTeSR with 10 μM ROCK inhibitor totaling 12 mL media. Dispense 2 mL per well of the 6-well plate with microwell inserts.

5. Centrifuge cell suspension in 6-well plate with microwell inserts at 200 rcf for 5 min (Fig. 1b).
6. Place the 6-well plate with cells in tissue culture incubator and allow the cells to aggregate overnight.

3.3 Plate down of Aggregates and Induction of CRISPRi

1. After overnight recovery, each microwell should contain a mixed population condensed aggregate (Fig. 1c).
2. Coat a 96-well optically clear flat-bottom plate with Growth Factor Reduced Matrigel at a final concentration of 80 μg/mL and let adsorb at room temperature for 1 h.
3. With a 1000-μL-wide bore pipette tip, gently pipette up and down to remove aggregates from microwells and transfer to 15 mL conical tube. Repeat with 1 mL of DPBS to wash out remaining aggregates from microwells. Repeat for each well of the 6-well plate and put each in separate 15 mL conical tube (*see* **Note 5**).
4. Centrifuge aggregates in 15 mL conical tubes at 100 rcf for 3 min, aspirate spent media, and resuspend cell pellet in 5 mL mTeSR to a concentration of 1000 aggregates/mL. Discard 4 mL and dilute the remaining suspension to 50 aggregates/mL in mTeSR (20 mL total).
5. Aspirate off Matrigel from 96-well plate and add 200 μL of aggregate suspension per well, making sure to mix aggregate suspension thoroughly before dispensing to ensure aggregates remain in suspension.
6. Allow plated aggregates to attach and spread overnight in incubator.
7. CRISPRi is induced by addition of doxycycline to culture media at a concentration of 2 μM. This can be done before or after co-aggregating different cell lines (*see* **Note 6**).

3.4 Time Lapse Microscopy

1. 24 h after plating, the aggregates should have adhered and spread on the plate, forming round colonies at desired cell line ratios depending on steps taken during creation of mixed aggregates (*see* **Note 4**) (Fig. 1d).
2. 30 min before imaging, turn on CO_2 and heating for the incubated stage. The incubator should be set to 5% CO_2 and 37 °C. Confirm the incubator has reached temperature and correct CO_2 concentration before transferring the sample.
3. Calibrate the two-axis automated stage in Zen before transferring the plate.

4. Immediately before transferring, feed the 96-well plate with 200 μL per well (a total of 19.2 mL) fresh mTeSR warmed to 37 °C. Add 100 μL per channel PBS to the space between wells (total of 9.6 mL) of the 96-well to prevent evaporation.
5. Transfer the 96-well to the incubated stage with the A1 well in the top left corner of the 96-well plate carrier. Ensure that the plate is situated flat and level in the plate carrier.
6. Select the 96-well plate layout in Zen. Using the 3-point method in Zen, calibrate the focal plane of the stage to the top left, top right, and bottom right corners of the 96-well plate by focusing manually in brightfield at 20× on the basal surface.
7. Set the Brightfield exposure time to 50 ms at 4 V power. To capture fluorescence from the doxycycline-induced mCherry reporter, set the 555 nm exposure time to 200 ms at 25% laser power (*see* **Note 7**). Disable all other light sources.
8. To minimize artifacts due to uneven illumination and evaporation, begin colony selection from row 2 and column B and do not image the outer wells (*see* **Note 8**). Beginning in the B2 well, continuing down to the G2 well, then right to the G3 well and back up to the B3 well, and so on, select individual colonies for longitudinal imaging. Accept only colonies that fill between one quarter to one half of the field of view at 20× (~110–225 μm in diameter), where no other colony is within one field of view (minimum of ~450 μm away on any side). Confirm by imaging at 555 nm that the colony contains the expected percentage of labeled cells. Center the colony in the field of view, focus the image in 555 nm, then add the colony to the tile positions window in Zen.
9. Repeat until between 30 and 40 total colonies have been added to the tile position window. If the above scanning pattern reaches the outer row 12, all acceptable colonies on a single plate have been exhausted.
10. Set the time course to acquire a single field of view for each colony every 5 min for 6 h (*see* **Note 9**).
11. Set the focus strategy to use Definite Focus for each tile for each time point.
12. After ensuring one last time that the incubation parameters are stable at 37 °C and 5% CO_2, start the experiment. Ensure that all selected tiles can be acquired in the 5-min period.

3.5 Image Analysis

All code for this section can be found at the following GitHub repository: https://github.com/david-a-joy/ProgrammedMorpho2019-QuantifyingPatterning

1. To analyze the data, first export the mCherry (555 nm) channel to individual frames for each tile in the Tagged Image File Format (TIFF) format. A colony imaged every 5 min for 6 h will result in 72 timepoint images per tile.
2. Load each image and convert to grayscale where white pixels have a value of 1.0 and black pixels have a value of 0.0. All out-of-range pixels should be clamped from 0 to 1 (i.e., pixel values lower than 0 or greater than 1 should be replaced with 0 and 1, respectively).
3. To remove background inhomogeneity using a difference of Gaussians, create a foreground and a background image from the clamped image. The foreground image should be smoothed with a 2D Gaussian filter with a standard deviation of three pixels. The background image should be smoothed with a 2D Gaussian filter with a standard deviation of 30 pixels. Subtract the background image from the foreground image, then clamp the resulting image to the range of 0.0–1.0. In this background corrected image, most of the frame should be black (near 0.0) with only mCherry-positive cell areas having nonzero values.
4. To estimate the threshold needed to segment the individual cells, fit a two-term mixture of Gaussians model to the background corrected image [13]. Use the mean of the higher of the two Gaussians to define the threshold to separate fluorescent cells from background, where positive pixels are any pixels above the threshold (*see* **Note 10**).
5. To extract cell areas, threshold the background corrected image using the threshold calculated above. Remove any positive detections less than 500 square pixels and any positive detections within 20 pixels of the border, then calculate a distance transform to the edge on the remaining masks [14]. Separate touching masks into raw segmentations using the watershed transform [15].
6. Discard any masks that are individually smaller than 500 pixels in area. The remaining masks are the detected cells (Fig. 2a).
7. To extract cell contours, for each individual cell mask, calculate a contour around the border of the mask using the marching squares algorithm [14].
8. Repeat this extraction process in **steps 5**–**7** for all images in the dataset.
9. To link cells into cell tracks, calculate the Boolean intersection for each individual cell mask between sequential frames within the dataset. Sort cell masks by pixel size in the current frame, then process each mask through **steps 10**–**13** from largest to smallest.

10. A cell mask that has no intersection in a prior frame is a new detection. Start a new track fragment for this cell, recording the mask, center of mass, and perimeter for this cell at this frame. All cells in the first frame of the time series should be processed this way.
11. A cell mask that has no intersection in a subsequent frame has failed to track to the next frame. Save the current track fragment for this cell, then assume any new cells that appear in this position are a new cell track fragment. All cells in the last frame of the time series should be processed this way.
12. A cell mask in a prior frame that has an intersection of at least 10 pixels with exactly one mask in the next frame should be linked. Record the new mask, center of mass, and perimeter using the same track index as the previous frame.
13. A cell mask in a prior frame that intersects at least 10 pixels each with two or more masks should be linked to the mask with the most overlap.
14. Once all frames have been tracked, secondary metrics such as velocity and track length can be calculated using the centers of mass for each track over time.
15. This algorithm is implemented for a directory containing sequential frames of one study using python 3 and the scikit-image [15] library.

4 Notes

1. The plasmid used to create the WTC CRISPRi Gen1C hiPSC cell line is deposited on Addgene by Bruce Conklin named pAAVS1-Ndi-CRISPRi (Gen1). In this case, refer to reference [7] for instructions on cell line creation.
2. The Broad website allows for design of multiple types of CRIPSR guides targeting any gene. The targeted gene in our example is CDH1; however, the technique can be extended to any gene of choice to observe how loss of gene expression affects colony organization. Additionally, the aforementioned Broad Institute website offers guide design for CRISPR, CRISPRi, and CRISPRa. To ensure proper guide design, make sure that CRISPRi is selected in the top tab.
3. Comparable AggreWell™400 plates may be purchased from StemCell Technologies.
4. In order to obtain different ratios of mixing, mix singularized cells from two different lines at the appropriate concentration to obtain the final desired size for the aggregate. For example, if creating a 100-cell aggregate wherein 25% of the aggregate is

CRISPRi Cell line 1 and 75% is the wild-type cell line, then for 1 well of the 6-well plate with microwell insert, a total of 125,000 CRISPRi cells are required (5000 microwells/well × 100 cells/microwell × 0.25) and 375,000 wild-type cells are required. The cells are mixed and diluted in mTeSR to a total of 2 mL and then added to one well of the 6-well plate with PDMS microwell insert plate. This will generate 5000 100-cell aggregates with 25% of each aggregate containing the CRISPRi cell line. These calculations can be done for a range of mixtures to titer the knockdown population within the adherent mosaic colonies (Fig. 2b).

5. When washing the aggregates out from the microwells, make sure to thoroughly wash the entire surface of the well to ensure all aggregates are physically removed from the microwells, but pipette gently in order to prevent shearing of the aggregates. It is helpful to ensure that aggregates have been washed out of the microwells by visually inspecting with a microscope after the second wash.
6. CRISPRi knockdown can be started before or after mixing populations based on when doxycycline is added to the tissue culture medium. The CRISPRi system contains an mCherry fluorescence cassette that labels manipulated cells and allows for cell tracking. A minimum of 3 h of doxycycline treatment is necessary before detection of mCherry fluorescence is possible.
7. The described exposure time, laser power, and emission wavelength produce sufficiently high signal to noise to segment the cytoplasmic mCherry signal from the WTC CRISPRi Gen1C hiPSC cell line while limiting cell death due to phototoxicity. Other fluorophores can also be used for segmentation, but the imaging settings will require adjustment. If image contrast is too low, increase the exposure time or laser power. If visible cell death occurs over the imaging period, reduce laser power or use a longer wavelength fluorophore to reduce cell damage and production of reactive species.
8. Colonies in the border wells (rows 1 and 8, and columns A and H) can be imaged; however, they are more susceptible to behavioral and imaging artifacts. Even over short imaging periods, wells along the edge experience more evaporation, leading to changes in cell behavior and increases in cell death. Furthermore, illumination in edge wells is less homogeneous than in center wells, making cells in these wells much harder to segment. To avoid plating aggregates in the border wells, in Subheading 3.3, **step 5** add 200 μL aggregate suspension only to the center 60 wells (rows 2 through 7 and columns B through G) of the 96-well plate and add 200 μL PBS instead to the border wells.

9. Image acquisition can be run for longer periods of time if needed; however, the longer an experiment is run, the more evaporation is a concern. To prevent this, place a dish of sterile water in the incubated chamber to help prevent evaporation of media off of the 96-well.
10. Automated threshold detection is often difficult, especially for images with very sparsely labeled cells (1% labeling for instance), or images with very strong background signal. Instead of attempting to calculate a threshold from the data, a user may supply a threshold. Values that work well to segment colonies of this type are typically in the range of 0.05–0.1.

References

1. Lancaster MA, Knoblich JA (2014) Organogenesis in a dish: modeling development and disease using organoid technologies. Science 345:1247125–1247125. https://doi.org/10.1126/science.1247125
2. Clevers H (2016) Modeling development and disease with organoids. Cell 165:1586–1597. https://doi.org/10.1016/j.cell.2016.05.082
3. Warmflash A, Sorre B, Etoc F et al (2014) A method to recapitulate early embryonic spatial patterning in human embryonic stem cells. Nat Methods 11:847–854. https://doi.org/10.1038/nmeth.3016
4. Bredenoord AL, Clevers H, Knoblich JA (2017) Human tissues in a dish: The research and ethical implications of organoid technology. Science 355:eaaf 9414. https://doi.org/10.1126/science.aaf9414
5. Hookway TA, Butts JC, Lee E et al (2016) Aggregate formation and suspension culture of human pluripotent stem cells and differentiated progeny. Methods 101:11–20. https://doi.org/10.1016/j.ymeth.2015.11.027
6. Ungrin MD, Joshi C, Nica A et al (2008) Reproducible, ultra high-throughput formation of multicellular organization from single cell suspension-derived human embryonic stem cell aggregates. PLoS One 3(e):1565. https://doi.org/10.1371/journal.pone.0001565
7. Mandegar MA, Huebsch N, Frolov EB et al (2016) CRISPR interference efficiently induces specific and reversible gene silencing in human iPSCs. Cell Stem Cell 18:541–553. https://doi.org/10.1016/j.stem.2016.01.022
8. Larson MH, Gilbert LA, Wang X et al (2013) CRISPR interference (CRISPRi) for sequence-specific control of gene expression. Nat Protoc 8:2180–2196. https://doi.org/10.1038/nprot.2013.132
9. Kurosawa H (2007) Methods for inducing embryoid body formation: in vitro differentiation system of embryonic stem cells. J Biosci Bioeng 103:389–398. https://doi.org/10.1263/jbb.103.389
10. Potter SW, Morris JE (1985) Development of mouse embryos in hanging drop culture. Anat Rec 211:48–56. https://doi.org/10.1002/ar.1092110109
11. King JA, Miller WM (2007) Bioreactor development for stem cell expansion and controlled differentiation. Curr Opin Chem Biol 11:394–398. https://doi.org/10.1016/j.cbpa.2007.05.034
12. Libby AR, Joy DA, So P-L et al (2018) Spatiotemporal mosaic self-patterning of pluripotent stem cells using CRISPR interference. elife 7:e36045. https://doi.org/10.7554/eLife.36045
13. Pedregosa F, Varoquaux G, Gramfort A et al (2011) Scikit-learn: machine learning in Python. J Mach Learn Res 12:2825–2830
14. Lorensen WE, Cline HE (1987) Marching cubes: a high resolution 3D surface construction algorithm. SIGGRAPH Comput Graph 21:163–169. https://doi.org/10.1145/37402.37422
15. van der Walt S, Schönberger JL, Nunez-Iglesias J et al (2014) Scikit-image: image processing in Python. PeerJ 2:e453. https://doi.org/10.7717/peerj.453

Part III

Early Developmental Engineering

Chapter 9

Fate-Patterning of 2D Gastruloids and Ectodermal Colonies Using Micropatterned Human Pluripotent Stem Cells

George Britton, Sapna Chhabra, Joseph Massey, and Aryeh Warmflash

Abstract

In the developing mammalian embryo, intercellular signaling allows cells to self-organize to create spatial patterns of different cell fates. This process is challenging to study because of the difficulty of observing or manipulating embryos on the spatial and temporal scales required. In vitro models can provide a complement to in vivo systems for addressing these issues. These models are also the only windows we have into early human development. Here we provide protocols for two systems based on differentiating human pluripotent stem cells in micropatterned colonies on defined size and shape. The first model replicates the patterning of the germ layers at gastrulation, while the second replicates the medial-lateral patterning of the ectoderm. These systems allow study of how signaling underlies self-organized patterning at stages of development which are otherwise inaccessible.

Key words Self-organization, Signaling, Human embryonic stem cells (hESCs), Micropatterns, Gastruloids, Ectoderm, Cellular communication, Tissue patterning

1 Introduction

Cell-to-cell communication via chemical and mechanical signals is integral to the formation of a spatially patterned organism. The interplay between signaling and tissue patterning is technically very challenging to study in a developing mammalian embryo. Micropatterning technology provides a platform to develop simplified, in vitro models of embryonic development that recapitulate tissue patterning. In these models, cells' attachment is restricted to regions of defined shapes and sizes [1]. Although submicron resolution can be achieved with micropatterning techniques, for tissue-patterning experiments, cells are typically confined to colonies in the range of 0.1–1 mm, the approximate size of a mammalian

George Britton, Sapna Chhabra, and Joseph Massey authors contributed equally to this work.

Mo R. Ebrahimkhani and Joshua Hislop (eds.), *Programmed Morphogenesis: Methods and Protocols*, Methods in Molecular Biology, vol. 2258, https://doi.org/10.1007/978-1-0716-1174-6_9,

embryo at gastrulation stage, or of an organ during its initial patterning. Spatial confinement has two advantages: First, controlling colony size removes variability from outcomes so that consistent patterns of signaling and cell fate are formed. Second, confinement leads to increased cell density, so that in micropatterns, but not in similarly sized colonies in standard culture, the density can be made to mimic that of the embryo. This in turn allows cell communication and self-organization similar to that which occurs in vivo. For instance, micropatterned 2D stem cell colonies, stimulated with appropriate growth factors or inhibitors, recapitulate gastrulation and ectodermal patterning in vitro [2, 3]. These simplified models provide a controlled, high-throughput and highly reproducible platform to quantitatively examine the role of signaling in patterning.

Previously, we have shown that micropatterned human embryonic stem cell (hESC) colonies, stimulated with BMP4 ligand, self-organize to form radial patterns of the three germ layers, thus recapitulating gastrulation in vitro (2D gastruloids) [2]. Starting from colony edge, the patterns comprise rings of trophectoderm, endoderm, and mesoderm with either ectoderm [2] or pluripotent cell-fates [4] at the colony center. This gastrulation protocol has been reproduced in other labs [5, 6], and a comparable system for mouse gastrulation has been developed [7]. The relative position of germ layers and the chemical signaling cascade underlying patterning are the same in micropattern gastrulation assays and the gastrulating mouse embryo [4, 8, 9]. Thus, these micropatterned systems provide a good platform to dissect the relationship between signaling and patterning, and can be utilized to uncover common and species-specific mechanisms underlying germ-layer patterning. In recent studies, we used the human gastrulation assay to show that dynamic waves of WNT and NODAL signaling, in the absence of an underlying spatial signaling gradient, control germ layer patterning [4, 10]. This suggests that the combinatorial dynamics of multiple signaling pathways, and not a concentration threshold in signaling, governs patterning during gastrulation.

Recently, we adopted micropatterning technology to create a system that recapitulates the medial-lateral (ML) patterning of the ectodermal germ layer [3]. This system provides an opportunity to understand how this layer is patterned into functionally distinct cell types, a topic of both fundamental interest and medical relevance as several of these fates are the subject of intense studies for regenerative therapies. Micropatterned hESCs are differentiated toward the ectodermal lineages, and patterning is then induced with BMP4. In response, the cells self-organize to form radial patterns containing the same cell fates in the same organization as found along the ML axis of mammalian embryos. Starting from colony edge, the patterns comprise surface ectoderm, placode, neural crest, and neural cell fates. This patterning is controlled by relative levels of BMP and WNT signaling. We used the information gained from the

micropatterned platform to improve differentiation protocols for the placodal cell fate. Thus, micropatterned assays can provide mechanistic insights into the signaling dynamics underlying patterning, with direct implications for improving differentiation protocols for regenerative medicine.

We have previously published a protocol for micropatterned 2D gastruloids in defined media [11]. Here, we modify that protocol for a 96-well format, include improvements for long-term storage of laminin-coated micropatterned surfaces, and introduce the protocol for ectoderm patterning.

2 Materials

2.1 Cell Culture

2.1.1 2D Gastruloid and Ectoderm Patterns

1. Human pluripotent stem cells. We routinely use ESI017 (ESI-BIO) and RUES2 (Ali Brivanlou, Rockefeller University) as well as induced pluripotent cells from the Coriell collection.
2. mTeSR1 culture media kit (basal media and 5× supplement) (STEMCELL Technologies; 85870).
3. Accutase (Fisher Scientific; NC9839010) for single-cell suspensions.
4. ROCK Inhibitor (RI) Y-27632 (Fisher Scientific; 50-175-998).
5. 35 mm Nunc Cell Culture/Petri Dish (Fisher Scientific; 1256591) for routine culture.
6. Cell culture incubator with controlled humidity and 5% CO_2.
7. Biological safety cabinet (Laminar Flow Hood).
8. 70% Ethanol for sterilizing work surfaces and tools.
9. 1, 5, 10, and 25 mL sterile serological pipettes and pipettor.
10. Micropipette tips with barrier and micropipettor.
11. PBS without calcium and magnesium (Caisson Labs; PBL01-6X500ML).
12. Dulbecco's Phosphate-Buffered Saline (DPBS), 1× with calcium and magnesium (VWR; 45000-430).
13. Inverted tissue culture microscope with phase contrast.
14. Hemocytometer.
15. Cell culture centrifuge.
16. Nalgene Rapid-Flow sterile disposable filter units with PES membrane (ThermoFisher; 569-0020).
17. Penicillin-streptomycin (Life Technologies; 15140-148).
18. Recombinant human BMP-4 (Fisher Scientific; 314BP050).
19. Fluoromount-G (Southern Biotech; 0100-01).
20. Microslides (VWR; 16004-382).

2.1.2 Additional Reagents Required for Ectoderm Pattern

1. Selective inhibitor of ALK4, Alk5, and ALK7. SB431542 (Stemgent; 04-0010-05).
2. DMEM-F12 (VWR; 45000-344).
3. Neurobasal media (Life Technologies; 21103-049).
4. N2 supplement 100× (Life Tehnologies; 17502048).
5. B27 supplement without vitamin A 50× (Life Technologies; 12587010).
6. Glutamax 100× (Life Technologies; 35050061).
7. ß-Mercaptoethanol (Fisher Scientific; 21985023).
8. WNT secretion inhibitor IWP2 (Stemcell Technologies; 72124).

2.2 Micropatterning

1. 96-Well micropatterned plate (CYTOO; 20-950-00) or chip (CYTOO; 10-021-00-18)
2. PBS with calcium and magnesium (VWR; 45000430).
3. Recombinant human laminin 521 (Biolamina, R021599/X0086842).
4. A multichannel micropipettor for high-throughput experiments.

2.3 Immunofluorescence and Imaging

1. 4% Paraformaldehyde (wt/vol). Prepared from 16% stock (EM Sciences; 15710) diluted in PBS.
2. Blocking solution: 3% normal donkey serum (EMD Millipore; S30-100ML) with 0.1% Triton X-100 (Sigma; 1001843780) in PBS. Stores for 1 week at 4 °C.
3. PBST washing solution: 0.1% Tween-20 (Sigma; P1379) in PBS.
4. Human Brachyury antibody, goat-derived (R&D Systems; AF2085), 1:300 dilution.
5. Human Sox2 antibody, rabbit-derived (Fisher Scientific; 5024S), 1:200 dilution.
6. Human CDX2 antibody, mouse-derived (Abcam; AB15258), 1:50 dilution.
7. Human N-CAD antibody, mouse-derived (Sigma; C2542), 1:100 dilution.
8. Human E-CAD antibody, rabbit-derived (Fisher Scientific; 31955), 1:200 dilution.
9. Human SOX9 antibody, goat-derived (R&D Systems; AF3075), 1:200 dilution.
10. 4,6-Diamidino-2-phenylindole, dihydrochloride (DAPI) (Life Technologies; D1306).

11. Secondary antibodies: Donkey anti-Mouse Alexa Fluor 488, anti-Goat Alexa Fluor 555, and anti-Rabbit Alexa Fluor 647 (Thermo Fisher; A-21202, A-21432, and A-31573), dilution 1:500.
12. Inverted fluorescence microscope for imaging (e.g., Olympus FV1200).

3 Methods

Embryonic gene expression patterns for both gastruloids and ectoderm have successfully been generated on CYTOO micropatterned coverslips and 96-well plates. There are advantages and disadvantages to each micropattern format, and we suggest potential users to select the one that best suits their research question. For example, the 96-well plate is easily amendable to live-cell imaging, and well suited for multiplexing experimental conditions, technical repeats, and primary antibody cocktail combinations. Additionally, the benefit of lower media volumes to conduct a single experiment translates to using fewer resources such as recombinant laminin for coating, antibodies for immunohistochemistry and small molecules and ligands for differentiation protocols. One potential drawback to the 96-well plate is the limited number of shapes, sizes, and replicate number of micropatterned surfaces in each well. On the other hand, the larger culture surface on CYTOO chips allows one to study, in a single experiment, the role of size and shape during embryonic patterning events. However, the large media volume needed to conduct a single experiment on CYTOO chips means it is far less economical and difficult to scale for experiments that require multiple experimental conditions and controls. In the method that follows below, we provide detailed procedures to coat, wash, and seed hESCs to each micropattern format. We then provided the necessary signaling conditions and media volumes to generate either gastruloid or ectodermal gene expression patterns on CYTOO chips and 96-well plates.

An important consideration for any experiment conducted on micropatterned surfaces (CYTOO chip or 96-well plate) is that the position and intensity of cell fate markers in resulting patterns is sensitive to experimental variation. These include minor variations in initial seeding density, the duration of differentiation, and the duration of each step of immunofluorescence staining. For these reasons, we recommend always making comparisons against controls that are done alongside each experimental condition, and not at separate times.

3.1 Base Media Preparation

1. mTeSR
   (a) Thaw mTeSR 5× supplement overnight at 2–8 °C. Mix thoroughly once completely thawed.
   (b) Working in a sterile culture hood, add 400 mL of mTeSR basal medium and 100 mL of mTeSR 5× supplement to 500 mL Nalgene Rapid-Flow sterile filter unit.
   (c) Connect and apply vacuum to Rapid-Flow unit for sterile filtration of mTeSR.
   (d) Store filtered mTeSR at 4 °C for up to 2 weeks or at −20 °C for up to 6 months.
2. N2B27
   (a) Thaw N2 and B27 supplements at room temperature.
   (b) Working in a sterile culture hood add 250 mL of DMEM/F12, 250 mL of neurobasal media, 5 mL glutamax 100×, 5 mL B27 50× supplement, 2.5 mL N2 100× supplement, and 0.5 mL ß-mercaptoethanol to 500 mL Nalgene Rapid-Flow Sterile filter unit.
   (c) Connect and apply vacuum to Rapid-Flow unit for sterile filtration of N2B27 media.
   (d) Store-filtered N2B27 media at 4 °C for up to 4 weeks or at −20 °C for up to 6 months.

3.2 Coat Micropatterned Surface with Laminin and Seed Cells

All of these procedures should be done inside the tissue culture hood while observing proper aseptic technique unless otherwise noted. Media and PBS++ should be at room temperature or pre-warmed to 37 °C.

For experiments conducted in a 96-well plate, it is important to consider that unused wells can be used in subsequent experiments. We have found hESC attachment and their potential to form gene expression patterns on previously unused micropatterned surfaces remain unaffected. To increase the lifespan of the 96-well plate, we store plates at 4 °C between experiments and only prepare wells for seeding as needed. A few of our plates have gone through upwards of five cycles of experiments spread over more than 6 months. To be clear, we never reuse the same wells. It is the previously unused wells which remain available for subsequent experiments.

3.2.1 Prepare Laminin Coated Micropattern Surface

96-Well CYTOO Micropattern Plate

1. Add 5 μg/mL laminin 521 (diluted in PBS with Calcium and Magnesium, hereafter PBS++) to each well. For a 96-well plate, we typically use 100 μL per well (*see* **Note 1**).
2. Incubate plate at 37 °C for 2.5 h.
3. Gently wash each well with PBS++ with the pipette tip placed against the edge of the well. A multichannel pipettor can be used for multiple wells.

(a) Begin with four partial washes by adding and removing 250 μL PBS++. A remaining 100 μL PBS++ should be present between washes.

(b) Remove the remaining 100 μL PBS++ and perform one complete wash by adding and withdrawing 250 μL PBS++. Perform this step quickly to be sure micropattern surfaces do not dry between washes.

(c) Add 100 μL PBS++ to each coated and washed microwell. Micropatterns are available to use immediately or can be stored in PBS++ at 4 °C for up to 2 weeks.

CYTOO Micropattern Chip

1. Place each CYTOO micropattern chip face up in one 35 mm plate.
2. Add 5 μg/mL laminin 521 diluted in PBS++ to each 35 mm plate. Each chip will require 2 mL of diluted laminin solution.
3. Incubate the chip at 37 °C for 2.5 h.
   (a) Press the corners of the chip to the surface of the 35 mm plate with a 1-mL pipette tip in case the micropattern chip begins to float upon addition of laminin-PBS++ solution.
4. Gently wash each chip with PBS++.
   (a) Begin with five partial washes by adding and removing 6 mL of PBS++ using a 10-mL serological pipette. A remaining 2 mL PBS++ should be present between washes.
   (b) Remove the remaining 2 mL PBS++ and perform one complete wash by adding and withdrawing 8 mL of PBS++. Perform this step quickly to be sure micropattern surfaces do not dry between washes.
   (c) Add 2 mL PBS++ to each coated and washed micropatterned chip. The chip is available to use immediately or can be stored in PBS++ at 4 °C for up to 2 weeks.

3.2.2 Seed Cells

1. Prepare single cell suspension of hESCs for seeding.
   (a) Calculate the total volume of mTeSR media with 10 μM ROCK inhibitor Y-27632 (RI) needed to harvest, count, and seed cells to micropattern surfaces. Volume of media required for each step: ***Harvesting cells***: Each plate will require 1 mL of mTeSR with RI to harvest cells following accutase treatment (e.g., need 2 mL of mTeSR with RI to harvest cells from 2.35 mm plates). ***Counting cells***: To resuspend cells following centrifugation, one can expect to use 0.5–1 mL of mTeSR with RI for every ~1 × 10^6 cells. ***Seeding cells***: The media volume will scale with the number of wells coated in a 96-well plate (100 μL mTeSR+RI/well) and/or the number of coated chips (2 mL mTeSR+RI/chip).

(b) To harvest cells, aspirate media from plate with adherent hESCs and wash with PBS without calcium and magnesium twice.

(c) Add 500 mL of accutase to each 35 mm plate and incubate at 37 °C for 5 min or until cells have detached.

(d) Add 1 mL of mTeSR with RI to each 35 mm plate to dilute accutase. Use pipette to break hESC colonies into a single cell suspension.

(e) Transfer cell suspension to 15 mL tube and pellet cells in centrifuge at 180 RCF for 4 min.

(f) Aspirate media and resuspend cells in 0.5–1 mL mTeSR with RI (10 μM) for every ~1 × 10^6 cells collected (Estimated. For reference, a nearly confluent 35 mm dish typically contains about 3 × 10^6 hESCs.)

(g) Count the number of cells/mL using a hemocytometer.

2. Aspirate/remove PBS++ from wells in CYTOO plate/chips.

3. Seed cells to micropatterned surfaces. The number of cells will depend on the micropatterned format (96-well plate vs. chip) and pattern model (gastruloid vs. ectoderm). ***For 96-well plate***, seed 180,000 cells/well for gastruloid patterns or 120,000 cells/well for ectodermal patterns. For both models, cells are seeded to wells using 100 μL of mTeSR plus RI. ***For chips***: seed 1.8 × 10^6 cells/chip for gastruloid patterns or 1.2 × 10^6 cells/chips for ectodermal patterns. For both models, cells are seeded to chips in 35 mm plates using 2 mL of mTeSR plus RI.

4. Place chips or 96-well plates in the incubator for 45 min at 37 °C. Note: incubation time can go up to 1.5 h if needed (*see* **Note 2**).

5. Prepare differentiation media prior to washing cells.

3.3 Wash Nonspecifically Bound Cells

1. Completely wash cells with PBS (250 μL/well of a 96-well plate and 1 mL/chip in 35 mm dish) without calcium and magnesium (PBS– –) 1–6 times until the majority of cells outside of the pattern have been removed. First washes should be gentler and against the side of the well of a 96-well plate or 35 mm dish. It is best practice to continually check progress on phase contrast microscope and gradually pipette more aggressively as needed. It is not necessary to remove all of the non-patterned cells at this point; many will die and detach once RI is removed at a later step (Fig. 1).

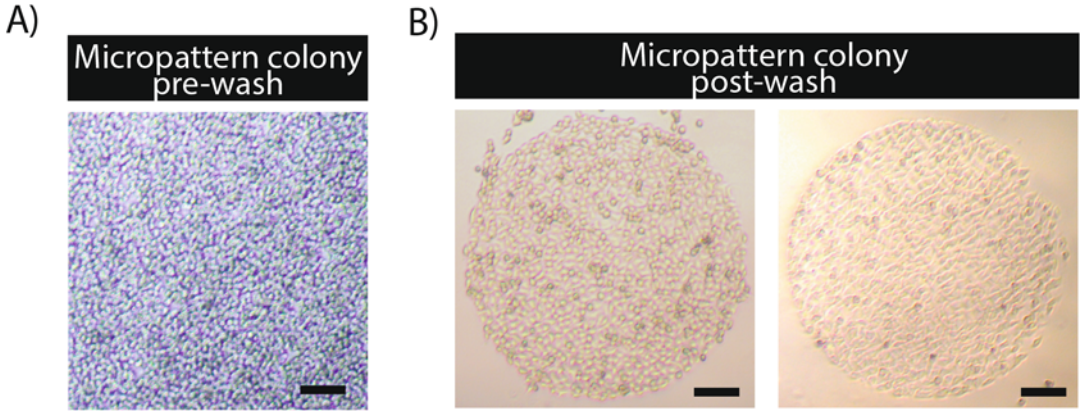

Fig. 1 Images of hESCs on micropatterns at the time of seeding. (**a**, **b**) Representative phase contrast images of hESCs seeded to a micropattern surface before (**a**) and after (**b**) washing. Colony diameter: 700 μm. Scale bar: 100 μm

3.4 Differentiate

Proceed to either gastruloid differentiation or ectodermal differentiation

3.4.1 Gastruloid Differentiation

The induction media is introduced only at the beginning and uses a volume of 200 μL for 96-well plates and 2 mL for chips.

1. After washing micropatterned cell colonies, replace PBS with mTeSR containing 50 ng/mL BMP4 and Pen/Strep (1%). Note that this media no longer contains RI. For 96-well plates, use 200 μL media. For chips use 2 mL. media.
2. Incubate at 37 °C for 42–48 h.

3.4.2 Patterned Ectoderm Differentiation

There are several treatment protocols that provide different ectoderm patterns described in our initial report [3]. Here we describe one of the protocols that results in patterns consisting of placodes, neural crest, and neural cell fates.

Media is changed daily with the media used on each day described below. Use 100 μL/well of a 96-well plate and 2 mL/chip in a 35 mm plate. Note RI is absent throughout the induction protocol.

1. After washing micropatterned cell colonies, replace PBS with mTeSR supplemented with SB431542 (10 μM) and pen/strep (1%).
2. After 24 h, exchange the media for N2B27 supplemented with SB431542 (10 μM) and pen/strep (1%) for the following two nights.
3. After three nights of induction with SB431542, introduce 1–3 ng/mL of BMP4 to N2B27 media with 10 μM SB431542 and pen/strep (1%).

4. On the following day, BMP4 signaling is maintained while WNT secretion is inhibited with N2B27 media containing 1–3 ng/mL BMP4, 10 μM SB431542, 3 μM IWP2, and pen/strep (1%).
   (a) Use the same concentration of BMP4 as the prior day.
5. Cells are fixed on the sixth day.

3.5 Fix Cells, Stain for Immunofluorescence, and Image

PFA should only be used in a chemical safety hood. PFA fixation and immunofluorescence staining can be performed using standard techniques for cell culture while being especially careful while pipetting not to disturb patterned cells.

3.5.1 Common to CYTOO 96-Well Plates and Chips

1. Fix cells by replacing media with 4% Paraformaldehyde (Wt/Vol; 100 μL/well of 96-well plate or 1 mL/chip in 35 mm dish) in PBS and incubating at room temperature for 20 min.
2. Aspirate PFA and wash cells with PBS twice (300 μL/well of 96-well plate and 2 mL/chip in 35 mm dish).
3. Add blocking solution (100 μL/well of 96-well plate and 1 mL/chip in 35 mm plate) to cells and incubate at room temperature for 1 h.
4. Replace blocking solution with primary antibodies diluted in blocking solution (50 μL/well of 96-well plate and 1 mL/chip in 35 mm dish) and incubate at room temperature for 1 h or overnight at 4 °C.
5. Perform three 20-min washes at room temperature with PBST (300 μL/well of 96-well plate and 2 mL/chip in 35 mm dish).
6. Replace final PBST wash with secondary antibody solution diluted in blocking solution (50 μL/well of 96-well plate and 1 mL/chip in 35 mm dish) and incubate at room temperature for 30 min.
7. Wash three more times with PBST (same volume as **step 5**) for 20 min each at room temperature.
8. Replace PBST wash with DAPI diluted in PBS to a final concentration of 300 nM (50 μL/well of 96-well plate and 1 mL/chip in 35 mm dish) and incubate at room temperature for 30 min.
9. Perform two 5-min washes with PBS (300 μL/well of 96-well plate and 2 mL/chip in 35 mm dish).
10. Replace final PBS wash with PBS (200 μL/well of 96-well plate and 2 mL/chip in 35 mm dish).
11. Mount CYTOO chips on a slide.

(a) Add 30 μL of fluoromount to a clean microslide and carefully transfer the CYTOO chip to the slide with its face oriented down on the microslide.

(b) Let each sample dry in a dark environment overnight.

12. Image cells using a fluorescent microscope (Fig. 2).

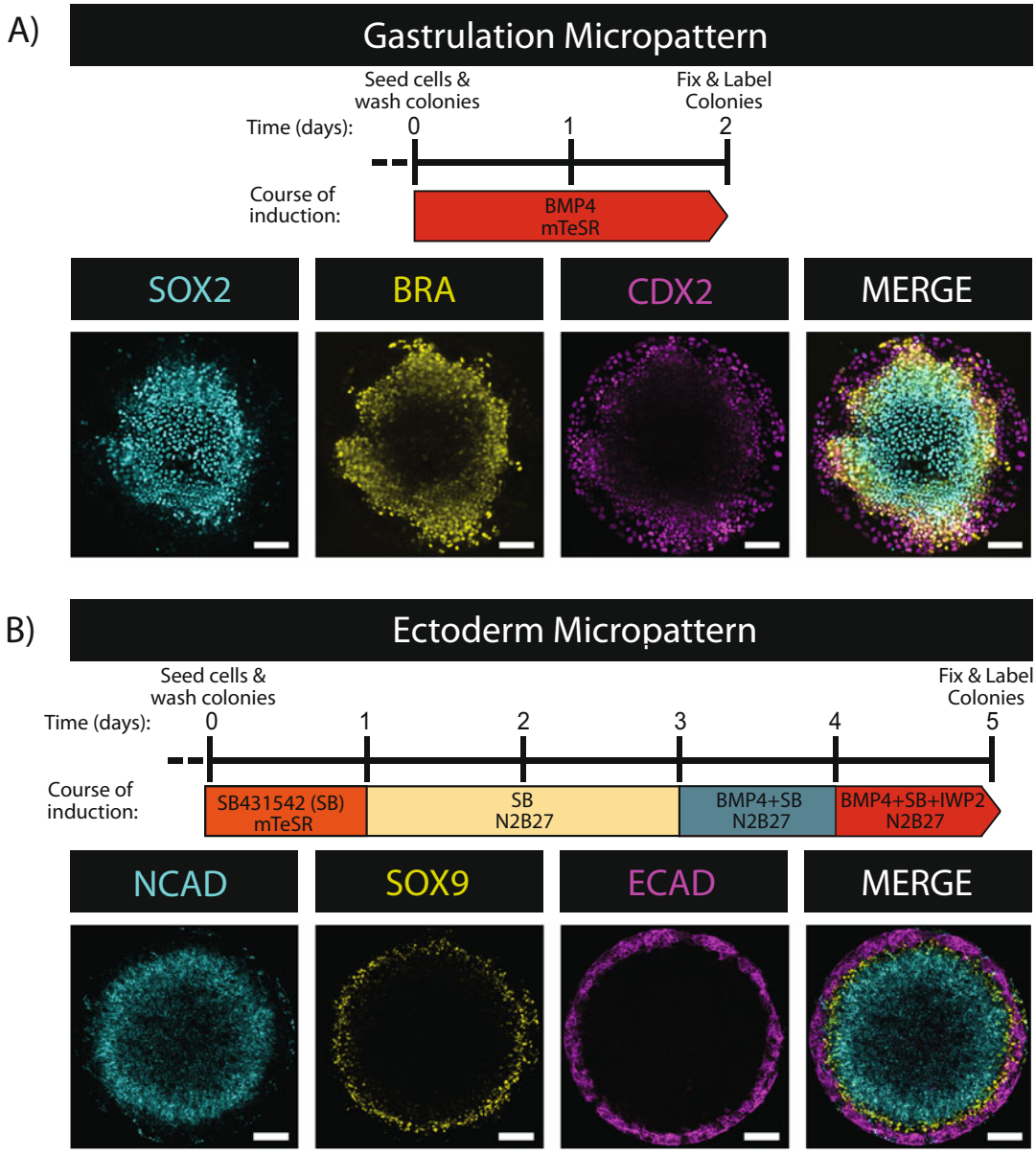

Fig. 2 Induction protocol and fate patterning in 2D gastruloids and ectodermal patterns. (**a**, **b**) Representative images of colonies with the indicated single or merged immunolabels following a gastruloid (**a**) or ectoderm (**b**) induction protocol with 50 ng/mL of BMP4 (**a**) or 1 ng/mL of BMP4 (**b**). The base media for each day is indicated below the cocktail of supplied agonists and inhibitors. Colony diameter: 700 μm. Scale bar: 100 μm

4 Notes

1. Sometimes batch-to-batch variability in laminin 521 results in the need for empirically determining the optimal coating concentration, though this is rare. We typically find the optimal concentration is between 5 and 20 μg/mL.
2. Number of seeded cells may need to be determined empirically for each cell line. A lower number of cells is seeded for ectoderm patterning experiments due to the longer growth time, while for gastruloids the seeding density can be higher. For gastruloids in particular, it is important that patterns are completely full after seeding, and it is generally better to err on the side of having more cells than having too few.

Acknowledgments

George Britton, Sapna Chhabra, and Joseph Massey contributed equally to this work.

References

1. Théry M (2010) Micropatterning as a tool to decipher cell morphogenesis and functions. J Cell Sci 123:4201–4213
2. Warmflash A, Sorre B, Etoc F et al (2014) A method to recapitulate early embryonic spatial patterning in human embryonic stem cells. Nat Methods 11:847–854. https://doi.org/10.1038/nmeth.3016
3. Britton G, Heemskerk I, Hodge R et al (2019) A novel self-organizing embryonic stem cell system reveals signaling logic underlying the patterning of human ectoderm. Development 146(20):dev179093. https://doi.org/10.1242/dev.179093
4. Chhabra S, Liu L, Goh R et al (2019) Dissecting the dynamics of signaling events in the BMP, WNT, and NODAL cascade during self-organized fate patterning in human gastruloids. PLoS Biol 17:e3000498. https://doi.org/10.1371/journal.pbio.3000498
5. Tewary M, Ostblom J, Prochazka L et al (2017) A stepwise model of reaction-diffusion and positional information governs self-organized human peri-gastrulation-like patterning. Development 144:4298–4312. https://doi.org/10.1242/dev.149658
6. Manfrin A, Tabata Y, Paquet ER et al (2019) Engineered signaling centers for the spatially controlled patterning of human pluripotent stem cells. Nat Methods 16:640–648. https://doi.org/10.1038/s41592-019-0455-2
7. Morgani SM, Metzger JJ, Nichols J et al (2018) Micropattern differentiation of mouse pluripotent stem cells recapitulates embryo regionalized cell fate patterning. elife 7:e32839. https://doi.org/10.7554/eLife.32839
8. Martyn I, Kanno TY, Ruzo A et al (2018) Self-organization of a human organizer by combined Wnt and Nodal signalling. Nature 558:132–135. https://doi.org/10.1038/s41586-018-0150-y
9. Arnold SJ, Robertson EJ (2009) Making a commitment: cell lineage allocation and axis patterning in the early mouse embryo. Nat Rev Mol Cell Biol 10:91–103. https://doi.org/10.1038/nrm2618
10. Heemskerk I, Burt K, Miller M et al (2019) Rapid changes in morphogen concentration control self-organized patterning in human embryonic stem cells. elife 8:e40526. https://doi.org/10.7554/eLife.40526.001
11. Deglincerti A, Etoc F, Guerra MC et al (2016) Self-organization of human embryonic stem cells on micropatterns. Nat Protoc 11:2223–2232. https://doi.org/10.1038/nprot.2016.131

Chapter 10

Gastruloids: Embryonic Organoids from Mouse Embryonic Stem Cells to Study Patterning and Development in Early Mammalian Embryos

Kerim Anlas, Peter Baillie-Benson, Krisztina Arató, David A. Turner, and Vikas Trivedi

Abstract

Gastruloids are embryonic organoids made from small, defined numbers of mouse embryonic stem cells (mESCs) aggregated in suspension culture, which over time form 3D structures that mimic many of the features of early mammalian development. Unlike embryoid bodies that are usually disorganized when grown over several days, gastruloids display distinct, well-organized gene expression domains demarcating the emergence of the three body axes, anteroposterior axial elongation, and implementation of collinear Hox transcriptional patterns over 5–7 days of culture. As such *gastruloids* represent a useful experimental system that is complementary to in vivo approaches in studying early developmental patterning mechanisms regulating the acquisition of cell fates. In this protocol, we describe the most recent method for generating gastruloids with high reproducibility, and provide a comprehensive list of possible challenges as well as steps for protocol optimization.

Key words Gastruloids, Gastrulation, Organoids, Mouse embryo, Axial development, Mouse embryonic stem cells

1 Introduction

The initial body plan of the embryo is established during early development, where specific regions of gene expression are defined that serve as a blueprint for coordinating the growth and patterning of the embryo over time. In mammalian embryos, the zygote develops two distinct cell populations, inner cell mass (ICM), and trophectoderm, the former being the source of embryonic stem cells. Around implantation, the ICM segregates into the primitive

Kerim Anlas and Peter Baillie-Benson authors contributed equally to this work.

The former name of the author "Peter Baillie-Benson" was "Peter Baillie-Johnson".

Mo R. Ebrahimkhani and Joshua Hislop (eds.), *Programmed Morphogenesis: Methods and Protocols*, Methods in Molecular Biology, vol. 2258, https://doi.org/10.1007/978-1-0716-1174-6_10,

endoderm and epiblast, with the epiblast giving rise to all tissues of the embryo proper. Prior to gastrulation (which transforms a bilayered embryo into one comprised of three germ layers), a subpopulation in the proximal posterior region of the epiblast initiates the expression of *T/Brachyury* (T/Bra) defining the site of gastrulation and the formation of the primitive streak.

Owing to the inaccessibility of mammalian embryo at these early stages of development, studying many of the cellular processes involved in lineage specification in vivo has been technically challenging. Embryonic stem cells (ESCs) provide a potential, inexpensive solution to dissect these events as they can generate all tissues of the embryo proper, can be maintained indefinitely in culture, and their directed differentiation can yield different cell fates [1–8]. Studies conducted with mouse ESCs (mESCs) in particular have informed our understanding of the role and requirement of specific signaling molecules and transcription factors in early mouse development. However, these studies have been performed on cells grown in a monolayer (two-dimensional; 2D) which lack the architecture of a three-dimensional (3D) embryo.

Recently, more attention has been given to developing techniques that allow cells to be cultured in 3D, building on previous work on hanging-drop and mechanically supported cultures [9] to generate 3D structures termed *organoids*. Organoids, which can be derived from stem cells (embryonic and adult) or fragments of in vivo tissues (such as intestinal crypts), mimic the structural architecture and, to some extent, the function of their in vivo counterparts. Examples include mesodermal derivatives [10, 11], intestinal [12], gut [13], kidney [14, 15], brain [16, 17], retinal [18, 19], and neural [20] organoids. Together, they represent a class of new approaches and model systems to understand embryogenesis in vitro [21, 22].

1.1 Gastruloids and Other Embryonic Organoids

Work by van den Brink et al. [23] showed that a defined number of mESCs when aggregated to form initially spherical 3D structures mimic morphogenetic events of early mouse embryos, such as polarization of gene expression, primary axis formation, elongation, and associated patterning, notably in the absence of extraembryonic tissues and nearly all associated signaling cues. This system, termed *gastruloids*, has been developed since then, demonstrating that mESCs in such aggregates, in a serum- and matrigel-free environment, display gastrulation-like movements and develop gene expression domains associated with all germ layers as well as the three body axes, accompanied by timely implementation of collinear Hox transcriptional patterns over 5–7 days of culture [24–27]. In this article, we outline a unified protocol for generating *gastruloids* that has been developed across several labs.

As an alternative to in vivo studies of early embryogenesis and pattern formation, several embryonic organoid model systems have been developed, each with its own unique strengths, and it is

important to recognize key differences between them and *gastruloids* discussed in this protocol. Embryoid bodies, for example, have been used by a number of groups to study axis formation and polarised gene expression [10], however these differ in both the protocol (in terms of number of cells and media composition) as well as the final outcome. Unlike *gastruloids*, which are grown in serum-free media and start with approximately 300 mESCs, embryoid bodies are typically grown in media with serum and can start with a cell number ranging from hundreds to thousands of cells in suspension [9]. Two other remarkable systems use both embryonic and extraembryonic stem cells to mimic embryogenesis in vitro at two distinct stages: (a) *blastoids*, which are aggregates of trophoblast and embryonic stem cells that resemble embryonic day 3.5 blastocysts [28, 29]; (b) ETX embryos that consist of embryonic, trophoblast, and extraembryonic endoderm stem cells and mimic an epiblast with embryonic and extraembryonic compartments [30, 31]. These differ from gastruloids that consist of only embryonic stem cells and thereby provide an opportunity to study the self-organizing potential of embryonic cells in the absence of any extraembryonic tissue. Altogether, gastruloids represent a highly tractable, medium-throughput in vitro system that is suitable for live imaging, and for dissecting and elucidating the underlying events involved in early mouse development such as symmetry breaking, cell fate decisions, and tissue patterning dynamics.

2 Materials

2.1 Cell Lines Tested with this Protocol

We have tested a number of cell lines from various backgrounds, assessed their ability to generate gastruloids, and modified their culture conditions to ensure they are in a similar responsive state just prior to *gastruloid* formation. We usually consider the frequency and extent of elongation observed in *gastruloids* at around 96–120 h as a proxy for assessing how "competent" the cells are in responding to differentiating signals when taken from culture prior to the gastruloid protocol. While the number of cells that usually yields gastruloids that initiate elongation at 72 h in culture is typically 300 cells, certain cell lines require the plating number to be optimised. Certain cell lines might also require a day long exposure to 2i + LIF medium (termed "2iL-Pulse," [ESL-2iL]) prior to the *gastruloid* protocol.

2.2 Routine Culture Medium

For the following medium, ensure the maximum volume remains 500 mL, removing sufficient volume of the base medium to allow for the total volume of medium supplements. Always avoid using "old" medium where the pH is too high (i.e., purple medium where phenol red is the pH indicator). Store all complete medium at 4 °C and warm to 37 °C before use.

1. ESL Medium

   This is the standard medium for culturing most mESC lines.

   (a) Base medium (*see* **Notes 1** and **2**).

   - 500 mL Glasgow's Minimal Essential Medium (GMEM, Gibco 11710-035).

   Or

   - 500 mL Dulbecco's Modified Eagle's Medium (DMEM, Gibco 11960044).

   (b) 550 µL Mouse Leukemia Inhibitory Factor (mLIF; 1000 U, either inhouse or commercial).

   (c) 50 mL Fetal bovine serum (FBS; 10% final concentration, requires batch testing for specific applications).

   (d) 5 mL Non-Essential Amino Acids (NEAA; 100×, Thermo Fisher Scientific 11140050).

   (e) 5 mL Sodium Pyruvate (100×, Thermo Fisher Scientific 11360070).

   (f) 5 mL Glutamax (100×, Thermo Fisher Scientific 35050038).

   (g) 1 mL 2-mercaptoethanol (0.1 mM final concentration, Thermo Fisher Scientific 31350010).

2. N2B27/NDiff227

   This medium can either be commercially bought (NDiff227; Takara Y40002) (*see* **Notes 3** and **4**) or made in-house (N2B27) as described previously [4, 32] and in the following:

   (a) 250 mL DMEM/F12 (50:50; Thermo Fisher Scientific 11320074).

   (b) 250 mL Neurobasal (Thermo Fisher Scientific 21103049).

   (c) 2.5 mL N2 (100×; Thermo Fisher Scientific 17502048).

   (d) 5 mL B27 (50×; Thermo Fisher Scientific 17504044).

   (e) 5 mL glutamax (100×; Thermo Fisher Scientific 35050038).

   (f) 1 mL 2-mercaptoethanol (Thermo Fisher Scientific 31350010).

   (g) BSA fraction V (Gibco™ 15260037).

3. 2iL

   (a) 50 mL N2B27 (or NDiff227).

   (b) 3 µM CHIR99021 (Chi; 10 mM stock dissolved in DMSO, Tocris Bioscience 4423).

(c) 1 μM PD0325901 (PD03; 10 mM stock dissolved in DMSO, Tocris Bioscience 4192).

(d) 55 μL mLIF.

4. Tissue culture reagents
   (a) 1× $PBS^{+/+}$ (with Ca^{2+} and Mg^{2+}).
   (b) Gelatin; a 1% (w/v) stock solution prepared in sterile water and autoclaved. Further diluted to 0.1% (v/v) in PBS (with Ca^{2+} and Mg^{2+}). *Alternatively acquire ready-to-use 0.1% gelatin in H_2O suitable for ESC culture applications.*
   (c) Trypsin-EDTA (0.05%, Thermo Fisher Scientific 25300054).
5. Tissue culture plastics and equipment
   (a) Tissue culture-treated flasks: 25cm^2 flasks routinely used; coated in 0.1% gelatin before use.
   (b) 50 mL or 15 mL sterile centrifuge tubes.
   (c) Sterile reservoir.
   (d) U-bottomed 96-well plate (Greiner Bio-One 650185).
   (e) U-bottomed 96-well plate with low adherence (for extended culture to 144 h; Greiner Bio-One 650970 or Corning® CLS7007).
   (f) Low-adherence 24-well plate for extended culture (from 120 to 168 h) (Corning, 3473).
   (g) Cell counter/hemocytometer.
   (h) BSL-2 biosafety cabinet.
   (i) Benchtop centrifuge with capacity for 15 mL or 50 mL centrifuge tubes.
   (j) Water bath set to 37 °C.
   (k) An optional requirement for an incubator-compatible horizontal shaker (Infors Celltron 69222) for extended culture up to 168 h after aggregation.
   (l) Inverted benchtop tissue culture microscope.
   (m) Multichannel pipette(s) for 40 μL and 150 μL volumes.

3 Methods

3.1 Routine Cell Culture

In order to generate consistent gastruloids, it is essential that the cells are well maintained and that they are competent to respond to differentiating signals. Ensure cells are *Mycoplasma*-free and have not been maintained in culture for excessive passage numbers which, while naturally dependent on the "age" of the respective

cell line, generally amounts to a maximum of around 25–30 passages from thawing a fresh aliquot. Cells must be in culture for 2–3 passages after defrosting before making gastruloids. Typically, cells are cultured in 25 cm^2 tissue culture-treated flasks that have been coated with 0.1% gelatin/PBS or 0.1.% gelatin/H_2O, in GMEM or DMEM containing serum and LIF (*see* above for formulation; ESL). Ensure medium and trypsin is warmed up to 37 °C prior to use.

1. Prepare a fresh 25 cm^2 tissue culture flask and coat with 3 mL 0.1% gelatin/PBS for at least 30 min at RT. Coating can continue overnight at room temperature (RT) if required. Aspirate gelatin solution just prior to use.
2. When the flask containing mESCs is approximately 60% confluent, aspirate the culture medium and wash twice with PBS to remove traces of serum. Aspirate PBS and incubate at 37 °C until cells have detached (<5 min) in the humidified tissue culture incubator with 2 mL trypsin. Gentle mechanical agitation aids cell detachment.
3. Once the cells have detached, inactivate the trypsin with 8 mL ESL, gently pipetting up and down with a 10-mL pipette over the growth surface ~3–4 times to dislodge any cells still adherent and to break up any remaining clumps of cells.
4. Transfer cells to a centrifuge tube (50 mL or 15 mL) and centrifuge for 3 min at 170 × *g* (~1000 rpm). Following centrifugation, aspirate the supernatant carefully to prevent the pellet being dislodged, and resuspend in an appropriate volume of fresh ESL (i.e., 1 mL). Ensure generation of a homogeneously dispersed single-cell suspension by gentle repeated pipetting with a P1000 pipette, avoiding the generation of bubbles.
5. Determine the cell density by counting with an automated cell counter or a hemocytometer. Remove gelatin from the fresh tissue culture flask, and plate an appropriate number of cells in 6 mL ESL (*see* **Note 5**).
6. Place the flask carefully in the humidified 37 °C incubator (5% CO_2), and ensure the cells are evenly spread along the tissue culture flask.
7. The next day, check the cells to ensure they are growing well (estimated confluency at this stage is ~20%). Aspirate medium and replace with fresh ESL.

3.2 Preparation of N2B27

If using commercial N2B27 (NDiff227), extreme care is required when defrosting the stock bottle to ensure there is no precipitation in the medium which would interfere with gastruloid aggregation and their ongoing culture. It has been found that NDiff227 readily precipitates during defrosting, and the following method (adapted from the manufacturer's instructions) prevents this from occurring.

1. Place NDiff227 in the water bath set to 37 °C and immediately protect from light via covering with aluminum foil or using a darkened incubator lid.
2. After 15 min, remove the stock bottle from water bath and gently invert it repeatedly (~3–4 times) to gradually equilibrate the temperature around the bottle. Place the bottle back in the water bath (protected from light).
3. Continue to return to and invert the bottle every 5 min. Remove the bottle from the water bath at the point where the ice has dissolved to the size of a ball of ~4–5 cm, invert the bottle once more and place in the fridge at 4 °C overnight.
4. The next day, check for precipitate and if clear, invert the bottle 3–4 times (to fully mix and avoid any concentration gradients that have formed) and aliquot. Store aliquots at 4 °C protected from light for a month.

3.3 Preparing Cells for Gastruloid Plating

We have developed two protocols for culturing cells in preparation for gastruloid formation (Fig. 1): Protocols [ESL-ESL] and [ESL-2iL]. The first protocol [ESL-ESL] is the "standard protocol" [24–28], where cells are exposed to their normal culture medium for the duration of the passage, whereas the second

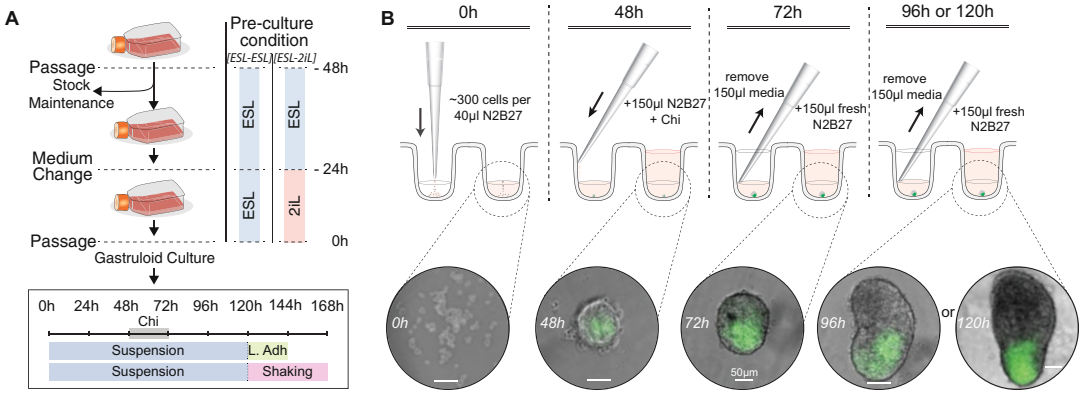

Fig. 1 The generic workflow for gastruloid generation. (**a**) General mouse embryonic stem cell (mESC) maintenance. For making gastruloids, flasks (25 cm^2) with ~60% confluency are passaged, and cells are plated for stock maintenance or for gastruloid culture in normal growth medium (ESL), and changed into either ESL or 2iL depending on their requirement (*see* Subheadings 3.1–3.3). Cells are then passaged the next day to generate gastruloids. The timeline of gastruloid development is shown in Subheading 3.4. (**b**) A 40 µL droplet containing the required number of mESCs (*see* Subheading 3.4) is plated directly into the center of the wells of a 96-well plate (0 h; left panel) with a multichannel micropipette. At 48 h, 150 µL fresh N2B27/NDiff227 containing 3 µM Chi is added carefully to the sides of the well (second panel from left). From 72 h onward, cell culture (150 µL) medium is replaced every 24 h with fresh N2B27/NDiff227 by carefully removing the medium from the base of the vertical sides of the well so as not to disturb the developing gastruloid, holding the pipette at an angle to the well. 40 µL is always left in the well to prevent gastruloids from drying out. Image panels below show representative gastruloids, made with Bra+/GFP cell line [33], at the indicated timepoints after aggregation. All scalebars denote 50 µm

Table 1
Cell lines that have been successfully tested with this protocol and specific requirements

Cell line	Strain/background	Requirement of [ESL-2iL] pre-gastruloid
E14-Tg2A [33]	129/Ola	Yes
$Bra^{+/GFP}$ [34]	129P2/OlaHsd	No
$Nodal^{+/YFP}$ [35]	129S2/SvPas	No
$Gata6^{H2BVenus}$ [36]	(C57BL/6 × 129S4/SvJae)F1	Yes
$Sox1^{eGFP}$; $Bra^{mCherry}$ [37]	129P2/OlaHsd	No
AR8::mCherry [38]	129S6/SvEvTac	No
$FoxA2^{+/YFP}$	(C57BL/6J × 129S6/SvEvTac)F1	Not tested
Sox1GFP (46C) [39]	129/Ola	Not tested

The following table details the specific cell lines we have tested with respect to the gastruloid protocol. Some cell lines, as highlighted in the text, require a 24 h pretreatment with 2iL the day before gastruloid formation [ES-2iL] and that information has been indicated here. The number of cells needed for "successfully" making gastruloids is around 300; however, depending upon specific conditions in the lab and composition of ESL (GMEM- or DMEM-based), starting cell numbers might need to be optimized (*see* Subheading 4, **Note 3**)

protocol [ESL-2iL] requires a pulse of 2iL medium on the second day in culture. It must be stressed that this second protocol is not necessary for all cell lines, and is only necessary if the cells produce variable gastruloid morphology by 120 h (i.e., <70% consistent elongation). Further, the end results in terms of gastruloid morphology and gene expression may be different for the two protocols. *See* Table 1 for the cell lines we have tested and their requirement for 2iL pretreatment [ESL-2iL].

1. For the passage before plating gastruloids, passage the cells as described above (Subheading 3.1) and plate the required number of cells into two 25 cm^2 tissue culture flasks in 6 mL routine cell culture medium. Incubate overnight in a humidified incubator (37 °C; 5% CO_2). The first flask is to continue the culture of cells ("passage flask" Fig. 1; Subheading 3.1), whereas the other is solely for gastruloid culture ("gastruloid flask"; Fig. 1).
2. The next day, aspirate the medium in the "gastruloid flask," and replace with either 6 mL of routine tissue culture [ESL-ESL] or wash cells with 6 mL $PBS^{+/+}$ and then replace with 2iL [ESL-2iL], depending on the cell line. Incubate cells overnight in a humidified incubator (37 °C; 5% CO_2).
3. Aspirate the medium in the "passage flask," and replace with normal culture medium. This flask will be used to continue the culture of the cell line in parallel to gastruloid culture (Subheading 3.1).

3.4 Gastruloid Generation and Culture

This section describes the method of producing a single 96-well plate of gastruloids from the abovementioned "gastruloid flask." Once the experimenter is familiar with the protocol, it is possible to scale up the quantities for multiple 96-well plates. However, we do not recommend more than four plates setup at a time (as this will increase the time the cells are out of the incubator, possibly leading to an increase in variability). Prior to starting this section of the protocol, ensure the flask is ~60% confluent, and the cells appear healthy by examining the flask of cells on an inverted tissue culture microscope.

3.4.1 0 h After Aggregation (AA): Cell Plating

1. Pre-warm all media (ESL and N2B27/NDiff227), trypsin, and $PBS^{+/+}$ in a water bath set to 37 °C.
2. Aspirate medium from the mESC culture flask ("gastruloid flask"), wash once with 5 mL PBS+/+, and incubate cells with 2 mL Trypsin/EDTA for <5 min in a humidified incubator (37 °C; 5% CO_2). Excessive incubation with trypsin has a detrimental effect on gastruloid formation, so it is imperative that the cells are checked every ~2 min. Rock the cells to aid detachment of the cells from the flask and remove the flask from the incubator once cells are no longer adhering to the flask growth surface.
3. Inactivate trypsin by the addition of 8 mL ESL, and dissociate the colonies by pipetting up and down ~3 times across the growth surface. Transfer the 10 mL cell suspension to a 15-mL or 50-mL centrifuge tube and centrifuge the cell suspension at approximately 170 × *g* for 3 min.
4. Aspirate the supernatant and dissociate the cell pellet by adding 10 mL warm $PBS^{+/+}$. Centrifuge the cell suspension at 170 × *g* for 3 min.
5. Aspirate the supernatant and dissociate the cell pellet for a second time by adding 10 mL warm $PBS^{+/+}$ and centrifuge at 170 × *g* for 3 min.
6. Aspirate the supernatant, ensuring minimal carryover of PBS while maintaining integrity of pellet by tilting the tube to ~45° and removing the liquid from the side of the tube.
7. Cover the pellet in 1 mL warm N2B27/NDiff227 and fully resuspend the pellet using a p1000 pipette set to 1 mL. Pipette up and down (~3 times for most cell lines) to ensure a single-cell suspension is obtained, minimizing bubbling. This solution can be further diluted with a suitable volume of N2B27/NDiff227 (e.g., 3 mL) if required.
8. Accurately determine the concentration of the cell suspension with either an automated cell counter or a hemocytometer, and calculate the required volume of cell suspension for one 96-well

plate, e.g., if one is plating 300 cells per well, transfer 37,500 cells to 5 mL medium such that the final concentration is 300 cells/40 μL. The 5 mL volume is sufficient for 40 μL to be transferred to each well and includes adequate dead volume following later pipetting.

9. Transfer the correct volume of cell suspension to fresh, warm N2B27 to give a final volume of 5 mL, and mix the tube gently by hand, or carefully pipette the solution up and down with a 5 mL pipette (avoiding bubbles). Transfer this cell suspension to a reservoir.
10. Using a multichannel micropipette, transfer 40 μL from the reservoir to each well of a sterile U-bottomed, non-tissue culture-treated 96-well plate, pipetting the droplet into the center of each well (Fig. 1b; 0 h, top panel). If needed, gently tap each of the four sides of the plate to force any droplets that were pipetted to the sides on to the bottom of their wells. If gastruloid culture to 144 h or 168 h after aggregation is desired, it is recommended to use low adherence 96-well plates (*see* Subheading 2.2, **item 5e**).
11. Confirm that cells have been transferred by sampling a region of the plate under an inverted tissue culture microscope (Fig. 1b; 0 h, bottom panel).
12. Transfer the 96-well plate to the humidified incubator (37 °C; 5% CO_2) and incubate for 48 h.
13. At this stage, if the cell stock is being maintained, follow the steps in Subheading 3.1 for the "passage flask."
14. Following aggregation gastruloid culture can be halted at this or any following stage for imaging, fixation, or other downstream techniques (*see* Subheading 3.5) (*see* **Note 6**).

3.4.2 48 h After Aggregation: Addition of Secondary Medium with Chiron

1. Pre-warm the required volume of N2B27/NDiff227 in a water bath set to 37 °C.
2. Prepare a 3 μM solution of Chi in 16 mL N2B27/NDiff227; this volume is sufficient for a single 96-well plate including "dead-volume" following pipetting. Mix well by hand, avoiding excessive medium bubbling (*see* **Note 7**).
3. Assess the quality of the gastruloids by observing them on an inverted benchtop microscope. They should have formed a single, spherical aggregate of smooth appearance approximately 150 μm in diameter (Fig. 1b; 48 h). Only slight deviations from this morphology can be expected depending on the cell line (e.g., slightly ovoid) (*see* **Notes 8–13** for trouble shooting).

4. Pipette the Chi solution to a sterile reservoir, and gently transfer 150 μL to each well of the 96-well gastruloid plate using a multichannel micropipette, ejecting the medium at the side of the well, above the 40 μL volume (Fig. 1b; 48 h).
5. Incubate the plate in a humidified incubator (37 °C; 5% CO_2) for 24 h.

3.4.3 72 h After Aggregation: Removal of Chiron Pulse and Medium Change

1. Pre-warm the required volume of N2B27/NDiff227 in a water bath set to 37 °C.
2. Assess the quality and progression of the gastruloids on an inverted benchtop microscope. Gastruloids should still have a smooth appearance, but, depending on the cell line, they may have advanced to an ovoid morphology. For instance, wild-type (E14-Tg2A) gastruloids tend to maintain a spherical appearance at this stage, whereas for $Bra^{+/GFP}$ gastruloids start elongating by 72 h. In the particular case of $Bra^{+/GFP}$ gastruloids, the expression of the reporter will be highly polarized to the "posterior" region (Fig. 1b; 72 h).
3. Remove 150 μL from each well with a multichannel micropipette, holding the pipette at an angle and carefully removing the medium from the side of the well at the interface between the vertical side and the inverted dome of the well (Fig. 1b; 72 h). Note, it is important to leave 40 μL in the wells to prevent gastruloids from drying out.
4. As an optional control measure to ensure the gastruloids have not been aspirated, gently place the side of the pipette (still holding the aspirated medium) on top of a tip box to maintain the sterility of the tip ends, and confirm the presence of gastruloids using the bench-top microscope. Eject the medium if gastruloids have not been aspirated, or replace the medium and return to these wells after the rest of the plate's secondary medium has been removed.
5. Transfer a sufficient quantity of fresh, warm N2B27/NDiff to a reservoir and pipette 150 μL directly into each well of the 96-well plate as in Subheading 3.4, **step 18**. Note that the medium should be ejected into the wells with sufficient force to agitate the gastruloids, preventing them from adhering to the bottom of the wells. Forceful pipetting is not necessary when using low-adherence 96-well plates listed in Subheading 2.2, **item 5e**.
6. Incubate the plate in a humidified incubator (37 °C; 5% CO_2) for 24 h.

3.4.4 96 h After Aggregation: Medium Change

1. Repeat **steps 1–5** in Subheading 3.4.3 to exchange 150 μL medium with fresh, warm N2B27/NDiff227.

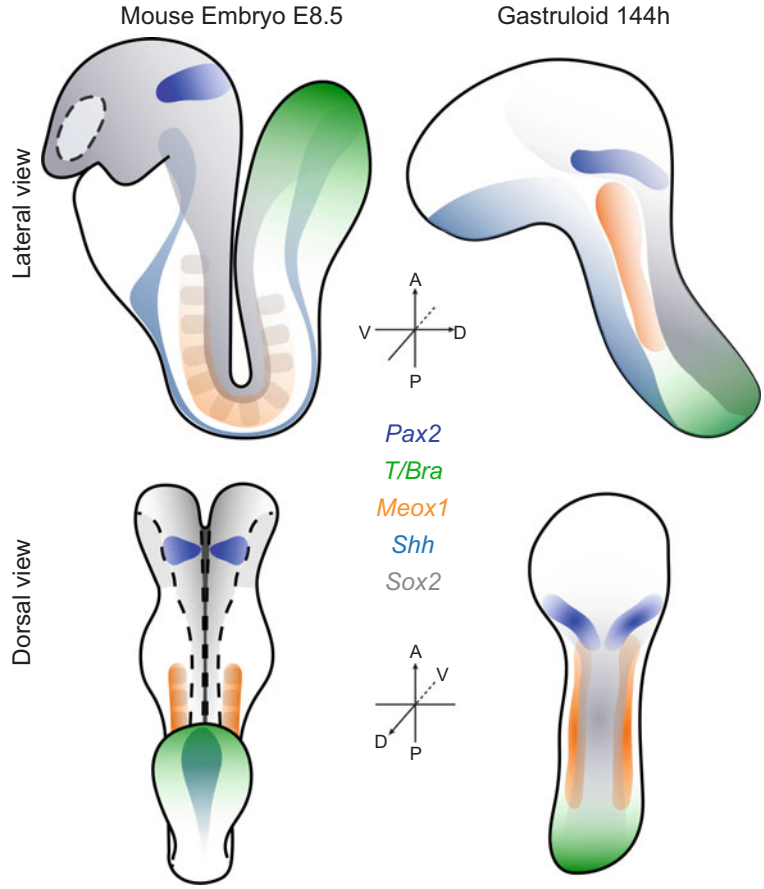

Fig. 2 Overview of gene expression progression and axes formation in gastruloids. Schematic diagrams showing candidate genes denoting the three axes (T/Bra denoting anteroposterior [AP], Shh denoting dorsoventral [DV], Meox and Pax2 denoting medio-lateral [ML] axes) and the three germ layers (T/Bra denoting mesoderm, Sox2 and Pax2 denoting ectoderm, Shh denoting endoderm) in relation to their expression in mouse embryo at E8.5. *A* anterior, *P* posterior, *D* dorsal, *V* ventral, axis lines without arrowheads denote medio-lateral axis

3.4.5 120 h After Aggregation: Medium Change and Continued Culture

1. At this stage, gastruloids ought to be highly elongated, and display polarized expression of Brachyury in the posterior ([23–26], Fig. 2), as well as expression of anterior markers localized to the opposite pole of Brachyury expression such as GATA6 [26]. Typically, the gastruloid culture is halted at this point for imaging, fixation, or other downstream techniques (*see* Subheading 3.5 and **Note 14**).
2. If continuing the culture to 144 h, repeat **steps 1–5** in Subheading 3.4.3 to exchange 150 μL medium with fresh, warm N2B27/NDiff227. When using standard round-bottom 96-well plates (*see* Subheading 2.2, **item 5d**) and if culture is

to be prolonged to 144 h, gently withdraw the entire volume of the well using a p1000 micropipette set to 200 μL, and individually transfer gastruloids to a fresh, low-adherence 96-well plate (see Subheading 2.2 **item 5e**, and incubate in a humidified incubator (37 °C; 5% CO_2) for 24 h (*see* **Note 15**).

3. If the culture is to be continued to 168 h, individually remove the gastruloids from the wells as in **step 2** of this section, but transfer them into low-attachment 24-well plates holding 700 μL fresh N2B27/NDiff227 (*Note: one gastruloid per well*). Incubate on an incubator-compatible horizontal shaker (e.g., Infors Celltron 69222) in a humidified incubator (37 °C; 5% CO_2) for 48 h at ~40 rpm [27], replacing 400 μL medium with fresh, warm N2B27/NDiff227 at 144 h.

3.5 Removing Gastruloids for Downstream Applications

1. Pipette a suitable volume of $PBS^{-/-}$ into a bacterial-grade 10 cm^2 dish (~5 mL) (*see* **Note 16**).
2. At the required timepoint, remove the 96-well gastruloid plate from the incubator and replace 150 μL medium with 200 μL warm $PBS^{-/-}$ using the method described in **steps 1–5** in Subheading 3.4.3.
3. Using a multichannel micropipette with the pipette tips cut 5 mm from the end, pipette up and down once, and then transfer the whole contents of the wells to the 10 cm^2 dish. Check that all gastruloids have been removed from the wells by sampling each well rapidly on an inverted bench-top microscope; collect any that have not been removed using a p200 set to 200 μL with the tips cut as above.
4. Swirl the 10 cm^2 dish to drive all the gastruloids to the center of the well, collect and transfer to 1.5 mL or 2 mL microcentrifuge tubes for downstream processing (e.g., fixation for immunofluorescence or in situ hybridization). To prevent gastruloids sticking to the inside of the tubes and pipette tips, coat with FBS or detergent (e.g., 2% Pluronic® F-127 in PBS) prior to use

4 Notes

1. Other base media can be used depending on the mESC line in question. For most mESC lines, either GMEM or DMEM is sufficient. Also, different labs might use slightly different concentrations of the components b–g for making ESL medium that works for lab-specific culture conditions.
2. Although we do not routinely use antibiotics in mESC culture for making gastruloids, their use is optional. It is important to monitor the cell line over time as low-level infection suppressed

by antibiotics may be misrepresented as non-contamination, and the downstream effects of this have not been examined regarding gastruloid culture.

3. N2 and B27 show batch variability, and each batch must be tested prior to use. Note that NDiff227 must be defrosted carefully as described in Subheading 3.2. BSA fraction V is optional. Also note that the concentration of N2 used is 0.5× final concentration.
4. N2B27 can be modified depending on the downstream application, as indicated in a recent publication [4], where three versions of N2B27 are provided.
5. An appropriate number of cells plated is the number which is required to produce a flask after 2 days that is 60–70% confluent. This is specific for each cell line. Depending on an experimentalist's experience, cell counting can be omitted and cells can be split into a new gelatin-coated flask at a ratio between 1:5 and 1:20, provided that appropriate confluency is reached after 2 days.
6. By observing the gastruloids at 24 h, one can get a good sense of whether they are forming correctly or whether too many/too few cells have been plated which will affect their development over the next days.
7. Other combinations of factors can be added to the medium [23, 25], and this will yield different results in morphology and gene expression.
8. Composition of basal medium. Some cell lines require DMEM, GMEM, or other formulations depending on their growth conditions. Grow cells for two passages in ESL containing different basal medium compositions, form gastruloids, and assess their aggregation, growth, and morphology throughout the timecourse.
9. Pretreatment of mESCs in culture with 2iL [ESL-2iL] medium prior to gastruloid protocol: Test the effect of either [ESL-ESL] or [ESL-2iL] preculture on gastruloid formation. Some lines do not require the 2iL pulse before passaging, and for others 2iL pulse might be essential for robust formation of gastruloids. The concentration of Chi/PD03 and LIF might need to be optimized depending on the cell line.
10. Number of mESCs used for making gastruloids: Different cell lines require optimization of the number of cells needed for making robust gastruloids (i.e., >70% consistent elongation in a plate by 120 h). Test the effect of different plating densities of cells during gastruloid formation from 200 to 500 cells/well.

11. Genetic background of mESCs used for making gastruloids: For reasons not clear yet from a molecular point of view, genetic background of the mESCs (i.e., source mouse strain from which mESCs were derived) can impact the formation of gastruloids. As a result, it will be necessary to optimize the culture conditions for uncharacterized cell lines, as well as cell lines that have recently been derived following genetic manipulation (i.e., insertion of reporter genes).
12. Dosage of Chi pulse on gastruloid formation and progression: We have found that the dose of Chi during the 48–72 h pulse to be cell-line-dependent, resulting in fewer or more elongated gastruloids by 120 h [40]. Test the effect a range of Chi concentrations has on gastruloid formation and progression.
13. General procedural precautions: Avoid plating more than four 96-well plates at the same time as this will increase the time cells are out of the incubator, to potentially detrimental effect.
14. Analysis: For qualitative assessment, gastruloids are scrutinized by visual inspection under an inverted tissue culture microscope. For quantitative assessment, images from a 96-well plate can be analyzed to identify shape, size (length, width, aspect ratio, etc.), localization, and intensity of gene expression following in situ hybridization or immunofluorescence, etc.
15. For some cell lines, these expression domains might be visible earlier or later than 120 h and so this needs to be confirmed individually.
16. Using a p1000 tip cut ~5 mm from the end with sterile scissors may help reduce damage to individual gastruloids.
17. As an alternative to Subheadings 3.5, **steps 1–4**, one can also use recently designed collector plates for pooling together gastruloids from a plate [41].

Acknowledgments

The authors wish to thank members of Alfonso Martinez Arias' lab, University of Cambridge, UK, for discussions. Additionally, for kindly sharing their cell lines, we are indebted to Heiko Lickert (FoxA2^{H2BYFP}), Gordon Keller (Bra$^{+/GFP}$), Austin Smith (E14Tg2A, 46C Sox1^{GFP}), Palle Serup (AR8mCherry), Jérôme Collignon (Nodal$^{+/YFP}$), Anna-Katerina Hadjantonakis (GATA6^{H2BVenus}), and David Suter (Sox1^{eGFP}; Bra^{mCherry}). We thank K. Hötte-Lohmeier, F. Pampaloni, and E.H.K. Stelzer from Goethe Universität Frankfurt am Main, Germany, for providing collectors and multi-collectors. KA, KA, and VT are funded by the European Molecular Biology Laboratory (EMBL) Barcelona; P B-B is funded as part of a Wellcome Strategic Award to Professor

Jennifer Nichols and a European Research Council advanced grant to Professor Alfonso Martinez Arias (834580). The Cambridge Stem Cell Institute is supported by core funding from Wellcome and the Medical Research Council. DAT is funded by an NC3Rs David Sainsbury Research Fellowship (NC/P001467/1), a Wellcome Trust Institutional Strategic Support Fund (ISSF), and by an award from the University of Liverpool Technology Directorate Voucher Scheme. We acknowledge the Liverpool Centre for Cell Imaging (CCI) for provision of imaging equipment and technical assistance. Kerim Anlas and Peter Baillie-Benson contributed equally to this work.

References

1. Evans MJ, Kaufman MH (1981) Establishment in culture of pluripotential cells from mouse embryos. Nature 292:154–156
2. Schröter C, Rué P, Mackenzie JP et al (2015) FGF/MAPK signaling sets the switching threshold of a bistable circuit controlling cell fate decisions in embryonic stem cells. Development 142:4205–4216
3. Turner DA, Rué P, Mackenzie JP et al (2014) Brachyury cooperates with Wnt/β-Catenin signalling to elicit Primitive Streak like behaviour in differentiating mouse ES cells. BMC Biol 12:63
4. Mulas C, Kalkan T, von Meyenn F et al (2019) Defined conditions for propagation and manipulation of mouse embryonic stem cells. Development 146:dev178970-17
5. Turner DA, Trott J, Hayward P et al (2014) An interplay between extracellular signalling and the dynamics of the exit from pluripotency drives cell fate decisions in mouse ES cells. Biol Open 3:614–626
6. Turner DA, Hayward PC, Baillie-Johnson P et al (2014) Wnt/β-catenin and FGF signalling direct the specification and maintenance of a neuromesodermal axial progenitor in ensembles of mouse embryonic stem cells. Development 141:4243–4253
7. Kalmar T, Lim C, Hayward P et al (2009) Regulated fluctuations in nanog expression mediate cell fate decisions in embryonic stem cells. PLoS Biol 7:e1000149
8. Lowell S, Benchoua A, Heavey B et al (2006) Notch promotes neural lineage entry by pluripotent embryonic stem cells. PLoS Biol 4:e121
9. Turner DA, Baillie-Johnson P, Martinez Arias A (2016) Organoids and the genetically encoded self-assembly of embryonic stem cells. BioEssays 38:181–191
10. ten Berge D, Koole W, Fuerer C et al (2008) Wnt signaling mediates self-organization and axis formation in embryoid bodies. Cell Stem Cell 3:508–518
11. Marikawa Y, Tamashiro DAA, Fujita TC et al (2009) Aggregated P19 mouse embryonal carcinoma cells as a simple *in vitro* model to study the molecular regulations of mesoderm formation and axial elongation morphogenesis. Genesis (New York, NY) 47:93–106
12. Spence JR, Mayhew CN, Rankin SA et al (2011) Directed differentiation of human pluripotent stem cells into intestinal tissue in vitro. Nature 470:105–109
13. McCracken KW, Catá EM, Crawford CM et al (2014) Modelling human development and disease in pluripotent stem-cell-derived gastric organoids. Nature 516:400–404
14. Xia Y, Nivet E, Sancho-Martinez I et al (2013) Directed differentiation of human pluripotent cells to ureteric bud kidney progenitor-like cells. Nat Cell Biol 15:1507–1515
15. Taguchi A, Kaku Y, Ohmori T et al (2014) Redefining the *in vivo* origin of metanephric nephron progenitors enables generation of complex kidney structures from pluripotent stem cells. Cell Stem Cell 14:53–67
16. Lancaster MA, Renner M, Martin C-A et al (2013) Cerebral organoids model human brain development and microcephaly. Nature 501:373–379
17. Qian X, Nguyen HN, Song MM et al (2016) Brain-region-specific organoids using mini-bioreactors for modeling ZIKV exposure. Cell 165:1238–1254
18. Eiraku M, Takata N, Ishibashi H et al (2011) Self-organizing optic-cup morphogenesis in three-dimensional culture. Nature 472:51–56

19. Eiraku M, Sasai Y (2012) Mouse embryonic stem cell culture for generation of three-dimensional retinal and cortical tissues. Nat Protoc 7:69–79
20. Meinhardt A, Eberle D, Tazaki A et al (2014) 3D reconstitution of the patterned neural tube from embryonic stem cells. Stem Cell Rep 3:987–999
21. Huch M, Koo B-K (2015) Modeling mouse and human development using organoid cultures. Development 142:3113–3125
22. Simunovic M, Brivanlou AH (2017) Embryoids, organoids and gastruloids: new approaches to understanding embryogenesis. Development 144:976–985
23. van den Brink SC, Baillie-Johnson P, Balayo T et al (2014) Symmetry breaking, germ layer specification and axial organisation in aggregates of mouse embryonic stem cells. Development 141:4231–4242
24. Baillie-Johnson P, van den Brink SC, Balayo T et al (2015) Generation of aggregates of mouse embryonic stem cells that show symmetry breaking, polarization and emergent collective behaviour *in vitro*. J Vis Exp 105:53252
25. Turner DA, Girgin M, Alonso-Crisostomo L et al (2017) Anteroposterior polarity and elongation in the absence of extraembryonic tissues and spatially localised signalling in Gastruloids, mammalian embryonic organoids. Development 144:dev150391-3906
26. Beccari L, Moris N, Girgin M et al (2018) Multi-axial self-organization properties of mouse embryonic stem cells into gastruloids. Nature 562:272–276
27. Girgin M, Turner DA, Baillie-Johnson P et al (2018) Generating gastruloids from mouse embryonic stem cells. Protoc Exchange:1–8. https://doi.org/10.1038/protex.2018.094
28. Rivron NC, Frias-Aldeguer J, Vrij EJ, Boisset J-C, Korving J, Vivié J, Truckenmüller RK, van Oudenaarden A, van Blitterswijk CA, Geijsen N (2018) Blastocyst-like structures generated solely from stem cells. Nature 2018 (557):106–111
29. Rivron NC (2018) Formation of blastoids from mouse embryonic and trophoblast stem cells. Protoc Exchange. https://doi.org/10.1038/protex.2018.051
30. Harrison SE, Sozen B, Christodoulou N et al (2017) Assembly of embryonic and extraembryonic stem cells to mimic embryogenesis in vitro. Science 356:eaal1810
31. Sozen B, Amadei G, Cox A et al (2018) Self-assembly of embryonic and two extraembryonic stem cell types into gastrulating embryo-like structures. Nat Cell Biol 20:979–989
32. Ying Q-L, Smith AG (2003) Defined conditions for neural commitment and differentiation. Methods Enzymol 365:327–341
33. Hooper M, Hardy K, Handyside A et al (1987) HPRT-deficient (Lesch-Nyhan) mouse embryos derived from germline colonization by cultured cells. Nature 326:292–295
34. Fehling HJ, Lacaud G, Kubo A et al (2003) Tracking mesoderm induction and its specification to the hemangioblast during embryonic stem cell differentiation. Development 130:4217–4227
35. Papanayotou C, Benhaddou A, Camus A et al (2014) A novel nodal enhancer dependent on pluripotency factors and smad2/3 signaling conditions a regulatory switch during epiblast maturation. PLoS Biol 12:e1001890
36. Freyer L, Schröter C, Saiz N et al (2015) A loss-of-function and H2B-venus transcriptional reporter allele for Gata6 in mice. BMC Dev Biol 15:38
37. Deluz C, Friman ET, Strebinger D et al (2016) A role for mitotic bookmarking of SOX2 in pluripotency and differentiation. Genes Dev 30:2538–2550
38. Serup P, Gustavsen C, Klein T et al (2012) Partial promoter substitutions generating transcriptional sentinels of diverse signaling pathways in embryonic stem cells and mice. Dis Model Mech 5:956–966
39. Ying Q-L, Stavridis M, Griffiths D et al (2003) Conversion of embryonic stem cells into neuroectodermal precursors in adherent monoculture. Nat Biotechnol 21:183–186
40. Baillie-Johnson P (2017) The generation of a candidate axial precursor in three dimensional aggregates of mouse embryonic stem cells
41. EP3404092A1- Method and apparatus for centrifugation-based accumulation and collection of cell cultures

Part IV

Organoids, Tissue Barriers, and Disease Models

Chapter 11

A Synergistic Engineering Approach to Build Human Brain Spheroids

Djuna von Maydell and Mehdi Jorfi

Abstract

Self-assembling brain spheroids derived from human stem cells closely emulate the tangled connectivity of the human brain, recapitulate aspects of organized tissue structure, and are relatively easy to manipulate compared to other existing three-dimensional (3D) cellular models. However, current platforms generate heterogeneously sized and short-lived spheroids, which do not robustly and reproducibly model human brain development and diseases. Here, we present a method to generate large-scale arrays of homogeneously sized 3D brain spheroids derived from human-induced pluripotent stem cells (hiPSCs) or immortalized neural progenitor cells to recapitulate Alzheimer's disease (AD) pathology in vitro. When embedded in extracellular matrix, these brain spheroids develop extensive outward projection of neurites and form networks, which are mediated by thick bundles of dendrites. This array facilitates cost-effective, high-throughput drug screening and mechanistic studies to better understand human brain development and neurodegenerative conditions, such as AD.

Key words Brain spheroids, 3D cell culture, Alzheimer's disease, Disease modeling, High-throughput, Drug screening

1 Introduction

Neuronal differentiation in three-dimensional (3D) cell culture allows precise spatial and temporal control, facilitates synapse formation, neurite outgrowth, and emulates network connectivity of the brain compared to conventional 2D cultures [1, 2]. Besides emulating the 3D connectivity of the brain, 3D cell cultures prevent rapid diffusion of pathogenic proteins, which is key to modeling neurodegenerative proteinopathies, such as AD [3]. In brief, 3D cell culture systems are broadly classified into three categories (Fig. 1); (a) microfluidic-based microsystems, also known as organs-on-chips or microphysiological systems (MPS), emulate organ-level pathophysiology on a microscale [4]; (b) matrix-based models, rely on artificial extracellular matrices that promote neural

Mo R. Ebrahimkhani and Joshua Hislop (eds.), *Programmed Morphogenesis: Methods and Protocols*, Methods in Molecular Biology, vol. 2258, https://doi.org/10.1007/978-1-0716-1174-6_11,

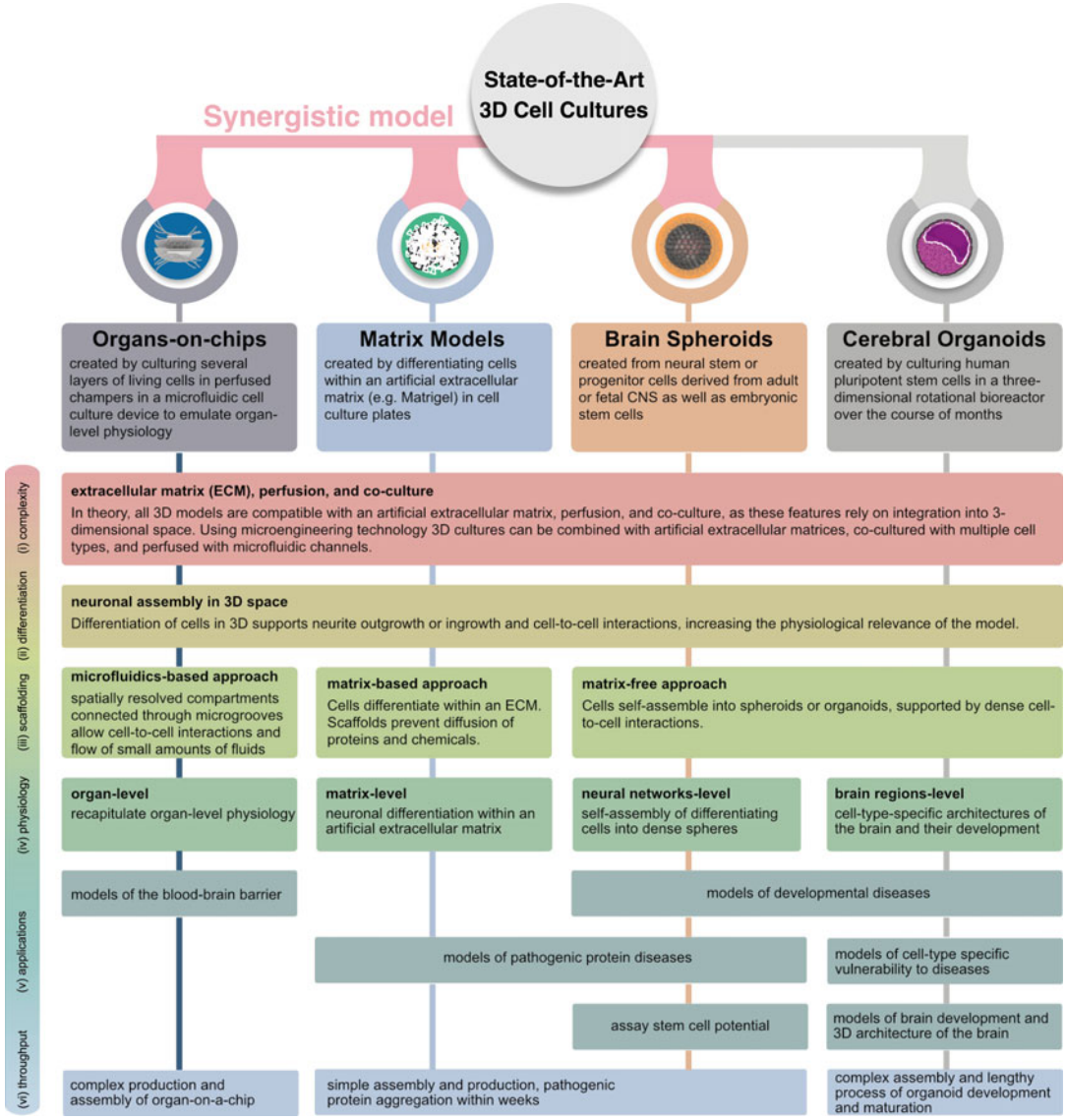

Fig. 1 Overview of state-of-the-art 3D cell culture systems and their main features. Our 3D brain spheroids array combines multiple features, including microfluidics technology, extracellular matrices, and the self-assembly of human stem cells

differentiation in 3D space [5]; and (c) matrix-free systems, including cerebral organoids and brain spheroids, rely on self-assembly of human stem cells into 3D spheroids [6–9]. A number of studies have begun to examine 3D cell culture models as a necessary alternative to AD rodent models and 2D cell cultures [10, 11]. For example, Choi et al. showed that genetically engineered human stem cells, embedded within an artificial extracellular matrix (i.e., Matrigel), recapitulated the two main pathological hallmarks of AD, including amyloid plaques and tauopathy

[11]. This has not been possible in 2D cell cultures and animal models, mainly due to diffusion of pathogenic proteins and differences in genetic background, respectively [12–14]. While an attempt to model AD pathology was also made using human-induced pluripotent stem cell (hiPSC)-derived brain spheroids, these spheroids were highly heterogenous in size and lacked robust pathology [14]. However, very recent progress toward hiPSC-derived organoids has provided substantial insights into the cellular basis of AD [15]. This is well-exemplified in the work undertaken by Lin *et al.*, which found an important contribution of the APOE4 AD risk allele to impaired glial clearance of AD pathology using an hiPSC-derived organoids model [16]. For further details on modeling neurological diseases in brain spheroids and organoids, readers are referred to recent reviews [7, 17].

Although brain spheroids constitute promising platforms to study brain development and diseases in vitro, these models are still in their infancy. Multiple limiting factors constrain robust disease modeling in existing systems, including (a) size heterogeneity, which limits reproducibility and data consolidation between studies, (b) inward projection of neurites, (c) short life spans of brain spheroids, likely due to the lack of pro-survival signals from a physiologically relevant matrix environment, and (d) diffusion of pathogenic proteins in the absence of an extracellular matrix. To overcome these limitations, we have merged microfluidic technology, brain spheroids derived from human stem cells, and an artificial extracellular matrix, to create a single synergistic model that combines multiple key advantages from recent advances in 3D systems (Fig. 1) [6]: Our microengineered array (a) consistently generates uniformly sized brain spheroids, (b) mimics the brain microenvironment via an extracellular matrix, which promotes outward projection of neurites and increases brain spheroid lifespan, (c) is compatible with hiPSCs and genetically engineered human neural progenitor cells (hNPCs) that generate high levels of aggregated pathogenic amyloid-β (Aβ) to model AD pathology, (d) facilitates high-throughput biochemical and imaging readouts as well as automated drug screening, (e) is straightforward to manipulate experimentally, and (f) enables monitoring of individual brain spheroids during long-term cell culture.

The brain spheroids array comprises 1536 microwells of 500 μm in diameter, which physically constrain uniformly sized spheroids derived from hiPSCs or hNPCs. After self-assembly, the brain spheroids are embedded within an extracellular matrix, which promotes extensive outward projections of neurites and neural network formation. The array is highly customizable to other neurobiological questions of interest. Spheroid size is easy to modify by altering microwell diameters, while the extent of network formation is controlled by changing the microwell depth. The formation of extensive neural networks unlocks numerous possibilities for

basic mechanistic studies, including disease pathology propagation and compound toxicity. The extracellular matrix limits diffusion of pathogenic proteins, which generates aggregated protein pathology associated with numerous neurodegenerative diseases, including AD. Using this novel array platform, we robustly recapitulated hallmarks of AD in uniformly sized brain spheroids derived from hNPCs that overexpress familial AD (fAD) genes with multiple disease mutations [6]. We also found reduced production of Aβ species by treating the fAD brain spheroids with β-secretase inhibitor, a commonly used inhibitor of APP processing and a primary candidate in AD therapeutics. Overall, this unique synergistic model constitutes a reliable platform for modeling specific disease phenotypes and cost-effective, high-throughput drug screening for new interventions. Moreover, the array is a promising substrate for the design of next-generation spheroid platforms to answer a range of niche neurobiological questions.

2 Materials

2.1 Array Platform

1. MakerBot Replicator 2 desktop 3D printer and ABS material.
2. AutoCAD and MakerBot Printing software.
3. SU8–100 photoresist (MicroChem Co.).
4. SU8 developer, BTS-220 (Doe & Ingalls).
5. Silicon wafer 6-in. (NOVA Electronic Materials).
6. High reflective chrome photomask (Front Range Photomask LLC).
7. Polydimethylsiloxane (PDMS)-Sylgard 184 Silicon (Ellsworth Adhesives).
8. Glass slides (Nexterion, Applied Microarrays, Inc.).
9. MTP 96-well superstructures and sealing film (Nexterion, Applied Microarrays, Inc.).
10. Plate lid (Nexterion, Applied Microarrays, Inc.).

2.2 Cell Culture

Carry out all procedures under a sterile biosafety cell culture hood.

1. 20 μg/mL human recombinant epidermal growth factor (EGF) stock solution: Filter 10 mM acetic acid through a 0.2-μm membrane. Add 2.0 mL of the filtered acetic acid to 2.0 mg of lyophilized EGF (Sigma-Aldrich; 1 mg/mL) and mix thoroughly. Make up a final concentration of 20 μg/mL by further diluting with 0.2 μm filtered 0.1% (wt/vol) bovine serum albumin (BSA) solution. Prepare 1.0 mL aliquots and store at −80 °C (*see* **Note 1**).

2. 25 μg/mL human recombinant basic fibroblast growth factor (bFGF) stock solution: Filter 10 mM Tris (pH 7.6) through a 0.2 μm membrane. Add 2.0 mL of the filtered Tris to 50 μg of lyophilized bFGF (Stemgent), mix thoroughly, and make 0.2 mL aliquots. Store aliquots at −80 °C (*see* **Note 1**).
3. ReN-cell proliferation medium: 484.5 mL DMEM/F12 medium, 0.5 mL heparin, 10 mL B27, 5.0 mL 100× penicillin/streptomycin, 0.5 mL amphotericin B, 0.5 mL EGF (20 μg/mL, Sigma-Aldrich), 0.4 mL bFGF (25 μg/mL, Stemgent).
4. hiPSC proliferation medium: 99 mL ENStem—A neural proliferation medium, 1.0 mL EmbryoMax L-Glutamine solution (100×, 200 mM), 1.0 mL 100× EmbyroMax ES Cell-Qualified Penicillin—Streptomycin solution (EMD Millipore).
5. ReN-cell differentiation medium: 484.5 mL DMEM/F12 medium, 0.5 mL of heparin, 10 mL of B27, 5.0 mL 100× penicillin/streptomycin, and 0.5 mL amphotericin B.
6. ENStem.
7. IRES-mediated polycistronic lentiviral vectors CSCW-GFP (control), CSCW-APPSL-GFP (AD), and CSCW-APPSL-PS1Δe9-mCherry (AD) (all constructs are available through the corresponding author). For more details on the constructs, readers are referred to ref. [5].
8. Human iPSC-derived neural progenitor cells (EMD Millipore).
9. Matrigel (Corning).
10. Matrigel-coated vented T25 cell culture flasks: Add 3 mL of Matrigel:DMEM-F12 medium (1:100 dilution) to the bottom of each vented T25 flask, shake gently to cover the surface, and incubate at 37 °C for at least 1 h. Aspirate the media and store flasks at 4 °C until use (*see* **Note 2**).
11. Accutase (Life Technologies).
12. Phosphate-buffered saline (PBS).
13. ReN-cell neural stem cell freezing medium (EMD Millipore).
14. Cell counting machine, cell counting slides, and Trypan Blue (Invitrogen).

2.3 Immunohistochemistry

1. Blocking solution: Add 2.5 g of BSA (Sigma-Aldrich), 5.63 g of glycine, and 0.25 g of gelatin to 200 mL of Tris-buffered saline (TBS-T, Boston BioProducts). Incubate the solution at 55 °C for ~10 min for gelatin to dissolve. Add 10 mL of donkey serum (Sigma-Aldrich) and TBS-T to a final volume of 250 mL. Filter the solution through a 0.4-μm filter unit and store at 4 °C.

2. Primary and secondary antibodies:
   (a) Anti-MAP 2 (EMD Millipore, AB5543, 1:500).
   (b) Anti-Tuj1 (Sigma, T2200, 1:100).
   (c) Anti-DCX (Abcam, Ab135349, 1:200).
   (d) AT-8 (ThermoFisher Scientific, MN1020, 1:30).
   (e) β-amyloid (1–42 specific) (Cell Signaling Technology, D9A3A, 1:200).
   (f) Alexa Fluor 488 Secondary antibody (Abcam, Ab150077, 1:200).
   (g) Alexa Fluor 568 Secondary antibody (Life Technology, A-11041, 1:400).
   (h) Cy5 Secondary antibody (Jackson ImmunoResearch, 715–175–150, 1:200).
   (i) Cy5 Secondary antibody (Jackson ImmunoResearch, 711–175–152, 1:200).
3. 4% Paraformaldehyde.
4. Nikon Eclipse Ti microscope.
5. ImageJ software.

2.4 Scanning Electron Microscopy

1. Aluminum Mounts.
2. Conductive Adhesive Tabs (double-sided adhesion).
3. SEM Pin Stub Mount Gripper 45° angle (TED PELLA, INC.).
4. Universal Specimen Mount Holder.
5. Glutaraldehyde 2.5% in 0.1 M Phosphate Buffer.
6. Hexamethyldisilazane.
7. Osmium tetroxide solution 4% in H_2O.
8. Ultra55 Field Emission Scanning Electron Microscope.

2.5 ELISA

1. Human amyloid-β ELISA Kit (Wako Pure Chemicals).
2. MesoScale Discovery 96-well Mouse Pro-Inflammatory V-PLEX Assay (Meso Scale Discovery).
3. Synergy 2 ELISA plate reader (BioTek Instruments).
4. Meso QuickPlex SQ 120 (Meso Scale Discovery).

3 Methods

3.1 Fabricating the Brain Spheroids Array

All designs can be generated using AutoCad software. All designs in this chapter are available through https://github.com/jorfilab/brainspheroids. An overview of the fabrication process is shown in Fig. 2a.

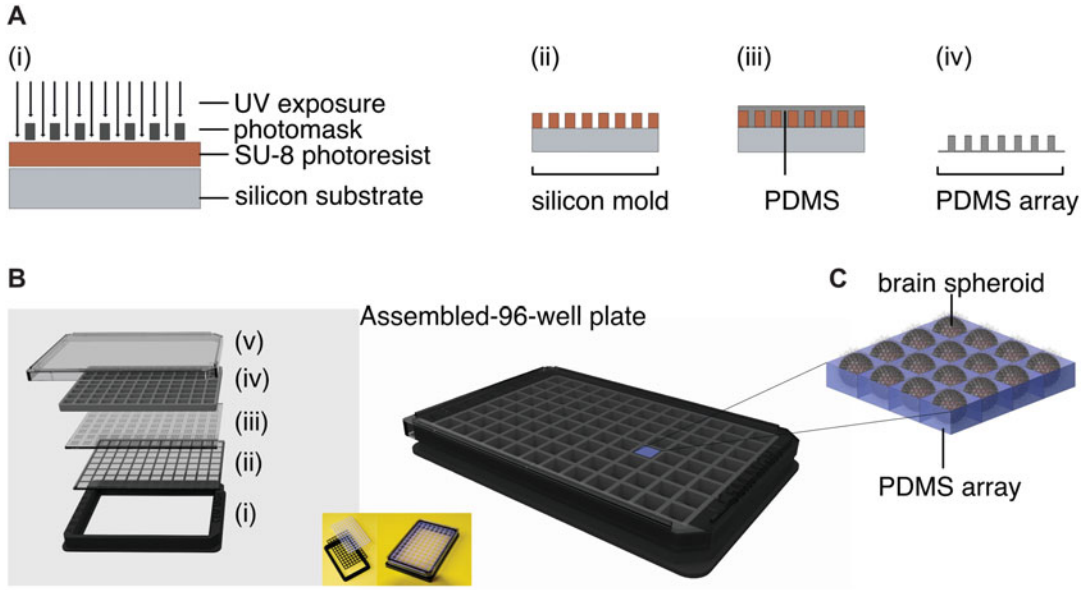

Fig. 2 Microfabrication process of the 3D brain spheroids array. (**a**) Generation of the PDMS brain spheroids array using soft lithography technique. (*i*) Expose masked SU8–100 photoresist to UV light. (*ii*) Remove the unexposed photoresist. (*iii*) Cast PDMS over silicon mold. (*iv*) Remove cured PDMS from mold. (**b**) The assembled 96-well array has five components: (*i*) a 3D designed and printed 96-well frame, (*ii*) a high-quality glass with transmittance of over 92% and high optical clarity for fluorescence wavelengths, (*iii*) a microfabricated PDMS microwell array of 1536 microwells, (*iv*) a 96-well silicon superstructure that groups 16 microwells into a single superstructure well, and (*v*) a plate lid. Adapted with permission [6]. Copyright 2018, Nature Publishing Group. (**c**) A single superstructure well in a 96-well plate holds 16 brain spheroids, each cultured in a 500-μm diameter microwell in the PDMS array

3.1.1 Master Fabrication

1. Design the microfluidic spheroids array using AutoCad software and print it onto the chrome photomask.
2. Dehydrate a silicon wafer in an oven at 250 °C for 30 min. Allow the silicon wafer to cool down to room temperature before proceeding to the next step.
3. Plasma-treat the silicon wafer using an oxygen plasma machine (March Plasma System) for 3 min at 100 watts.
4. After plasma treatment, blow-dry the silicon wafer with nitrogen gas, place it onto the spinner chuck, and turn on the vacuum.
5. Cover the silicon surface with ~5 mL of SU8–100 and spin the silicon wafer at 600 rpm for 5 s, followed by spinning at 1650 rpm for 30 s. This spinning protocol produces a photoresist thickness of ~200 μm.
6. Place the coated silicon wafer onto a hot plate. Soft-bake the wafer at 70 °C for 25 min, followed by baking at 100 °C for 80 min. Allow the coated silicon wafer to cool down to room temperature before proceeding to the following step.

7. Repeat **steps 5** and **6** three times to achieve ~600 μm photoresist thickness suitable for the 500 μm brain spheroids array (*see* **Note 3**).
8. Place the coated silicon wafer onto the exposure stage, facing the UV lamp. Place the photomask with the microwell design onto the exposure stage. Open the shutter of the UV lamp and expose the photoresist for 80 s.
9. Place the exposed silicon wafer onto a hot plate, with the SU8–100 coating facing upwards. Post-bake the silicon wafer at 70 °C for 1 min, followed by baking at 100 °C for 16 min. Allow the coated silicon wafer to cool down to room temperature.
10. Develop the exposed silicon wafer using the developer solution for ~1 h, followed by developing in a fresh developer for another 2 min. Rinse the silicon wafer with fresh developer and blow-dry using nitrogen gas.
11. Place the silicon wafer onto the exposure stage with the SU8–100-coated surface facing the UV lamp. Place a clear photomask or glass on top of the silicon wafer. Post-expose the photoresist for another 65 s in case of uncompleted reactions initiated during the first exposure.
12. Place the flood-exposed silicon wafer onto a hot plate with the coated layer on top. Post-bake the wafer at 70 °C for 2 min, followed by baking at 100 °C for 6 min. Allow the coated silicon wafer to cool down to room temperature and store for later use.

3.1.2 PDMS Mold Fabrication

1. Prepare 10:1 PDMS by combining 40 g of Sylgard 184 base with 4 g of curing agent in a plastic dish. Mix thoroughly and degas the mixture for 2–3 h inside a desiccator connected to a vacuum to remove all air bubbles generated during mixing.
2. Gently pour the PDMS mixture over the silicon wafer mold to avoid generation of new air bubbles.
3. Bake the PDMS-coated silicon wafer in an oven at 75 °C for 12 h.
4. Cut out the PDMS spheroids array from the silicon wafer substrate using a sharp blade.
5. Place the PDMS spheroids array block (containing 1536 microwells, 500 μm in diameter) on a clean tray inside the oxygen plasma machine with the microwells facing down. Place the glass slide onto the same tray and expose both surfaces to plasma for 70 s at 50 watts.
6. Invert the PDMS spheroids array block and bond it to the glass slide. Bake the bonded PDMS-glass slide in a 70 °C hot plate for 20 min.

3.1.3 Brain Spheroids Array Assembly

1. Print the 96-well frame plate using MakerBot Replicator 2 desktop 3D printer and ABS material following the vendor protocol.
2. Assemble the 96-well plate as shown in Fig. 2b. Note that each superstructure well supports the formation of 16 brain spheroids (Fig. 2c).
3. Store the plate in a clean environment for future use (*see* **Note 4**).

3.2 Generating the Genetically Engineered AD hNPCs

1. Package lentiviral vectors. Transfect ReN cells with CSCW constructs (*see* **Note 5**). Enrich the transfected cells for top 2% GFP/mCherry-expressing cells using fluorescence-activated cell sorting (FACS).
2. Generate clonal control and fAD ReN cell lines by FACS-assisted 96-well single-cell cloning into Matrigel-coated 96-well plates (Fig. 3).
3. Sequentially expand the cells in 6-well plates, T25, and T75 flasks. Change the proliferation medium twice a week.

   Once cells reach confluency, aspirate media, wash cells with PBS to remove dead residual cells, incubate cells in Accutase (0.5 mL for T25 and 1.5 mL for T75) at 37 °C until cells are dissociated from the plate, and neutralize the reaction with an equal volume of proliferation medium. Centrifuge cells at 1500 rpm for 3 min. Re-suspend cell pellets in corresponding freezing medium and transfer cells into appropriate freezing vials to store in liquid nitrogen for later use.

3.3 Maintaining ReN Cells and hiPSCs

Carry out all procedures under a sterile biosafety cell culture hood.

1. Quickly thaw control, AD ReN cells, and hiPSCs by placing frozen stocks into a bead bath at 37 °C. Equilibrate thawed cells into proliferation medium by slowly adding a small volume of appropriate proliferation medium directly to the cells. Pipette up and down and transfer the entire solution to a new

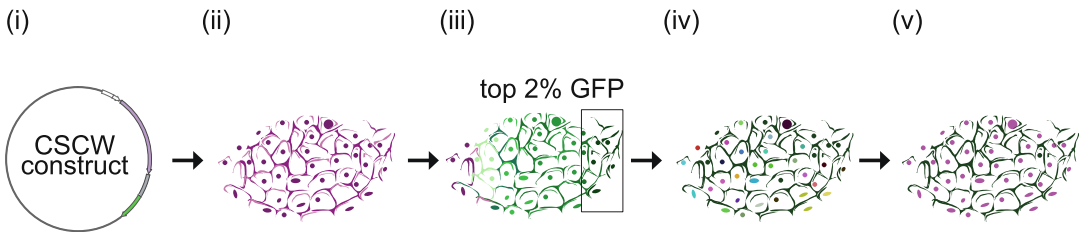

Fig. 3 Workflow to generate single-clonal fAD-ReN cell lines. (*i*) fAD mutations are introduced into the CSCWW-APP-(PS1)-GFP construct by site-directed mutagenesis. (*ii*) hNPCs are transfected with the construct. (*iii*) Transfected hNPCs are FACS-enriched by GFP signal. (*iv*) The sorted cells are heterogeneous for genomic integration of the construct. (*v*) Single-cell-FACS enrichment generates single-clonal hNPCs

tube. Centrifuge cells at 1500 rpm for 3 min, aspirate the supernatant, and re-suspend the cell pellets in 4–7 mL pre-warmed proliferation medium.

Transfer the cells to a matrigel-coated vented T25 flask and place in a cell culture incubator at 37 °C and 5% CO_2 (*see* **Notes 6** and **7**).

2. Maintain cells at 37 °C in proliferation medium with full biweekly medium changes until the cells become confluent. Proliferation medium may be changed more frequently if cells are dividing slowly.

3.4 Generating Brain Spheroids from Stem Cells

Carry out all procedures in a sterile biosafety cell culture hood to avoid contamination.

1. Once cells have reached 90–100% confluency, aspirate medium, wash cells with PBS, and incubate cells with Accutase (0.5 mL for T25 and 1.5 mL for T75) at 37 °C until cells are dissociated from the flask. Then, neutralize Accutase with an equal volume of proliferation medium. Centrifuge the cell mixture and resuspend the cell pellets in 5 mL of fresh proliferation medium. Mix cells thoroughly by pipetting up and down so that cells are evenly dispersed and cell counting is accurate.
2. Dilute the cells 1:10 by adding 10 μL of resuspended cells to 90 μL of medium and mix thoroughly. Further dilute the cells 1:1 with Trypan Blue, by mixing 15 μL of cells with 15 μL of Trypan Blue and mix thoroughly. Dispense 10 μL of the solution into each side of the cell counting chip. Count the cells in each side of the chip using an automated cell counter, average the values, and adjust for the dilution (*see* **Note 8**). Centrifuge the cells at 1500 rpm for 3 min. Resuspend the cells in appropriate volume of proliferation medium to achieve a final concentration of 12×10^6 cells/mL (*see* **Note 9**).
3. If the cell count is insufficient, cells must be expanded further. To passage the cells for further proliferation. Following **step 1**, resuspend the cell pellets in proliferation medium and transfer them into three Matrigel-coated T25 flasks. Keep changing medium until the cells become confluent. Count the cells as described in **step 2** and proceed with the following steps.
4. Plate 100 μL of the cells from **step 2** into each suprastructure well of the brain spheroids array (Fig. 4, **Step 1**).
5. After 20 min, add 200 μL of proliferation medium against the wall of each suprastructure well. Aspirate the medium to remove floating cells from the wells and add fresh 200 μL of proliferation medium to each well (Fig. 4, **Step 2**).

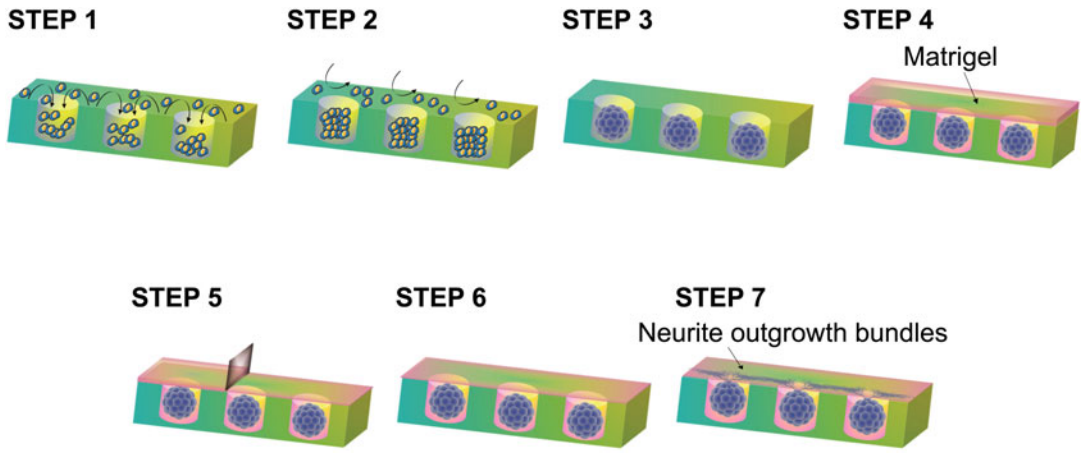

Fig. 4 Workflow for plating stem cells in the 3D array platform. **Step 1**. Plate stem cells into the array. **Step 2.** Once cells aggregate, remove floating cells. **Step 3.** Allow 3D spheroids to form during incubation. **Step 4.** Cover array with extracellular matrix. **Step 5.** Remove excess matrix. **Steps 6** and **7**. Allow spheroids to differentiate and form neurite projections during incubation

6. Incubate the arrays at 37 °C and 5% CO_2 atmosphere (Fig. 4, **Step 3**). Change the proliferation medium after 24 h and incubate the arrays at 37 °C and 5% CO_2 atmosphere for another 24 h to generate fully formed brain spheroids.
7. After 48 h, aspirate the entire proliferation medium and apply 100 μL of 1:4 Matrigel:differentiation medium (for ReN-derived spheroids) or 1:1 proliferation:differentiation medium (for hiPSC-derived spheroids) to each well to cover the whole surface area (Fig. 4, **Step 4**). Incubate at 37 °C for 2 h to allow Matrigel to solidify (*see* **Note 10**).
8. Remove excess Matrigel from the surface of the brain spheroids array by gently scraping a gel loading tip tilted at 90° across the surface of the PDMS array (Fig. 4, **Step 5**). Replace the media with 200 μL fresh pre-warmed differentiation medium.
9. Maintain the cell culture up to 8 weeks, changing half of the differentiation media every 4 days.
10. OPTIONAL: For applications that require the removal of the brain spheroids from the arrays, following **step 7**, place the array in a 6-well plate tilted at 45° and spray proliferation medium over the array using a 1-mL tip. Repeat this step three times to extract all the spheroids from the arrays. Images can be captured using the Z-stacking function on an inverted Nikon Eclipse Ti microscope, to allow visualization of full brain spheroids after removal (*see* Fig. 5a). Process images for quantification of spheroid diameters using ImageJ software (Fig. 5b).

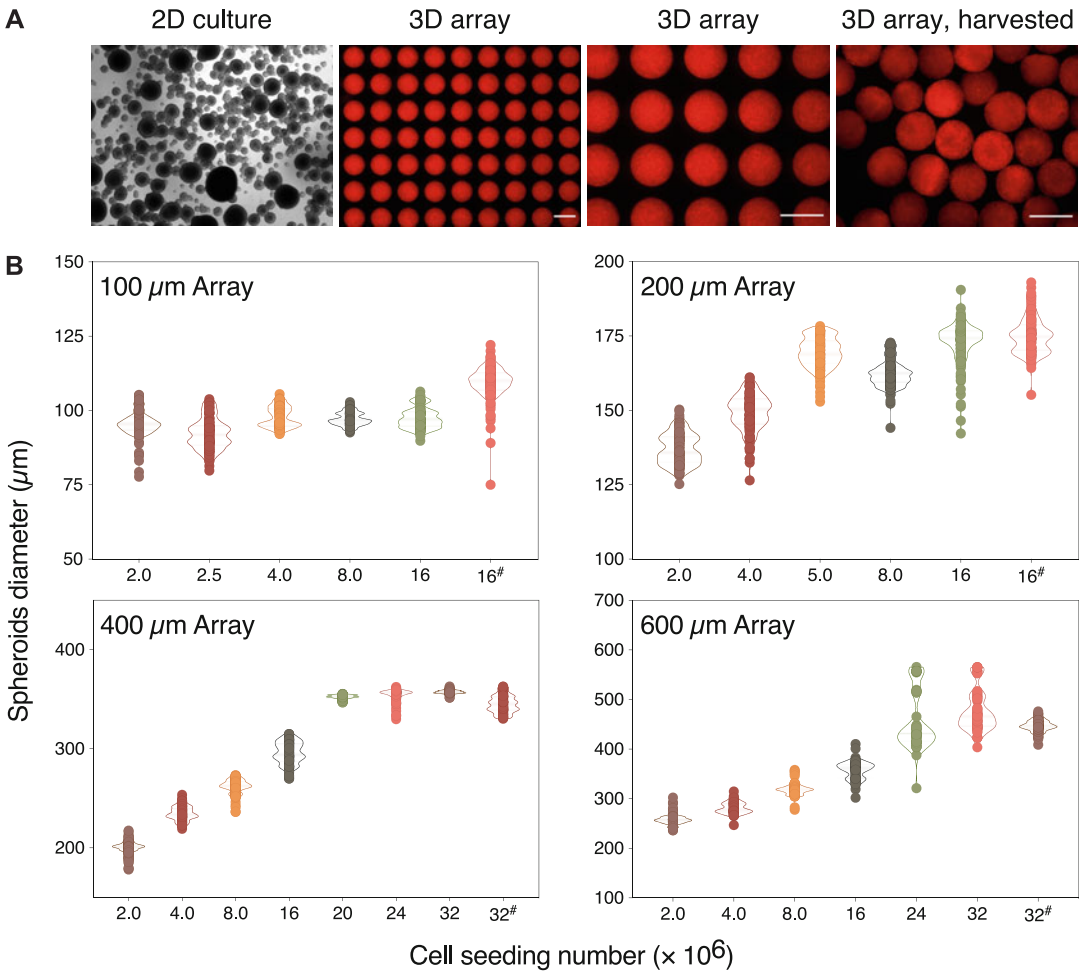

Fig. 5 Generation and recovery of uniformly sized brain spheroids in high-throughput arrays. (**a**) Confocal images show plated and harvested homogenously sized brain spheroids generated in the 3D array platform compared to conventional 2D platforms. Scale bars indicate 400 μm. (**b**) Violin plots show the relationship between cell seeding concentration, microwell diameter, and spheroid diameter after a 24-h formation period in the 3D array platform. $n > 100$ spheroids for each condition

3.5 Application I: Imaging Brain Spheroids Morphology

1. Rinse plates with PBS and fix in 4% paraformaldehyde (PFA) overnight at 4 °C. Wash plates three times with 1× Tris Buffered Saline with Tween 20 (TBS-T). Keep cells overnight at 4 °C in blocking solution. Then, permeabilize the cellular membrane of the cells with 0.1% Triton X-100 for 45–60 min at room temperature. Next, wash the cells three times with 1× TBS-T, leaving each wash in for 15 min. Incubate the brain spheroids with primary antibodies in blocking solution at 4 °C overnight, followed by incubation with species-specific secondary antibodies at 4 °C overnight in the dark. Alternatively, after secondary antibody staining and washing three times with 1× TBS-T, cell nuclei can be stained with Hoechst 3342 (1:2000 dilution) for 20 min at room temperature. Following staining

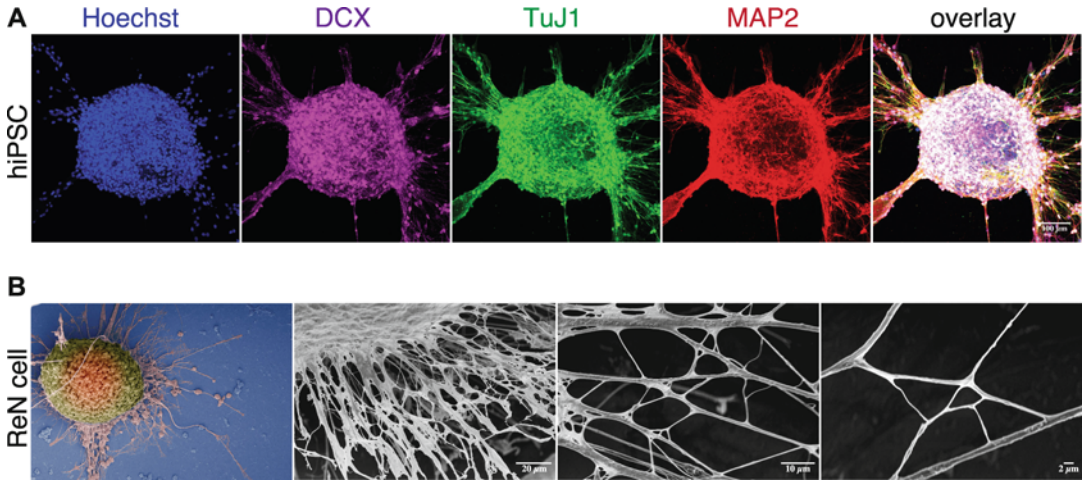

Fig. 6 Uniformly sized brain spheroids generated in the 3D array form extensive neurite networks. (**a**) Representative confocal images show expression of neuronal markers (MAP-2, microtubule-associated protein 2; TuJ1, ß-tubulin III; and DCX, doublecortin) and nuclei (Hoechst) in hiPSC-derived spheroids at 2-weeks differentiation in the 3D array platform. (**b**) Scanning electron microscopy images for control and fAD ReN cells differentiated as spheroids in the 3D array platform for 8 weeks. Outward neurite projections enable formation of spheroid networks (right three panels). Reproduced with permission [6]. Copyright 2018, Nature Publishing Group

of the brain spheroids, a series of images can be captured using the Z-stacking function on an inverted Nikon Eclipse T*i* microscope, to allow visualization of full brain spheroids (Fig. 6a) (*see* **Note 11**). Process images using ImageJ software.

2. To visualize brain spheroids using electron microscopy, fix the differentiated spheroids in 2.5% glutaraldehyde for 30 min, wash three times with PBS, and then post-fix in aqueous 1% OsO_4 in a certified chemical hood with personal protective equipment for 60 min (*see* **Note 12**). Then, wash the brain spheroids with PBS three times, leaving each wash in for 15 min. Dehydrate through a graded series of ethanol diluted in PBS (30–90% v/v) for 15 min each, followed by washing with absolute ethanol three times before drying in hexamethyldisilazane solution. Air-dry under safety hood overnight. Mount the arrays with fixed brain spheroids onto aluminum stubs, sputter-coat with 5 nm of platinum/palladium, and image in an Ultra55 Field Emission Scanning Electron Microscope at 10 kV with In lens SE detector (Fig. 6b).

3.6 Application II: Monitoring Pathophysiology

1. Immunohistochemical detection of Aβ and tau pathology: Follow **step 1** in Subheading 3.5 for fixing, permeabilizing, and blocking the brain spheroids. Next, choose appropriate anti-Aβ and anti-phosphorylated tau primary and secondary antibodies (*see* Subheading 2.3, **item 2**) to immunostaining the brain spheroids for Aβ and tau pathology (Fig. 7a, b).

2. Quantify Aβ isoform levels using Human Amyloid-β ELISA Kit: Collect the conditioned media from differentiated ReN-brain spheroids at the timepoint of interest and dilute 1:2 in the provided dilution buffer. Use a Synergy 2 ELISA plate reader to quantify Aβ40 and Aβ42 fluorescent signals (Fig. 7c).

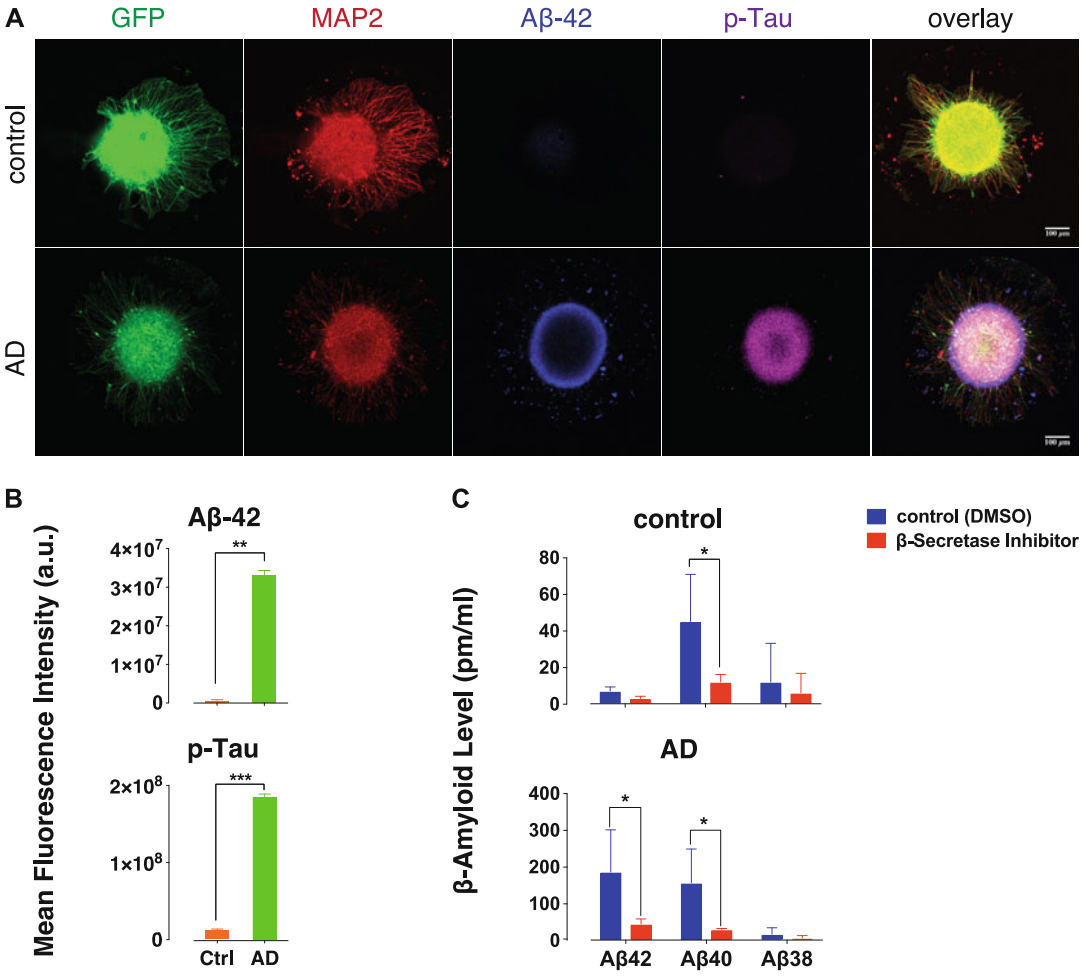

Fig. 7 Modeling AD pathology in the 3D brain spheroids array. (**a**) fAD ReN-cell-derived spheroids were differentiated in the array for 8 weeks and stained for Aβ and phospho-Tau (p-Tau). Pathological hallmarks show distinct localization throughout the spheroids, with Aβ aggregated along the perimeter of the spheroids and p-Tau present throughout the spheroids. (**b**) MAP 2, Aβ42, and p-Tau levels quantified by immunofluorescence in control and AD ReN-cell spheroids. (**c**) Aβ42, Aβ40, and Aβ38 levels in the media quantified by ELISA for control and AD ReN cells differentiated for 7 weeks in the array platform and treated with β-secretase inhibitor. *$P < 0.05$; **$P < 0.01$; ***$P < 0.001$; ****$P < 0.0001$; ANOVA followed by a post hoc Dunnett's test; means ± SEM; $n = 6$ per each sample. Reproduced with permission [6]. Copyright 2018, Nature Publishing Group

3. Quantify Aβ isoform levels using MesoScale Discovery 96-well Mouse Pro-Inflammatory V-PLEX Assay: Add 150 μL of provided diluent to the plate, which is coated with an array of Aβ capture antibodies. Incubate the plate at room temperature while shaking for 1 h. Wash the plate with the washing buffer. Add 25 μL of detection antibody solution and 25 μL of the prepared samples to the plate according to the manufacturer's protocol. Incubate the plate at room temperature for 2 h with vigorous shaking. Wash the plate in washing buffer and add 150 μL of 2× Read Buffer T. Immediately read the fluorescent signal on a Meso QuickPlex SQ 120.
4. Aβ levels in the media can be quantified by ELISA at various timepoints to monitor the effect of treatment (*see* Subheading 3.7, **Application III**) with active compounds on levels of secreted pathogenic proteins in the media (Fig. 7c).

3.7 Application III: High-Throughput Drug Screening of AD Brain Spheroids with Automated Readouts

1. Plate control and fAD ReN-cells into the brain spheroids array platform at a concentration of 12×10^6 cells/mL in proliferation medium.
2. After 20 min, add 200 μL of proliferation medium against the wall of each suprastructure well. Aspirate the medium to remove floating cells from the wells and add fresh 200 μL of proliferation medium.
3. Incubate the arrays at 37 °C and 5% CO_2 atmosphere for 48 h to allow full spheroids formation.
4. Add drugs of choice to the proliferation medium to achieve the desired concentration. Treat the brain spheroids with different drugs at varying concentrations 2 days after plating (Fig. 8). Make fresh working stock for each media change.
5. Repeat the drug treatment after 4 days.
6. Maintain the brain spheroids for 7 days at 37 °C and 5% CO_2 atmosphere. After 7 days, rinse the brain spheroids with PBS and fix in 4% PFA overnight at 4 °C. Wash three times in PBS for 15 min each, and leave 200 μL PBS in each well.
7. For high-throughput drug screening, set up an automated imaging-job on the Nikon Eclipse T*i* microscope. Since the x and y dimensions of each microwell are known and the brain spheroids are homogenous in size, confocal images of the 1536 spheroids (16 brain spheroids per well in a 96-well plate) can be acquired in an automated high-throughput manner. Toxicity readouts, including brain spheroid diameters and neurite extensions, can also be quantified as part of this automated process through postprocessing, using ImageJ software (Fig. 9).

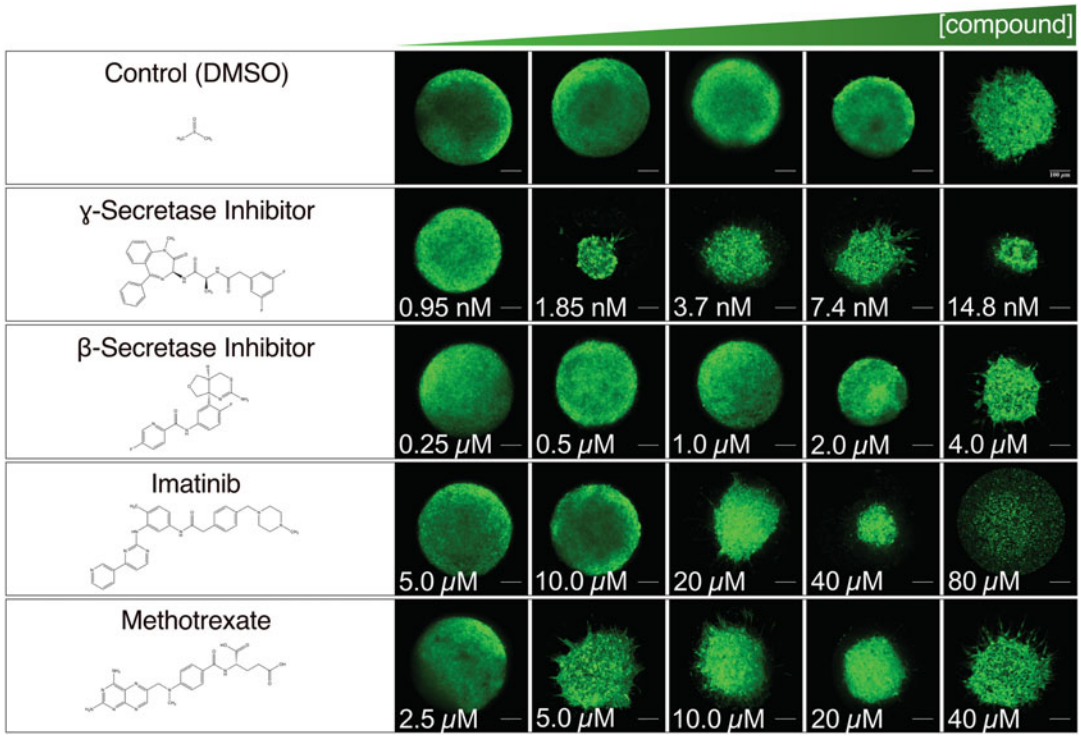

Fig. 8 Monitoring the effect of active compounds on AD ReN-cell-derived spheroids cultured in the 3D array platform. Confocal images of representative brain spheroids after a 7-day drug treatment with DMSO, γ-secretase inhibitor (Compound E), β-secretase inhibitor (LY2886721), Imatinib, or Methotrexate at five different concentrations. Reproduced with permission [6]. Copyright 2018, Nature Publishing Group

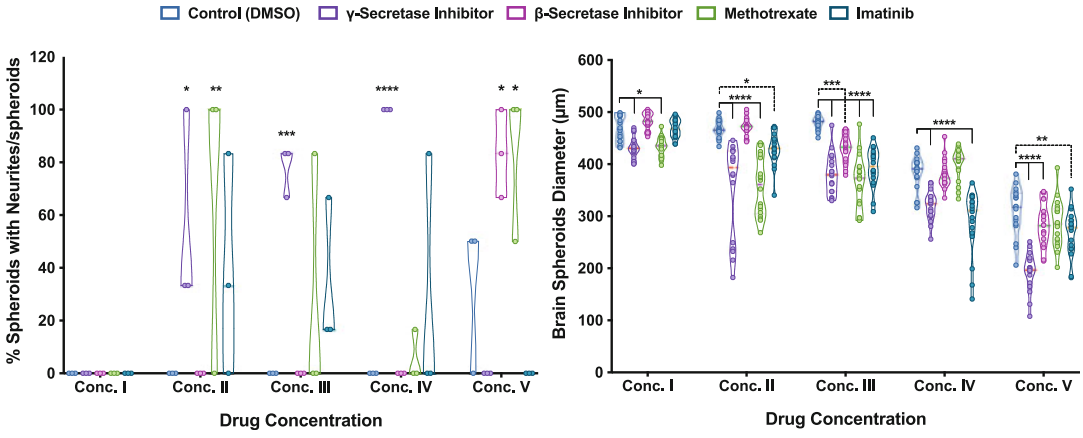

Fig. 9 Quantifying the effect of active compounds on AD ReN-derived spheroids cultured in the 3D array platform. Quantification of neurite number and brain spheroids diameter after 7-day drug treatments from Fig. 8. *$P < 0.05$; **$P < 0.01$; ***$P < 0.001$; ****$P < 0.0001$; ANOVA followed by a post hoc Dunnett's test; means ± SEM; $n = 6$ per each sample. Adapted with permission [6]. Copyright 2018, Nature Publishing Group

4 Notes

1. Stock aliquots can be stored for up to 1 year at −80 °C. Once thawed, store aliquots at 4 °C and use within 2–3 weeks to avoid activity loss associated with multiple freeze–thaw cycles.
2. Take out Matrigel stock from −80 °C freezer and store at 4 °C 1 day prior to experiment to give the gel plenty of time to thaw. Make fresh working solution each time. Precool pipettes in cold DMEM-F12 medium prior to taking up Matrigel to prevent the gel from solidifying. Keep Matrigel and Matrigel: DMEMF12 solution on ice throughout coating. Make sure the Matrigel:DMEMF12 solution covers the base of each T25 flask evenly prior to incubating. Matrigel-coated flasks can be stored for up to 2 months at 4 °C.
3. The spheroids array design can be customized using AutoCAD software according to specific needs and interests. For example, one can modify the spheroids array diameter, spheroid–spheroid distance, number of spheroids per well, or add connections between the spheroids. Repeat **steps 5** and **6** (Subheading 3.1.1) once to achieve ~200 μm photoresist thickness that is suitable for the 100 and 200 μm brain spheroids arrays or twice to achieve ~400 μm photoresist thickness that is suitable for the 400 μm brain spheroids array.
4. Place the assembled 96-well brain spheroids plate without a lid onto a tray inside the oxygen plasma machine and expose the array surface to plasma for 70 s at 50 watts before adding the cell suspension to the array.
5. Cells were transfected with the CSCW-APPSL-GFP construct, encoding full-length β-amyloid precursor protein (APP695) with the London (V717F), Swedish (K670N/M671L) mutations, and GFP reporter gene, the CSCW-APPSL-PS1Δe9-mCherry construct, additionally encoding the PS1 gene with the Δe9 mutation, or a control CSCW-GFP control construct as described in ref. [11].
6. Thaw cells quickly in the water bath (37 °C) until no crystals remain. Add proliferation medium to the thawed cells in small increments, while gently shaking the vial to disperse the medium and avoid cell membrane rupture. Keep the cells on UV-sterilized ice whenever possible.
7. Excess cells may be frozen down. Alternatively, the cell pellet may be split into multiple flasks. Ensure that flasks are not overpopulated with cells as they may reach confluency too quickly. Once cells settle, they should occupy about one-third of the surface area so that cells have plenty of room to proliferate.

Under these conditions, ReN cells usually take 2–3 days to become confluent. A single 95% confluent T25 flask yields ~2–3 $\times$ 10^6 cells.

8. Trypan Blue stains dead cells, allowing the cell counter to generate a "live," "dead," and "total" cell count. When using Trypan Blue, average the live cell counts from both readings. Please note that the cell counter may be set to automatically account for the 1:1 Trypan Blue dilution. If the counts are discrepant by $>10^6$ cells, mix cells thoroughly before recounting.
9. To optimize the cell density in brain spheroids arrays with different microwell diameters, resuspend the cells in an appropriate volume of proliferation medium to achieve a final concentration of 2, 2.5, 4, 8, 16, 20, 24, or 32 $\times$ 10^6 cells/mL.
10. This is a key step that prevents brain spheroids from diffusing out of the microwells.
11. The excitation wavelengths of mCherry and anti-chicken Alexa Fluor 568 antibodies (MAP 2 staining) partially overlap. However, the major differences in signal strength allows differentiation between the MAP 2 signal versus mCherry.
12. Osmium tetroxide (OsO_4) is an oxidizing and highly toxic material. OsO_4 solution must be handled in a certified chemical hood with personal protective equipment (PPE) including lab coat, protective gloves, and eye/face protection. Read thoroughly the material safety data sheet (MSDS) before using the OsO_4 solution. To dispose the leftover OsO_4 solution, neutralize it by twice its volume of vegetable oil (e.g., corn oil) by pouring the oil into the OsO_4 solution and wait for the oil to completely turn black.

Acknowledgments

This work was supported by the National Institutes of Health (P30 NS045776). All microfabrication procedures of the brain spheroids array were performed at the BioMEMS Resource center (EB00002503). Scanning Electron Microscopy was performed at the Center for Nanoscale Systems (CNS) at Harvard University, supported by the National Science Foundation (Award No. 1541959). The authors acknowledge Anika Marand for her help with the brain spheroids extraction.

References

1. Paşca SP (2018) The rise of three-dimensional human brain cultures. Nature 553:437–445
2. Frega M, Tedesco M, Massobrio P et al (2014) Network dynamics of 3D engineered neuronal cultures: a new experimental model for in-vitro electrophysiology. Sci Rep 4:5489
3. Choi S, Kim Y, Quinti L et al (2016) 3D culture models of Alzheimer's disease: a road map to a "cure-in-a-dish". Mol Neurodegener 11:75
4. Zhang B, Korolj A, Lai B et al (2018) Advances in organ-on-a-chip engineering. Nat Rev Mater 3:257–278
5. Kim Y, Choi S, D'Avanzo C et al (2015) A 3D human neural cell culture system for modeling Alzheimer's disease. Nat Protoc 10:985–1006
6. Jorfi M, D'Avanzo C, Tanzi RE et al (2018) Human neurospheroid arrays for in vitro studies of Alzheimer's disease. Sci Rep 8:2450
7. Jorfi M, D'Avanzo C, Kim D et al (2018) Three-dimensional models of the human brain development and diseases. Adv Healthc Mater 7:1700723
8. Kim S, Cho A, Min S et al (2019) Organoids for advanced therapeutics and disease models. Adv Ther 2:1800087
9. Raja WK, Mungenast AE, Lin Y-T et al (2016) Self-organizing 3D human neural tissue derived from induced pluripotent stem cells recapitulate Alzheimer's disease phenotypes. PLoS One 11:e0161969
10. Joseph JV, van Roosmalen IA, Busschers E et al (2015) Serum-induced differentiation of glioblastoma neurospheres leads to enhanced migration/invasion capacity that is associated with increased MMP9. PLoS One 10: e0145393
11. Choi S, Kim Y, Hebisch M et al (2014) A three-dimensional human neural cell culture model of Alzheimer's disease. Nature 515:274–278
12. Dawson TM, Golde TE, Lagier-Tourenne C (2018) Animal models of neurodegenerative diseases. Nat Neurosci 21:1370–1379
13. Duval K, Grover H, Han L-H et al (2017) Modeling physiological events in 2D vs. 3D cell culture. Physiology 32:266–277
14. Lee H-K, Sanchez C, Chen M et al (2016) Three dimensional human neuro-spheroid model of Alzheimer's disease based on differentiated induced pluripotent stem cells. PLoS One 11:e0163072
15. Meyer K, Feldman HM, Lu T et al (2019) REST and neural gene network dysregulation in iPSC models of Alzheimer's disease. Cell Rep 26:1112–1127
16. Lin Y-T, Seo J, Gao F et al (2018) APOE4 causes widespread molecular and cellular alterations associated with Alzheimer's disease phenotypes in human iPSC-derived brain cell types. Neuron 98:1141–1154
17. Wang H (2018) Modeling neurological diseases with human brain organoids. Front Synapt Neurosci 10:15

Chapter 12

Directed Differentiation of Human Pluripotent Stem Cells for the Generation of High-Order Kidney Organoids

Idoia Lucía Selfa, Maria Gallo, Nuria Montserrat, and Elena Garreta

Abstract

Our understanding in the inherent properties of human pluripotent stem cells (hPSCs) have made possible the development of differentiation procedures to generate three-dimensional tissue-like cultures, so-called organoids. Here we detail a stepwise methodology to generate kidney organoids from hPSCs. This is achieved through direct differentiation of hPSCs in two-dimensional monolayer culture toward the posterior primitive streak fate, followed by induction of intermediate mesoderm-committed cells, which are further aggregated and cultured in three-dimensions to generate kidney organoids containing segmented nephron-like structures in a process that lasts 20 days. We also provide a concise description on how to assess renal commitment during the time course of kidney organoid generation. This includes the use of flow cytometry and immunocytochemistry analyses for the detection of specific renal differentiation markers.

Key words Kidney organoid, Human pluripotent stem cells, Differentiation, Primitive streak, Intermediate mesoderm, Nephron progenitor cells, 2D Monolayer, 3D Organotypic culture, Nephrons, Flow cytometry, Immunocytochemistry

1 Introduction

Human pluripotent stem cells (hPSCs) can be exposed to a series of developmental cues in form of cytokines, growth factors, chemical compounds, and biophysical cues [1] to direct their differentiation toward specific cell lineages occurring during kidney development [2]. Under these renal inductive signals, differentiating hPSCs are able to self-organize in three-dimensional (3D) culture resulting in the formation of tissue-like structures that partially resemble in structure and function the human developing kidney, known as kidney organoids (reviewed in [3–5]). Several studies have described different approaches to generate hPSC-derived kidney organoids containing nephron-like structures [1, 6–9]. Most of the procedures developed up to date account with a first stage of

Mo R. Ebrahimkhani and Joshua Hislop (eds.), *Programmed Morphogenesis: Methods and Protocols*, Methods in Molecular Biology, vol. 2258, https://doi.org/10.1007/978-1-0716-1174-6_12,

differentiation in where undifferentiated hPSCs are guided to the posterior primitive streak (PPS) fate by the endogenous activation of WNT using the GSK-3ß inhibitor CHIR99201 (CHIR). To that end, different lengths and doses of CHIR treatment have been described [1, 6–11]. In the same manner, different laboratories have shown that the commitment of PPS toward intermediate mesoderm (IM) and nephron progenitor cells (NPCs) can vary among protocols [1, 6–11]. In this chapter, we explain in detail a procedure to generate kidney organoids from hPSCs, during which hPSCs are induced for a short period of 4 days in a two-dimensional (2D) culture fashion toward IM-like cells that are then aggregated into 3D spheroids and cultured under organotypic conditions for 16 additional days (Fig. 1). After aggregation, IM-committed spheroids are kept in the presence of growth factors for 5 days to induce NPC commitment. Three additional days are then required for the formation of renal vesicle (RV) structures—the precursor structures of the nephrons—that appear within the organoids 24 h after complete growth factor removal due to a process of mesenchymal to epithelial transition. During the following 8 days, RVs acquire proximal–distal polarity and develop into nephron-like structures by recapitulating in vitro the process known as nephron patterning (Fig. 1). Day 16 kidney organoids reveal the presence of segmented nephron-like structures containing glomeruli with podocyte-like cells connected to proximal and distal tubular structures [1]. In contrast to recent works that showed the possibility to differentiate hPSCs into kidney organoids transcriptomically matching first trimester gestational kidney in a process of 25 days, the method described here takes advantage of the aggregation of IM-like cells very early during the differentiation process to boost cell-to-cell and cell-to-extracellular matrix interactions to efficiently generate kidney organoids with a similar transcriptomic profile as that found in second-trimester human gestational kidney [1].

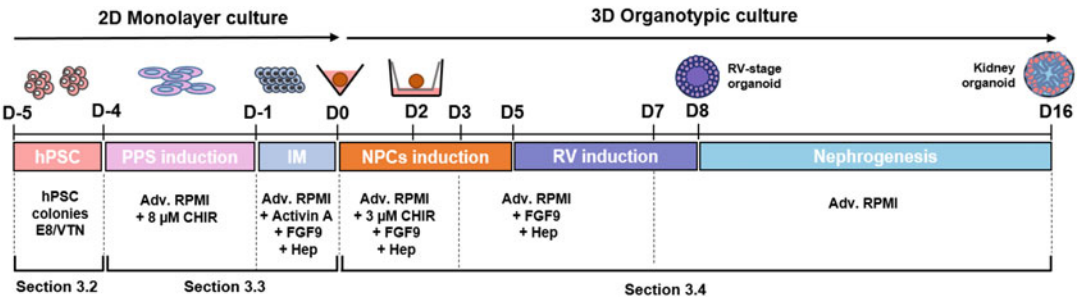

Fig. 1 Kidney organoid differentiation protocol. The days of the protocol are indicated as "D". *hPSCs* human pluripotent stem cells, *PPS* posterior primitive streak, *IM* intermediate mesoderm, *NPCs* nephron progenitor cells, *RV* renal vesicles, *E8* essential 8 medium, *VTN* vitronectin, *Adv RPMI* advanced RPMI 1640 basal medium, *Hep* heparin

During the last decade, several laboratories have demonstrated the generation of organoids from hPSCs resembling not only kidney but also a variety of organs including eye cup, brain, intestine, and lung among others [5]. The field is rapidly evolving, and several studies have recently highlighted organoids' potentiality for modeling organ development and disease in the human context, opening the door to future drug discovery and regenerative medicine applications. However, the organoid field is still facing major challenges, in part associated to the lack of control in the self-organizing events occurring during organoid formation in current methodologies, leading to high organoid variability as well as lack of essential cellular components (i.e., vascularization) and incomplete maturation. In this regard, emergent bioengineering technologies including biomimetic materials, microtechnologies, and 3D bioprinting [12, 13] can be used to harness and control organoid morphogenesis by precisely tuning the organoid niche (i.e., cell–cell and cell–extracellular matrix interactions) (reviewed in [5, 14]). Recently, we have shown that kidney organoids can vascularize upon implantation onto the chick chorioallantoic membrane (CAM), thus acquiring relevant features of podocyte maturity [1]. Of note, when the soft CAM microenvironment was mimicked in vitro using polyacrylamide hydrogels, these accelerated the formation of kidney organoids that indeed contained more nephron-like structures in comparison to a rigid microenvironment [1]. Overall, the exploitation of bioengineering tools as well as other emergent disciplines (i.e., gene editing, single-cell analysis, force mapping, computational modeling, among others) in combination with the morphogenetic potential of organoids represents a promising scenario toward the development of next-generation organoid models.

2 Materials

2.1 Culture and Passage of hPSCs

1. Air-vented 10 cm Petri dishes, Nunclon Delta™ (150350, Thermo Scientific).
2. Phosphate-buffered saline (PBS) pH 7.4 (1×) (1001–015, Life Technologies).
3. Vitronectin (VTN-N) (A14700, Fisher Scientific). The vitronectin coating is prepared by diluting the vitronectin stock solution (0.5 mg/mL) at a 1:100 ration in 1× PBS. Coating of an air-vented 10 cm Petri dish is performed by diluting 50 μL of the vitronectin stock solution in 5 mL of PBS to have a final concentration of 0.5 μg of vitronectin/mL. For 24-well plates (*see* Subheading 2.2), 400 μL of diluted vitronectin (5 μg/mL) per well is used. Plates containing the vitronectin solution are left at room temperature for 1 h or kept at 4 °C overnight until further use.

4. Essential 8 medium (A1517001, Life Technologies). It is provided as a two-component kit (500 mL basal medium bottle and 10 mL supplement). Besides adding the 10 mL supplement, add 5 mL of Penicillin/Streptomycin (10,000 units/mL of penicillin and 10,000 μg/mL of streptomycin, 15140122, Life Technologies).
5. 0.5 M EDTA (15575-038, Life Technologies): dilute the EDTA stock solution (0.5 M) at a 1:1000 ratio in 1× PBS to have a working solution of 0.5 mM EDTA.

2.2 Plating of hPSCs for Differentiation

1. 24-well plate, Nunclon Delta™ (142475, Thermo Scientific).
2. Round coverslips, diameter 12 mm, #1.5 (CBA-D00120RAC20MNZ#0, Fischer Scientific). Autoclave the coverslips before use for cell culture.
3. Microfuge tubes, 1.5 mL (200400P, Deltalab).
4. Accumax (07921, Stem Cell Technologies).
5. Dulbecco's modified eagle medium (DMEM) (11966025, Life Technologies).
6. Fetal Bovine Serum (FBS) (10270-106, Gibco).
7. Neubauer chamber (0640010, Superior Marienfeld).

2.3 Differentiation of hPSCs Toward IM-Committed Cells and Generation of Kidney Organoids

1. Advanced RPMI 1640 basal medium (12633-012, Life Technologies): A bottle of 500 mL of advanced RPMI 1640 basal medium is supplemented with 5 mL of L-GlutaMAX (200 mM, 35050–038, Life Technologies) and 5 mL of Penicillin/Streptomycin (10,000 units/mL of penicillin and 10,000 μg/mL of streptomycin, 15140122, Life Technologies).
2. 12 μM CHIR99021 (SML1046-5MG, Sigma): dilute 5 mg of CHIR99021 in 896 μL of dimethyl sulfoxide (D2650, Sigma), aliquot, and store at −20 °C.
3. 50 μg/mL Recombinant human FGF9 (100-23B, Peprotech): reconstitute in cell-culture-grade distilled water (15230-089, Life Technologies), aliquot, and store at −20 °C.
4. 50 mg/mL Heparin (H3149-10KU, Sigma): reconstitute in cell-culture-grade distilled water (15230-089, Life Technologies), aliquot, and store at 4 °C.
5. 50 μg/mL Activin A (338-AC-050, R&D Systems): reconstitute in sterile 4 mM hydrochloric acid (HCl), aliquot, and store at −20 °C.
6. 96-well plate, V-bottom, Nunc™ (249935, Thermo Scientific).
7. Corning® Transwell® polyester membrane cell culture inserts (CLS3460, Sigma).
8. Thin glass Pasteur pipette, 150 mm (5426015, Normax).

9. 200 μL-wide orifice pipette tips (E1011-8400, Starlab). Tips need to be autoclaved for cell culture use.

2.4 Flow Cytometry Analysis of Differentiation Markers

1. eBioscience™ Foxp3/Transcription factor staining buffer set (00-5523-00, Invitrogen). Components are fixation/permeabilization concentrate (00-5123), fixation/permeabilization diluent (00-5223) and 10× permeabilization buffer (00-8333). Prepare fresh Foxp3 fixation/permeabilization working solution by mixing one part of Foxp3 fixation/permeabilization concentrate with three parts of Foxp3 fixation/permeabilization diluent. Prepare a 1× working solution of permeabilization buffer by mixing one part of 10× permeabilization buffer with nine parts of distilled water.
2. Accumax (07921, Stem Cell Technologies).
3. Falcon® 5 mL Round-Bottom Polystyrene Test Tube, with Cell Strainer Snap Cap (352235, Corning).
4. LIVE/DEAD™ Fixable violet dead cell stain kit (L34963, Invitrogen).
5. Fetal bovine serum (FBS) (10270-106, Gibco).

Antibodies and Isotype Controls

6. Oct3/4, mouse IgG1 κ, Alexa Fluor (AF) 488, Clone 40/Oct3 (560253, BD Pharmigen).
7. Mouse IgG1 κ, AF488-conjugated isotype control, clone MOPC-21 (557721, BD Pharmigen).
8. Brachyury, goat IgG, APC (IC2085A, R&D Systems).
9. Goat IgG, APC-conjugated isotype control (IC108A, R&D Systems).
10. PAX2, goat IgG (AF3364, R&D Systems). Before use, conjugate PAX2 antibody to AF488 using the Lightning-Link® Rapid conjugation kit (322-0010, Innova Biosciences) following manufacturer instructions.
11. Goat IgG, AF488-conjugated isotype control (IC108G, R&D Systems).

2.5 Immunocytochemistry Analysis of Differentiation Markers

1. Fixation solution of 4% paraformaldehyde. In the fume hood, prepare this solution by mixing 2.5 mL of 16% paraformaldehyde (153799, Aname) with 7.5 mL of 1× PBS. Prepare fresh and use it upon preparation.
2. Tris–buffered saline (TBS), 10× (pH 7.4–7.5). To prepare this buffer, dissolve 132.2 g of Trizma–HCl (T6666, Sigma), 19.4 g of Trizma base (T6791, Sigma), and 90.0 g of NaCl (S7653, Sigma) in 855 mL of distilled water. Keep the solution at 4 °C and use it within 1 month.

3. TBS, 1× (pH 7.4–7.5). To prepare this buffer, dilute 10× TBS at 1:10 ratio by mixing 900 mL of distilled water and 100 mL of 10× TBS. Keep the solution at 4 °C and use it within 2 weeks.
4. TBS, 1× (pH 7.4–7.5) supplemented with 1% Triton X-100 (50 mL). To prepare this buffer, dilute 500 μL of Triton X-100 (T8787, Sigma) in 50 mL of TBS, 1× (pH 7.4–7.5). Keep the solution at 4 °C and use it within 2 weeks.
5. TBS, 1× (pH 7.4–7.5) supplemented with 0.5% Triton X-100 (50 mL). To prepare this buffer, dilute 250 μL of Triton X-100 (T8787, Sigma) in 50 mL of TBS, 1× (pH 7.4–7.5). Keep the solution at 4 °C and use it within 2 weeks.
6. Blocking solution (10 mL) containing 1% Triton X-100 and 6% donkey serum. To prepare this solution, dilute 600 μL of donkey serum (S30-KC, Sigma) in 9.4 mL of TBS, 1× (pH 7.4–7.5) containing 1% Triton X-100. Prepare fresh blocking solution and use it upon preparation.
7. Streptavidin/Biotin blocking kit (SP-2002, Vector Labs) is used as an additional blocking step when biotinylated Lotus Tetragonolobus Lectin (LTL) is used to stain proximal tubule-like structures. Briefly, use 4–5 drops of streptavidin solution and incubate 20 min. Wash once with 1× TBS for 15 min at RT. Then use 4–5 drops of biotin solution and incubate 20 min. Wash once with 1× TBS for 15 min at RT.
8. For diluting the antibodies and for the washing steps, prepare a solution (25 mL) of 1× TBS containing 0.5% Triton X-100 and 6% donkey serum by mixing 1500 μL of donkey serum (S30-KC, Sigma) in 23.5 mL of 1× TBS containing 1% Triton X-100. Prepare fresh and use it upon preparation.
9. In case LTL is used to stain proximal tubule-like structures, for diluting the antibodies and LTL, and for the washing steps, prepare a solution (25 mL) of 1× TBS containing 0.5% Triton X-100 and 1% bovine serum albumin (BSA) by dissolving 0.25 g of BSA (A4503, Sigma) in 25 mL of 1× TBS containing 0.5% Triton X-100. Prepare fresh and use it upon preparation.

2.6 Primary Antibodies

1. Brachyury, goat IgG (AF2085, R&D Systems).
2. Oct4, mouse IgG, clone C10 (Sc-5279, Santa Cruz Biotechnology).
3. PAX2, goat IgG (AF3364, R&D Systems).
4. SALL1, mouse IgG2a, clone K9814 (PP-K9814-00, R&D Systems).
5. SIX2, rabbit IgG (11562-1-AP, Proteintech).

6. WT1, rabbit IgG, clone CAN-R9(IHC)-56-2 (ab89901, Abcam).
7. E-Cadherin, mouse IgG2a,κ, clone 36 (610181, BD Bioscience).
8. Podocalyxin, goat IgG (BAF1658, R&D Systems).

2.7 Secondary Antibodies and Other Reagents

1. Donkey anti-goat IgG AF488 (705-545-147, Jackson ImmunoResearch).
2. Donkey anti-mouse IgG Cy3 (715-165-151, Jackson ImmunoResearch).
3. Donkey anti-mouse IgG AF488 (A21202, Fischer Scientific).
4. Donkey anti-rabbit IgG Cy3 (711-165-152, Jackson ImmunoResearch).
5. Donkey anti-goat IgG AF555 (A21432, Fischer Scientific).
6. Donkey anti-mouse IgG AF647 (715-605-151, Jackson ImmunoResearch).
7. Biotinylated Lotus Tetragonolobus Lectin (LTL) (B-1325, Vector Laboratories).
8. DyLight 488 Streptavidin (SA-5488, Vector Labs).
9. 4′,6-Diamidino-2-Phenylindole, dihydrochloride (DAPI) (D1306, Invitrogen). To make a 5 mg/mL (14.3 mM) DAPI stock solution, dissolve the contents of one vial (10 mg) in 2 mL of distilled water. For long-term storage, aliquot the stock solution and store at −20 °C.

2.8 Other Materials

1. Histology mold, plastic (20447200820, Laboquimia). To embed the organoids, prepare a solution of 0.8% low gelling temperature type VII agarose (A4018, Sigma) by dissolving 0.8 g of agarose in 100 mL of distilled water. Use the plastic mold to place the organoids together with pre-warmed 0.8% agarose. Leave at 4 °C to obtain an agarose block containing the organoids.
2. Dako Pen (S200230, Agilent). Use it to surround tissue sections on the slide to create a smaller area for antibody incubation.
3. Fluoromount-G (0100-01, Southern Biotech).
4. Round coverslips, diameter 12 mm, #1.5 (CBA-D00120RAC20MNZ#0, Thermo Scientific).
5. Rectangular coverslip, 24 × 50 mm, #1.5 (BBAD02400500#SC13MNZ#0##, Thermo Scientific).
6. Microscope slide, 25 × 75 × 1.0 mm (J1800AMNZ, Thermo Scientific).
7. Nail polish to fix the coverslips when mounting the samples.

3 Methods

The methodology to generate kidney organoids from hPSCs (Fig. 1) has been divided into four methodological stages involving the culture and passage of hPSCs (Subheading 3.1), the plating of hPSCs for differentiation (Subheading 3.2), the differentiation of hPSCs toward posterior primitive streak (PPS) and intermediate mesoderm (IM) (Subheading 3.3), and the formation and culture of kidney organoids (Subheading 3.4). Next, by means of flow cytometry (Subheading 3.5) and immunocytochemistry (Subheading 3.6) analyses, a methodology to analyze the differentiation outcomes at different time points during the generation of kidney organoids is also described.

3.1 Culture and Passage of hPSCs

1. hPSCs are grown on vitronectin-coated air-vented 10 cm Petri dishes in Essential 8 Medium and incubated with 5% CO_2 at 37 °C. In order to avoid their spontaneous differentiation, hPSCs need to be passaged before they reach 100% confluency.
2. For enzymatic passaging, aspirate the Essential 8 medium from hPSCs monolayers at approximately 80% confluency.
3. Perform a quick and gentle wash by rinsing twice with 8 mL of 1x PBS.
4. Add 5 mL of 0.5 mM EDTA. Place the cells in an incubator at 37 °C for 3–4 min. Gently aspirate the EDTA solution without disrupting the hPCS colonies. Then disaggregate the hPSCs colonies by flushing 1 mL of Essential 8 media to the hPSCs colonies in order to detach the cells into small clusters (*see* **Note 1**). Collect the clumps of cells into a tube. To prevent excessive dissociation of cells, use a fresh 1 mL of Essential 8 Media each time and repeat the process until complete detachment of all cells in the plate. Normally, 10 mL of Essential 8 Media is used to collect the cell clumps in a 15-mL tube.
5. Take 500 μL of the cell suspension and complete to 10 mL with Essential 8 media in a new 15-mL tube to passage the cells at a 1:20 ratio (*see* **Note 2**).
6. Aspirate the vitronectin of a new air-vented 10 cm Petri dish (for vitronectin coating preparation, *see* Subheading 2.1, **item 3**) and directly plate the diluted cell suspension. Gently move the plate in all directions to evenly distribute the cell clusters on the plate.
7. Culture the cells in an incubator at 37 °C with 5% CO_2 for approximately 6 days, changing the Essential 8 media every second day (*see* **Note 2**).

3.2 Plating of hPSCs for Differentiation

1. Prepare fresh 24-well plates coated with vitronectin. Prepare also an additional 24-well plate containing 12 mm round glass coverslips coated with vitronectin, which will be further used to analyze the extent of differentiation into PPS and IM by immunocytochemistry (*see* Subheading 3.6).
2. Start the procedure as if it is a normal hPSCs passage and collect the undifferentiated cells in 10 mL of Essential 8 media in a 15-mL tube (*see* Subheading 3.1, **steps 1–4**).
3. For cell counting, take 1 mL of the cell suspension, place it in a 1.5 mL microfuge tube, and centrifuge for 5 min at 100 *g* to obtain a cell pellet (*see* **Note 3**).
4. Remove the Essential 8 media, add 1 mL of 1× PBS to wash the cell pellet, and centrifuge again for 5 min at 100 *g*.
5. Remove the 1× PBS and add 300 μL of Accumax and incubate at 37 °C for 5 min to allow single-cell dissociation for cell counting.
6. After the incubation time, cancel Accumax activity by adding 700 μL of DMEM media supplemented with 10% FBS.
7. Take 10 μL of the single-cell suspension and place it in a Neubauer chamber for cell counting (*see* **Note 4**).
8. Based on cell number, resuspend the cells in the appropriate volume of Essential 8 media to have 2×10^5 cells/mL. Plate 500 μL of the resultant cell suspension per well of a 24-well plate to have 10^5 cells in each well (*see* **Note 5**).
9. Plating density and cell colony distribution is essential for an efficient differentiation. In order to prevent cell clusters to come together in the center of the wells of a 24-well plate, shake the plate in all directions and carefully place the plate in the incubator. Avoid opening and closing the incubator during the next 2 h to ensure an even distribution of the adhered cells in the plate.
10. Culture the cells at 37 °C with 5% CO_2 for 24 h before starting the differentiation (Fig. 2a, b; *see* **Note 6**) (Fig. 1, day −5).

3.3 Differentiation of hPSCs Toward Posterior Primitive Streak (PPS) and Intermediate Mesoderm (IM)

1. Once cell colony density and distribution are adequate (Fig. 3a), aspirate the Essential 8 media from the 24-well plate and rinse once with 1× PBS to remove remnants of it (Fig. 1, day −4).
2. Add 500 μL/well of advanced RPMI 1640 basal media supplemented with 8 μM CHIR (Fig. 1, day −4).
3. Every 24 h, replace the media with fresh advanced RPMI 1640 basal media supplemented with 8 μM CHIR for two additional consecutive days (Fig. 1, day −3 and day −2). Note that hPSCs start to change their morphology (Fig. 3b).

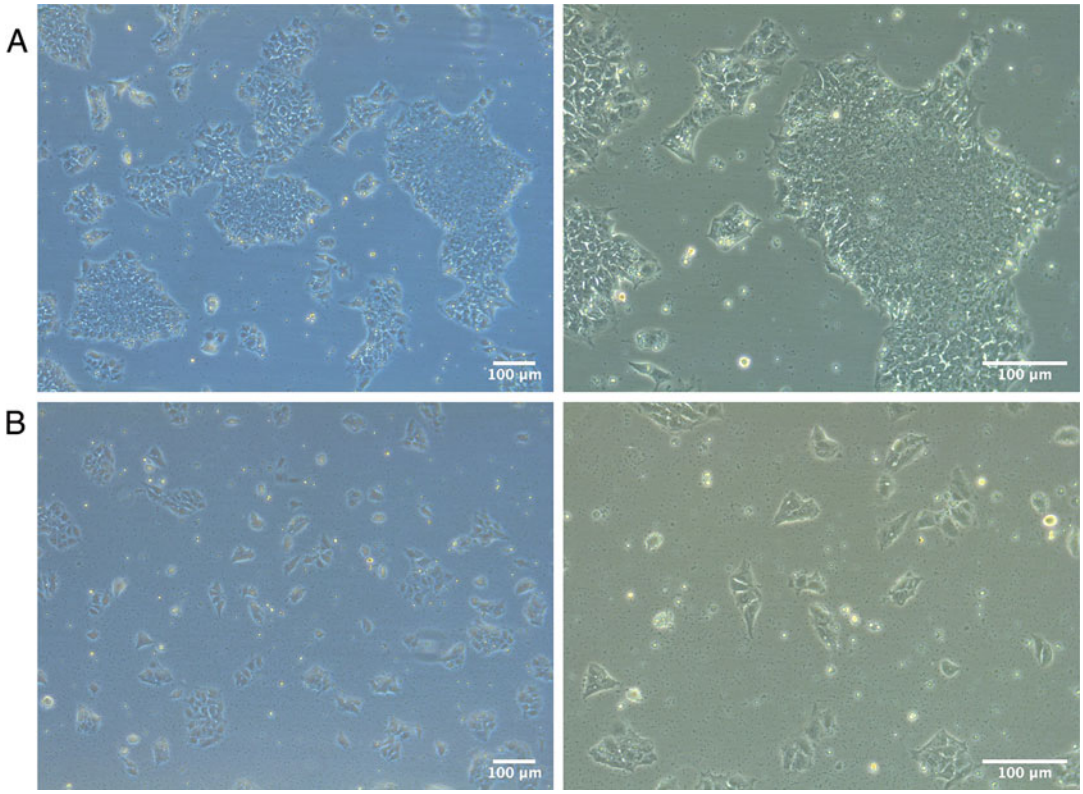

Fig. 2 Optimal plating density and colony distribution of undifferentiated hPSCs cultured in Essential 8 media that is required for starting the differentiation. Representative bright-field images of ES[4] hPSCs 24 h after plating (day −4). (**a**) Differentiation is started from hPSCs colonies presenting a good compaction. (**b**) When hPSCs colonies are too small or are not well compacted, wait 24 h more before starting the differentiation. If waiting 24 h does not improve hPSCs colony compaction or the right confluency is not achieved, then repeat the plating of hPSCs. Higher magnification images (10×) on the right correspond to the images shown on the left (5×). Scale bars: 100 µm

4. After the 3 days of 8 µM CHIR treatment (Fig. 1, day −1), cultured cells show an appearance of dense clusters (Fig. 3c). In order to confirm that cells have started to acquire a PPS-related fate, the differentiation extent is measured at the molecular level by the collection of cells and analysis for the loss of pluripotency-related markers such as OCT4, and the acquisition of the primitive streak marker Brachyury through both flow cytometry (*see* Subheading 3.5) and immunocytochemistry analysis (Fig. 4a; *see* Subheading 3.6).
5. On day −1, remove the advanced RPMI 1640 basal media supplemented with 8 µM CHIR and gently rinse once with 1× PBS (*see* **Note 7**).

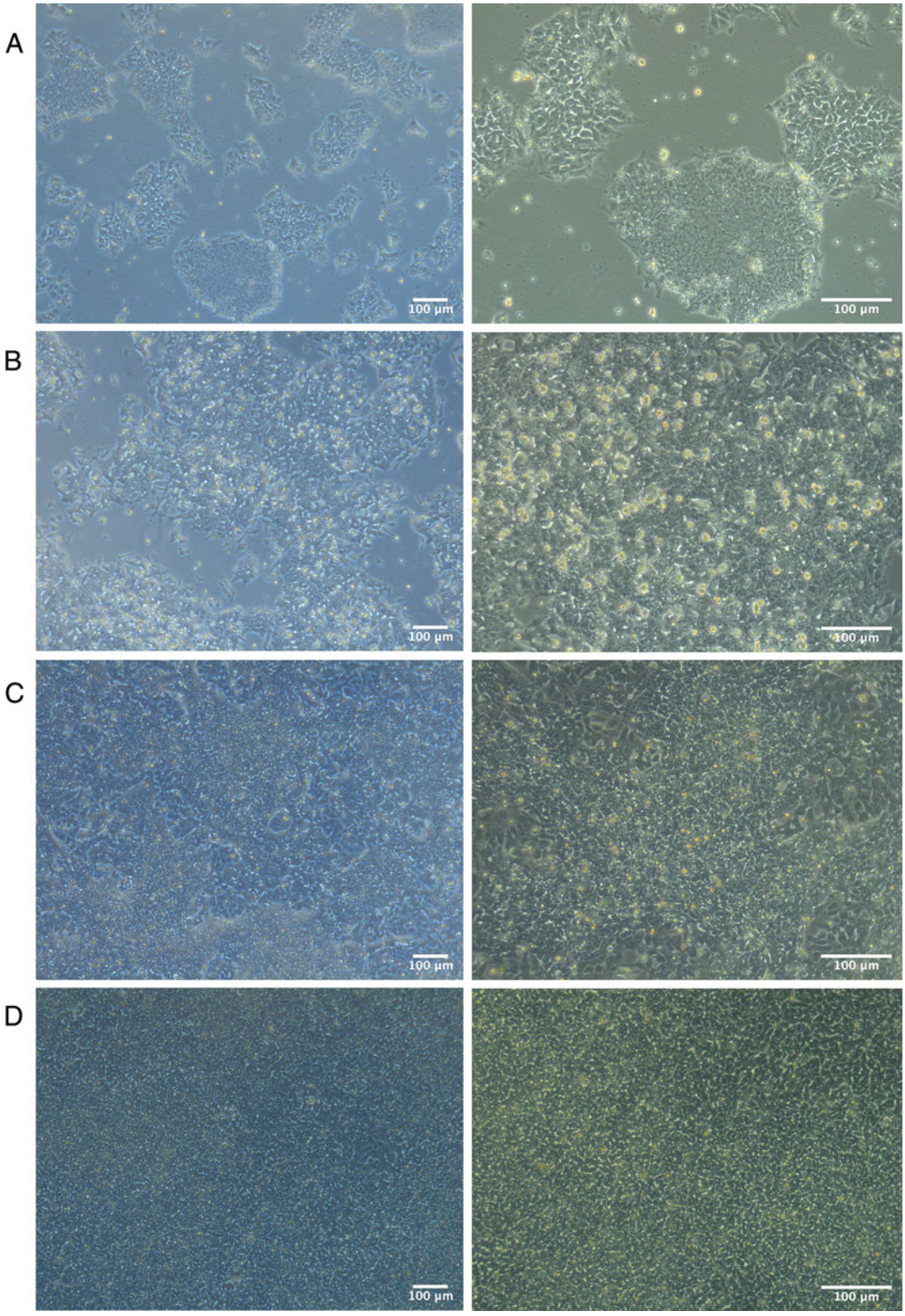

Fig. 3 Morphological changes in hPSCs during the first 4 days of 2D monolayer differentiation. Representative bright-field images. (**a**) Day −4: ES[4] hPSCs 24 h after plating that show the optimal confluency (40–50%) and morphology needed for starting the 8 µM CHIR treatment. (**b**) Day −2: morphology of differentiating hPSCs after 48 h of 8 µM CHIR treatment. (**c**) Day −1: appearance of cells after 72 h of

6. Add 500 μL per well of advanced RPMI 1640 basal media supplemented with 200 ng/mL FGF9, 1 μg/mL heparin, and 10 ng/mL activin A (Fig. 1, day −1).
7. After 24 h (Fig. 1, day 0), cells should appear under the microscope as a tight monolayer (Fig. 3d).
8. Cells at this point can be analyzed for the expression of the IM marker PAX2, using both flow cytometry (*see* Subheading 3.5) and immunocytochemistry analysis (Fig. 4b; *see* Subheading 3.6).

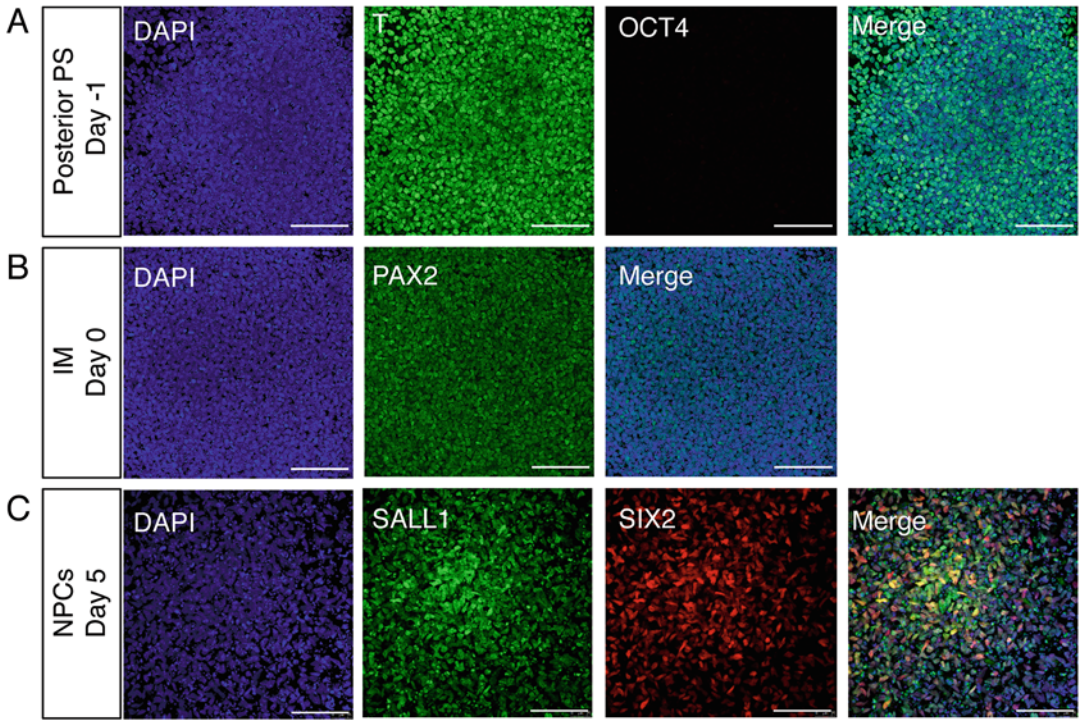

Fig. 4 Immunocytochemistry analysis for the assessment of the differentiation extent of monolayer cell cultures at different time points during the differentiation protocol. (**a**) Immunocytochemistry is performed at day -1 to detect the expression of Brachyury (T), one of the major markers related to PPS identity. Notice that T-positive cells do not express OCT4, one of the core pluripotency-related markers. (**b**) The commitment of PPS toward the IM is assessed by the detection of PAX2 at day 0. (**c**) The NPC signature in day 5 cells is assessed by the detection of SALL1 and SIX2 markers. Scale bars: 100 μm

Fig. 3 (continued) 8 μM CHIR treatment that induces the PPS fate. A compact cell monolayer is starting to form, but still loose clusters of cells are found at this stage. (**d**) Day 0: appearance of cells after treatment with FGF9, activin A, and heparin for 24 h that induces the derivation of intermediate mesoderm-committed cells. The cell monolayer appears uniform and compacted. At this stage, monolayers are ready to aggregate into 3D organoids. Higher magnification images (10×) on the right correspond to the images shown on the left (5×). Scale bars: 100 μm

3.4 Formation and Culture of Kidney Organoids

1. On day 0, remove the media and rinse twice with 1× PBS. Place 500 μL of Accumax per well of the 24-well plate and incubate for 1 min at 37 °C. Carefully, aspirate the Accumax without disrupting the cell monolayer. Then, use 500 μL of fresh advanced RPMI 1640 basal media to dissociate the cell monolayer in each well and collect the single-cell suspension in a 15-mL tube (*see* **Note 8**). Normally, 12 mL of advanced RPMI 1640 basal media is used to collect the cells from a 24-well plate.
2. Usually, since large amounts of cells are recovered after cell dissociation, an aliquot of the cell suspension is diluted at 1:4 ratio in advanced RPMI 1640 basal media to have a proper cell density to correctly perform the cell counting. Then, 10 μL of the single-cell suspension are placed in a Neubauer chamber and cells are counted (*see* **Note 3**).
3. Based on cell number, resuspend the cells in the appropriate volume of advanced RPMI 1640 basal media supplemented with 3 μM CHIR, 200 ng/mL FGF9, and 1 μg/mL heparin to have 5×10^6 cells/mL. Pipette 150 μL of the cell suspension in each well of a 96-well plate (V-bottom) to have 5×10^5 cells per well (*see* **Note 9**).
4. Centrifuge the 96-well plate (V-bottom) for 3 min at 300 *g* (Fig. 1, day 0).
5. Maintain the 96-well plate in an incubator at 37 °C with 5% CO_2 for 48 h without medium change to allow cells to self-aggregate and induce the differentiation toward nephron progenitor cells (NPCs).
6. After 48 h (day 2), the self-aggregated spheroids are transferred to 12-well plate transwells. Carefully transfer one spheroid per transwell by placing the spheroid on top of the transwell membrane (*see* **Note 10**).
7. Immediately, add 450 μL of advanced RMPI 1640 basal media with 3 μM CHIR, 200 ng/mL FGF9, and 1 μg/mL heparin to the base of each transwell to generate an air–liquid interface organotypic culture condition (Fig. 1, day 2).
8. On day 3, aspirate the media from the transwells with thin glass Pasteur pipettes and replace it with 450 μL of advanced RMPI 1640 basal media containing only 200 ng/mL FGF9 and 1 μg/mL heparin, and culture for 48 h without media changes.
9. On day 5, aspirate the media from the transwells with thin glass Pasteur pipettes and replace it with 450 μL of fresh advanced RMPI 1640 basal media containing 200 ng/mL FGF9 and 1 μg/mL heparin, and culture for 48 h without media changes. At this point, NPCs induction can be assessed by analyzing the expression of NPC-associated markers by immunocytochemistry (Fig. 4c, *see* Subheading 3.6).

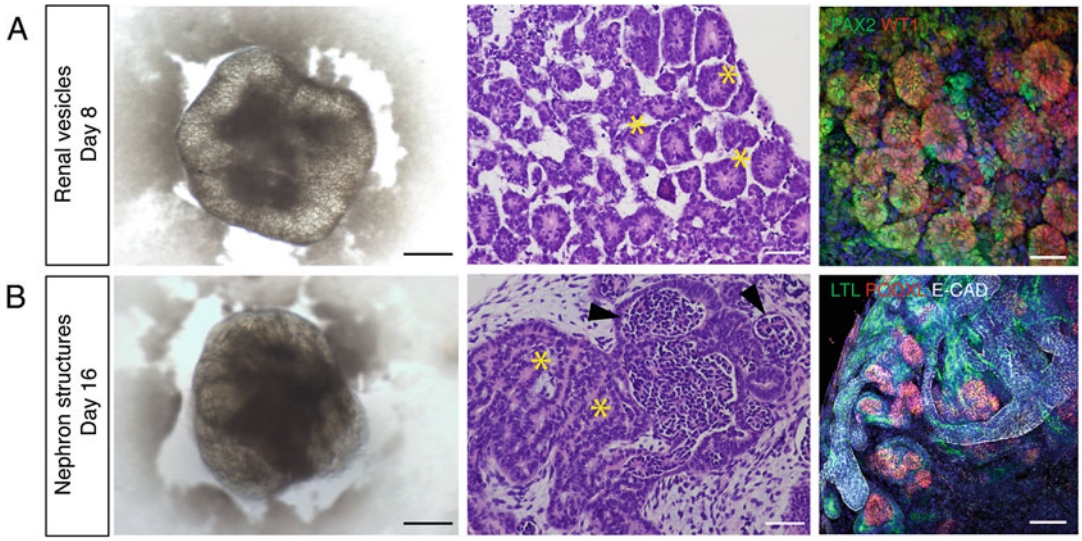

Fig. 5 Characterization of renal vesicles (RVs) and segmented nephron-like structures in hPSC-derived kidney organoids. (**a**) RV-stage kidney organoids contain RV-like structures that can be detected by different techniques. From left to right: bright-field image of a RV-stage kidney organoid, hematoxylin-eosin staining on a paraffin section of a RV-staged kidney organoid, and immunocytochemistry for the detection of PAX2 and WT1 in a RV-stage kidney organoid at day 8 of differentiation. Asterisks point to renal vesicle structures. (**b**) Segmented nephron-like structures are analyzed at day 16 of differentiation by different techniques. From left to right: bright-field image of a day 16 kidney organoid, hematoxylin-eosin staining on a paraffin section of a day 16 kidney organoid, and immunocytochemistry for the detection of Podocalyxin (PODXL) in podocyte-like cells, and Lotus Tetragonolobus Lectin (LTL) and E-cadherin (ECAD) in proximal and distal segments of the tubular-like structures, respectively. Arrowheads point to glomerular-like structures, and asterisks point to tubular-like structures. Scale bars in bright-filed images correspond to 500 μm. Scale bars in hematoxylin-eosin staining correspond to 50 μm. Scale bars in immunocytochemistry staining correspond to 75 μm

10. On day 7, growth factors are removed by replacing the media with advanced RMPI 1640 basal media. After 24 h, multiple renal vesicles (RVs)—the precursor structures of the nephrons—clearly appear within the spheroid (Fig. 1, day 8 RV-stage organoid). RVs can be visualized in bright field, and further analyzed by performing hematoxylin and eosin staining of kidney organoid sections and immunocytochemistry for the expression of RV-associated markers (Fig. 5a; *see* Subheading 3.6).
11. Change the media every second day until day 16, when kidney organoids are fully developed and contain nephron-like structures (Fig. 1, day 16 kidney organoid). The nephron structures can be visualized in bright field and further analyzed by performing hematoxylin and eosin staining of kidney organoid sections and immunocytochemistry for the expression of nephron markers (Fig. 5b; *see* Subheading 3.6).

3.5 Flow Cytometry Analysis of Differentiation Markers

1. For analysis of PPS differentiation efficiency, harvest cells at day −1. PPS induction is characterized by a marked decrease in the expression of the pluripotency-associated marker OCT4 and upregulation of the primitive streak marker Brachyury. For analysis of IM differentiation efficiency, harvest cells at day 0. IM commitment is assessed by analyzing the expression of PAX2.
2. For intracellular staining of all the above markers, use the Foxp3/transcription factor staining buffer set (*see* Subheading 2.4 for buffer preparation).
3. A minimum number of 10^5 cells/tube should be used for the analysis hereafter. Therefore, harvest approximately 3–4 wells of the 24-well plate at day −2 and 2–3 wells of the 24-well plate at day −1, to perform the analysis.
4. Remove media and gently rinse twice with 1× PBS.
5. Add 300 μL/well of Accumax and incubate for 2–5 min at 37 °C.
6. Aspirate the Accumax, dissociate cells by flushing with 1× PBS, and collect them in 1× PBS. Collect the necessary wells and resuspend the cells in 1 mL of 1× PBS.
7. Pass the cell suspension to a flow cytometry tube with 35-μm-filter caps to ensure a single-cell suspension (*see* Subheading 2.4, **item 3**).
8. Add 1 μL of reconstituted LIVE/DEAD fixable violet stain (*see* **Note 11**; reconstituted reactive should be used in 2 weeks) and incubate for 30 min at room temperature (RT) in the dark.
9. Wash two times with 3 mL of 1× PBS and centrifuge for 3 min at 300 *g*. Discard the supernatant and pulse vortex the sample to completely dissociate the pellet.
10. Add 500 μL of Foxp3 fixation/permeabilization working solution to each tube and resuspend the cells in the solution.
11. Incubate for 30 min at RT in the dark.
12. Centrifuge the sample for 3 min at 300 *g* and discard the supernatant.
13. For permeabilization, wash two times with 3 mL of permeabilization buffer. Centrifuge the sample for 3 min at 300 *g* and discard the supernatant.
14. Resuspend the pellet with permeabilization buffer. At this point, divide the sample into the necessary tubes to perform the isotype control staining and the correspondent antibody stainings. For PPS analysis (day −1), resuspend in 2.5 mL of permeabilization buffer and pipette 500 μL of cell suspension per tube (five tubes). For IM analysis (day 0), resuspend in

1.5 mL of permeabilization buffer and pipette 500 μL of cell suspension per tube (three tubes).

15. Block the sample tubes with 2% FBS by adding 10 μL directly to each tube containing 500 μL of the cell suspension. Incubate for 15 min at RT.
16. Centrifuge the tubes for 3 min at 300 *g* and discard the supernatant by gently pouring the solution without disrupting the pellet.
17. Add 100 μL of permeabilization buffer to each tube and pulse vortex to dissociate the pellet.
18. Add the recommended amount of conjugated isotype controls and antibodies for detection of intracellular antigens to each tube, pulse vortex and incubate for 30 min at RT in the dark.
19. For PPS analysis (day −1), add the indicated isotype controls and antibodies:
    (a) Tube 1: do not add any reagent.
    (b) Tube 2: Goat IgG APC-conjugated isotype control (10 μL) + Mouse IgG1 AF488-conjugated isotype control (5 μL).
    (c) Tube 3: Brachyury-APC (10 μL).
    (d) Tube 4: Oct4-AF488 (20 μL).
    (e) Tube 5: Brachyury -APC (10 μL) + Oct4-AF488 (20 μL).
20. For IM analysis (day 0), add the indicated isotype controls and antibodies:
    (a) Tube 1: do not add any reagent.
    (b) Tube 2: Goat IgG AF488-conjugated isotype control (5 μL).
    (c) Tube 3: PAX2-AF488 (0.5 μL).
21. After incubation, add 1 mL of permeabilization buffer to each tube and centrifuge the tubes for 5 min at 300 *g*. Discard the supernatant.
22. Wash two times with 2 mL of permeabilization buffer to each tube, centrifuging the tubes for 5 min at 300 *g* and discard the supernatant.
23. Resuspend each cell pellet in 500 μL of 1× PBS supplemented with 2% FBS.

Acquire the sample tubes in a flow cytometer and analyze the data using a flow cytometry software such as FlowJo. The expected percentage of Brachyury$^+$ OCT4$^-$ cells in the PPS analysis (day −1) is around 80%. The expected percentage of PAX2$^+$ cells in the IM analysis (day 0) is around 85%.

3.6 Immunocytochemistry Analysis of Differentiation Markers

For the analysis of the extent of differentiation into PPS and IM, cells differentiated onto glass coverslips coated with vitronectin (*see* Subheadings 3.2 and 3.3) are collected at day −1 and day 0, respectively. For the analysis of the extent of differentiation into NPCs, RVs, and nephron structures (*see* Subheading 3.4), organoids are collected at days 5, 8, and 16, respectively. Immunocytochemistry is performed in whole-mount organoids. Alternatively, paraffin sectioning of organoids can be also performed (*see* **Note 12** for details on kidney organoid sample processing for paraffin sectioning and immunohistochemistry).

1. Remove the media from the correspondent wells containing the glass coverslips with cells. For organoids, remove the media from the transwells. Wash samples once with 1× PBS.
2. In the fume hood, fix the samples by adding 1 mL of 4% paraformaldehyde to each well. For organoids on transwells, add 0.5 mL of 4% paraformaldehyde inside the transwell and 1 mL of 4% paraformaldehyde in the base of the transwell. Incubate for 20–30 min at RT in the case of cells and 1 h at RT in the case of organoids.
3. In the fume hood, remove the fixative and wash the samples three times with 1× PBS at RT for 5 min each in the case of cells and three times for 15 min each in the case of organoids.
4. Block the samples with 500 μL of 1× TBS containing 1% Triton X-100 and 6% donkey serum. For organoids on transwells, add 0.5 mL of the blocking solution inside the transwell and 1 mL of the blocking solution in the base of the transwell. Incubate for 1 h at RT in the case of cells and 4 h at RT in the case of organoids. In this step and during the next steps (**steps 5–12**), place the samples over a shaker when possible.
5. For nephron structure analysis in which the biotinylated Lotus Tetragonolobus Lectin (LTL) is used to stain proximal tubule-like structures, an additional blocking step with the Streptavidin/Biotin blocking kit is required to block the organoid endogenous biotin. Briefly, use 4–5 drops of streptavidin solution and incubate for 20 min. Wash once with 1× TBS for 15 min at RT in the case of cells and 15 min at RT in the case of organoids. Then use 4–5 drops of biotin solution and incubate 20 min. Wash once with 1× TBS for 15 min at RT in the case of cells and 15 min at RT in the case of organoids. Notice that after using the Streptavidin/Biotin blocking kit, the solutions to dilute primary and secondary antibodies contain 1% BSA instead of donkey serum (*see* next **steps 6–10**).
6. After blocking, prepare the correspondent primary antibody combinations. At this point, the transwell membranes containing organoids are cut using a scalpel and placed into separate wells of a 24-well plate. Primary antibody combinations and

antibody dilutions are detailed below. Antibodies in combinations a., b., c., and d. are diluted in 1× TBS containing 0.5% Triton X-100 and 6% donkey serum. Antibodies and LTL in combination e. are diluted in 1× TBS containing 0.5% Triton X-100 and 1% BSA.

(a) For PPS analysis (day −1): Brachyury (1:20) + Oct4 (1:25).

(b) For IM analysis (day 0): PAX2 (1:20).

(c) For NPCs analysis (day 5): SALL1 (1:100) + SIX2 (1:500).

(d) For renal vesicles analysis (day 8): PAX2 (1:20) + WT1 (1:100).

(e) For nephron structures analysis (day 16): LTL (1:200) + Podocalyxin (PODXL) (1:100) + E-cadherin (ECAD) (1:50).

7. Remove the blocking buffer and incubate the samples with primary antibodies overnight at 4 °C. Use 250-μL volume per well of a 24-well plate.

8. The following day, wash the samples with 1× TBS containing 0.5% Triton X-100 and 6% donkey serum (instead of donkey serum, use 1% BSA for samples assayed for LTL) three times for 5 min each at RT in the case of cells and three times for 15 min each at RT in the case of organoids.

9. Prepare the correspondent secondary antibody combinations and dilutions as detailed below. Antibodies in combinations a., b., c., and d. are diluted in 1× TBS containing 0.5% Triton X-100 and 6% donkey serum. Antibodies and LTL in combination e. are diluted in 1× TBS containing 0.5% Triton X-100 and 1% BSA:

(a) For PPS analysis (day −1): anti-goat 488 (1:100), anti-mouse Cy3 (1:100).

(b) For IM analysis (day 0): anti-goat 488 (1:100).

(c) For NPCs analysis (day 5): anti-mouse 488 (1:200), anti-rabbit Cy3 (1:100).

(d) For RVs analysis (day 8): anti-goat 488 (1:100), anti-rabbit Cy3 (1:100).

(e) For nephron structures analysis (day 16): DyLight 488 Streptavidin (1:40), anti-goat 555 (1:200), anti-mouse 647 (1:100).

10. Incubate the samples with secondary antibodies diluted in 1× TBS containing 0.5% Triton X-100 and 6% donkey serum (instead of donkey serum, use 1% BSA for samples assayed for LTL) for 2 h in the case of cells and 4 h in the case of organoids

at RT in the dark. Use 250 μL volume per well of a 24-well plate.

11. Wash the samples three times with 1× TBS for 5 min each at RT in the case of cells and three times for 15 min each at RT in the case of organoids.
12. For nuclei detection, incubate the samples with DAPI at a 1:5000 ratio in 1× TBS for 30 min at RT in the case of cells and 1 h at RT in the case of organoids.
13. Remove the DAPI solution and mount the samples with coverslips using Fluoromount-G as mounting medium. For cells, deposit one or two drops of Fluoromount-G on top of a microscope slide, and then place the coverslip on top of it, with the growing cells facing the microscope slide. For transwell organoids, place first the transwell membrane with the organoid on top of the slide, add one or two drops of Fluoromount-G on top of the organoid, and then carefully place a round coverslip to cover the sample. Dry the excess of mounting medium and cover the borders with nail polish to fix the coverslips to the slides.
14. Keep the slides at 4 °C in darkness until microscopic observation. Sample fluorescence is well preserved for about 2 weeks. After this time, the intensity of the fluorescence staining could substantially decrease.
15. Acquire images on a confocal microscope.

4 Notes

1. It is essential for hPSCs not to be dissociated into single cells to prevent reduced attachment and poor survival. Therefore, it is best to first check if undifferentiated hPSCs are ready to detach by flushing a small volume of EDTA after 3 min of incubation at 37 °C. If cells do not come off, wait an extra minute before checking again and removing the EDTA. It is also important to visually check under the microscope the borders of the colonies since when hPSCs colonies are ready to be detached, the borders are shinier and refracting.
2. The plating dilution can vary among the hPSC cell line. When starting to culture hPSCs, try different passaging dilutions until finding the one that allows growth of the cells for approximately 5–6 days until reaching 80% confluency for next passage.
3. Always keep the cell suspension in the 15-mL tube in an incubator at 37 °C during the preparation of the cells for cell counting (Subheading 3.2, **steps 3**–7, and Subheading 3.4, **steps 1** and **2**).

4. The number of hPSCs collected out of a 10-cm Petri dish usually range from seven to ten million.
5. To have a 24-well plate for differentiation, a total number of 2.4 million cells are needed. Generally, cell suspensions are performed in 12 mL of Essential 8 media at a concentration of 2×10^5 cells/mL. In this manner, each 500 μL contain the needed number of cells (10^5 cells) per well of a 24-well plate. The starting plating density of 10^5 cells was optimized for ES [4], H1 and H9 hPSCs lines. Importantly, the starting cell density should be tested in case other hPSCs lines are used.
6. As mentioned, plating density and cell colony distribution are essential for an efficient differentiation (Fig. 2a). If colonies are too small after 24 h of plating, wait additional 24 h before starting the differentiation (Fig. 2b).
7. After starting the differentiation, media changes and 1× PBS washes should be performed very gently. As cells start to differentiate, they tend to become looser and can easily detach from the plate, leaving spaces without cells that can greatly detriment differentiation efficiency and formation of monolayer on day 0.
8. On day 0, cells are very loosely attached to the plate surface, so a mild enzymatic treatment is sufficient to detach them and obtain a single-cell suspension.
9. Using the ES[4] human embryonic stem cell line, the monolayer differentiation of one 24-well plate (from day −4 to day 0) should be sufficient enough to generate one 96-well plate of kidney organoids (from day 0 to day 16). Expected cell numbers on day 0 should be approximately $2.5–3 \times 10^6$ cells per well of a 24-well.
10. To transfer the spheroid onto transwells, use a 200-μL-wide orifice pipette tip to prevent damaging or fragmenting the spheroid. Carefully place the spheroid in the middle of the transwell membrane and remove with the 200 μL-micropipette, the remaining medium from the membrane to leave only the spheroid. Afterwards, add 450 μL of media through the side of the transwell into the base of the well to maintain the organoid under the air–liquid interface organotypic culture condition.
11. Once LIVE/DEAD fixable violet stain solution has been reconstituted, it should be used in the following 2 weeks.
12. For performing organoid sections, after organoid fixation (*see* Subheading 3.6, **steps 1–3**), place the organoids in a $7 \times 7 \times 5$ mm histology mold and embed the organoids in 0.8% low gelling temperature agarose. Once solidified, embed the block of agarose containing the organoids into paraffin following the classic histology procedure. Then, perform

5 μm thick sections using a microtome. Next, dewax and rehydrate organoid sections following the classic histology procedure. Then, proceed with an antigen retrieval consisting of citrate buffer (pH 6) at 95 °C for 30 min. Afterwards, continue with the blocking step and antibody incubations steps using 3% instead of 6% donkey serum in blocking, washing, and antibody solutions (*see* Subheading 3.6, **steps 4–9**). Use 1 mL of blocking buffer to incubate each slide. After blocking, use Dako pen to surround the tissue section on the slide to create a smaller area for antibody incubation. Create an area with one tissue section for negative control (only secondary antibody incubation). The Dako pen ink is water repelling and prevents diffusion of the antibody dilutions during incubations. Use 300 μL for primary and secondary antibody dilutions and incubation per slide, following the combinations described in the protocol (Subheading 3.6, **steps 6–12**). After DAPI incubation, add three or four drops of Fluoromount-G on top of the slide and carefully cover it with a coverslip. Dry the excess of mounting medium and seal the borders with nail polish.

Acknowledgments

I.L.S. has received financial support through the "la Caixa" INPhINIT Fellowship Grant for Doctoral studies at Spanish Research Centres of Excellence, "la Caixa" Banking Foundation, Barcelona, Spain. The fellowship code is LCF/BQ/IN17/11620003. E.G. and N.M. were funded by the EFSD/Boehringer Ingelheim European Research Programme in Microvascular Complications of Diabetes. This research has been supported by EIT Health under grant ID 20366 (R2U-Tox-Assay) to E.G. and N.M.
This work has received funding from the European Research Council (ERC) under the European Union's Horizon 2020 research and innovation program (StG-2014-640525_REGMAM KID to E.G. and N.M.), the Spanish Ministry of Economy and Competitiveness/FEDER (SAF2015-72617-EXP to N.M., SAF2017-89782-R to M.G. and N.M., and RYC-2014-16242 to N.M.), the Generalitat de Catalunya and CERCA program (2017 SGR 1306 to N.M.), la Asociación Española contra el Cáncer (LABAE16006 to N.M.). N.M. is also supported Instituto de Salud Carlos III (Cardiocel and ACE2ORG)). IBEC is the recipient of a Severo Ochoa Award of Excellence from MINECO.

References

1. Garreta E, Prado P, Tarantino C et al (2019) Fine tuning the extracellular environment accelerates the derivation of kidney organoids from human pluripotent stem cells. Nat Mater 18:397–405. https://doi.org/10.1038/s41563-019-0287-6
2. Little MH, McMahon AP (2012) Mammalian kidney development: principles, progress, and projections. Cold Spring Harb Perspect Biol 4:3. https://doi.org/10.1101/cshperspect.a008300
3. Garreta E, González F, Montserrat N (2018) Studying kidney disease using tissue and genome engineering in human pluripotent stem cells. Nephron 138:48–59
4. Morizane R, Bonventre JV (2017) Kidney organoids: a translational journey. Trends Mol Med 23:246–263
5. Xia Y, Izpisua Belmonte JC (2019) Design approaches for generating organ constructs. Cell Stem Cell 24:877–894
6. Taguchi A, Kaku Y, Ohmori T et al (2014) Redefining the in vivo origin of metanephric nephron progenitors enables generation of complex kidney structures from pluripotent stem cells. Cell Stem Cell 14:53–67. https://doi.org/10.1016/j.stem.2013.11.010
7. Takasato M, Er PX, Chiu HS, Maier B, Baillie GJ, Ferguson CPR, Wolvetang EJ, Roost MS, Chuva de Sousa Lopes SM, Little MH (2015) Kidney organoids from human iPS cells contain multiple lineages and model human nephrogenesis. Nature 526:564–568
8. Morizane R, Lam AQ, Freedman BS, Kishi S, Valerius MTBJ (2015) Nephron organoids derived from human pluripotent stem cells model kidney development and injury. Nat Biotechnol 33:1193–1200
9. Freedman BS, Brooks CR, Lam AQ, Fu H, Morizane R, Agrawal V, Saad AFLM, Hughes MR, Werff RV, Peters DT, Lu J, Baccei A, Siedlecki AMVM, Musunuru K, McNagny KM, Steinman TI, Zhou J, Lerou PHBJ (2015) Modelling kidney disease with CRISPR-mutant kidney organoids derived from human pluripotent epiblast spheroids. Nat Commun 6:8715
10. Lam AQ, Freedman BS, Morizane R et al (2014) Rapid and efficient differentiation of human pluripotent stem cells into intermediate mesoderm that forms tubules expressing kidney proximal tubular markers. J Am Soc Nephrol 25(6):1211–1225. https://doi.org/10.1681/ASN.2013080831
11. Toyohara T, Mae S-I, Sueta S-I et al (2015) Cell therapy using human induced pluripotent stem cell-derived renal progenitors ameliorates acute kidney injury in mice. Stem Cells Transl Med 4:980–992. https://doi.org/10.5966/sctm.2014-0219
12. Garreta E, Oria R, Tarantino C et al (2017) Tissue engineering by decellularization and 3D bioprinting. Mater Today 20(4):166–178. https://doi.org/10.1016/j.mattod.2016.12.005
13. Kratochvil MJ, Seymour AJ, Li TL, Paşca SP, Kuo CJ, Heilshorn SC (2019) Engineered materials for organoid systems. Nat Rev Mater 4:606–622
14. Brassard JA, Lutolf MP (2019) Engineering stem cell self-organization to build better organoids. Cell Stem Cell 24:860–876. https://doi.org/10.1016/j.stem.2019.05.005

Chapter 13

Methods for Controlled Induction of Singular Rosette Cytoarchitecture Within Human Pluripotent Stem Cell-Derived Neural Multicellular Assemblies

Alireza Aghayee and Randolph Ashton

Abstract

Neurally differentiating human pluripotent stem cells (hPSCs) possess the ability to self-organize into structures reminiscent of the developing fetal brain. In 2- and 3D cultures, this phenomenon initiates with formation of polarized areas of neural stem cells (NSCs), known as rosettes that resemble cross-sectional slices of the embryonic neural tube, i.e., the central nervous system (CNS) anlage. Thus, neural rosettes serve as an excellent starting point for bioengineering tissue models of all CNS tissues. Here, we provide detailed methods for bioengineering controlled induction of hPSC-derived neural assemblies with a biomimetic, singular neural rosette cytoarchitecture.

Key words Morphogenesis, Bioengineering, Neural stem cells (NSCs), Neural rosettes, Embryonic neural tube

1 Introduction

Aggregates of human pluripotent stem cell (hPSC)-derived neural stem cells (NSCs) exhibit emergent properties via cell-intrinsic self-assembly that yields biomimetic tissue structures in 2- and 3D culture. In 3D, these "neural organoids" initiate from structures known as neural rosettes that are comprised of NSCs and recapitulate the apico-basal polarity of the neural tube. Then, the rosettes execute additional stages of central nervous system (CNS) developmental morphogenesis to generate tissues with gene expression programs, cell phenotype diversity, and microscale cytoarchitectures mimetic of developing brain and spinal tissues [1–6]. As such, neural organoids have been used to model aspects of human CNS development, physiology, evolution, and neuropathology in manners previously infeasible for model organisms [7–12]. However, the spontaneous self-assembly that drives neural organoid

Mo R. Ebrahimkhani and Joshua Hislop (eds.), *Programmed Morphogenesis: Methods and Protocols*, Methods in Molecular Biology, vol. 2258, https://doi.org/10.1007/978-1-0716-1174-6_13,

morphogenesis also limits the platform's utility to serve as a scalable and reproducible basis for bioengineering tissues that replicate CNS anatomy [13, 14]. Careful attention to details in organoid derivation protocols can ensure reproducibility of their cellular composition [15, 16]. Still, the spontaneous formation of numerous neural rosettes of variable shape and size and at indeterminate locations within the initial NSC aggregates yields an unpredictable and non-mimetic organoid cytoarchitecture at the macroscale. This potentially hinders organoid maturation and renders reproducibility of the organoid's anatomy infeasible.

Here we describe methodology to bioengineer hPSC-derived NSC tissues with controlled induction of a biomimetic singular rosette cytoarchitecture. As described in Knight et al., control of the NSC aggregates morphology is provided using micropatterned culture substrates and enables induction of a singular rosette cytoarchitecture [13]. The resulting rosette tissues model the cytoarchitecture of a transverse slice of the embryonic neural tube. Since the neural tube forms along the entire rostrocaudal (R/C) axis of the developing embryo, methods to generate forebrain [17] and hindbrain through spinal cord [18] NSC tissues are also described. Reproducible derivation of NSC tissues with a singular rosettes cytoarchitecture represents a promising first step in bioengineering neural organoids with biomimetic CNS anatomy. Integration of these methods with biomaterial [19, 20], microfluidic [21, 22], and genetic engineering [23] platforms that enable additional spatiotemporal control of neural organoid morphogenesis will advance the field toward the next-generation neural organoids that reproducibly replicate CNS anatomy, circuitry, and thereby physiology.

2 Materials

2.1 Micropatterned Culture Substrate Fabrication

1. Type 1, 18 × 18 mm glass microscope coverslips.
2. Absolute ethanol and highly pure toluene and acetone.
3. Highly pure gold and titanium.
4. Poly(dimethyl siloxane) (PDMS; Slygard 184 Kit).
5. Silicon wafers were designed using AutoCAD and were purchased from FlowJEM.
6. ω-Mercaptoundecyl bromoisobutyrate (Sigma-Aldrich) in absolute ethanol solution (2 mM).
7. Stock solution of Atom Transfer Radical Polymerization (ATRP) reaction mixture: Dissolve (16.7 mmol, 8 g) of oligo (ethylene glycol) methyl ether methacrylate (OEGMEMA, Mn = 475) in water (7.5 mL) and methanol (7.5 mL) and

add copper(II) bromide (0.08 mmol, 17.9 mg), and 2′,2-bipyridine (0.24 mmol, 37.5 mg).

8. L-sodium ascorbate stock solution in ultrapure water (400 mM).

2.2 Cell Culture

1. WA09 human embryonic stem cells (hESCs) or other hPSC line.
2. Gibco™ Essential 8™ Medium (ThermoFisher).
3. Gibco™ Essential 6™ Medium (ThermoFisher).
4. DMEM/F-12 Medium (ThermoFisher).
5. Tissue-culture polystyrene (TCPS) plates.
6. Sodium bicarbonate (Sigma).
7. Ascorbic acid (L-ascorbic acid-2-phosphate magnesium; Sigma).
8. Sodium selenite (Sigma-Aldrich).
9. Recombinant human albumin solution (Sigma-Aldrich).
10. Versene (ThermoFisher).
11. bFGF (WiCell).
12. TGFβ (Peprotech or R&D Systems).
13. Growth factor-reduced Matrigel (BD Biosciences, variable concentration).
14. Phosphate buffered saline (PBS; ThermoFisher).
15. Dimethyl sulfoxide (DMSO; Sigma-Aldrich).
16. 6-Well TCPS plates (ThermoFisher).
17. ROCK inhibitor Y-27632 (R&D Systems).
18. Accutase (Invitrogen).
19. CHIR99021 (Tocris).
20. FGF8b (Peprotech).
21. Retinoic acid (RA; Sigma-Aldrich).

2.3 Immunostaining

1. 4% Paraformaldehyde (in PBS).
2. PBS, pH 7.4.
3. Tris-Buffered Saline (TBS), pH 7.5.
4. Donkey serum (Sigma-Aldrich).
5. Triton X-100 (Sigma-Aldrich).
6. TBS-DT: TBS, 5% donkey serum, 0.3% Triton X-100.
7. TBST: TBS, 0.3% Triton X-100.
8. Primary antibodies: Rabbit Anti-Pax6 (Biolegend), Mouse Anti-N-cadherin (BD Biosciences).

9. Secondary Alexa Fluor™ antibodies (ThermoFisher).
10. 4′,6-Diamidino-2-phenylindole (DAPI) (Abcam).
11. Anti-Fade Reagent (Molecular Probes).
12. Microscope coverslides 24 × 24 mm.
13. Clear nail polish.

3 Methods

3.1 Generating Micropatterned Substrates

1. Clean Type 1, 18 × 18 mm glass microscope coverslips by sequential immersion in toluene and methanol followed by sonication for 1 min in acetone. Dry completely using a nitrogen gas stream (*see* **Note 1**).
2. Deposit 35 Å of titanium followed by 180 Å of gold onto the coverslips using a CHA-600 Metal Evaporator (Telemark) (*see* **Note 2**).
3. Rinse gold-coated coverslips with absolute ethanol prior to use (*see* **Note 3**).
4. To create micropatterned silicon masters for generating PDMS stamps, use Autocad software to design the photomask's feature patterns. The micropattern design should be an $n \times n$ array of circles with 250 μm diameters and 375 μm center-to-center spacing for forebrain tissues and 150 μm diameter and 225 μm center-to-center spacing for hindbrain and spinal tissues. Final photomask designs are sent to FlowJEM for silicon wafer manufacture (*see* **Note 4**).
5. To make elastomeric stamps for soft lithography, prepare the poly(dimethyl siloxane) (PDMS; Slygard 184 Kit) mixture according to manufacturer instructions, i.e., a 10:1 mixture of PDMS and curing agent. Pour the mixture on top of the micropatterned silicon wafer and cure overnight at 60 °C.
6. Carefully peel the cured PDMS elastomer from the silicon wafer surface, and use a straight edge razor to trim excess cured elastomer from the PDMS stamp.
7. For microcontact printing, ink the PDMS stamp's micro-well features by spreading 40 μL of ω-mercaptoundecyl bromoisobutyrate solution over the surface using a micropipette tip. Dry completely under a gentle nitrogen gas stream (*see* **Note 5**).
8. Create conformal contact between the inked PDMS stamp and a gold-coated coverslip. Remove the PDMS stamp without any horizontal translation motions (*see* **Note 6**).
9. Wash the micropatterned coverslips with absolute ethanol and dry under nitrogen.

10. Transfer a single coverslip to a sealed 50 mL Schlenk flask and apply vacuum to remove excess oxygen (*see* **Note 7**).
11. Add 5 mL of ATRP stock solution via a syringe to the Schlenk flask.
12. Add 0.5 mL of L-sodium ascorbate stock solution via a syringe to the Schlenk flask to initiate the reaction (*see* **Note 8**).
13. Allow the reaction to continue for 16 h at room temperature under a steady stream of nitrogen gas (*see* **Note 9**).
14. Remove the micropatterned coverslip from the Schenk flask, and rinse with ethanol, water, and ethanol. Dry under a gentle nitrogen stream (*see* **Note 10**).

3.2 Human PSCs Culture

3.2.1 Matrigel Coating of TCPS Plates

1. Add 12 mL of DMEM/F12 media to a 15-mL conical.
2. From the conical, add 1 mL of media to each well of a 6-well plate.
3. Take a Matrigel aliquot out of the −80 °C freezer and let it thaw at room temperature in biosafety cabinet until the pellet is slightly melted (*see* **Note 11**).
4. Remove 1 mL of DMEM/F12 from the 15 mL conical and use it to dissolve the Matrigel pellet (*see* **Note 12**).
5. Resuspend the Matrigel suspension in the remaining DMEM/F12 media in the 15 mL conical by pipetting up and down several times.
6. Add 1 mL of the dissolved Matrigel solution to each well of the 6-well plate, and allow Matrigel coating to form overnight in a 37 °C cell culture incubator or 4 °C refrigerator.
7. Matrigel plates are good for 1 week at 37 °C or stored at 4 °C for up to 2 weeks (*see* **Note 13**).

3.2.2 hPSC Culture

1. Remove a vial of hPSCs from liquid nitrogen storage.
2. Let the vial sit for 60 s at room temperature, then use your hands to warm it up for another 15 s.
3. Swirl the vial gently in the water bath until it is approximately 75% thawed (*see* **Note 14**).
4. Spray copiously with ethanol and transfer the vial to a biosafety cabinet. Use a 2-mL glass pipette to gently transfer the contents of the vial to a 15-mL conical, then add 4 mL of E8 medium DROPWISE to the cell suspension.
5. Spin down for 5 min at 1000 rpm (150 × *g*).
6. Aspirate the supernatant and resuspend the pellet in 12 mL of E8 medium containing 10 μM Y27632, a.k.a. Rock inhibitor (*see* **Note 15**).

7. Add 2 mL of cell suspension into each well of a 6-well TCPS plate, place the plate in incubator, and shake side to side and then back and forth to distribute the cells evenly.
8. Change 100% of E8 medium daily thereafter. Cells should be ready to passage after approximately 4–5 days of culture depending on the density at which they were seeded. Cells are ready to passage when the plate is ~80% confluent or when colonies have become so large that debris begins to accumulate in the middle of the colonies.

3.3 Derivation of Hindbrain and Spinal Neuromesodermal (NMP) Progenitors

1. Rinse cells with PBS and dissociate hPSCs with 1 mL of Accutase per well for 5 min at 37 °C.
2. Seed cells onto matrigel-coated, 6-well TCPS plates at 150,000 cells/cm^2 in E8 media with 10 mM ROCK inhibitor. This is denoted as Day −1 (Fig. 1).
3. On Day 0, change media to E6 medium.
4. On Day 1, change media to E6 medium with 200 ng/mL FGF8b.
5. On Day 2, dissociate the cells with 1 mL of Accutase per well for 1:45 min and seed onto TCPS plates at a 1:1.5 well ratio in E6 media with 200 ng/mL FGF8b, 3 mM CHIR, and 10 mM ROCK inhibitor (*see* **Note 16**). The addition of the Wnt agonist, i.e., CHIR99021 (CHIR), induces acquisition of a Sox2$^+$/Brachyury$^+$ neuromesodermal phenotype that becomes more caudal over time under these conditions. The level of caudalization is indicated by *HOX* gene expression as detailed in Lippman et al. [18]. The duration of culture maintenance under these media conditions will determine the degree of NMP caudalization.
6. On Day 4, the media is switched to E6 + FGF8b + CHIR for an additional day of culture to generate cervical spinal NMPs.

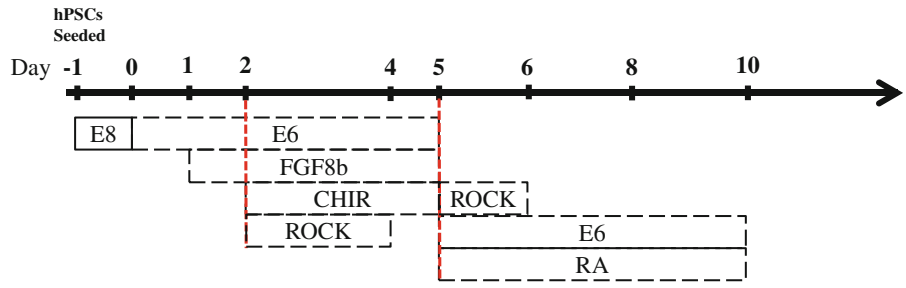

Fig. 1 Schematic for derivation of hindbrain and spinal neuroepithelial tissues. Subculture/seeding onto a new well plate (i.e., Day 2) or micropatterned coverslips (i.e., Day 5) is indicated by dotted red lines

3.4 Generation of Micropatterned Forebrain NSC Tissues

1. Rinse micropatterned coverslips five times with sterile PBS in a biosafety cabinet.
2. Transfer each coverslip using tweezers to an individual well of a new 6-well TCPS plate.
3. Coat micropatterned coverslips with 1 mg/mL Matrigel in DMEM/F-12 media by incubation at 37 °C overnight.
4. Rinse hPSCs at 80% confluency with PBS.
5. Dissociate cells with Accutase for 5 min at 37 °C.
6. Collect singularized cells in Accutase using a pipette and transfer into a conical tube with 6 mL of E8 media.
7. Centrifuge the conical tube at 1000 rpm for 5 min.
8. Resuspend the hPSCs in E8 media with 10 mM ROCK inhibitor.
9. Seed hPSCs onto micropatterned coverslips at 100,000 cells/cm^2 using 4 mL of media per well. This is denoted as Day −1 (Fig. 2a, *see* **Note 17**).
10. On Day 0, add 4 mL E6 to each well of a new 6-well TCPS plate.
11. Transfer each micropatterned, hPSC-seeded coverslip into a new well containing E6 media (*see* **Note 18**).

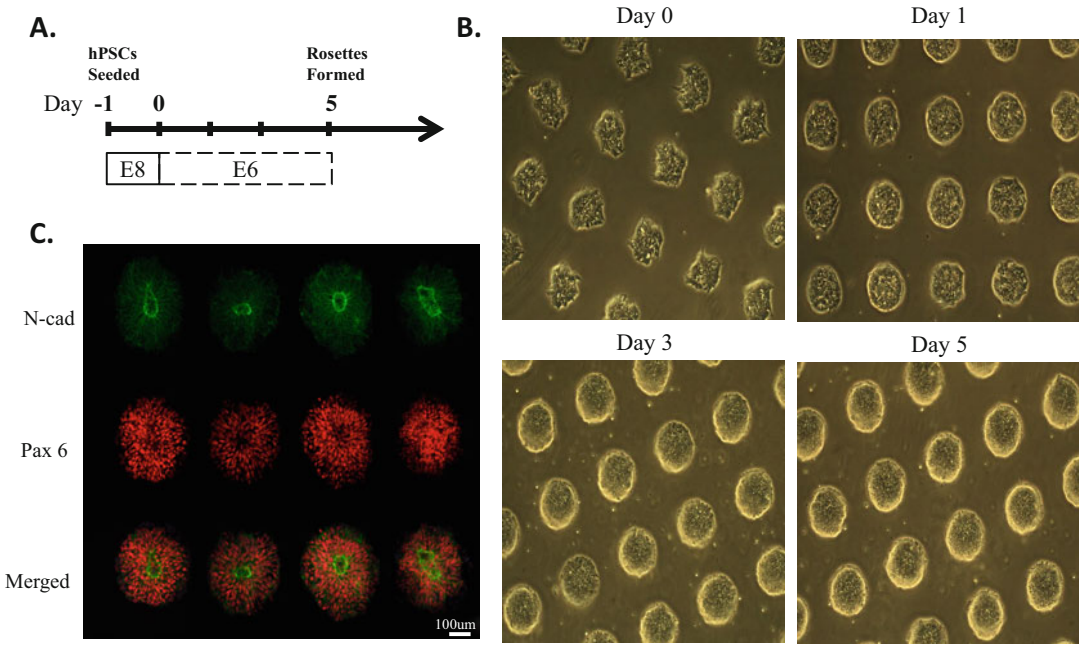

Fig. 2 Neural Rosette microarray derivation. (**a**) Experimental timeline for generating micropatterned forebrain NSC tissues. (**b**) Bright field images of forebrain NSC tissues on micropatterned coverslips with 250 μm circular adhesive areas and 375 μm center-to-center spacing over 5 days of culture. (**c**) Representative confocal images of immunostained single rosettes on micropatterned coverslip

12. On Day 1, aspirate 2 mL of E6 media from each well and add 2 mL of fresh E6 media (50% media change).
13. Performed 50% media changes daily until Day 5.

3.5 Generation of Micropatterned Hindbrain and Spinal NCS Tissues

1. Rinse micropatterned coverslips five times with sterile PBS in a biosafety cabinet.
2. Transfer each coverslip using tweezers to an individual well of a new 6-well TCPS plate.
3. Coat micropatterned coverslips with 1 mg/mL Matrigel in DMEM/F-12 media by incubation at 37 °C overnight.
4. Dissociate NMP cultures with 1 mL of Accutase per well for 5 min to singularize the cells. Seed the cell suspension onto each micropatterned substrate at 150,000 cells/cm^2 in 4 mL of E6 media with 1 mM retinoic acid and 10 mM ROCK inhibitor to initiate transition to a $Pax6^+$ NSC phenotype. This is denoted as Day 5 (Fig. 1).
5. On Day 6, change the media to E6 media with 1 mM retinoic acid. Perform 50% media changes every 24 h for the next 4 days.

3.6 Immunostaining

1. Wash micropatterned NSC tissue arrays with PBS to remove cell debris prior to fixation. Use 50% PBS washes to avoid lifting tissues from surface.
2. Fix the cells in 4% paraformaldehyde for 10 min at room temperature.
3. Wash the cells 2–3 times in PBS to remove excess PFA. After carefully removing PFA completely, perform 50% media changes to avoid lifting cells from surface of plate/slide for all wash steps (*see* **Note 19**).
4. Block and permeabilize the cells in TBS-DT for at least 1 h at RT. Store at 4 °C for longer incubation periods.
5. Incubate tissues with appropriate primary antibody diluted in fresh TBS-DT. This step may be performed overnight at 4 °C. Alternatively, for "speed staining" incubate for 3 h at RT.
6. Wash 2–3 times in TBST for 10 min each on a rocker.
7. Incubate cells with appropriate Alexa Fluor secondary antibody at a 1:500 dilution in the dark for at least 2 h at RT. Store at 4 °C for longer incubation periods (*see* **Note 20**).
8. Wash two times with TBS for 15 min each on rocker.
9. To stain nuclei with DAPI, add diluted DAPI solution (1:2000 DAPI stock solution into TBS; stored in foil at 4 °C) to each well and incubate for 10 min at RT.
10. Wash one time with TBS for 15 min each on rocker. Add fresh TBS to well-plates and store at 4 °C until mounting.

11. Place a 50-μL droplet of Anti-Fade Reagent (PVA-DAPCO) on a microscope coverslide and mount the micropatterned coverslip. Leave in the dark at room temperature overnight to dry. Seal edges of coverslip to microscope coverslide with clear nail polish before storage/imaging (Fig. 2c).

4 Notes

1. Toluene and acetone should only be handled in a chemical fume hood.
2. Gold-coated substrates are also available via commercial suppliers. Optically transparent substrates will facilitate microscopic analysis.
3. Store gold-coated slides protected from light and under vacuum in a desiccator.
4. In designing stamps, feature depths lower than 100 μm can cause abnormal deformation of stamps prior to contact with substrate surfaces. Designate features as "posts" when emailing template to FlowJem.
5. Incomplete drying can result in partial loss of pattern fidelity.
6. Gentle conformal contact will be enough for pattering coverslips. Too much pressure on the PDMS stamp can result in patterning defects. The slide can stick to the PDMS stamp upon conformal contact. Therefore, to remove the slide, invert to stamp/slide combo, use your index finger and thumb to pull down on opposite corners of the stamp, and use tweezers to remove the slide by lifting straight upward.
7. Use a rubber stopper to seal each Schlenk flask.
8. Reaction color will change from light green to dark brown following addition of L-sodium ascorbate.
9. The length of the PEG brushes increases over time and a 16-h reaction time should provide an optimal brush thickness.
10. Patterns should be visible to the eye and can be imaged and analyzed under a microscope following surface initiated (SI)-ATRP.
11. Matrigel stock concentration is listed on the package, and should be used to calculate the appropriate volume to create 1 mg aliquots.

    Example: if the concentration of Matrigel is listed at 9.7 mg/mL, the volume in each tube will be (1 mg)/(9.7 mg/mL) = 0.103 mL = 103 μL.

12. Forceful pipetting will cause liquid to shoot out of the microfuge tube when trying to dissolve the Matrigel pellet. Use gentle pipetting.
13. To use a Matrigel-coated plate, it must be warmed in the incubator for a MINIMUM of 4 h.
14. When thawing cells, do not let any water touch the vial cap.
15. When resuspending the cell pellet in E8 media, it is okay if you cannot see the pellet in the centrifuged conical. The cells are still present.
16. Cells should be subcultured as clumps avoiding singularization. Use wide-bore or cut pipette tips for handling cells.
17. Add cell suspension directly on top of the micropatterned coverslips to make sure they remain on the well bottom and are fully covered with media.
18. This coverslip transfer step helps to remove nonadherent cells from the micropatterned surface to enhance patterning fidelity [20]. Keep the slide level when transferring to ensure that the slide does not dewet, which will cause removal of neural tissues.
19. Use care when handling PFA as it is neurotoxic. Bleach PFA and dilute with plenty of water prior to disposing.
20. Cover plates in aluminum foil during all immunostaining steps where the secondary antibody is present.

References

1. Lancaster MA, Renner M, Martin C-A, Wenzel D, Bicknell LS, Hurles ME et al (2013) Cerebral organoids model human brain development and microcephaly. Nature 501:373–379
2. Xiang Y, Tanaka Y, Cakir B, Patterson B, Kim K-Y, Sun P et al (2019) hESC-derived thalamic organoids form reciprocal projections when fused with cortical organoids. Cell Stem Cell 24:487–497.e7
3. Camp JG, Badsha F, Florio M, Kanton S, Gerber T, Wilsch-Bräuninger M et al (2015) Human cerebral organoids recapitulate gene expression programs of fetal neocortex development. Proc Natl Acad Sci U S A 112:15672–15677
4. Renner M, Lancaster MA, Bian S, Choi H, Ku T, Peer A et al (2017) Self-organized developmental patterning and differentiation in cerebral organoids. EMBO J 36:1316–1329
5. Jo J, Xiao Y, Sun AX, Cukuroglu E, Tran H-D, Göke J et al (2016) Midbrain-like organoids from human pluripotent stem cells contain functional dopaminergic and neuromelanin-producing neurons. Cell Stem Cell 19:248–257
6. Duval N, Vaslin C, Barata T, Frarma Y, Contremoulins V, Baudin X et al (2019) BMP4 patterns Smad activity and generates stereotyped cell fate organisation in spinal organoids. Development 146:dev175430
7. Lemke KA, Aghayee A, Ashton RS (2017) Deriving, regenerating, and engineering CNS tissues using human pluripotent stem cells. Curr Opin Biotechnol 47:36–42
8. Qian X, Nguyen HN, Song MM, Hadiono C, Ogden SC, Hammack C et al (2016) Brain-region-specific organoids using mini-bioreactors for modeling ZIKV exposure. Cell 165:1238–1254
9. Pollen AA, Bhaduri A, Andrews MG, Nowakowski TJ, Meyerson OS, Mostajo-Radji MA et al (2019) Establishing cerebral organoids as models of human-specific brain evolution. Cell 176:743–756.e17
10. Trujillo CA, Gao R, Negraes PD, Chaim IA, Domissy A, Vandenberghe M et al (2019) Nested oscillatory dynamics in cortical

organoids model early human brain network development. Cell Stem Cell 25:558–569

11. Wells MF, Salick MR, Wiskow O, Ho DJ, Worringer KA, Ihry RJ et al (2016) Genetic ablation of AXL does not protect human neural progenitor cells and cerebral organoids from zika virus infection. Cell Stem Cell 19:703–708
12. Bagley JA, Reumann D, Bian S, Lévi-Strauss J, Knoblich JA (2017) Fused cerebral organoids model interactions between brain regions. Nat Methods 14:743–751
13. Knight GT, Lundin BF, Iyer N, Ashton LM, Sethares WA, Willett RM et al (2018) Engineering induction of singular neural rosette emergence within hPSC-derived tissues. elife 7:e37549
14. Marti-Figueroa CR, Ashton RS (2017) The case for applying tissue engineering methodologies to instruct human organoid morphogenesis. Acta Biomater 54:35–44
15. Velasco S, Kedaigle AJ, Simmons SK, Nash A, Rocha M, Quadrato G et al (2019) Individual brain organoids reproducibly form cell diversity of the human cerebral cortex. Nature 570:523–527
16. Yoon S-J, Elahi LS, Paşca AM, Marton RM, Gordon A, Revah O et al (2019) Reliability of human cortical organoid generation. Nat Methods 16:75–78
17. Lippmann ES, Estevez-Silva MC, Ashton RS (2014) Defined human pluripotent stem cell culture enables highly efficient neuroepithelium derivation without small molecule inhibitors. Stem Cells 32:1032–1042
18. Lippmann ES, Williams CE, Ruhl DA, Estevez-Silva MC, Chapman ER, Coon JJ et al (2015) Deterministic HOX patterning in human pluripotent stem cell-derived neuroectoderm. Stem Cell Rep 4:632–644
19. McNulty JD, Marti-Figueroa C, Seipel F, Plantz JZ, Ellingham T, Duddleston LJL et al (2019) Micro-injection molded, poly(vinyl alcohol)-calcium salt templates for precise customization of 3D hydrogel internal architecture. Acta Biomater 95:258–268
20. Knight GT, Sha J, Ashton RS (2015) Micropatterned, clickable culture substrates enable in situ spatiotemporal control of human PSC-derived neural tissue morphology. Chem Commun (Camb) 51:5238–5241
21. Manfrin A, Tabata Y, Paquet ER, Vuaridel AR, Rivest FR, Naef F et al (2019) Engineered signaling centers for the spatially controlled patterning of human pluripotent stem cells. Nat Methods 16(7):640–648
22. Uzel SGM, Amadi OC, Pearl TM, Lee RT, So PTC, Kamm RD (2016) Simultaneous or sequential orthogonal gradient formation in a 3D cell culture microfluidic platform. Small 12:612–622
23. Cederquist GY, Asciolla JJ, Tchieu J, Walsh RM, Cornacchia D, Resh MD et al (2019) Specification of positional identity in forebrain organoids. Nat Biotechnol 37:436–444

Chapter 14

3D Self-Organized Human Blood–Brain Barrier in a Microfluidic Chip

Marco Campisi, Sei Hien Lim, Valeria Chiono, and Roger Dale Kamm

Abstract

A preclinical blood–brain barrier (BBB) model is important for the study of fundamental transport mechanisms and in accessing the delivery of small molecules and antibodies that target brain. Transwell assays for BBB models are easy to create and use but lack the true 3D anatomy of the brain microvasculature and also often the cell–cell and cell–matrix interactions that are important in ensuring a tight BBB. Here we describe the formation of a BBB that expresses neurovascular membrane transporters, tight junction, and extracellular matrix proteins using the coculture of human-induced pluripotent stem cell-derived endothelial cells (iPSC-EC), brain pericytes (PC), and astrocytes (AC) in a microfluidic device. The BBB model recapitulates human brain vascular permeability with values that are lower than conventional in vitro models and are comparable to in vivo measurements in rat brain. This in vitro BBB model can therefore be used to screen for brain-targeting drugs or to study neurovascular functions.

Key words Human blood–brain barrier, BBB preclinical model, In vitro drug testing, BBB-on-a-chip, Microphysiological systems

1 Introduction

The human blood–brain barrier (BBB) is a highly selective barrier between brain tissue and the microcirculation [1]. It has a fundamental role to maintain brain homeostasis and protect the brain from harmful agents [2]. However, the same mechanisms also regulate drug delivery to the brain, thus restricting the variety of therapeutic candidates available for neurological disorders [3, 4]. Although animal and 2D BBB models have been widely adopted to assess the permeability of drugs, they fail to faithfully recapitulate the genetic and anatomical characteristics of the human brain barriers [5].

Marco Campisi and Sei Hien Lim authors contributed equally to this work.

Mo R. Ebrahimkhani and Joshua Hislop (eds.), *Programmed Morphogenesis: Methods and Protocols*, Methods in Molecular Biology, vol. 2258, https://doi.org/10.1007/978-1-0716-1174-6_14,

Microfluidic technologies have provided invaluable tools for modeling microphysiological living systems that recapitulate human structures and biological interactions that cannot be replicated in more conventional in vitro models [6, 7]. Recently, microfluidic technology has led to the development of complex BBB-on-chip models that could potentially be used as preclinical drug screening tools [8, 9].

Here we describe the methods to develop a self-organized 3D human BBB microvasculature model on a microfluidic chip that can recapitulate the microvascular structures and the transport processes in the brain [10]. The BBB model uses human-induced pluripotent stem cell-derived endothelial cells, brain pericytes, and brain astrocytes to form a self-assembled microvasculature within a 3D fibrin gel. The 3D culture is made possible by using a microfluidic chip that consists of three fluid channels whereby the center gel channel can accommodate the cell-containing 3D hydrogel while the two flanking media channels provide nutrients as well as access to the microvessels for vascular perfusion.

After the initial cell seeding, a microvascular network forms within 1–2 days, and is perfusable in 4–5 days. Over time, cells remodel their 3D microenvironment by degrading the initial hydrogel and replacing it with extracellular matrix (ECM) molecules that they secrete. As cells are brought together in close proximity within the fibrin gel, they will interact through not only paracrine but also juxtacrine signaling where the brain pericytes and astrocytes can adhere to and envelope the microvessels partially, mimicking the BBB in vivo [11, 12]. These emergent collective behaviors are natural biological interactions that are facilitated by interactions among the different cell types in this 3D BBB microfluidic model. The formation of microvasculature in this model recapitulates some aspects of the vascular morphogenesis process of brain development in embryogenesis [13, 14].

This physiologically relevant BBB model exhibits perfusable microvasculature, with vascular permeability that is lower than previously reported 2D and 3D models [15, 16], and comparable to in vivo measurements in the rat brain microcirculation [17]. The human BBB model has value as a model of transendothelial exchange between the vascular and tissue compartments, and is thus useful as in pharmacokinetic/pharmacodynamic modeling, and could potentially be employed for the characterization and screening of drug candidates to improve the drug design and predict therapeutic transport across the human BBB [18, 19].

2 Materials

Prepare the solutions in a biosafety cabinet; every item should be sterilized before use.

2.1 Microfluidic Technology

1. The microfluidic system that consists of a hydrogel channel and two flanking media channels. An example of a commercial chip from AIM Biotech is shown here for illustrative purposes (Fig. 1).

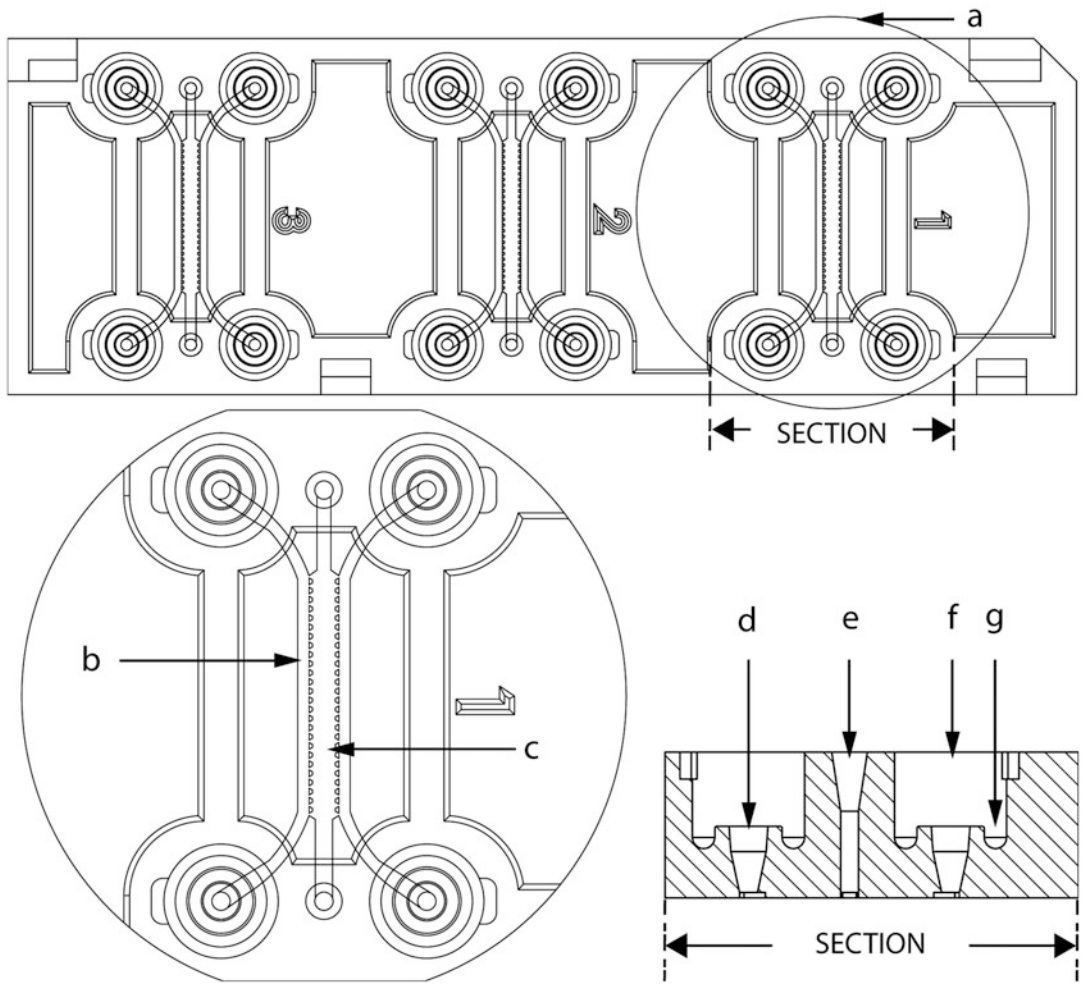

Fig. 1 Schematic diagrams of the microfluidic chip from AIM Biotech. The following are the features of the chip: (**a**) site, a chip contains three sites; (**b**) media channel, two flanking media channels to provide nutrients to the cells in the gel; (**c**) gel channel in the center; (**d**) media inlet for loading coating solution and cells; (**e**) gel inlet for loading hydrogel; (**f**) port acts as a reservoir for medium; (**g**) trough for easy aspiration of medium

2.2 Fibrin Gel

1. Fibrinogen working solution: Dissolve 12 mg of fibrinogen from bovine plasma in 2 mL of 1× PBS to yield 6 mg/mL of fibrinogen working solution. Incubate in a 37 °C water bath for >1 h until the fibrinogen powder completely dissolves. Filter the fibrinogen working solution with a 0.22-μm syringe filter. Keep the working solution on ice (*see* **Note 1**).
2. 100 units/mL thrombin stock solution in a 0.1% (w/v) BSA solution (water) (*see* **Note 2**). Sterilize thrombin stock solution by passing through a 0.22-μm bottle top filter or syringe filter. Aliquot the thrombin stock solution and store it at −20 °C.
3. Thrombin suspension medium: Add 40 μL of thrombin stock solution (100 U/mL) into 960 μL of endothelial medium to yield 4 U/mL of suspension medium. Keep the suspension medium on ice.

2.3 Cell Culture

As cell sources are critical in ensuring the success of the assay, the suppliers are listed here.

1. Human iPSC-ECs from Cellular Dynamics International.
2. Human brain pericytes and Pericyte medium from ScienCell.
3. Human brain astrocytes and Astrocyte medium from ScienCell.
4. Endothelial medium, from Cellular Dynamics International, with growth factors (5 ng/mL of rh FGF, 50 μg/mL of ascorbic acid, 1 μg/mL of hydrocortisone hemisuccinate, 4 mM of L-glutamine, 15 ng/mL of rh IGF-1, 5 ng/mL of rh EGF, 5 ng/mL of rh VEGF, 0.75 U/mL of heparin sulfate, 30 mg/mL of gentamicin and 15 μg/mL of amphotericin B), and iPSC-EC medium supplement (*see* **Note 3**).
5. Trypsin and TrypLE.

2.4 Coating Solution and Growth Factor-Enriched Culture Media

1. Human fibronectin solution: 60 μg/mL in endothelial medium.
2. VEGF stock solution: Reconstitute recombinant human $VEGF_{165}$ at 100 μg/mL in sterile PBS containing at least 0.1% BSA. Aliquot it into smaller volumes and store them at −20 °C. Dilute the aliquots to 10 μg/mL with PBS as secondary stock solutions before use.
3. Growth factor-enriched medium A: Add 5 μL of VEGF (10 μg/mL) and 10 μL of Astrocyte Growth Supplement (100×) per mL of endothelial medium, to reach 50 ng/mL VEGF and 1% v/v Astrocyte Growth Supplement final concentrations.
4. Growth factor-enriched medium B: Endothelial medium enriched with 1% v/v Astrocyte Growth Supplement.

2.5 Fluorescent Dextran Solution

1. 10 kDa FITC-dextran: Prepare 2 μg/mL of 10 kDa FITC-dextran in 1× PBS. Sterilize using 0.22 μm syringe filter.

3 Methods

3.1 Preparing and Filling Fibrin Gel with Cells

1. Trypsinize cells as per protocol. Briefly, wash the culture flasks/dishes with sterile 1× PBS twice. Use TrypLE (for iPSC-ECs) or trypsin (for astrocytes and pericytes) to dissociate cells. Add medium with FBS, at least five times the volume of TrypLE/trypsin, into the culture flasks/dishes to dilute/neutralize the TrypLE/trypsin. Transfer the cell suspensions to 15 mL tubes and pellet the cells by centrifuging at 250 × *g* for 5 min at room temperature.
2. Resuspend the cells in the suspension medium in 36 M cells/mL for iPSC-EC, 12 M cells/mL for pericytes, and 12 M cells/mL for astrocytes. This is to achieve the final seeding concentration of 6 M cells/mL, 2 M cells/mL and 2 M cells/mL for iPSC-EC, pericytes, and astrocytes, respectively (*see* **Note 4**).
3. Draw 30 μL of cell suspension from each tube, and mix them to make a 90-μL master cell suspension stock. This amount is sufficient for filling at least 12 experiments.
4. Mix 6 μL of master cell suspension with 6 μL of fibrinogen solution to make fibrin gel solution in a microcentrifuge tube (Fig. 2b). Make sure the fibrin gel solution is kept on ice at all times (*see* **Notes 5** and **6**).
5. Draw 10 μL of fibrin gel solution into a 1- to 10-μL micropipette (*see* **Note 7**).
6. Fill fibrin gel solution through either of the inlets and stop near the end of posts. Fill from the other inlet until the gel fronts merge as shown in Fig. 2c, d at room temperature (*see* **Notes 8** and **9**).
7. Prepare a humidified chamber to house the chips (e.g., by adding water into a pipette tip box until approximately one-third is filled; both water and pipette tip box should be sterile) (*see* **Note 10**).
8. Allow polymerization of hydrogel to take place for 15 min at room temperature (*see* **Notes 11** and **12**).

3.2 Hydrating and Coating Media Channels

1. After polymerization, insert a pipette tip into either inlet of the media channel and push gently until the tip fits. Inject 15 μL of fibronectin coating solution into the channel. Due to surface tension, the injected solution will form a spherical cap at the opposite inlet as shown in Fig. 3a (*see* **Notes 13** and **14**).

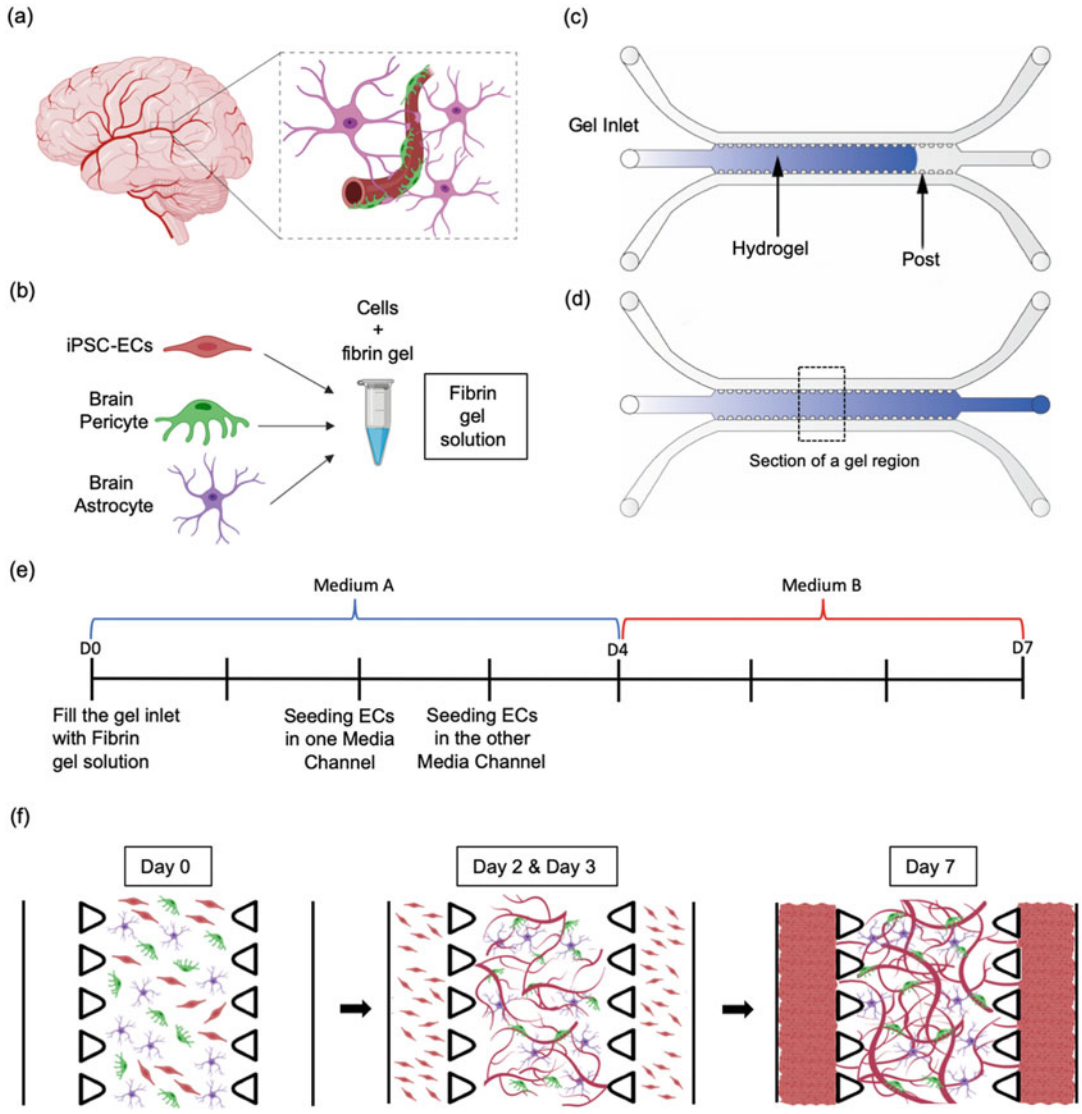

Fig. 2 Human blood–brain barrier in a microfluidic chip. (**a**) Schematic representation of the human blood–-brain barrier (BBB). (**b**) Schematic diagrams to illustrate the gel filling step. (**c**) Inject the hydrogel from one of the inlets and stop near the end of the posts and (**d**) inject the hydrogel from the other inlet until the gel fronts merge. (**e**) Timeline of medium filling. (**f**) Cell seeding configuration and experimental steps to form the human BBB model with self-organized microvasculature. Schematics (**a**, **b**, **f**) were created with BioRender

2. Incubate the media-channel-hydrated chips for 1 h in a 37 °C incubator.
3. Add 70 μL of medium A into one port and then add 50 μL into the opposite port of the same media channel to flush out the coating solution.
4. Keep the chips in an incubator and change medium daily.

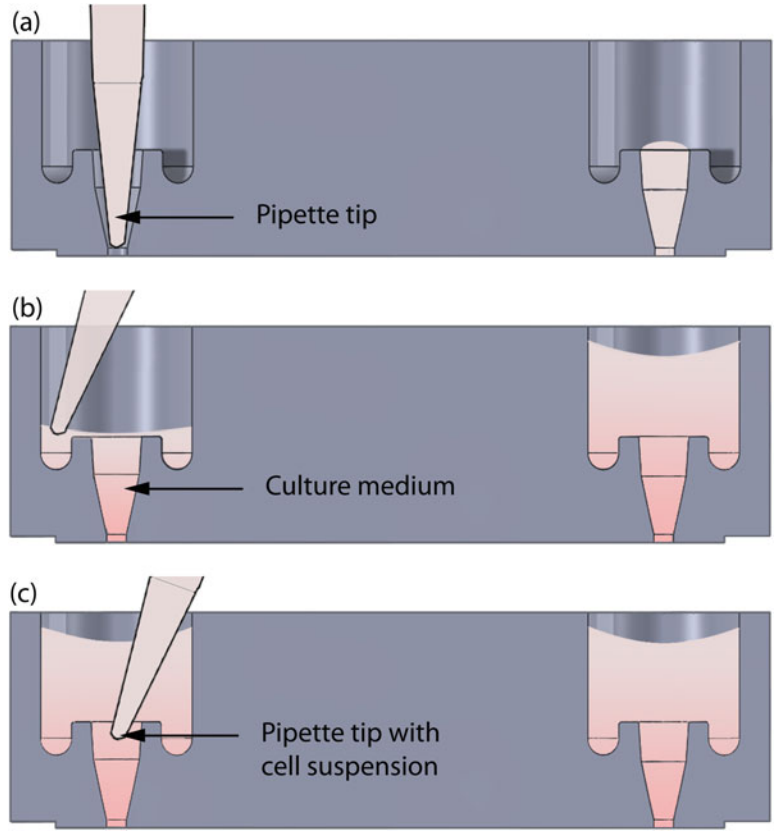

Fig. 3 Schematic diagrams that show the different positions of pipette tips during different steps. (**a**) To coat media channels with coating solution, insert a tip into an inlet until it fits then inject solution till it reaches the opposite inlet. (**b**) To change medium in the ports, the medium should be removed from the ports by pointing the pipette tip at the troughs. (**c**) To seed cells into the media channels, position the pipette tip near inlets while inject cell suspension. The pipette tips and medium are both shaded pink

3.3 Changing Medium

1. Remove medium from all four ports by carefully aspirating the medium out from the troughs as shown in Fig. 3b. To replace the medium in a media channel, add 70 μL of medium into one port and then add 50 μL into the opposite connected port (*see* **Notes 15** and **16**). Change the medium every 24 h.
2. Use medium A from day 0 to day 4 and switch to medium B from day 4 onward (Fig. 2e). Keep the chips in an incubator. Microvasculature shall start forming within 2 days and continue to mature in the chips (*see* **Note 17**) (Fig. 2f).

3.4 Seeding Endothelial Cells in Media Channels

1. Seed endothelial cells in one of the two media channels on day 2 after the daily medium change in order to obtain a better seal on the channel side of the gel (*see* **Note 18**).

2. Trypsinize endothelial cells as per protocol and resuspend the cells at 1.5 M cells/mL.
3. Add an additional 30 μL of medium A into one of the ports at the media channel that is to be seeded with cells.
4. Use a micropipette to withdraw 10 μL of endothelial cell suspension. Position the tip near the inlet of a media channel and inject the cell suspension as shown in Fig. 3c. The additional 40 μL of fluid (10 μL of cell suspension and 30 μL of medium) creates a height difference between the two media channels thus generating interstitial flow across the gel. This helps the attachment of endothelial cells on the gel interface (*see* **Notes 19** and **20**).
5. Visual inspection under a microscope is recommended. If the cell distribution is not optimal for your application, adjust the concentration of the cell suspension and repeat the seeding steps (*see* **Notes 21** and **22**).
6. Wait for 5 min and then remove medium from all the ports. Add 50 μL of medium A into each port.
7. Use a micropipette to withdraw 10 μL of endothelial cell suspension. Position the tip at the same inlet that has been injected with endothelial cell. Inject the cell suspension.
8. Flip the chips upside down and incubate for 1.5 h in a 37 °C incubator. This helps the attachment of endothelial cells on the top surface of the media channel (*see* **Note 23**).
9. Flip the chips back to their upright position after the incubation.
10. Keep the chips in an incubator. Allow the endothelial cells to grow for 24 h and repeat **steps 2–9** on day 3 for the other media channel.

3.5 Perfusing Microvasculature with Fluorescent Dextran

1. Remove medium from all four ports by carefully aspirating the medium out from the troughs.
2. Add 70 μL of dextran solution into one port and then add 70 μL of medium B into one port of the other media channel (*see* **Note 24**).
3. Add 50 μL of dextran solution and medium B into the respective empty ports as shown in Fig. 4a with a 20-s interval to allow the dextran solution to flow into the microvascular network.
4. Image the dextran-perfused microvasculature with confocal microscopy or high-content imaging system starting immediately after **step 3** with a 5-min interval for 30 min (Fig. 4b, d).

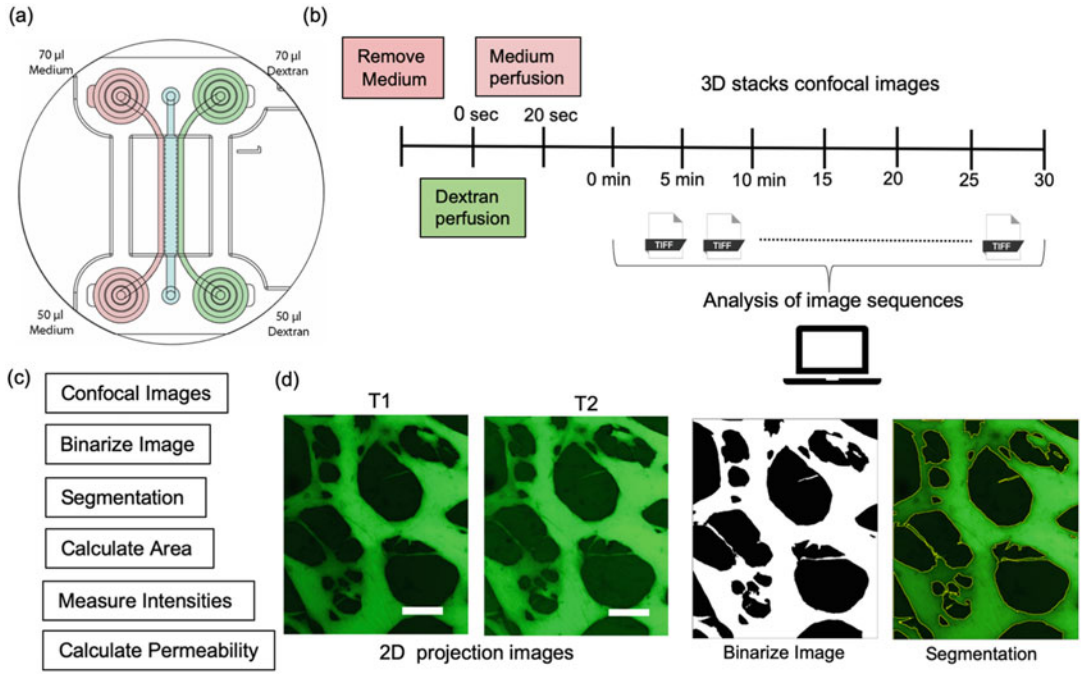

Fig. 4 A schematic diagram to illustrate the setup for perfusing microvasculature with fluorescent dextran to measure the apparent permeability. (**a**) Add 70 µL of dextran solution (green) and medium (pink) into the top ports and then add 50 µL of dextran solution and medium into the bottom ports to allow dextran to diffuse into gel (blue) without additional hydrostatic pressure. (**b**) Timeline of the permeability experiment. 3D confocal images were captured every 5 min for 30 min. (**c**) Workflow of image analysis to calculate the apparent permeability. (**d**) Maximum 2D image projections at two time points. Projections were binarized after thresholding to identify microvascular borders. Then, microvasculature was recognized by segmentation of vascular borders. Scale bar indicates 50 µm

3.6 Quantification of Microvascular Permeability

The quantification is based on confocal images of microvasculature that is perfused with fluorescent-labelled dextran. ImageJ is used in the quantification steps (Fig. 4c).

1. Project a stack of confocal images at time point 1 (t_1) into 2D images based on the maximum intensity projection method. Duplicate the projected image.
2. Preprocess the duplicated image if necessary. Depending on the image quality, you may apply preprocessing techniques such as enhance contrast. You should always preprocess your image as a whole.
3. Binarize the duplicated image (Fig. 4d).
4. Use the built-in Selection: Create Selection function in ImageJ to select the binarized microvasculature as first region of interest (ROI) and add that into the ROI manager.

5. Use the built-in Selection: Make Inverse function in Image J to select the area outside of the microvasculature as second ROI and add that into the ROI manager.
6. Select the original projected image so that it is the active window. Use the Measure function in the ROI manager to measure the fluorescent intensities of vessels (I_V), fluorescent intensities of tissue (I_T), the perimeter of the microvasculature (P), and lateral tissue area ($A_{lateral\_tissue}$) at t_1 (typically $t_1 = 0$ min).
7. Repeat **steps 1–6** to determine the fluorescent intensities at time point 2, t_2 (typically $t_2 = 30$ min).
8. Calculate the apparent permeability P_{app} by using the following equation:

$$P_{app} = \frac{1}{\left(I_V^{t1} - I_T^{t1}\right)} \frac{\left(I_T^{t2} - I_T^{t1}\right)}{\Delta t} \frac{V_{tissue}}{A_{surface}}$$

V_{tissue} is the volume of the tissue space and $A_{surface}$ is the surface area of the microvasculature. Based on the assumption that the ratio $V_{tissue}/A_{surface}$ can be approximated as $A_{lateral\_tissue}/P$, the P_{app} can be calculated as followed:

$$P_{app} = \frac{1}{\left(I_V^{t1} - I_T^{t1}\right)} \frac{\left(I_T^{t2} - I_T^{t1}\right)}{\Delta t} \frac{A_{lateral\_tissue}}{P}$$

3.7 Quantification of Microvascular Geometry

In order to quantify the microvascular geometry, we recommend using fluorescently tagged-cells (such as GFP) or labelling the cells through immunocytochemistry (such as VE-cadherin staining that is specific to endothelial cells) in situ. The quantification is based on confocal images of the microvasculature. ImageJ is used in the quantification steps.

1. Project the stacks of confocal images into 2D images based on the maximum intensity projection method.
2. Preprocess the images if necessary. Depending on the image quality, you may reduce noise through despeckle and background reduction or apply a Gaussian filter to smoothen the edges and fill up the gaps between the bright signals around the cell membrane if the endothelial cells are stained for junction proteins (e.g., VE-cadherin) (*see* **Note 25**).
3. Try all threshold methods on at least three individual projected images. Choose the method that segments your data best and produces the closest estimation to the original images. Threshold the preprocessed images to binarize the images.
4. Use Measure (a built-in function of ImageJ) on the binarized images to obtain the area of the images and the area fraction of

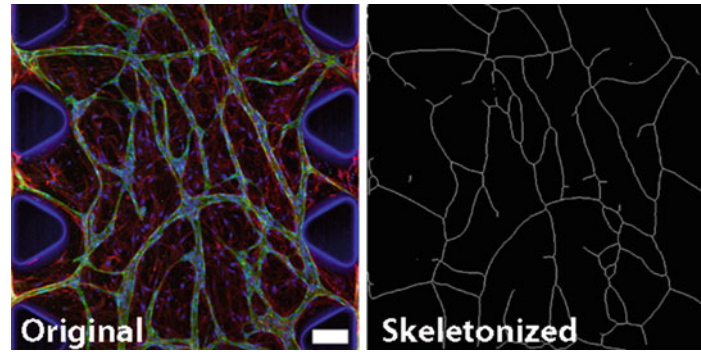

Fig. 5 A 3D projection of a stack of confocal images (left) and its corresponding skeletonized image (right). Scale bar indicates 100 μm

the microvascular network. Multiply the total area by the area fraction to get lateral vessel area (A_{lateral}) (*see* **Note 26**).

5. Use Skeletonize (2D/3D) plugin (http://imagej.net/Skeletonize3D) in ImageJ to find the centerlines (also known as skeleton) of objects in the input image as shown in Fig. 5.
6. Use AnalyzeSkeleton plugin (http://imagej.net/AnalyzeSkeleton) in ImageJ to analyze the skeletons you have generated. This yields information including the average branch length and the number of branches. Multiply the average branch length by the number of branches to get total branch length (L_{branch}).
7. Derive the lateral diameter (D_{lateral}) by dividing the lateral vessel area by the total branch length.

$$D_{\text{lateral}} = \frac{A_{\text{lateral}}}{L_{\text{branch}}}$$

8. Preprocess the images if necessary. Depending on the image quality, you may apply preprocessing techniques such as despeckle and background subtraction (*see* **Note 27**).
9. Try all threshold methods and choose the method that segments your data best and produces the closest estimation to the original images based on at least three individual stacks of images. Threshold the preprocessed images to binarize the images.
10. Use Trainable Weka Segmentation 3D plugin (https://imagej.net/Trainable_Weka_Segmentation) in ImageJ to segment the duplicated binarized images as obtained from **step 5**. Briefly, select representative region of interest (ROI) of the microvascular network and add that as first classifier. The region outside of microvasculature network is selected as the second classifier. Train the classifiers and create results afterwards.

11. Adjust the segmented image into 8-bit.
12. Use 3D geometrical measure in 3D ImageJ Suite (http://imagejdocu.tudor.lu/doku.php?id=plugin:stacks:3d_ij_suite:start) to measure the 3D vessel volume (V) and 3D surface area ($A_{surface}$).
13. Derive the transverse diameter ($D_{transverse}$) by using the following equations:

$$A_{lateral} = D_{lateral} L_{branch}$$

$$A_{surface} = \pi \sqrt{\frac{D_{transverse}^2 + D_{lateral}^2}{2}} L_{branch}$$

$$V = \frac{\pi D_{lateral} D_{transverse} L_{branch}}{4}$$

$$D_{lateral} = 2R_{major} = \frac{A_{lateral}}{L_{branch}}$$

$$D_{transverse} = \sqrt{\frac{D_{lateral}^2}{\frac{A_{surface}^2 D_{lateral}^2}{8V^2} - 1}}$$

14. Compute circularity by dividing the transverse diameter by the lateral diameter (*see* **Note 28**).

$$\text{Circularity} = \frac{D_{transverse}}{D_{lateral}}$$

4 Notes

1. The fibrinogen working solution can be kept in 4 °C for not more than 2 weeks.
2. Water is used instead of PBS to keep the pH at 6.5 which is optimum to maintain the stability of thrombin.
3. The iPSC-EC medium supplement substitutes for the FBS that comes from the endothelial medium kit.
4. Individual cell suspensions are mixed to obtain a master cell suspension stock. The master stock is then mixed with fibrinogen solution in a 1:1 ratio to form fibrin gel. Therefore, the seeding concentrations are multiplied by the number of cell types and the dilution factor of two to obtain the concentrations of cell suspensions.
5. Prepare fibrin gel that is only sufficient for one experiment at a time to avoid polymerization from taking place in the microcentrifuge tube.

6. Fibrinogen polymerizes very quickly when it is mixed with thrombin. This mixing step should be done in less than 10 s. If unsure, pipette up and down for not more than 15 times.
7. Limit the volume of fibrin gel to 10 μL to prevent the fibrin gel from overflowing into media channels.
8. Inject the fibrin gel deftly (but not abruptly) to complete the gel filling step before it polymerizes. If unsure, fill the gel within 5 s.
9. Hold the plunger firmly while removing the micropipette from the inlets, otherwise the negative pressure will suck the gel up.
10. AIM chips are laminated with a gas-permeable film that enables gas exchange to take place. The bottom of the chips should therefore be exposed to allow for air circulation. Custom-made PDMS chips do not need to be supported to allow air circulation as PDMS is highly gas-permeable.
11. Chips with unpolymerized gel must be handled with care. Excessive agitation or impact may cause the unpolymerized gel to leak out of the gel channel.
12. Large fibrin fibers may form in the gel and affect the EC cell alignment due to early polymerization of fibrin gel or old fibrinogen stock. This can be avoided by not mixing the fibrin gel for too long before injecting it into the chips and by preparing a new batch of fibrinogen solution.
13. Hold the plunger firmly while removing the micropipette from the inlets, otherwise the negative pressure will suck the solution up.
14. Do not inject more than 20 μL of solution at this step or the high injection pressure may disrupt the fibrin gel.
15. The differential volumes in the two ports allow the replacement of medium to take place in the channel. The minimum volume of medium is 30 μL to ensure the inlets are covered and the troughs are wetted. If less than 30 μL of medium is used, the surface tension at the inlets will prevent the medium from flowing through the channel. We recommend using 50 μL of medium for easier handling.
16. Do not aspirate medium from inlets to avoid accidental removal of medium from the channels.
17. If the microvasculature is too narrow, the seeding density of endothelial cells should be increased. Similarly, if the microvasculature turns into a sheet-like structure, the seeding density of endothelial cells should be reduced.
18. Endothelial cells are seeded in the media channels to increase the cell coverage on the gel interface, to fill gaps at the gel-post borders and to improve the connections between the microvascular network and media channels.

19. Do not insert the tip completely into the inlets to avoid introducing cells into the media channels at a high flow rate. High flows will not allow cells to settle along the channel, resulting in uneven distribution.
20. Lay chips on a flat surface while seeding cells into chips. Inclination of the chips affects the cell distribution.
21. Reduce the seeding density if there are too many endothelial cells in the media channel, and vice versa.
22. Increase the volume of cell suspension to apply greater pressure head if there are insufficient endothelial cells adhered to the gel interface.
23. If the chips are supported by spacers or in the dedicated AIM holder, the surface tension at the ports prevents the medium from dripping even though the chips are flipped.
24. The surface tension at the media channel inlets prevents the dextran solution/medium from flowing through the channels at this step.
25. Optimize the preprocessing steps based on the stained proteins/organelles and the image quality. You should always preprocess your images as a whole.
26. Select area fraction as one of the measurements and set the scale according to your images.
27. The confocal images are not projected to 2D images as the 3D vessel volume, 3D surface area, and transverse diameter will be determined in the following steps.
28. The circularity of a circle is 1.

Acknowledgments

M.C. was supported by Ermenegildo Zegna Founder's scholarship and then by the MIT-POLITO grant (BIOMODE—Compagnia di San Paolo) under the joint "Doctorate of Bioengineering and Medical-Surgical Sciences" of University of Turin and Politecnico di Torino. R.D.K. acknowledges the support from the Cure Alzheimer's Fund and National Science Foundation for a Science and Technology Center on Emergent Behaviors of Integrated Cellular Systems (CBET-0939511). and R.D.K. were supported by the National Cancer Institute (U01 CA202177). M.C., V.C., and R.D.K. also acknowledge the support of the research collaborations and exchanges program between MIT and POLITO (MITOR project NANOCAB). M.C. and S.H.L. contributed equally to this manuscript.

Competing Interests: *R.D.K. is the cofounder of AIM Biotech that makes microfluidic systems. S.H.L. is an employee of AIM Biotech.*

References

1. Abbott NJ, Patabendige AAK, Dolman DEM, Yusof SR, Begley DJ (2010) Structure and function of the blood–brain barrier. Neurobiol Dis 37(1):13–25. https://doi.org/10.1016/j.nbd.2009.07.030
2. Serlin Y, Shelef I, Knyazer B, Friedman A (2015) Anatomy and physiology of the blood–brain barrier. Semin Cell Dev Biol 38:2–6. https://doi.org/10.1016/j.semcdb.2015.01.002
3. Cecchelli R, Berezowski V, Lundquist S, Culot M, Renftel M, Dehouck M-P, Fenart L (2007) Modelling of the blood–brain barrier in drug discovery and development. Nat Rev Drug Discov 6:650. https://doi.org/10.1038/nrd2368
4. Sweeney MD, Sagare AP, Zlokovic BV (2018) Blood–brain barrier breakdown in Alzheimer disease and other neurodegenerative disorders. Nat Rev Neurol 14:133. https://doi.org/10.1038/nrneurol.2017.188
5. Pamies D, Hartung T, Hogberg HT (2014) Biological and medical applications of a brain-on-a-chip. Exp Biol Med (Maywood) 239 (9):1096–1107. https://doi.org/10.1177/1535370214537738
6. van der Helm MW, van der Meer AD, Eijkel JCT, van den Berg A, Segerink LI (2016) Microfluidic organ-on-chip technology for blood-brain barrier research. Tiss Barriers 4 (1):e1142493. https://doi.org/10.1080/21688370.2016.1142493
7. Kamm RD, Bashir R, Arora N, Dar RD, Gillette MU, Griffith LG, Kemp ML, Kinlaw K, Levin M, Martin AC, McDevitt TC, Nerem RM, Powers MJ, Saif TA, Sharpe J, Takayama S, Takeuchi S, Weiss R, Ye K, Yevick HG, Zaman MH (2018) Perspective: the promise of multi-cellular engineered living systems. APL Bioeng 2(4):040901. https://doi.org/10.1063/1.5038337
8. Gribkoff VK, Kaczmarek LK (2017) The need for new approaches in CNS drug discovery: why drugs have failed, and what can be done to improve outcomes. Neuropharmacology 120:11–19. https://doi.org/10.1016/j.neuropharm.2016.03.021
9. Osaki T, Shin Y, Sivathanu V, Campisi M, Kamm RD (2018) In vitro microfluidic models for neurodegenerative disorders. Adv Healthcare Mater 7(2):1700489. https://doi.org/10.1002/adhm.201700489
10. Campisi M, Shin Y, Osaki T, Hajal C, Chiono V, Kamm RD (2018) 3D self-organized microvascular model of the human blood-brain barrier with endothelial cells, pericytes and astrocytes. Biomaterials 180:117–129. https://doi.org/10.1016/j.biomaterials.2018.07.014
11. Abbott NJ, Rönnbäck L, Hansson E (2006) Astrocyte–endothelial interactions at the blood–brain barrier. Nat Rev Neurosci 7 (1):41–53. https://doi.org/10.1038/nrn1824
12. Winkler EA, Bell RD, Zlokovic BV (2011) Central nervous system pericytes in health and disease. Nat Neurosci 14:1398. https://doi.org/10.1038/nn.2946
13. Obermeier B, Daneman R, Ransohoff RM (2013) Development, maintenance and disruption of the blood-brain barrier. Nat Med 19:1584. https://doi.org/10.1038/nm.3407
14. Hagan N, Ben-Zvi A (2015) The molecular, cellular, and morphological components of blood–brain barrier development during embryogenesis. Semin Cell Dev Biol 38:7–15. https://doi.org/10.1016/j.semcdb.2014.12.006
15. Herland A, van der Meer AD, FitzGerald EA, Park TE, Sleeboom JJ, Ingber DE (2016) Distinct contributions of astrocytes and pericytes to neuroinflammation identified in a 3D human blood-brain barrier on a chip. PLoS One 11(3):e0150360. https://doi.org/10.1371/journal.pone.0150360
16. Adriani G, Ma DL, Pavesi A, Kamm R, Goh ELK (2016) A 3D neurovascular microfluidic model consisting of neurons, astrocytes and cerebral endothelial cells as blood-brain barrier. Lab Chip 17(3):448–459. https://doi.org/10.1039/c6lc00638h
17. Yuan W, Lv Y, Zeng M, Fu BM (2007) Non-invasive measurement of solute permeability of rat pial microvessels. In: 2007 IEEE 33rd Annual Northeast Bioengineering Conference, 10–11 March 2007. pp 185–186. https://doi.org/10.1109/nebc.2007.4413340
18. Hajal C, Campisi M, Mattu C, Chiono V, Kamm RD (2018) In vitro models of molecular and nano-particle transport across the blood-brain barrier. Biomicrofluidics 12(4):042213. https://doi.org/10.1063/1.5027118
19. Lee SWL, Campisi M, Osaki T, Possenti L, Mattu C, Adriani G, Kamm RD, Chiono V (2020) Modeling Nanocarrier Transport across a 3D In Vitro Human Blood-Brain–Barrier Microvasculature. Adv Healthc Mater. 1901486:1–12. https://doi.org/10.1002/adhm.201901486

Chapter 15

Modeling the Complexity of the Metastatic Niche Ex Vivo

Amanda M. Clark

Abstract

Cancer mortality predominantly results from distant metastases that are undetectable at diagnosis and escape initial therapies to lie as dormant micrometastases for years. To study the behavior of micrometastases—how they resist initial treatments and then awaken from a dormant state—we utilize the Legacy LiverChip®, an all-human ex vivo hepatic microphysiological system. The functional liver bioreactor, comprising hepatocytes and non-parenchymal cells in a 3D microperfused culture format, mimics the dormant-emergent metastatic progression observed in human patients: (a) a subpopulation of cancer cells spontaneously enter dormancy, (b) cycling cells are eliminated by standard chemotherapies, while quiescent dormant cells remain, and (c) chemoresistant dormant cells can be stimulated to emerge. The system effluent and tissue can be queried for proteomic and genomic data, immunofluorescent imaging as well as drug efficacy and metabolism. This microphysiological system continues to provide critical insights into the biology of dormant and re-emergent micrometastases and serves as an accessible tool to identify new therapeutic strategies targeting the various stages of metastasis, while concurrently evaluating antineoplastic agent efficacy for metastasis, metabolism, and dose-limiting toxicity.

Key words Organ-on-a-chip, Microphysiological system, Model of metastasis, Cancer, Dormancy, Emergence

1 Introduction

Metastatic disease remains largely incurable and is responsible for ~90% cancer-related deaths. Advances in our abilities to remove or treat primary tumors have not translated into sustained success against metastases. It is a dynamic, multistep process whereby cells within the primary tumor undergo a cancer-associated epithelial to mesenchymal transition, which enables motility to disseminate into the circulation followed by extravasation into and colonization of distant organs [1]. The tumor cells that successfully colonize can either outgrow immediately into metastases or do so after a period of inactivity (i.e., dormancy). This delayed emergence arises from a subset of cells that lie dormant for months, years, or

Mo R. Ebrahimkhani and Joshua Hislop (eds.), *Programmed Morphogenesis: Methods and Protocols*, Methods in Molecular Biology, vol. 2258, https://doi.org/10.1007/978-1-0716-1174-6_15,

even decades before re-emerging into clinically detectable metastases [2].

In late-relapsing patients, the underlying mechanisms of metastatic dormancy and re-emergence are not well understood. Understanding the foundations of this post-dissemination phase is key to reducing the mortality associated with metastatic cancer. The mechanisms remain muddled due in no small part to challenges in creating tractable experimental models that can faithfully recapitulate the cellular complexity and microenvironmental dynamics of metastatic disease. While animal models have been valuable for dissecting biological mechanisms, they are not fully representative of the human situation due to issues of interspecies functions (e.g., immune and metabolic) [3, 4] and the use of immunocompromised mice [5–7]. To address this problem, microphysiological systems—ex vivo models of human tissues and organs—have been developed; employing 3D tissue engineering approaches with microfluidic control [8, 9].

One such example is the all-human biologically complex Legacy LiverChip® microphysiological system (technological details described in Subheading 1.1) which can be used to mimic dormant-emergent metastatic progression that is physiologically reflective of the human situation [10–12]. The liver is a highly relevant organ for deciphering these important questions as it is a major site of metastasis for a wide range of carcinomas and its involvement correlates poorly with patient survival [13–16]. Moreover, it is the main organ of drug metabolism and dose-limiting toxicity for most chemotherapies [17].

Metastatic progression is recapitulated by firstly isolating hepatic cells from therapeutic partial hepatectomies. The hepatic cells comprise donor-matched parenchymal hepatocytes and an array of non-parenchymal cells; predominant subtypes include liver sinusoidal endothelial cells, Kupffer cells, stellate cells, and lymphocytes [12]. Following isolation they are seeded into the constructed Legacy LiverChip® microphysiological system (Fig. 1, **Day 0**). Hepatic tissue is given 3 days to establish after which a limited number of fluorescently labeled cancer cells are seeded into the system (Fig. 1, **Day 3**). The cancer cells colonize and establish as two populations: actively growing and quiescently dormant. Importantly, they integrate and reside alongside the liver tissue, and spontaneous attainment of dormancy occurs among a subpopulation of cancer cells (Fig. 1, **Day 7**). Following treatment with chemotherapy, the proliferating cells are eliminated and only dormant cells remain (Fig. 1, **Day 13**). Upon exposure to pathophysiologically relevant inflammatory stimuli, the surviving dormant populations can be induced to outgrow or "emerge" from dormancy (Fig. 1, **Day 15**) [10].

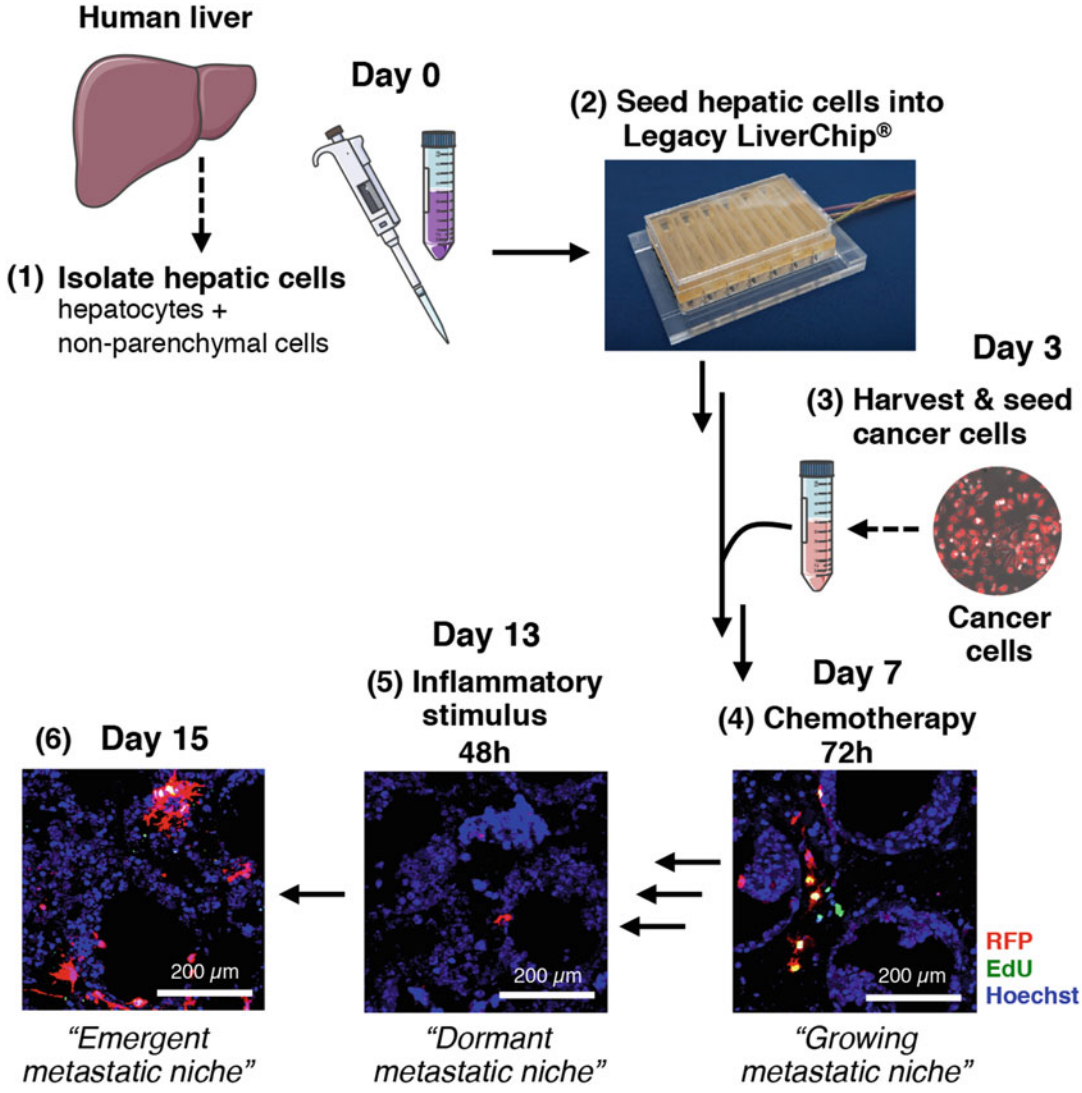

Fig. 1 Schematic representation of modeling dormant-emergent metastatic progression using the Legacy LiverChip® microphysiological system. (*1*) On day 0, hepatic cells (hepatocytes and non-parenchymal cells) are obtained and isolated from human livers and (*2*) seeded into the Legacy LiverChip® plate. (*3*) On day 3, cancer cells are harvested and seeded on top of the hepatic tissue. (*4*) By day 7, cancer cells have colonized—the majority establish as actively growing cells (red and yellow cells), while subpopulation spontaneously enter a dormant state (red and pink cells). Treatment with chemotherapy is given for 72 h after which (*5*) only the dormant cells remain. (*6*) Emergence of the remaining dormant cells is achieved by adding an inflammatory stimulus on day 13 for 48 h. Immunofluorescent images: red—RFP (cancer cells), green—EdU (proliferating cells), blue—Hoechst (nucleus). *Steps* (*4–6*) adapted from Clark et al. [10] A model of dormant-emergent metastatic breast cancer progression enabling exploration of biomarker signatures, Molecular & Cellular Proteomics (17:4) pp. 619–630. Copyright © 2018 (The American Society for Biochemistry and Molecular Biology, Inc.). DOI: https:/doi.org/10.1074/mcp.RA117.000370

1.1 Overview of Legacy LiverChip® Microphysiological System Technology

The Legacy LiverChip® microphysiological system was devised to recreate a liver microenvironment in terms of cellular composition, fluid flow, oxygen gradient, and shear stress, and can be maintained for up to a month [10]. The system is presently commercialized and available from CN Bio Innovations Ltd., but was originally developed by Linda Griffith's laboratory [18, 19]. The Legacy LiverChip® platform consists of 12 fluidically isolated liver bioreactors. The scaffold enables the formation of an array of 3D microtissues, specifically designed to recreate the architecture of the liver sinusoid and comprises 301 individual channels (Fig. 2a, b). Each liver bioreactor has a surface channel that allows for efficient re-oxygenation of the media by gaseous exchange with the atmosphere (Fig. 2a, c). A pneumatic controlled underlay enables re-oxygenation via continuous perfusion (1 μL/s), and the oxygen concentrations are similar to that observed in the liver sinusoid [18]. Additionally, both the flow rate (0.5–5.4 μL/s) and direction (up or down) can be easily adjusted as needed (Fig. 3). The platform is covered with a single loose lid (as per a standard microtiter plates) enabling direct access to each of the 12 liver bioreactors for cell seeding, media changes, and sampling (Fig. 2c). The system is housed in a humidified cell culture incubator at 37 °C with 5% CO_2.

1.2 Strengths and Limitations for Investigating Metastatic Disease

With respect to metastasis, a major strength of the Legacy LiverChip® microphysiological system is that each scaffold can be processed to collect a wide variety of visual information, including metastatic phase, cell–cell interactions, as well as tumor burden as a measure of therapeutic activity or efficacy [10–12, 20–22]. It also affords real-time, high volume sampling with each well able to hold up to 2.5 mL. Such specimens can be utilized for elucidation of communication networks, biomarker discovery [11, 19, 21, 23], and important pharmacological information such as drug metabolism, toxicity, clearance, efficacy, and interactions [10, 11, 20, 24, 25]. These features are facilitated by a combination of the bioengineering behind the system and the incorporation of a full complement of donor-matched primary human hepatocytes and non-parenchymal cells. The latter is a critical feature for accurately recapitulating the metastatic microenvironment as each of the cellular components of the host organ plays just as much of an important role as the tumor cells [10, 12, 21–23, 26, 27].

The Legacy LiverChip® microphysiological system is however not without limitations. In terms of imaging, the optical windows of the early interactions [28] were traded for enhanced throughput. As a result, real-time image tracking of cancer cells from colonization, during chemotherapy, and onto emergence/recurrence is presently not possible as scaffolds must be harvested at the time

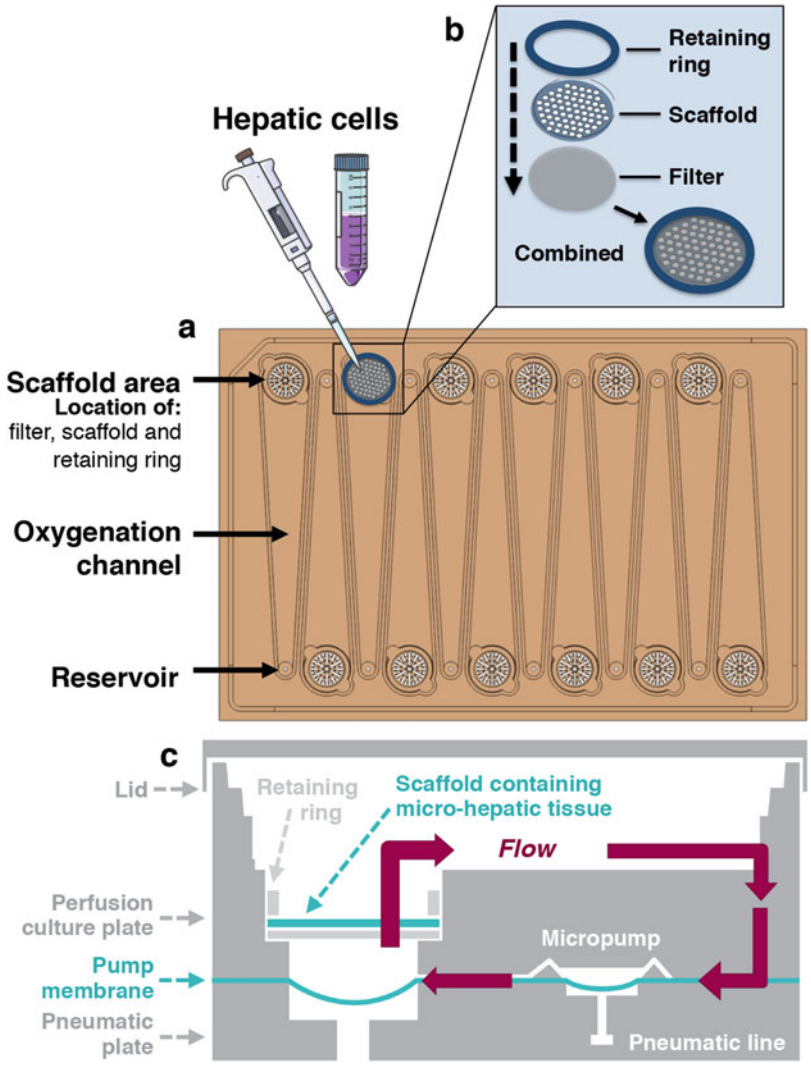

Fig. 2 Configuration and perfusion dynamics of the Legacy LiverChip® microphysiological system. (**a**) An aerial view of the Legacy LiverChip® plate showing the 12 fluidically isolated wells, also called liver bioreactors. (**b**) Each liver bioreactor contains an engineered collagen-coated scaffold (depth of 250 μm) placed atop a filter and held in place by a retaining ring. Hepatic cells are seeded onto the scaffolds and form microtissues. (**c**) Schematic representation of a single liver bioreactor on the Legacy LiverChip® plate. Pneumatically driven micropumps are embedded within plate and control the direction and speed of medium flow within each well. The micropumps are set using an electronic controller (*see* Fig. 3; image courtesy of CN Bio Innovations Ltd.). Both (**a**, **b**) are adapted from Clark et al. [23] Liver metastases: microenvironments and ex vivo models, Experimental Biology and Medicine (241) pp. 1639–1652. Copyright © 2016 (Society for Experimental Biology and Medicine). DOI: https:/doi.org/10.1177/1535370216658144

point of interest. Furthermore, although the system affords the ability to sample sufficient effluent for numerous downstream assays, it comes at a cost of requiring a considerable number of hepatocytes per well.

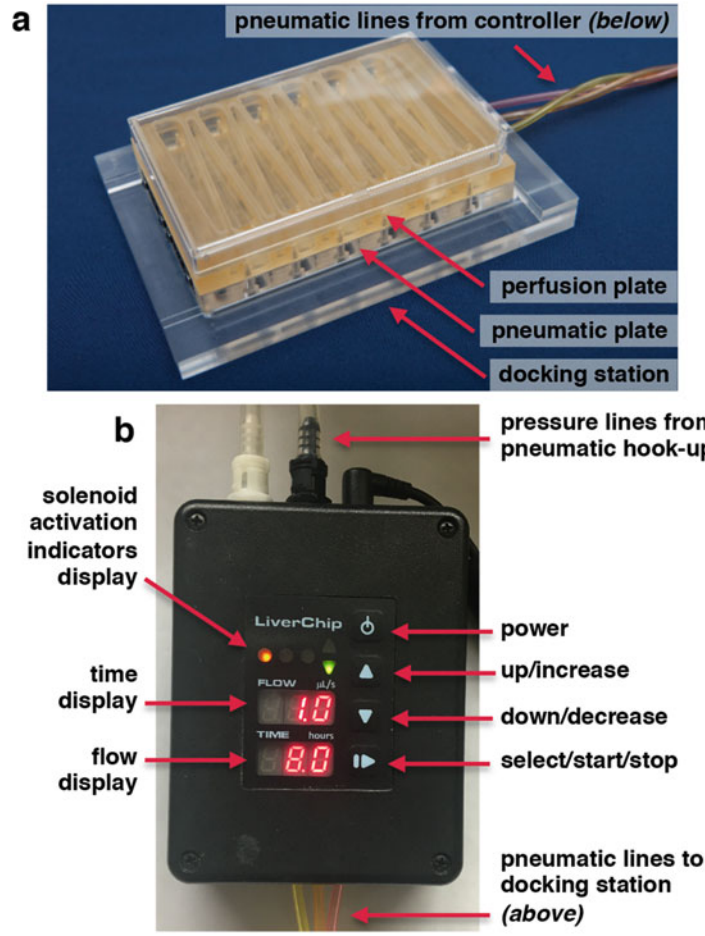

Fig. 3 Docked Legacy LiverChip® plate and electronic controller. (**a**) The fully constructed Legacy LiverChip® plate depicted within its docking station (image courtesy of CN Bio Innovations Ltd.). (**b**) Electronic dock controller that controls the perfusion of the Legacy LiverChip® plate while in the docking station depicted in (**a**). Three microprocessors control the movement of the solenoid valves which drive micropumps in the Legacy LiverChip® perfusion culture and pneumatic plates. The controller must be used in conjunction with a pneumatic hookup (not pictured)

1.3 Applications

The Legacy LiverChip® microphysiological system enables investigations into the post-dissemination stages of metastatic progression as observed in human patients [10]. The protocol described herein serves as a canvas for mimicking metastatic progression as modifications can be made at any time point. This affords the user the ability to examine any of the individual stages (e.g., colonization, dormancy, and emergence). For example, the system can be used to discern factors that influence a cancer cell's ability to colonize a foreign microenvironment, as well as whether that cancer cell outgrows immediately or transitions to a dormant state [12, 21]. It can

also investigate the role individual metastatic niche cellular components have in regulating emergence [10, 22] and therapeutics to block this lethal transition [20]. Additionally, by changing the scaffolding biomaterial, the impact imparted by the biomechanics of the metastatic microenvironment can be assessed [11]. It has also been extensively characterized in terms of its ability to assess drug efficacy [10, 11], interactions, and metabolism [10–12, 29].

2 Materials

2.1 Legacy LiverChip® Microphysiological System Setup and Preparation

1. Legacy LiverChip® hardware system: for information regarding the purchase and setup of the necessary hardware (e.g., docking station, controller, pneumatic hook-ups, and setup tools), contact the manufacturer, CN Bio Innovations Ltd. (https://cn-bio.com or enquiries@cn-bio.com).
2. Tools: ring pusher, tweezers, automatic torque driver/power supply/cable/bits (CN Bio Innovations Ltd.).
3. Legacy LiverChip® plates: Legacy LiverChip® perfusion culture plate, Legacy LiverChip® pneumatic plate, screw pack, and bevel washer pack (CN Bio Innovations Ltd.).
4. Consumables: Legacy LiverChip® Consumables kit (contains 13 high-impact polystyrene scaffolds (*see* **Note 1**), 13 retaining rings, 13 filters, 1 pump membrane, 24 culture plate lids; CN Bio Innovations Ltd.). All items are shipped sterilized.
5. Scaffold coating: 1% collagen type I rat tail (Corning™ Fisher Scientific) in phosphate buffered saline (PBS), 100 mm Petri dish.
6. Priming solution: 1% bovine serum albumin (BSA) in deionized water filter-sterilized using a 500 mL 0.22 μm vacuum filter/storage bottle system (Corning™ Fisher Scientific).
7. Hepatic cells: human hepatocytes and non-parenchymal cells (including Kupffer cells, endothelial cells, and stellate cells) are isolated from the normal margins of therapeutic partial hepatectomies. Patient donors can include both males and females as no discernable differences among the genders have been observed [10]. The normal human hepatic cells can be obtained through the Liver Tissue Cell Distribution System (LTCDS), Pittsburgh, Pennsylvania, which is funded by NIH Contract #HSN276201200017C (*see* **Note 2**). Hepatocytes and non-parenchymal cells are received as separate isolations with the non-parenchymal fraction further purified via Percoll gradients as described in Subheading 3.
8. Cancer cells: the triple-negative breast cancer cell line, MDA-MB-231, can be purchased from ATCC and maintained in complete RPMI-1640 (*see* **step 11**). It should be modified to

express a red fluorescent protein (RFP; described previously [26]) (*see* **Notes 3–5**). Remove the selection antibiotic to maintain RFP expression approximately 24 h before harvesting and seeding the cancer cells into the microphysiological system.

9. Hepatocyte plating medium: phenol-free William's E medium (Gibco™ ThermoFisher Scientific) plus Primary Hepatocyte Thawing and Plating Supplements (Gibco™ ThermoFisher Scientific). For these supplements, 25 mL fetal bovine serum (FBS), 50 μL dexamethasone, and 18 mL cocktail A are added to William's E medium.
10. Hepatocyte maintenance medium: phenol-free William's E medium plus Primary Hepatocyte Maintenance Supplements (Gibco™ ThermoFisher Scientific). For these supplements, 5 μL dexamethasone and 20 mL cocktail B are added to William's E medium.
11. Complete RPMI-1640: RPMI-1640 (Gibco™ ThermoFisher Scientific) supplemented with 10% heat-inactivated FBS (Gemini Bio-Products) and 25 IU/mL penicillin and streptomycin (Gibco™ ThermoFisher Scientific).
12. Percoll gradients: use Percoll (pH 8.5–9.5; Sigma-Aldrich) and PBS to make 25% (7.5 mL Percoll + 22.5 mL PBS) and 50% solutions (15 mL Percoll + 15 mL PBS).
13. Cell counting: hemocytometer and 0.4% Trypan Blue Solution (working solution 0.1% in PBS; Gibco™ ThermoFisher Scientific).
14. Treatments: doxorubicin (APP Pharmaceuticals LLC), lipopolysaccharide (LPS; Sigma-Aldrich), mouse epidermal growth factor (mEGF; Corning™ Fisher Scientific), EdU (*see* Subheading 2.2, **item 5a**).

2.2 Immunofluorescence

1. Consumables: 35 mm glass bottom dish with a 14 mm microwell (MatTek Corporation), 24 well plate, tweezers.
2. Fixation buffer: 2% paraformaldehyde in PBS.
3. Permeabilization buffer: 0.5% Triton X-100 in PBS.
4. Blocking buffer: 3% BSA in PBS.
5. EdU proliferation kit: Click-iT™ Plus EdU Alexa Fluor 488 Imaging Kit (Invitrogen™ ThermoFisher Scientific) (*see* **Note 6**). Prepare each component as follows:
   (a) 10 mM solution of EdU (component A): add 2 mL DMSO (component C) to the component A. Working solution is 10 μM (1:1000 dilution).
   (b) Reaction buffer (component D): add 4 mL component D bottle to 36 mL deionized water. Store at 4 °C.

(c) 10× buffer additive (component F): add 2 mL deionized water to the vial and mix until fully dissolved. Store any remaining stock solution at ≤ –20 °C. Before use in detection cocktail, dilute 1:10 using deionized water.

3 Methods

The methods described for the construction and use of the Legacy LiverChip® were modified from the manufacturer's protocols, CN Bio Innovations Ltd.

3.1 Legacy LiverChip® Microphysiological System Preparation

3.1.1 Legacy LiverChip® Plate Assembly

1. Move the sterile pump membrane, perfusion cell culture plate, lid, and tweezers into the biosafety cabinet (Fig. 3a). Spray the pneumatic plate with 70% ethanol, place in the biosafety cabinet, and wipe dry with a Kimwipe.
2. Begin assembly by using the tweezers to place the pump membrane on the pneumatic plate being careful to only let the bottom side of the membrane come into contact with the pneumatic plate. The top side must remain sterile. Using the tweezers, adjust the pump membrane as required to ensure the holes in the membrane align with the screw holes in the pneumatic plate. Place the perfusion plate on top followed by the sterile lid.
3. Turn over the Legacy LiverChip® plate to ensure the pump membrane is not folded over or obstructing any of the screw holes.
4. While the plate is turned over, add the 43 screws and bevel washers into the base of the pneumatic plate. Start at the center and work outwards.
5. Screw together using the calibrated torque driver. Again, start at the center and work outwards. This step can be done outside the biosafety cabinet. Ensure the unit remains as one.
6. Check that each of the screws aligns evenly (*see* **Note 7**).

3.1.2 Priming

1. Move the Legacy LiverChip® plate back into the biosafety cabinet along with the docking station.
2. With the Legacy LiverChip® plate residing within the docking station (Fig. 3a), add 700 μL 1% BSA priming solution into each of the 12 reservoirs (Fig. 2a).
3. Set the controller to upward flow at a rate of 1 μL/s (Fig. 3b, **left**).
4. Once the solution is observed in all the wells, stop flow and add 1 mL 1% BSA priming solution to the channel of each liver bioreactor.

5. Return the Legacy LiverChip® plate to the incubator and set the controller to upward flow at a rate of 1 μL/s for at least 1 h of priming.

3.1.3 Coat Scaffolds

1. In the biosafety cabinet, transfer the scaffolds into a 100 mm Petri dish.
2. Add 20 mL cold 1% collagen type I solution. Ensure the scaffolds are free of bubbles by tapping them with the sterile tweezers to release any trapped in the channels.
3. Incubate at 37 °C for 1 h.
4. Return the dish to the biosafety cabinet, aspirate the collagen solution, and replace with PBS.

3.1.4 Legacy LiverChip® Plate Construction

1. Move all the required items into the biosafety cabinet (Legacy LiverChip® plate, filters, retaining rings, coated scaffolds, ring pusher, and tweezers).
2. Situate the Legacy LiverChip® plate within the docking station.
3. Before constructing, check each well of the Legacy LiverChip® plate for bubbles. If present, use a pipet to dislodge them by aspirating the medium up and down.
4. Using tweezers, sequentially add a filter, scaffold and retaining ring to each well (Fig. 1a).
5. Using the sterile ring pusher, push the retaining ring firmly into place. This is typically accompanied by a clicking sound. Check the sides of the perfusion cell culture plate to confirm the retaining rings have been successfully pushed flush to the base. Repeat if necessary.
6. Return the Legacy LiverChip® plate to the docking station located in the incubator and set the controller to upward flow at a rate of 1 μL/s until the hepatic cells are ready for seeding.

3.2 Creating Hepatic Tissue (Day 0)

Isolation of non-parenchymal cells: calculations and steps are based on a 40–50 mL specimen of non-parenchymal cells taken from a human liver isolation (*see* **Note 8**).

1. Prepare the Percoll gradients by first dividing 25% Percoll solution into two 50 mL tubes (15 mL each). Using a 10-mL serological pipette and the pipet aid set to slow, aspirate up 14.5 mL 50% Percoll solution, place at the bottom of the 25% Percoll layer and slowly dispense (*see* **Note 9**). Place on ice until the non-parenchymal cells are ready.
2. Centrifuge the tube containing non-parenchymal cells at 50 × *g* for 5 min at 4 °C (*see* **Note 10**).
3. Transfer supernatant to a new tube and centrifuge at 350 × *g* for 10 min at 4 °C.

4. Aspirate supernatant and resuspend the pellet in 20 mL cold PBS.
5. Layer 10 mL of the non-parenchymal cells on top of each Percoll gradient.
6. Centrifuge at 900 × *g* for 20 min with no brake at 4 °C.
7. Collect the second flocculent layer (i.e., interface between the 50% and 25% layers). This may need to be repeated a few times until the interface between layers is clear.
8. Dilute the cells collected from the flocculent layer 1:2 with PBS and centrifuge at 900 × *g* for 10 min on low brake at 4 °C.
9. Aspirate supernatant and resuspend in 3–5 mL of cold hepatocyte plating medium and store on ice until needed (*see* **Note 11**).

   Seeding hepatic cells: On day 0, hepatocytes and non-parenchymal cells are combined into one tube, seeded into the Legacy LiverChip® plate, and cultured with downward flow at 1 μL/s for 8 h to establish the hepatic tissue (Fig. 4).
10. Count the hepatocytes and non-parenchymal cells using a hemocytometer and 0.1% Trypan Blue solution.
11. Make the hepatic cell suspension using cold hepatocyte plating medium: 6×10^5 hepatocytes and 6×10^5 non-parenchymal cells per 400 μL (equal to 1.5×10^6/mL each). Be sure to rock the conical tube back and forth before transferring cells as the hepatocytes sediment very quickly. Avoid pipetting the cells to resuspend where possible and keep on ice until needed.
12. Warm hepatocyte plating medium.

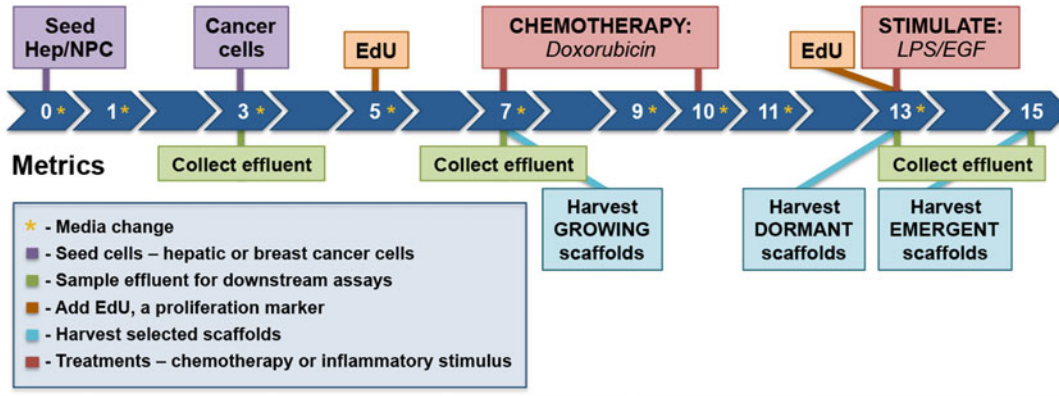

Fig. 4 Experimental outline to mimic dormant-emergent metastatic progression using the Legacy LiverChip® microphysiological system. Adapted from Clark et al. [10] A model of dormant-emergent metastatic breast cancer progression enabling exploration of biomarker signatures, Molecular & Cellular Proteomics (17:4) pp. 619–630. Copyright © 2018 (The American Society for Biochemistry and Molecular Biology, Inc.). DOI: https:/doi.org/10.1074/mcp.RA117.000370

13. Move all the required items into the biosafety cabinet (Legacy LiverChip®, plate docking station, pipets, pre-warmed media, hepatic cells, etc.)
14. Aspirate the 1% BSA priming solution from the wells, channels, and reservoirs of each liver bioreactor.
15. Using a swirling motion, ensure the hepatic cell mixture from **step 1** is resuspended homogenously.
16. Transfer 400 μL hepatic cell mixture to each well. Remember to swirl and keep cells homogenously suspended each time before transferring. When dispensing cells into the well, do so in a slow dropwise manner and over different spots of the scaffold.
17. Turn on flow by setting the controller to downward flow at a rate of 1 μL/s.
18. Aspirate medium from the reservoirs approximately every 30 s until the meniscus in the well aligns with the top of the retaining ring (~3–4 min).
19. Stop flow and add 1.4 mL hepatocyte plating medium to the channel of each liver bioreactor in a dropwise manner being careful not to disturb the cells that were seeded.
20. Return the Legacy LiverChip® plate to the docking station located in the incubator and set the controller to downward flow at a rate of 1 μL/s for 8 h (Fig. 3b, **right**; *see* **Note 12**). The system will automatically switch to the standard upward flow after 8 h (*see* **Note 13**).

3.3 Media Change (Day 1)

On day 1, after allowing the hepatic cells to attach to the scaffold overnight and form tissue, a media change is performed (Fig. 4). The media is switched from hepatocyte plating medium to hepatocyte maintenance medium. Also note, the precise detail of subsequent media change depends upon the experimental protocol (*see* **Note 14**).

1. Warm the hepatocyte maintenance medium.
2. Move the docking station, Legacy LiverChip® plate, and warm medium into the biosafety cabinet.
3. Aspirate approximately half the effluent from each well. Move the aspirator to the channel and aspirate up and down the sides. Move the aspirator to the reservoir and aspirate effluent. Return to the well, place the tip of the aspirator in the groove located in the top left-hand corner and gently remove media until the meniscus aligns with the retaining ring (*see* **Note 15**).
4. Add 400 μL hepatocyte maintenance medium to each well and aspirate any residual medium from the reservoirs.

5. Turn on flow by setting the controller to downward flow at a rate of 1 μL/s.
6. Aspirate medium from the reservoirs approximately every 30 s until the meniscus in the well aligns with the top of the retaining ring.
7. Stop flow and add 1.4 mL hepatocyte maintenance medium to the channel of each liver bioreactors in a dropwise manner.
8. Return the Legacy LiverChip® plate to the docking station located in the incubator and set the controller to upward flow at a rate of 1 μL/s.

3.4 Metastatic Progression (Days 3–15)

To create metastatic progression, three different metastatic stages will be mimicked: growing metastases (hepatic cells + cancer cells), dormant metastases (hepatic cells + cancer cells + chemotherapy), and emergent metastases (hepatic cells + cancer cells + chemotherapy + pathophysiological stimulus). When designing the experiment, each experimental group is performed in duplicate, and a hepatic niche condition without cancer cells is always included for baseline. Also, additional scaffolds that extend out to day 15 can be included for each metastatic group. For the growing and dormant niches, this will involve media changes with hepatocyte maintenance media for the days that follow-up to day 15 (Fig. 4).

1. On day 3, warm the hepatocyte maintenance medium.
2. Trypsinize MDA-MB-231 cells, centrifuge at 200 × *g* for 5 min, resuspend in hepatocyte maintenance medium, and count cells using a hemocytometer and 0.1% Trypan Blue solution.
3. Prepare MDA-MB-231 cells so that the number needed is per 400 μL (e.g., prepare as 2500 cells/mL if 500 cells per 400 μL is desired).
4. Move the docking station, Legacy LiverChip® plate, warm maintenance medium and cells into the biosafety cabinet.
5. Aspirate approximately half the effluent from the wells. Move the aspirator to the channel and aspirate up and down the sides. Move the aspirator to the reservoir and aspirate effluent. Return to the well, place the tip of the aspirator in the groove located in the top left-hand corner and gently remove media until the meniscus aligns with the retaining ring.
6. Transfer 400 μL MDA-MB-231 cell suspension to each well. When dispensing cells into the hepatic tissue, do so in a slow dropwise manner. For those wells not receiving cancer cells, add 400 μL hepatocyte maintenance medium.
7. Aspirate any residual media from the reservoirs.

8. Turn on flow by setting the controller to downward flow at a rate of 1 μL/s.
9. Aspirate medium from the reservoirs approximately every 30 s until the meniscus aligns with the top of the retaining ring.
10. Stop flow and add 1.4 mL of hepatocyte maintenance medium to the channel of each liver bioreactor in a dropwise manner being careful not to disturb the cancer cells that were seeded.
11. Return the Legacy LiverChip® plate to the docking station located in the incubator and set the controller to downward flow at a rate of 1 μL/s for 8 h.
12. On day 5, perform a media change as per Subheading 3.3. Modification—the growing and dormant metastases groups should receive hepatocyte maintenance medium containing 10 μM EdU solution (1:1000 dilution of component A of the Click-iT™ Plus EdU Alexa Fluor Imaging kit).
13. On day 7, harvest and fix two growing metastases scaffolds for imaging (*see* Subheading 3.5) and perform a media change on all other wells as per Subheading 3.3. Modification—the dormant and emergent metastases groups should receive hepatocyte maintenance medium containing a clinically relevant chemotherapeutic (e.g., 1 μM doxorubicin). Follow institutional protocols for the safe use and disposal of chemotherapy (*see* **Note 16**).
14. On day 9, repeat the media change as per **step 13**.
15. On day 10, perform a media change on the wells that received chemotherapy as per Subheading 3.3.
16. On day 11, perform a media change on all other wells as per Subheading 3.3.
17. On day 13, harvest and fix two dormant metastases scaffolds for imaging (*see* Subheading 3.5) and perform a media change on all other wells as per Subheading 3.3. Modification—the emergent metastases group should receive hepatocyte maintenance medium containing an inflammatory stimulus (1 μg/mL LPS and 20 nM mEGF) and 10 μM EdU.
18. On day 15, place the Legacy LiverChip® plate inside the biosafety cabinet and collect effluent from each liver bioreactor and store at −20 °C for downstream assays (*see* **Note 17**). Harvest and fix two emergent metastases scaffolds for imaging (*see* Subheading 3.5).

3.5 Immunofluorescence Staining and Imaging

Immunofluorescence enables quantification and assessment of cancer burden. For example, this could be used as a measure of drug efficacy or the effect molecules have on promoting or inhibiting colonization or growth of cancer cells.

3.5.1 Harvesting and Fixing Scaffolds

1. Add 500 μL 2% paraformaldehyde into a 24 well plate (one scaffold per well). Store at 4 °C for at least 1 h prior to harvesting scaffolds.
2. Remove and discard the retaining ring using tweezers.
3. Then using the tweezers, transfer each scaffold into a well of a 24 well plate containing 2% paraformaldehyde and incubate for 1 h at 4 °C (*see* **Note 18**).
4. Remove the fixative and wash each scaffold twice with 500 μL PBS.
5. Add 1 mL PBS and store scaffolds at 4 °C, protected from light until imaging. Image scaffolds within 1 week.

3.5.2 Quantification of Cancer Burden

1. To image a scaffold, transfer it to the coverslip well of a 35 mm glass bottom dish and submerge in a small amount of PBS.
2. Using a fluorescent microscope equipped with a 2× objective, take full-field image of both sides of each scaffold.
3. The presence of RFP cells can be quantified using MetaMorph Image analysis software (Molecular Devices LLC.). The image of the scaffold is inclusively thresholded and the RFP positive portion measured as a percentage of total scaffold area.

3.5.3 Detection of Proliferating Cancer Cells

1. Aspirate the PBS and wash each scaffold twice with 500 μL 3% BSA in PBS.
2. Aspirate the wash solution. Add 500 μL 0.5% Triton X-100 in PBS to each scaffold and incubate in the dark for 20 min at room temperature.
3. Prepare the Click-iT™ EdU cocktail (200 μL/scaffold): 176 μL buffer additive (component D), 4 μL copper protectant (component E), 0.48 μL Alexa Fluor® picolyl azide (component B), and 20 μL reaction buffer additive (component F). Prepare this solution fresh and use within 15 min.
4. Add 200 μL Click-iT™ EdU cocktail to each scaffold and incubate in the dark with gentle rocking for 30 min at room temperature.
5. Aspirate the Click-iT™ EdU cocktail and wash each scaffold once with 500 μL 3% BSA in PBS.
6. Aspirate the wash solution and wash each scaffold once with 500 μL PBS (*see* **Note 19**).
7. Dilute the Hoechst® 33342 in PBS (1:2000).
8. Aspirate PBS and add 500 μL Hoechst® 33342 solution to each scaffold. Incubate in the dark for 30 min at room temperature.
9. Aspirate the Hoechst® 33342 solution and wash each scaffold twice in 500 μL PBS.

10. Add 1 mL PBS and store scaffolds at 4 °C protected from light until imaging. Image scaffolds within 1 week.
11. Use a confocal fluorescent microscope to take Z-stacked images (Fig. 1). To image a scaffold, transfer it to the coverslip well of a 35 mm glass bottom dish and submerge in a small amount of PBS.

3.6 Effluent Collection, Assays and Analyses

The effluent can be collected and stored at −20 °C for a wide range of downstream assays. To date, the following have been performed.

1. Proteomic analyses.

   Cytokine, chemokine, and growth factor protein levels determined by enzyme-linked immunosorbent assays (ELISAs) or Luminex® multiplexed immunoassays and analyzed using Ingenuity Pathway Analysis [10–12, 24].
2. Genomic analyses.

   RNA isolated and sequenced from scaffolds to identify differentially regulated gene sets using Gene Set Enrichment Analysis [30].
3. Therapeutic agent and metabolism analyses.

   The activity of cytochrome P450 enzymes determined by P450-Glo kit for CYP3A4 (Promega) [24] or multiple cytochrome P450 enzymes using an established liquid chromatography–tandem mass spectrometry (LC-MS/MS) method [12, 31].

   Metabolic profiles, clearance correlations, toxicological responses, and acute phase responses determined using LC-MS/MS [25].

4 Notes

1. Should dormancy be the main focus of a study, the Legacy LiverChip® plate can be retrofitted with a softer scaffolding material (PEGDa-SynKRGD hydrogel), which is associated with a larger proportion of cancer cells spontaneously entering dormancy as it more closely mimics the biomechanical environment of liver [11].
2. If researchers do not have access to the LTCDS, cryopreserved vials of hepatocytes, Kupffer cells, liver sinusoidal endothelial cells, and hepatic stellate cells are available for purchase. Immortalized cell lines are also available. Both have been used with success in the Legacy LiverChip® microphysiological system [22, 24, 25].
3. The model is not limited to breast cancer cells. Any carcinoma that is known to metastasize to the liver is anticipated to work.

4. Cancer cells need to be tagged with a fluorescent protein in order to easily distinguish them from the hepatic tissue.
5. Cancer cells are preferably labeled with RFP as hepatocytes can autofluoresce green.
6. The Click-iT™ EdU kit is available in other fluorophores. Ensure it is different to the fluorescent label used to track the cancer cells.
7. If a screw does not align with the others, reverse the direction of the calibrated torque drive to unscrew and then re-screw. Should this not rectify the issue, exchange the screw and washer.
8. Increase the number of tubes for each additional 25 mL of non-parenchymal cell suspension. Lower yield percentages have been observed when loading cells at high densities.
9. Ensure to leave ~100 μL in the pipet so as not to release a bubble which may disrupt the delicate interface between the two Percoll layers.
10. This step removes hepatocytes that may be present.
11. The volume will be determined based on the size of the pellet. If the pellet forms a bullseye (center is clear), then 3 mL is recommended, but if the pellet covers the entire base of the 50 mL tube, then 5 mL is suggested.
12. Based on published calculations [32], a flow rate of 1 μL/s was determined to create sheer stress in the scaffold that is physiologically reflective of that in the liver sinusoid in vivo [18].
13. Downward flow is used temporarily for 8 h to allow the cells to attach and colonize the scaffolding before automatically returning to physiological upward flow.
14. Any time a media change is performed, the effluent can be collected (typically ~1 mL) for downstream assays or experiments (such as proteomic assays, conditioned media, and exosome isolation).
15. A 10 μL pipette tip is added to the end of the glass aspirator to reduce the suction intensity, which results in better tissue formation.
16. To determine the concentration of chemotherapy to use, it is recommended that a 2D cytotoxicity curve be performed on the relevant cancer cell line.
17. For information regarding the disassembly, cleaning, storage, and maintenance of the Legacy LiverChip® microphysiological system, contact the manufacturer, CN Bio Innovations Ltd (*see* https://cn-bio.com or enquiries@cn-bio.com).
18. It is important to do this at 4 °C in order to retain the RFP within the cancer cells.

19. If additional antibody labeling is desired, perform at this time. Following the recommendations from the manufacturer of the primary and secondary antibody. Ensure the samples are protected from light during incubations.

Acknowledgments

The methodologies were informed by studies funded by the VA Merit Award program, the National Institutes of Health (UH3TR000496, GM69668, and GM63569), and the United States Department of Defense (W81XWH-19-1-0494). The funders had no input over any aspects of this work. The author also thanks members of the Wells laboratory and those of Doug Lauffenburger and Linda Griffith (MIT) for informed discussions and suggestions.

References

1. Wells A, Yates C, Shepard CR (2008) E-cadherin as an indicator of mesenchymal to epithelial reverting transitions during the metastatic seeding of disseminated carcinomas. Clin Exp Metastasis 25(6):621–628
2. Giancotti FG (2013) Mechanisms governing metastatic dormancy and reactivation. Cell 155(4):750–764
3. Hackam DG, Redelmeier DA (2006) Translation of research evidence from animals to humans. JAMA 296(14):1731–1732
4. Mestas J, Hughes CC (2004) Of mice and not men: differences between mouse and human immunology. J Immunol 172(5):2731–2738
5. Fantozzi A, Christofori G (2006) Mouse models of breast cancer metastasis. Breast Cancer Res 8(4):212
6. Khanna C, Hunter K (2005) Modeling metastasis in vivo. Carcinogenesis 26(3):513–523
7. Teicher BA (2006) Tumor models for efficacy determination. Mol Cancer Ther 5 (10):2435–2443
8. Benam KH, Dauth S, Hassell B, Herland A, Jain A, Jang KJ et al (2015) Engineered in vitro disease models. Annu Rev Pathol 10:195–262
9. Wikswo JP (2014) The relevance and potential roles of microphysiological systems in biology and medicine. Exp Biol Med (Maywood) 239 (9):1061–1072
10. Clark AM, Kumar MP, Wheeler SE, Young CL, Venkataramanan R, Stolz DB et al (2018) A model of dormant-emergent metastatic breast cancer progression enabling exploration of biomarker signatures. Mol Cell Proteomics 17 (4):619–630
11. Clark AM, Wheeler SE, Young CL, Stockdale L, Shepard Neiman J, Zhao W et al (2016) A liver microphysiological system of tumor cell dormancy and inflammatory responsiveness is affected by scaffold properties. Lab Chip 17(1):156–168
12. Wheeler SE, Clark AM, Taylor DP, Young CL, Pillai VC, Stolz DB et al (2014) Spontaneous dormancy of metastatic breast cancer cells in an all human liver microphysiologic system. Br J Cancer 111(12):2342–2350
13. Wyld L, Gutteridge E, Pinder SE, James JJ, Chan SY, Cheung KL et al (2003) Prognostic factors for patients with hepatic metastases from breast cancer. Br J Cancer 89(2):284–290
14. Tas F (2012) Metastatic behavior in melanoma: timing, pattern, survival, and influencing factors. J Oncol 2012:647684
15. Ren Y, Dai C, Zheng H, Zhou F, She Y, Jiang G et al (2016) Prognostic effect of liver metastasis in lung cancer patients with distant metastasis. Oncotarget 7(33):53245–53253
16. Pond GR, Sonpavde G, de Wit R, Eisenberger MA, Tannock IF, Armstrong AJ (2014) The prognostic importance of metastatic site in men with metastatic castration-resistant prostate cancer. Eur Urol 65(1):3–6
17. King PD, Perry MC (2001) Hepatotoxicity of chemotherapy. Oncologist 6(2):162–176
18. Domansky K, Inman W, Serdy J, Dash A, Lim MH, Griffith LG (2010) Perfused multiwell

plate for 3D liver tissue engineering. Lab Chip 10(1):51–58

19. Clark AM, Wheeler SE, Taylor DP, Pillai VC, Young CL, Prantil-Baun R et al (2014) A microphysiological system model of therapy for liver micrometastases. Exp Biol Med (Maywood) 239(9):1170–1179
20. Beckwitt CH, Clark AM, Ma B, Whaley D, Oltvai ZN, Wells A (2018) Statins attenuate outgrowth of breast cancer metastases. Br J Cancer 119(9):1094–1105
21. Dioufa N, Clark AM, Ma B, Beckwitt CH, Wells A (2017) Bi-directional exosome-driven intercommunication between the hepatic niche and cancer cells. Mol Cancer 16(1):172
22. Khazali AS, Clark AM, Wells A (2018) Inflammatory cytokine IL-8/CXCL8 promotes tumour escape from hepatocyte-induced dormancy. Br J Cancer 118(4):566–576
23. Clark AM, Ma B, Taylor DL, Griffith L, Wells A (2016) Liver metastases: microenvironments and ex-vivo models. Exp Biol Med (Maywood) 241(15):1639–1652
24. Long TJ, Cosgrove PA, Dunn RT 2nd, Stolz DB, Hamadeh H, Afshari C et al (2016) Modeling therapeutic antibody-small molecule drug-drug interactions using a three-dimensional perfusable human liver coculture platform. Drug Metab Dispos 44 (12):1940–1948
25. Sarkar U, Ravindra KC, Large E, Young CL, Rivera-Burgos D, Yu J et al (2017) Integrated assessment of diclofenac biotransformation, pharmacokinetics, and omics-based toxicity in a three-dimensional human liver-immunocompetent coculture system. Drug Metab Dispos 45(7):855–866
26. Chao YL, Shepard CR, Wells A (2010) Breast carcinoma cells re-express E-cadherin during mesenchymal to epithelial reverting transition. Mol Cancer 9:179
27. Taylor DP, Clark A, Wheeler S, Wells A (2014) Hepatic nonparenchymal cells drive metastatic breast cancer outgrowth and partial epithelial to mesenchymal transition. Breast Cancer Res Treat 144(3):551–560
28. Yates C, Shepard CR, Papworth G, Dash A, Beer Stolz D, Tannenbaum S et al (2007) Novel three-dimensional organotypic liver bioreactor to directly visualize early events in metastatic progression. Adv Cancer Res 97:225–246
29. Tsamandouras N, Kostrzewski T, Stokes CL, Griffith LG, Hughes DJ, Cirit M (2017) Quantitative assessment of population variability in hepatic drug metabolism using a perfused three-dimensional human liver microphysiological system. J Pharmacol Exp Ther 360 (1):95–105
30. Chen WLK, Edington C, Suter E, Yu J, Velazquez JJ, Velazquez JG et al (2017) Integrated gut/liver microphysiological systems elucidates inflammatory inter-tissue crosstalk. Biotechnol Bioeng 114(11):2648–2659
31. Pillai VC, Strom SC, Caritis SN, Venkataramanan R (2013) A sensitive and specific CYP cocktail assay for the simultaneous assessment of human cytochrome P450 activities in primary cultures of human hepatocytes using LC-MS/MS. J Pharm Biomed Anal 74:126–132
32. Powers MJ, Domansky K, Kaazempur-Mofrad MR, Kalezi A, Capitano A, Upadhyaya A et al (2002) A microfabricated array bioreactor for perfused 3D liver culture. Biotechnol Bioeng 78(3):257–269

Chapter 16

Fabrication Method of a High-Density Co-Culture Tumor–Stroma Platform to Study Cancer Progression

Harpinder Saini and Mehdi Nikkhah

Abstract

Cancer has now been established as one of the most common chronic diseases due to high mortality rate. The early stage of non-invasive tumors can now be successfully treated leading to have high survival rates; however, the late stage invasive and metastatic tumors still suffer from poor treatment outcomes. Among multiple contributing factors, the role of tumor microenvironment and its complexities has been well recognized in cancer progression. Stromal cells including cancer-associated fibroblasts (CAFs), endothelial cells, adipocytes, immune cells as well as extracellular matrix (ECM) continuously interact with malignant cells and regulate various hallmarks of cancer including tumor growth, invasion, and intravasation. To better understand the role of the interaction between tumor cells and their surrounding microenvironment, numerous model systems ranging from two-dimensional (2D) assays to 3D hydrogels and in vivo murine xenografts have been utilized. While each one of these model systems exhibit certain advantages in studying biological facets of tumor progression, they are often limited to perform well-controlled mechanistic studies due to various factors including lack of tumor–stroma organotypic organization and presence of confounding biochemical and biophysical factors within the tumor microenvironment. In this regard, in the past few years, 3D in vitro microengineered model systems are becoming instrumental to precisely mimic the complexities of the native tumor microenvironment to conduct fundamental and well-designed studies for multiple purposes ranging from biological discovery to therapeutic screening. These model systems include microfluidics, micro-patterned features, and 3D organoids. In this chapter, we will outline the fabrication strategy of our microengineered 3D co-culture tumor–stromal model which comprises high-density array of tumor seeded microwells surrounded by stromal cells, such as CAFs encapsulated within collagen-based hydrogel. The developed platform provides excellent spatial organization of tumor and stromal entities with designated initial architecture and cellular positioning, therefore enabling to study the specific role of cell–cell and cell–ECM interaction on tumor proliferation/expansion, cancer cell migration as well as stromal activation. The developed platform is compatible with standard biological assays enabling gene and protein expression analyses across different types of cancer and co-culture of tumor and stromal cells.

Key words Microengineered systems, Tumor–stroma model, Tumor microenvironment, Co-Culture, Micromolding, Tumor progression

Mo R. Ebrahimkhani and Joshua Hislop (eds.), *Programmed Morphogenesis: Methods and Protocols*, Methods in Molecular Biology, vol. 2258, https://doi.org/10.1007/978-1-0716-1174-6_16,

Abbreviations

2D	Two dimensional
3D	Three dimensional
AFM	Atomic force microscopy
APTMS	(3-Aminopropyl) trimethoxysilane
CAFs	Cancer-associated fibroblasts
DCDMS	Dichlorodimethylsilane
ECM	Extracellular matrix
PDMS	Polydimethylsiloxane
TAM	Tumor-associated macrophages

1 Introduction

According to the statistics provided by the American Cancer Society, about 1.7 million new cancer cases were estimated in United States alone in the year 2019 [1]. While the enhanced awareness and advancements in early stage diagnosis of cancer have improved the outcome of noninvasive tumors, the invasive and metastatic cancers still suffer from poor therapeutic outcomes and high mortality rates [2]. Multiple studies have underlined the role of different factors contributing to tumor progression including genetic and epigenetic changes in cancer cell genome, the presence of cancer stem cells, and the role of the tumor microenvironment [3–5]. While numerous early studies focused on understanding the role of tumor cell genome in cancer progression, recent data has demonstrated the crucial role of tumor microenvironment components including stromal cells and extracellular matrix (ECM) on tumor cell survival and proliferation, invasion and immune evasion [6–8]. For instance, cancer-associated fibroblasts (CAFs) have been shown to extensively participate in stromal ECM remodeling through abundant deposition of matrix components including collagen I, collagen III, and fibronectin [9, 10]. Additionally, these cells (CAFs) have been shown to secrete high amounts of crosslinking enzymes such as lysyl oxidase to upregulate matrix stiffness leading to enhanced integrin-based mechanotransduction in both tumor and stromal cells [11]. Tumor-associated endothelial cells on the other hand form blood vessels to allow the supply of nutrients and gas exchange to the tumor cells which have undergone hyperproliferation and grown in mass beyond 1–2 mm^3 [12, 13]. Due to the imbalance between proangiogenic factors such as vascular endothelial growth factor, basic fibroblast growth factor, angiostatin, and anti-angiogenic factors including thrombospondin, interferon, and tissue inhibitor of metalloproteinases, the blood vessels formed in the tumor microenvironment are thin,

immature, and leaky in nature [14, 15]. The newly formed blood vessels also have reduced layer of pericytes and basement membrane around them as compared to normal vasculature which therefore aids in multiple steps of metastatic cascade including invasion and intravasation [14, 15]. Recent studies have also shed light on the role of immune cells such as macrophages within tumor environment on cancer progression [16, 17]. It has been observed that macrophages within tumor microenvironment can adopt multiple phenotypes ranging from classically activated M1-polarized macrophages to alternatively activated M2-polarized macrophages [17]. Since M1 macrophages are associated with secretion of pro-inflammatory cytokines, they are known to participate in activating the innate immune response against pathogens and thereby promoting antitumor immune response [17]. On the other hand, M2 macrophages promote tissue repair and secrete anti-inflammatory cytokines and therefore participates in tumor growth, immunosuppression, matrix remodeling, tumor invasion, and angiogenesis [16, 17]. While our knowledge about various components of the tumor microenvironment and their role in tumor progression has significantly increased in the past few years, there are still many unknowns about different components and biological signaling cascades within the complex milieu of the tumor microenvironment. Multiple attempts are being undertaken to build an in-depth understanding about the mechanism of action of the cross talk between cancer cells and the surrounding tumor microenvironment components to develop targeted therapies for treating late-stage tumors [18].

To date, various model systems have been developed and utilized to identify the mechanism of action for different phenotypic and genotypic changes within tumor cells due to their cross talk with specific stromal cells and ECM components. Many early studies in the past have utilized traditional two-dimensional (2D) assays since they are easy to develop and provide the capability to perform functional tests such as proliferation assays, migration assays as well as gene and protein expression assays [19]. However, it is now widely accepted that tumors within native conditions exist in three-dimensional (3D) microenvironment with spatial organization that is difficult to mimic within the 2D culture systems [20]. Such differences in dimensionality lead to significant alteration in phenotypic and genotypic signatures of cancer cells which can possibly explain failure of multiple drugs in clinical trials that were found successful in the initial in vitro studies utilizing conventional 2D assays [19, 20]. Animal models, such as murine xenografts, on the other hand provide tumor cells with accurate dimensionality and various complexities of the native tumor microenvironment. Similar to 2D systems, animal models enable visualization of multiple phenomenon including change in gene and protein expression, tumor growth, and metastatic burden

[13]. However, despite significant advantages over 2D conventional systems, animal models also suffer from several limitations. For instance, animal models exhibit multiple confounding factors, due to presence of different cell types and ECM components, which significantly limits the ability to perform cause and effect studies and dissect the role of a single component of the tumor microenvironment on cancer progression [13]. Additionally, due to inherent anatomical differences between humans and animals, including difference in their immune systems and drug permeation, they provide limited translational values for cancer therapy [21, 22]. In this regard, researchers have given significant attention toward development of next-generation 3D in vitro microengineered model systems that mimic the dimensionality and spatial arrangement of native tumor tissue with high precision and fidelity [13, 20]. Various components of the tumor microenvironment including stromal cells, ECM, and vasculature can be established with appropriate experimental controls within 3D in vitro microengineered models to study their individualistic and synergistic role on tumor progression [20].

Three-dimensional (3D) models including microscale surface topographies [23–27], organoid-based models [28–31], microfluidic systems [15, 32–35], and micro-patterned platforms [36–38] have been fabricated to study cancer cells behavior or establish the role of tumor microenvironment in cancer progression within both context of fundamental biological discoveries and therapeutic developments [13, 20]. For instance, organoid culture has been adopted by various researchers to study the role of cell–cell and cell–ECM interaction between tumor cells and stromal cells on different facets of tumor progression including tumor growth, tumor migration, and establishing the role of hypoxia on phenotypic and genotypic changes within tumor cells [30, 39]. Despite significant advantages, these models suffer from multiple limitations. Most of the organoid-based models rely on self-organization capabilities of the tumor and stromal cells and thus do not allow precise control over spatial arrangement between different cell types [39]. Additionally, organoid models still suffer from low reproducibility in terms of spheroid size using current approaches which can significantly impact tumor metabolism and crucial gene signatures [39]. Lastly, multiple crucial factors within the tumor microenvironment are difficult to reproduce within organoid-based models including mechanical stress and interstitial fluid flow with well-defined regime [13]. In contrast to organoid-based models, microfluidic systems, often integrated with hydrogel biomaterials, have provided unique capabilities to establish well-defined organization of the tumor and stromal entities and incorporate specific components of the tumor microenvironment such as vasculature to establish nutrient gradient and study different steps of the metastatic cascade (i.e., intravasation, extravasation) [13, 15, 32, 34,

35]. The tumor microenvironment developed using microfluidic systems are often within an enclosed setup which may not enable in-situ probing of the dynamic change in stromal ECM properties during active tumor cell migration, such as by using atomic force microscopy (AFM) as was shown in our earlier work [36]. Alternatively, micropatterned 3D tumor models, based on the use of hydrogel biomaterials [37], have provided the ability to incorporate the complexities of the native tumor microenvironment for defined biological studies. Such systems primarily provide the advantage of cell-specific cues by utilizing ECM-derived natural (e.g., collagen) or synthetic hydrogels with well-tuned properties [40]. In addition, micropatterning techniques enable spatial localization of target cell types, with a well-defined tissue architecture, to mechanistically study various biological processes such as tissue (e.g., mammary, vascular) morphogenesis, regeneration, stem cell differentiation, or disease progression [41–47].

Within the same context, our group has also utilized micromolding technique, similar to the techniques proposed by previous groups [37], to fabricate high-density 3D tumor–stroma platform with the co-culture of tumor and stromal cells (rather than monoculture) to perform numerous studies on tumor progression in response to various stromal cell types and ECM as well as to test anticancer drug resistance [36]. The platform also enables to study the specific change in gene and protein expression when tumor cells are co-cultured with stromal cells and ECM and mechanistically delineate the role of stromal components on tumor progression [48]. Notably, as stated earlier, due to the open top nature of the platform, our model provides the capability to integrate with nanoindentation techniques such as AFM to study the in-situ dynamic changes in ECM biophysical properties during active cancer cell migration [36, 48]. While our group utilized the tumor–stroma platform to study the specific role of CAFs in cancer progression in the presence of breast tumor cells [48] (i.e., MDA-MB-231, MCF7), we envision that the platform can be adapted to include different types of tumor and stromal cells from other type of cancers. Herein, we detail out the materials and the fabrication strategy to encapsulate cells within the collagen hydrogel and develop the proposed high-density tumor–stromal model.

2 Materials

2.1 Photolithography

1. SU8–2075 (Microchem).
2. Silicon Wafer (University Wafer).
3. Isopropyl alcohol.

2.2 Soft Lithography

1. Sylgard-184 PDMS kit (Dow Corning).
2. Dichlorodimethylsilane (DCDMS, Sigma Aldrich).

2.3 Surface Treatment

1. 98% Ethanol
2. 100% Ethanol
3. (3-Aminopropyl) trimethoxysilane (APTMS 97% solution, Sigma Aldrich)
4. Glutaraldehyde solution (50%, cell culture based, VWR).
5. Pluronic F127 (Sigma Aldrich).

2.4 3D Coculture of Tumor–Stroma Sample

1. High-concentration Rat Tail Collagen I solution (Corning).
2. Sodium hydroxide (Sigma Aldrich).
3. Phenol red (Sigma Aldrich).
4. 0.5% Trypsin-EDTA (Life Technologies).
5. DMEM media (Life Technologies).
6. Fetal Bovine Serum (Life Technologies).
7. PENSTREP (Life Technologies).
8. L-Glutamine (Life Technologies).

2.5 Instruments

1. Class 100 cleanroom.
2. UV lamp.
3. Air-based plasma.
4. High-frequency water-based sonicator.
5. Plate shaker.
6. Vacuum desiccators.
7. Vacuum oven.
8. 80 °C oven
9. Fluorescent microscope (Confocal or Apotome-based microscopy).
10. Cell culture chamber for microscope.

2.6 Software

1. AutoCAD®.
2. ImageJ.

3 Methods

3.1 Photolithography

1. In AutoCAD® software prepare 8 cm × 8 cm photomask of an array of circular microwells with diameter of each microwell set as 75 μm and center to center distance between each microwell as 250 μm. The depth of each microwell is defined to be 300 μm to generate thick microtissues.

2. Silicon wafer for each design is fabricated in a standard class 100 cleanroom. SU8–2075 is utilized as the photoresist to coat the wafer which is exposed to UV light to generate the desired features for both PDMS holders and stamps. The height of the SU8 photoresist will be optimized to be 300 μm, based on the rotational speed of the spinner. This will yield to the development of microwells with a depth of 300 μm.

3.2 Soft Lithography

The following steps will be followed to fabricate both PDMS stamps and PDMS holders.

1. In a plastic cup first add 10:1 ratio (w/w ratio) of Sylgard 184 PDMS base to the curing agent and mix properly to ensure equal distribution of all the parts.
2. Degas the solution to remove the bubbles formed due to mixing in a vacuum desiccator.
3. Take a new 100 mm plastic dish to secure the silicon wafer using scotch tape such that the feature side is facing upwards. *See* **Note 1**.
4. In a chemical safety cabinet, take a 100 mm glass dish containing 35 mm dish at the center filled with 0.5–1.5 mL of DCDMS. *See* **Note 2**.
5. Invert the plastic dish on top of the glass dish and keep it in well-ventilated area of the chemical hood for 10 min to allow vapor-based silanization.
6. After silanization is completed, pour the degassed PDMS solution prepared in **step 1** on the silicon wafer as quickly as possible and degas the assembly in a vacuum desiccator to remove any bubbles.
7. After all the bubbles are removed, keep the assembly of silicon wafer with PDMS in 80 °C oven overnight.
8. While the amount of Sylgard 184 base used for fabricating PDMS holder was about 30 mg; the amount of Sylgard 184 base solution required for PDMS stamps will be higher (~60–70 mg) such that the final thickness of the stamps is higher and therefore be utilized to micromold the collagen hydrogel.

3.3 Surface Treatment of the PDMS Holders

1. In a chemical safety cabinet, prepare a solution of 2% APTMS in 98% ethanol. *See* **Note 3**.
2. Cut the PDMS holders and clean them with feature side down on the sticky side of the scotch tape to take off any dust.
3. Next, with features side up, place the clean PDMS holders in a plasma-compatible dish (35 mm plastic dish) and treat them with air-based plasma for 4 min 30 secs at high frequency.

4. After completion of the plasma treatment, remove the PDMS holders and immerse them immediately in already prepared APTMS solution as prepared in **step 1**.
5. The APTMS solution containing PDMS holders is incubated at 60 °C for 1 h.
6. After the silanization treatment, remove the PDMS holders and sonicate them in a 100% ethanol in a water-based sonicator at high frequency for 20 min to remove any loosely bound silane.
7. Next, wash the PDMS holders in 100% ethanol at a high-speed shaker for 5 times at 10-min interval to remove all the excess APTMS. *See* **Note 4**.
8. Keep the PDMS holders in 80 °C oven for 30–60 min to increase the bond strength between hydroxyl group and silane groups on the holders.
9. In a chemical safety cabinet, prepare a 0.1% glutaraldehyde solution in DI water which are then poured over the silane-treated PDMS holders for 1 h at room temperature.
10. Remove the holders from the glutaraldehyde solution and wash them vigorously on the shaker with DI water for 5 times at 5-min interval.
11. To ensure complete removal of the excess glutaraldehyde, keep the PDMS holders exposed to the heat in the 80 °C oven overnight with the lid of the plastic dish off. *See* **Note 5**.

3.4 Surface Treatment of PDMS Stamps

1. The PDMS stamps are sterilized in a glass Petri dish first using liquid autoclave cycle followed by dry autoclave cycle. The stamps are then kept overnight in the 80 °C oven to allow complete drying of the PDMS stamps.
2. Next, 1–2% pluronic F127 solution is prepared in DI water and incubated the solution at 4 °C for at least 30 min to obtain a clear solution.
3. In a biosafety cabinet, the sterilized PDMS stamps are immersed into the prepared pluronic F127 solution which is then kept overnight at 4 °C to make the PDMS surface protein repellant to ensure easy detachment from the collagen hydrogel solution.

3.5 Development of the 3D Tumor–Stroma Coculture Model

1. The glutaraldehyde-treated PDMS holders are removed from the oven and then sterilized in 70% ethanol for more than 15 min. *See* **Note 6**.
2. Using clean sterilized forceps, the PDMS holders are transferred to a new plastic dish to allow them to dry.
3. On an ice bath, collagen-I hydrogel solution is prepared by mixing high-concentration rat tail collagen-I stock with 1 N

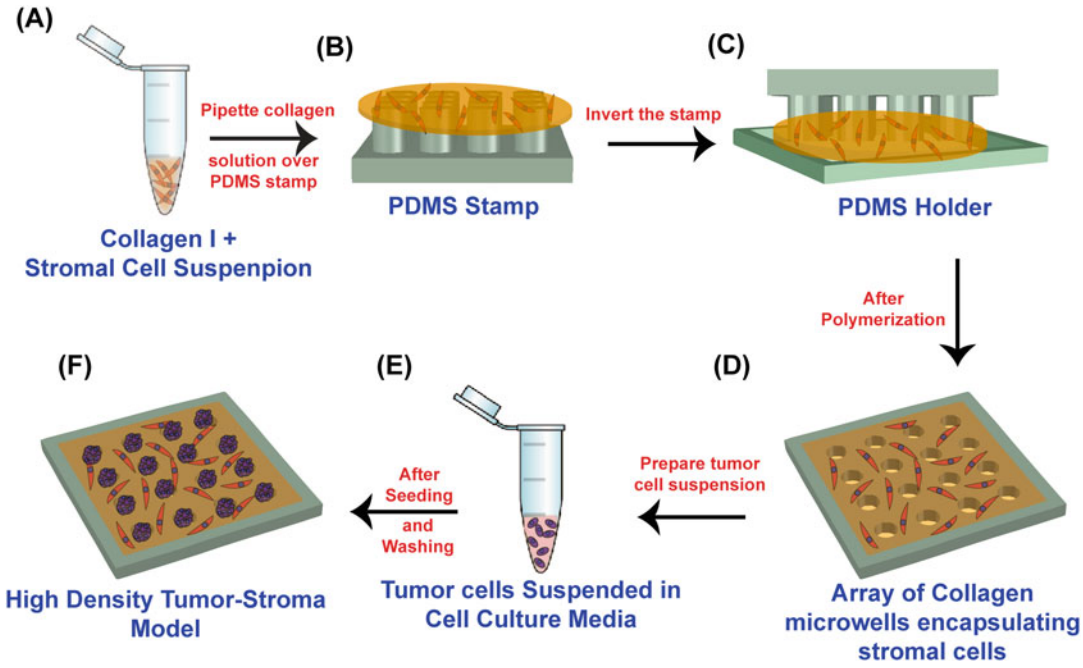

Fig. 1 Schematic of the fabrication method of micropatterned high-density tumor–stroma co-culture model. (**a**) Prepare a collagen + CAFs cell suspension by gently mixing. (**b**) Pipette about 50 μL collagen + CAF cell suspension onto the pluronic-treated PDMS stamp. (**c**) Invert the PDMS stamp onto surface-treated PDMS holder and allow this assembly to incubate at 37 °C for 30 min. (**d**) After polymerization of collagen hydrogel, gently remove the PDMS stamp to obtain an array of empty microwells surrounded by CAFs encapsulated within collagen. (**e**) Prepare high-density tumor cell suspension in media and break any clumps to obtain single cell suspension. (**f**) Seed a high-density drop of tumor cells (50 μL) on the platform, and after 3 min wash the unpatterned cells to obtain a high-density tumor–stroma model

NaOH, phenol red, and media to get a final concentration of 4 mg/mL. *See* **Note 7**.

4. The tumor cells (e.g., MDA-MB-231, MCF7) (purchased from commercial vendors such as ATCC) and cancer-associated fibroblasts (CAFs, ATCC) are then trypsinized using 0.05% Trypsin-EDTA in PBS and counted using hemocytometer and trypan blue to measure the viability of the cells.
5. CAFs are centrifuged and mixed gently with collagen hydrogel solution prepared above at a final density of 2×10^6 cells/mL (Fig. 1a). Avoid bubbles during mixing.
6. The PDMS stamps are removed from pluronic solution and then washed three times with PBS to remove any remaining pluronic solution.
7. About 50–70 μL of the CAF-embedded collagen-I hydrogel solution is pipetted onto the PDMS stamp and gently spread using pipette tip (Fig. 1b). *See* **Note 8**.

8. The cell solution-coated PDMS stamp is then inverted on top of the PDMS holder, and this assembly is incubated at 37 °C for 30 min to allow polymerization of the cell-embedded collagen-I hydrogel (Fig. 1c). *See* **Note 9**.
9. After polymerization of the hydrogel, the PDMS stamp is picked up gently using forceps in the upward direction to avoid the shearing of the microwells and distortion of the pattern (Fig. 1d).
10. The tumor cells are now centrifuged and resuspended in the media at a final cell density of 7–10 $\times$ 10^6 cells/mL (Fig. 1e).
11. About 50 μL of the tumor cell suspension solution is then pipetted onto the 3D culture sample for about 3 min and monitored under the microscope to observe filling of the microwells with the tumor cells (to enable easy distinction between tumor cells and stromal cells, tumor cells were transduced with mCherry protein). It is noteworthy to mention that this method is written for a micro-well diameter of 75 μm for proper positioning of the cells into the micro-wells. In case of larger micro-wells, further optimization may be required to avoid dislodging of the cells upon washing.
12. To remove the excessive tumor cells from the unpatterned regions upon seeding (in between micro-wells), the sample is tilted at 45° and then washed gently 2–3 times with 450 μL cell culture media. In between consecutive washes, it is crucial to check for cells in the unpatterned regions using a fluorescent microscope to ensure optimal washing and minimal dislodging of the tumor cells from the microwells (Fig. 1f).
13. Each sample can then be immersed in a well of 24-well plate with 500-μL media. *See* **Note 10**.

3.6 Microscopy for Subsequent Studies on Tumor Cell Behavior (e.g., Migration)

1. In order to visualize and quantify the tumor cell migration in the presence and absence of stromal cells such as CAFs as demonstrated in this work, the samples are imaged using a fluorescent microscope with Z-stack imaging modality every alternate day (Fig. 2a, b).
2. Since tumor cells are transduced to express mCherry protein, it is essential to image each sample separately from others to avoid the overexposure of the cells by fluorescent light that can lead to cell death due to high energy of the light.
3. The samples are placed in a plastic dish and then imaged in the environmental chamber. Z-stack images are taken from three random locations of each sample to average the cell migration parameters. *See* **Note 11**.

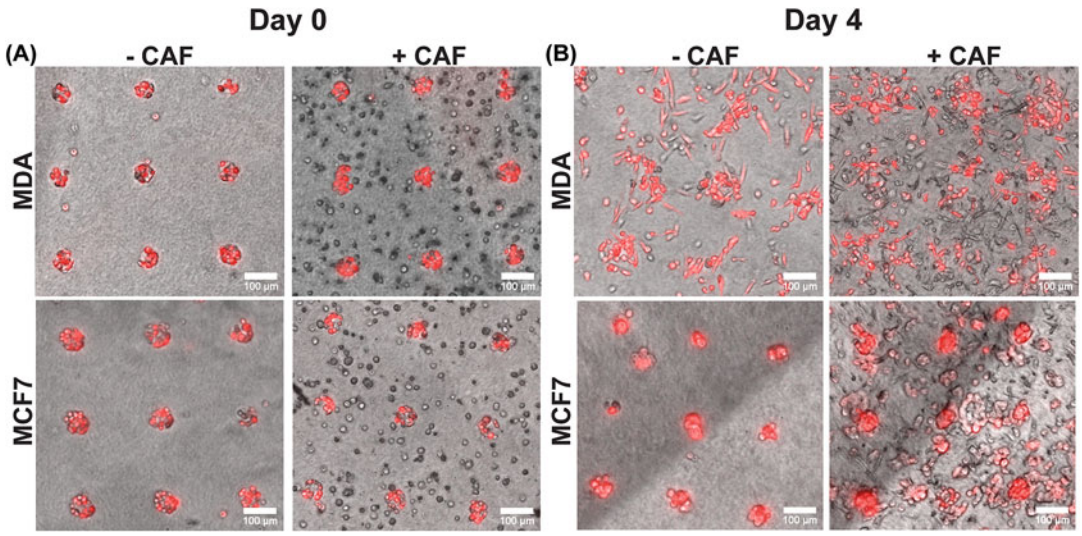

Fig. 2 (**a**) Representative phase contrast and fluorescent images of tumor–stroma model for mono-culture and co-culture groups of MDA-MB-231 and MCF7 cells (DsRed) along with CAFs at day 0. (**b**) MDA-MB-231 tumor cell migration and clustering of MCF7 cells can be visualized in mono-culture and co-culture groups at day 4. Scale bar represents 100 μm

4. Images should be taken from multiple replicates to allow quantification of cell migration parameters from a large dataset and for subsequent statistical analyses.
5. To perform live cell migration, each sample should be placed in a small size plastic dish filled with media in a chamber filled with 5% CO_2 at 33–34 °C for 14–16 h. Z-stack images are acquired from multiple locations of the samples at a frequency of 40–60 min within different regions of interest (ROIs) of each sample to accurately quantify parameters including cell speed, persistence, and directionality using various established software.

4 Notes

1. The silicon wafer is secured to the plastic dish using scotch tape over the edges. However, care should be taken that for generating PDMS mold the feature side of the wafer is free of any scotch tape.
2. The amount of DCDMS used for vapor-based silanization of the silicon wafer greatly depends on the humidity in the air. The amount of silane needed for successful silanization should be tested by the researcher. Along with the volume of the silane, researchers can also vary the amount of the time required for vapor deposition of the silane on the wafer. In order to check

for successful silanization, a clear DCDMS deposition can be seen on the scotch tape when smeared by a spatula. Overdeposition of silane vapors should also be avoided as this can lead to byproduct formation with PDMS when kept at high temperatures.

3. In order to ensure successful surface treatment of the PDMS holders, APTMS solution needs some amount of water for silane bond formation. Therefore, do not use 100% ethanol. Using lower percentage of ethanol such as 70% can lead to formation of various byproducts. Researchers need to optimize the amount of ethanol percentage for successful silanization of the PDMS holders. A good starting range of ethanol is about 97–98%.
4. It is important to remove any excess APTMS from the PDMS holders due to its nature to form orange-based fluorescent byproduct with glutaraldehyde solution which can later interfere with any fluorescent microscopy. In case any byproduct is formed, optimize the percentage of both APTMS and glutaraldehyde solutions along with rigorous washing at a plate shaker with high speed.
5. Do not use PDMS holders without overnight evaporation of glutaraldehyde as excess glutaraldehyde can lead to fixation of stromal cells embedded in the collagen hydrogel.
6. Surface-treated PDMS holders usually stick to the plastic dish. During ethanol sterilization, do not aspirate the ethanol solution, rather use the forceps for easy removal of these holders to a new Petri dish.
7. Always prepare the collagen hydrogel solution by mixing all the described components as per the manufacturer's instruction in an Eppendorf tube kept on an ice bath. The solution should be prepared by gentle mixing to avoid any bubble formation as this can interfere in micromolding of the hydrogel.
8. During pipetting of the cell-embedded hydrogel solution on top of the PDMS stamps, make sure that no bubbles are formed as they can lead to formation of microwells with distorted dimensions. Most of the bubbles formed at this step can be due to rigorous mixing of collagen solution and improper surface treatment of the PDMS stamps.
9. In order to obtain a homogenous distribution of the cells encapsulated within the collagen hydrogel solution, the dish containing PDMS stamp-collagen-holder assembly can be flipped every minute. At higher concentration of collagen such as 4 mg/mL, the need to flip is minimal since the hydrogel polymerization is very quick. However, if lower concentration of the collagen is used, then flipping the dish becomes more necessary and frequency needs to be varied.

10. The hydrogel-immobilized PDMS holders can float in the media within 24-well plate due to the hydrophobic nature of the PDMS. However, a gentle push by forceps in the downward direction will ensure their complete immersion in the media.
11. In order to avoid overexposure of the transduced cells within the 3D tumor–stroma samples, it is essential to minimize the number of Z-stacks. To ensure imaging of entire thickness of the sample, increase the optimal distance between two Z-stack slices to as high as 10 μm. In case exposure time for the transduced cells is high, it is better to re-transduce the cells to increase their brightness.

Acknowledgments

The authors would like to acknowledge National Science Foundation (NSF) Award Number 1914680 for supporting this study.

References

1. Siegel RL, Miller KD, Jemal A (2019) Cancer statistics, 2019. CA Cancer J Clin 69(1):7–34. https://doi.org/10.3322/caac.21551
2. Miller KD, Nogueira L, Mariotto AB, Rowland JH, Yabroff KR, Alfano CM, Jemal A, Kramer JL, Siegel RL (2019) Cancer treatment and survivorship statistics, 2019. CA Cancer J Clin 69(5):363–385. https://doi.org/10.3322/caac.21565
3. Liu Q, Zhang H, Jiang X, Qian C, Liu Z, Luo D (2017) Factors involved in cancer metastasis: a better understanding to "seed and soil" hypothesis. Mol Cancer 16(1):176. https://doi.org/10.1186/s12943-017-0742-4
4. Brabletz T, Jung A, Spaderna S, Hlubek F, Kirchner T (2005) Migrating cancer stem cells — an integrated concept of malignant tumour progression. Nat Rev Cancer 5 (9):744–749. https://doi.org/10.1038/nrc1694
5. Joyce JA, Pollard JW (2009) Microenvironmental regulation of metastasis. Nat Rev Cancer 9(4):239–252. https://doi.org/10.1038/nrc2618
6. Wang M, Zhao J, Zhang L, Wei F, Lian Y, Wu Y, Gong Z, Zhang S, Zhou J, Cao K, Li X, Xiong W, Li G, Zeng Z, Guo C (2017) Role of tumor microenvironment in tumorigenesis. J Cancer 8(5):761–773. https://doi.org/10.7150/jca.17648
7. Balkwill FR, Capasso M, Hagemann T (2012) The tumor microenvironment at a glance. J Cell Sci 125(23):5591–5596. https://doi.org/10.1242/jcs.116392
8. Walker C, Mojares E, Del Río Hernández A (2018) Role of extracellular matrix in development and cancer progression. Int J Mol Sci 19 (10):3028
9. Kalluri R (2016) The biology and function of fibroblasts in cancer. Nat Rev Cancer 16 (9):582–598. https://doi.org/10.1038/nrc.2016.73
10. Kalluri R, Zeisberg M (2006) Fibroblasts in cancer. Nat Rev Cancer 6(5):392–401. https://doi.org/10.1038/nrc1877
11. Jang I, Beningo KA (2019) Integrins, CAFs and mechanical forces in the progression of cancer. Cancers 11(5):721
12. Hillen F, Griffioen AW (2007) Tumour vascularization: sprouting angiogenesis and beyond. Cancer Metastasis Rev 26(3):489–502. https://doi.org/10.1007/s10555-007-9094-7
13. Peela N, Truong D, Saini H, Chu H, Mashaghi S, Ham SL, Singh S, Tavana H, Mosadegh B, Nikkhah M (2017) Advanced biomaterials and microengineering technologies to recapitulate the stepwise process of cancer metastasis. Biomaterials 133:176–207. https://doi.org/10.1016/j.biomaterials.2017.04.017

14. Nishida N, Yano H, Nishida T, Kamura T, Kojiro M (2006) Angiogenesis in cancer. Vasc Health Risk Manag 2(3):213–219. https://doi.org/10.2147/vhrm.2006.2.3.213
15. Nagaraju S, Truong D, Mouneimne G, Nikkhah M (2018) Microfluidic tumor–vascular model to study breast cancer cell invasion and intravasation. Adv Healthc Mater 7 (9):1701257. https://doi.org/10.1002/adhm.201701257
16. Liu Y, Cao X (2015) The origin and function of tumor-associated macrophages. Cell Mol Immunol 12(1):1–4. https://doi.org/10.1038/cmi.2014.83
17. Yang L, Zhang Y (2017) Tumor-associated macrophages: from basic research to clinical application. J Hematol Oncol 10(1):58. https://doi.org/10.1186/s13045-017-0430-2
18. Roma-Rodrigues C, Mendes R, Baptista PV, Fernandes AR (2019) Targeting tumor microenvironment for cancer therapy. Int J Mol Sci 20(4):840
19. Kapałczyńska M, Kolenda T, Przybyła W, Zajączkowska M, Teresiak A, Filas V, Ibbs M, Bliźniak R, Łuczewski Ł, Lamperska K (2016) 2D and 3D cell cultures – a comparison of different types of cancer cell cultures. Arch Med Sci 14(4):910–919. https://doi.org/10.5114/aoms.2016.63743
20. Infanger DW, Lynch ME, Fischbach C (2013) Engineered culture models for studies of tumor-microenvironment interactions. Annu Rev Biomed Eng 15(1):29–53. https://doi.org/10.1146/annurev-bioeng-071811-150028
21. Todo H (2017) Transdermal permeation of drugs in various animal species. Pharmaceutics 9(3):33
22. Wagar LE, DiFazio RM, Davis MM (2018) Advanced model systems and tools for basic and translational human immunology. Genome Med 10(1):73. https://doi.org/10.1186/s13073-018-0584-8
23. Nikkhah M, Strobl JS, Schmelz EM, Roberts PC, Zhou H, Agah M (2011) MCF10A and MDA-MB-231 human breast basal epithelial cell co-culture in silicon micro-arrays. Biomaterials 32(30):7625–7632. https://doi.org/10.1016/j.biomaterials.2011.06.041
24. Nikkhah M, Strobl JS, Peddi B, Agah M (2008) Cytoskeletal role in differential adhesion patterns of normal fibroblasts and breast cancer cells inside silicon microenvironments. Biomed Microdevices 11(3):585. https://doi.org/10.1007/s10544-008-9268-2
25. Nikkhah M, Strobl JS, Agah M (2008) Attachment and response of human fibroblast and breast cancer cells to three dimensional silicon microstructures of different geometries. Biomed Microdevices 11(2):429. https://doi.org/10.1007/s10544-008-9249-5
26. Nikk0hah M, Strobl JS, De Vita R, Agah M (2010) The cytoskeletal organization of breast carcinoma and fibroblast cells inside three dimensional (3-D) isotropic silicon microstructures. Biomaterials 31(16):4552–4561. https://doi.org/10.1016/j.biomaterials.2010.02.034
27. Nikkhah M, Edalat F, Manoucheri S, Khademhosseini A (2012) Engineering microscale topographies to control the cell–substrate interface. Biomaterials 33(21):5230–5246. https://doi.org/10.1016/j.biomaterials.2012.03.079
28. Liu T, Chien C-C, Parkinson L, Thierry B (2014) Advanced micromachining of concave microwells for long term on-chip culture of multicellular tumor spheroids. ACS Appl Mater Interfaces 6(11):8090–8097. https://doi.org/10.1021/am500367h
29. Tang Y, Liu J, Chen Y (2016) Agarose multiwells for tumour spheroid formation and anticancer drug test. Microelectron Eng 158:41–45. https://doi.org/10.1016/j.mee.2016.03.009
30. Xu H, Lyu X, Yi M, Zhao W, Song Y, Wu K (2018) Organoid technology and applications in cancer research. J Hematol Oncol 11 (1):116. https://doi.org/10.1186/s13045-018-0662-9
31. Singh M, Close DA, Mukundan S, Johnston AP, Sant S (2015) Production of uniform 3D microtumors in hydrogel microwell arrays for measurement of viability, morphology, and signaling pathway activation. Assay Drug Dev Technol 13(9):570–583. https://doi.org/10.1089/adt.2015.662
32. Truong D, Puleo J, Llave A, Mouneimne G, Kamm RD, Nikkhah M (2016) Breast cancer cell invasion into a three dimensional tumor-stroma microenvironment. Sci Rep 6 (1):34094. https://doi.org/10.1038/srep34094
33. Peela N, Barrientos ES, Truong D, Mouneimne G, Nikkhah M (2017) Effect of suberoylanilide hydroxamic acid (SAHA) on breast cancer cells within a tumor–stroma microfluidic model. Integr Biol 9(12):988–999. https://doi.org/10.1039/c7ib00180k
34. Truong DD, Kratz A, Park JG, Barrientos ES, Saini H, Nguyen T, Pockaj B, Mouneimne G,

LaBaer J, Nikkhah M (2019) A human organotypic microfluidic tumor model permits investigation of the interplay between patient-derived fibroblasts and breast cancer cells. Cancer Res 79(12):3139–3151. https://doi.org/10.1158/0008-5472.Can-18-2293

35. Truong D, Fiorelli R, Barrientos ES, Melendez EL, Sanai N, Mehta S, Nikkhah M (2019) A three-dimensional (3D) organotypic microfluidic model for glioma stem cells – vascular interactions. Biomaterials 198:63–77. https://doi.org/10.1016/j.biomaterials.2018.07.048
36. Saini H, Rahmani Eliato K, Silva C, Allam M, Mouneimne G, Ros R, Nikkhah M (2018) The role of desmoplasia and stromal fibroblasts on anti-cancer drug resistance in a microengineered tumor model. Cell Mol Bioeng 11 (5):419–433. https://doi.org/10.1007/s12195-018-0544-9
37. Nelson CM, Inman JL, Bissell MJ (2008) Three-dimensional lithographically defined organotypic tissue arrays for quantitative analysis of morphogenesis and neoplastic progression. Nat Protoc 3(4):674–678. https://doi.org/10.1038/nprot.2008.35
38. Peela N, Sam FS, Christenson W, Truong D, Watson AW, Mouneimne G, Ros R, Nikkhah M (2016) A three dimensional micropatterned tumor model for breast cancer cell migration studies. Biomaterials 81:72–83. https://doi.org/10.1016/j.biomaterials.2015.11.039
39. Cui X, Hartanto Y, Zhang H (2017) Advances in multicellular spheroids formation. J R Soc Interface 14(127):20160877. https://doi.org/10.1098/rsif.2016.0877
40. Bahlmann LC, Smith LJ, Shoichet MS Designer biomaterials to model cancer cell invasion in vitro: predictive tools or just pretty pictures? Adv Funct Mater 30 (16): 1909032. https://doi.org/10.1002/adfm.201909032
41. Saini H, Navaei A, Van Putten A, Nikkhah M (2015) 3D cardiac microtissues encapsulated with the co-culture of cardiomyocytes and cardiac fibroblasts. Adv Healthc Mater 4 (13):1961–1971. https://doi.org/10.1002/adhm.201500331
42. Zorlutuna P, Annabi N, Camci-Unal G, Nikkhah M, Cha JM, Nichol JW, Manbachi A, Bae H, Chen S, Khademhosseini A (2012) Microfabricated biomaterials for engineering 3D tissues. Adv Mater 24(14):1782–1804. https://doi.org/10.1002/adma.201104631
43. Hassanzadeh P, Kharaziha M, Nikkhah M, Shin SR, Jin J, He S, Sun W, Zhong C, Dokmeci MR, Khademhosseini A, Rolandi M (2013) Chitin nanofiber micropatterned flexible substrates for tissue engineering. J Mater Chem B 1(34):4217–4224. https://doi.org/10.1039/C3TB20782J
44. Annabi N, Tsang K, Mithieux SM, Nikkhah M, Ameri A, Khademhosseini A, Weiss AS (2013) Highly elastic micropatterned hydrogel for engineering functional cardiac tissue. Adv Funct Mater 23(39):4950–4959. https://doi.org/10.1002/adfm.201300570
45. Dolatshahi-Pirouz A, Nikkhah M, Kolind K, Dokmeci MR, Khademhosseini A (2011) Micro- and nanoengineering approaches to control stem cell-biomaterial interactions. J Funct Biomater 2(3):88–106. https://doi.org/10.3390/jfb2030088
46. Nelson CM, VanDuijn MM, Inman JL, Fletcher DA, Bissell MJ (2006) Tissue geometry determines sites of mammary branching morphogenesis in organotypic cultures. Science 314(5797):298–300. https://doi.org/10.1126/science.1131000
47. Nikkhah M, Eshak N, Zorlutuna P, Annabi N, Castello M, Kim K, Dolatshahi-Pirouz A, Edalat F, Bae H, Yang Y, Khademhosseini A (2012) Directed endothelial cell morphogenesis in micropatterned gelatin methacrylate hydrogels. Biomaterials 33(35):9009–9018. https://doi.org/10.1016/j.biomaterials.2012.08.068
48. Saini H, Rahmani Eliato K, Veldhuizen J, Zare A, Allam M, Silva C, Kratz A, Truong D, Mouneimne G, LaBaer J, Ros R, Nikkhah M (2020) The role of tumor-stroma interactions on desmoplasia and tumorigenicity within a microengineered 3D platform. Biomaterials 247:119975. https://doi.org/10.1016/j.biomaterials.2020.119975

Part V

In Vivo Therapeutic Applications

Chapter 17

A Method for Organoid Transplantation and Whole-Mount Visualization of Post-Engraftment Vascularization

Amy E. Emerson, Emily M. Slaby, and Jessica D. Weaver

Abstract

As the field of organoid development matures, the need to transplant organoids to evaluate and characterize their functionality grows. Decades of research developing islet organoid transplantation for the treatment of type 1 diabetes can contribute substantially to accelerating diverse tissue organoid transplantation. Biomaterials-based organoid delivery methods offer the potential to maximize organoid survival and engraftment. In this protocol, we describe a vasculogenic degradable hydrogel vehicle and a method to deliver organoids to intraperitoneal tissue. Further, we describe a method to fluorescently label and image functional vasculature within the graft as a tool to investigate organoid engraftment.

Key words Organoids, Transplantation, Vascularization, Engraftment

1 Introduction

Organoid development is an emergent field in regenerative medicine as a means to study and model tissue-level development and disease, as well as a means to potentially replace dysfunctional tissue [1]. As fields such as liver [2, 3], kidney [2, 4], intestinal [5, 6], and cancer [7] organoid development mature, the need to transplant organoids to evaluate and characterize their functionality grows. Many organoid models seek to study tissue development or use organoids wholly as in vitro assays; however, for organoids developed as a regenerative medicine application, transplantation of organoids in preclinical models to assess function is a crucial step toward clinical translation [2]. For example, cancer organoid transplantation enables the better understanding and evaluation of in vivo tumor dynamics, whereas organoids such as liver, kidney,

Amy E. Emerson and Emily M. Slaby authors contributed equally to this work.

Mo R. Ebrahimkhani and Joshua Hislop (eds.), *Programmed Morphogenesis: Methods and Protocols*, Methods in Molecular Biology, vol. 2258, https://doi.org/10.1007/978-1-0716-1174-6_17,

and intestinal organoids have therapeutic potential if they can adequately engraft and function.

Four decades of research into islet organoid transplantation for the treatment of type 1 diabetes can contribute substantially to accelerating diverse tissue organoid transplantation [8–11]. For example, we have learned that a key factor influencing islet organoid engraftment and function is tissue injury and inflammation during the transplantation procedure [9, 11]. One way this has been mitigated is through organoid delivery to the surface of intraperitoneal tissue such as the omentum (human, primate, rat) [2, 12–14] or murine equivalent, the epididymal fat pad (EFP) [15–17]. Transplantation to these sites requires some form of biomaterial vehicle that can deliver and physically localize islets to the transplant site. The past two decades have seen the development of delivery methods ranging from nondegradable scaffolds [18, 19] and hydrogels [12, 16] to degradable matrices from natural [13] or synthetic [15] sources.

In this protocol, we describe the use of a synthetic degradable hydrogel system [15] to deliver organoids to diverse tissue sites (Fig. 1). This system consists of a four-arm poly(ethylene glycol) (PEG) macromer functionalized with maleimide reactive groups. The maleimide functional groups react via Michael-type addition with free thiols, such as on the amino acid cysteine. As such, the hydrogel macromer can be readily functionalized with any bioactive proteins containing a terminal cysteine, thus enabling tailored, instructive signaling. For example, we incorporate the adhesive ligand RGD to promote cell adhesion and accelerate degradation of the hydrogel, as well as vascular endothelial growth factor (VEGF) to accelerate organoid engraftment and vascularization. To generate a gel, the macromer can be crosslinked with bifunctional thiol-containing reagents; in this case, we use a protease-

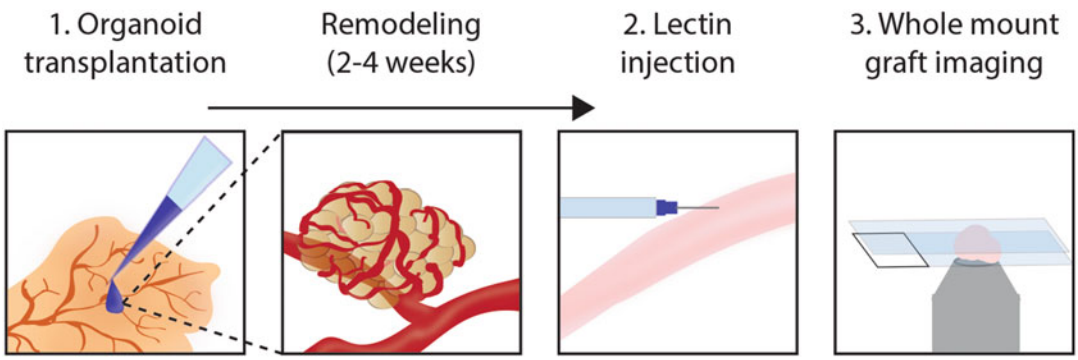

Fig. 1 Schematic illustrating the critical steps described in this protocol, including organoid delivery via a degradable synthetic hydrogel and intravenous lectin injection and whole-mount imaging to confirm organoid engraftment

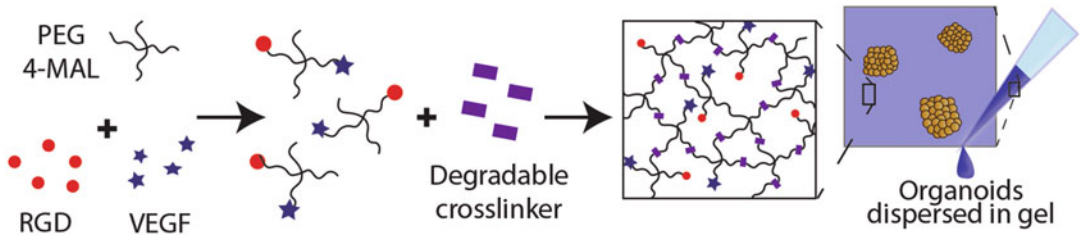

Fig. 2 Schematic illustrating the fabrication of degradable vasculogenic gels

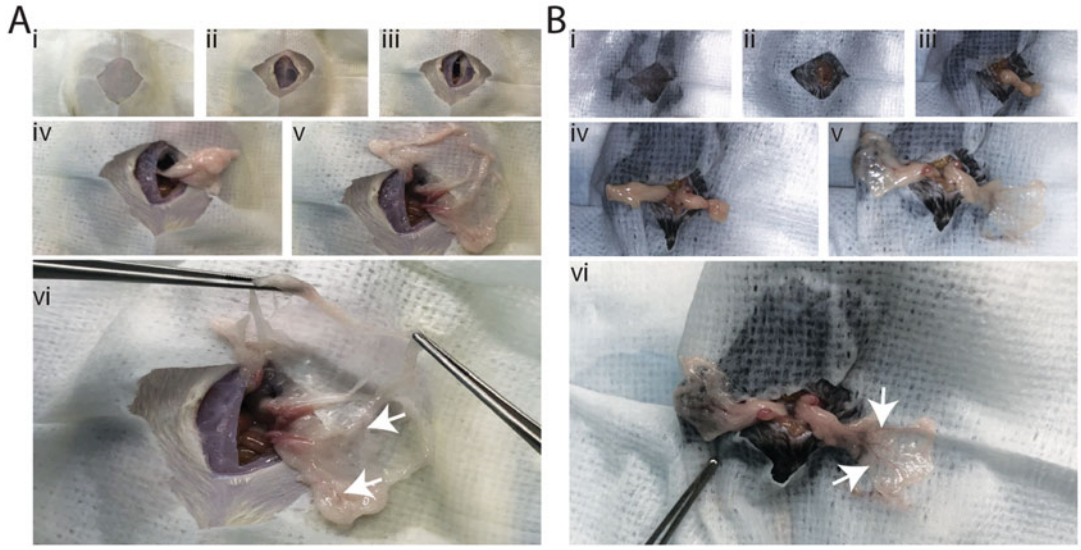

Fig. 3 Organoid transplantation in the rat omentum (**a**) or mouse EFP (**b**). (*i*) Surgical area preparation prior to midline incision, including shaving the surgical area and swabbing with chlorhexidine solution prior to applying a sterile drape. (*ii*) Midline incision through skin. (*iii*) Peritoneum wall incision. (*iv*) Exteriorized omentum (**a**) and EFP (**b**) laid on sterile, pre-wet gauze. (*v*) Omentum (**a**) and EFP (**b**) spread with saline solution. (*vi*) Magnified image demonstrating translucent nature of the tissue, and large blood vessels (white arrows)

sensitive peptide linker (VPM) to generate a gel that degrades in response to localized remodeling (Fig. 2).

Following transplantation (Figs. 3 and 4), organoid engraftment can be characterized by evaluating the degree of organoid vascularization and integration with host tissue. In this protocol, we describe the use of lectin labeling to visualize functional vasculature (Fig. 5) and a method of graft whole-mount imaging (Fig. 6) to evaluate three-dimensional organoid vasculature (Fig. 7).

1.1 Methodological Strengths and Weaknesses

This strategy of organoid delivery to intraperitoneal vascular tissue is a facile method to transplant organoids in rodents with minimal manipulation and stress on the cells. Organoids are delivered via a synthetic hydrogel that crosslinks in situ at the tissue site under physiological conditions. Crosslinking on the surface of tissue,

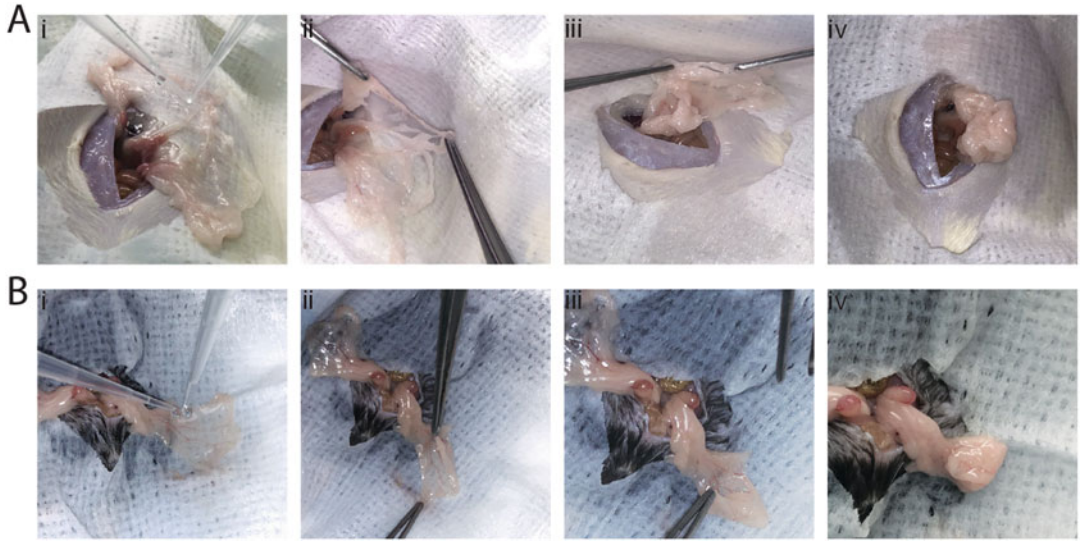

Fig. 4 Organoid delivery via degradable synthetic vasculogenic hydrogel to the rat omentum (**a**) and mouse EFP (**b**). Gel is delivered via separate pipettes (*i*), dripped directly on the surface of the tissue by alternating PEG+organoids and crosslinker. Allow a few seconds for gelation prior folding excess tissue around the gel starting with either the left or right side (*ii*), followed by the opposing side (*iii*), and last the third side opposing the omentum/EFP pedicle (*iv*)

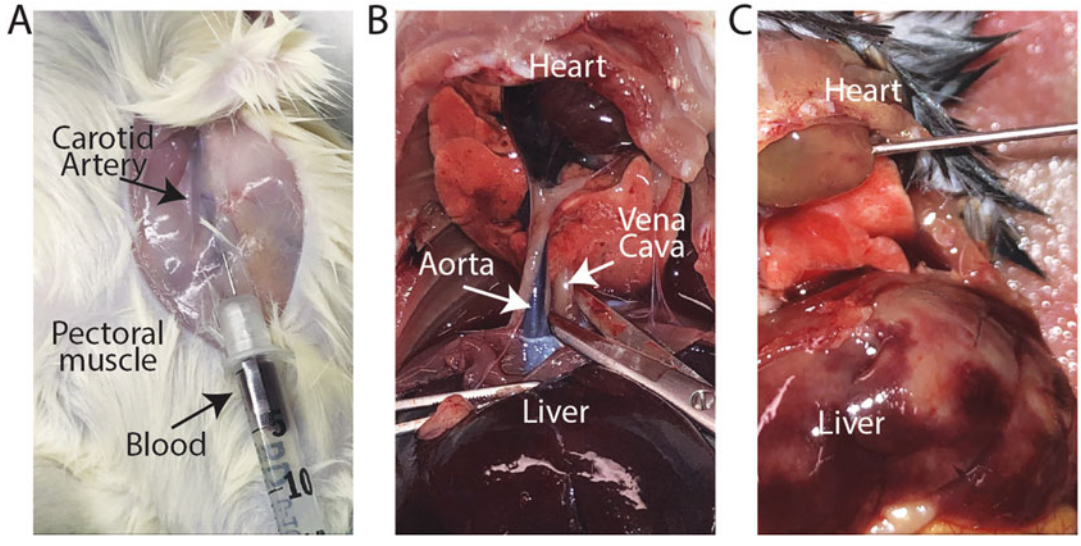

Fig. 5 Lectin injection to visualize functional vasculature and organoid engraftment. (**a**) First, a skin flap may be removed to visualize the carotid artery. Lectin is injected via insulin syringe after confirmation of successful puncture (presence of blood when plunger is extracted). (**b**) Sever the vena cava, the lighter vessel dorsal to the aorta, an obviously blood-filled vessel. (**c**) Puncture the left ventricle with a large-gauge needle attached to a syringe containing 10+ mL of saline. Blood should exit the severed vena cava and the organs should gradually blanche (note color difference of heart and liver between **b** and **c**)

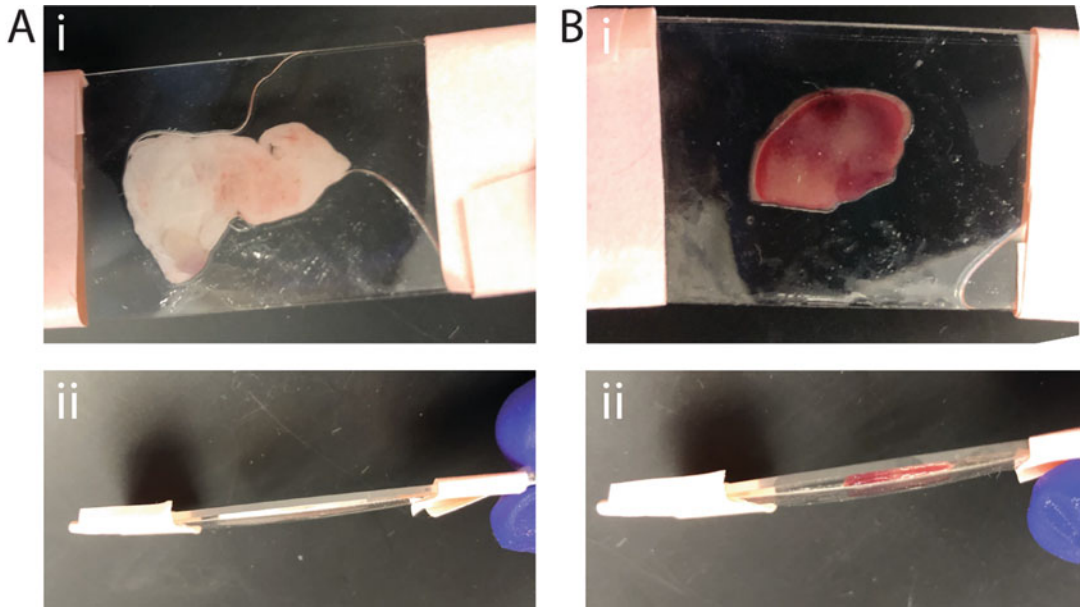

Fig. 6 Whole-mount imaging sample preparation. Example slide and coverslip assembly for whole-mount imaging of EFP (**a**) and liver (**b**) tissue samples. Note in (*ii*) that the EFP (**a**) compresses more easily than lobe of liver (**b**), which influences imaging depth and penetration

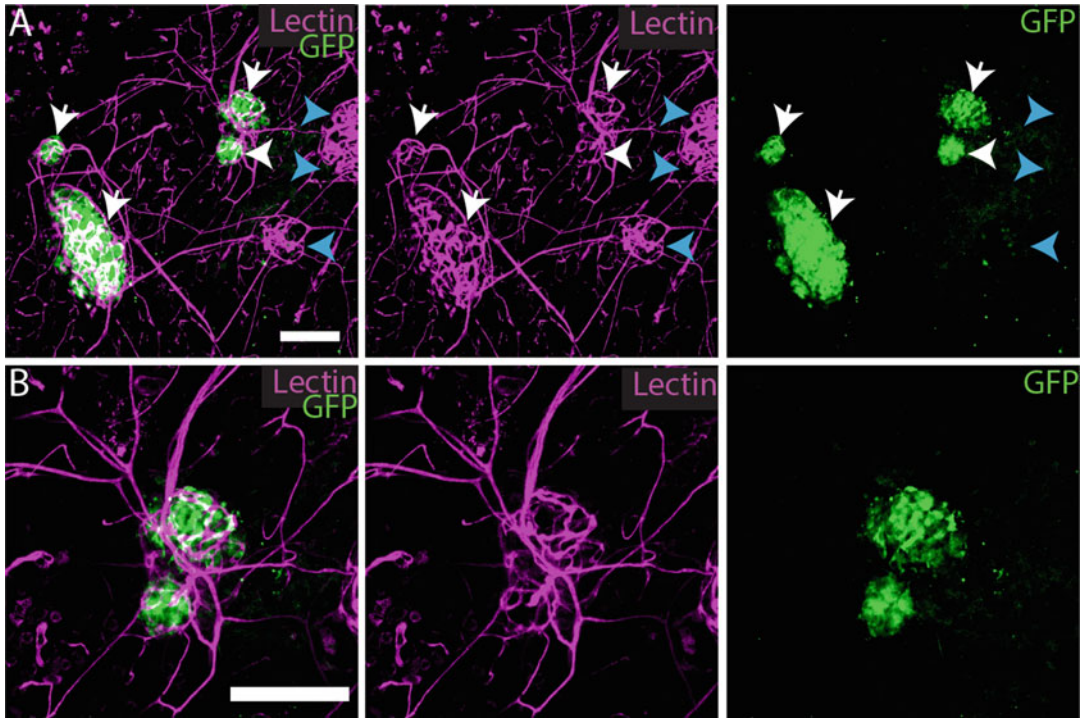

Fig. 7 Whole-mount imaging of transplanted organoids and functional vasculature to evaluate engraftment. (**a**) A mixture of wild-type and transgenic GFP-expressing islet organoids is visualized after lectin injection and whole-mount imaging. White arrows indicate GFP+ islets, and blue arrows indicate wild-type engrafted islets. (**b**) A magnified image of GFP-expressing islet integration with lectin-labeled vasculature. Images were acquired on a confocal microscope and are projections of z-stacks taken at 10–50 μm intervals to the extent of the objective working distance. Scale bars = 200 μm

rather than via injection, minimizes tissue damage and subsequent immune response. Localized VEGF delivery encourages organoid vascularization to maximize organoid survival, typically occurring within 2–4 weeks via this method, depending on transplantation site [12, 15]. Theoretically, any bioactive proteins of choice that possess a terminal cysteine resulting in a free thiol can be incorporated within the hydrogel matrix to undergo Michael-type addition with the maleimide moiety. Lectin injection and whole-mount imaging enables visualization of functional vasculature, which enables characterization and confirmation of organoid engraftment. Secondary staining of whole grafts can also be performed for confirmation of organoid presence and viability.

A potential disadvantage of this technique is that organoid engraftment and function within intraperitoneal vascular tissue may be limited by the organoid tissue type. For example, functional engraftment of intestinal or liver organoids within the omentum may be difficult to assess and impractical for clinical applications. Alternatively, this degradable hydrogel could be used to deliver organoids to matched tissue (i.e., intestinal or liver surface). Visualization of whole-mounted grafts from tissues with lower optical clarity than the EFP/omentum may be reduced, particularly if organoids are embedded deeply within the tissue. Methods to address this issue are discussed in the Notes section.

1.2 Applications

A multitude of emerging applications for organoid transplantation exist in the research field of tissue engineering. Organoid transplantation was first pioneered for primary islet organoid transplantation for the treatment of type 1 diabetes in the 1970s/1980s [8, 10, 20, 21]. The traditional intrahepatic infusion method destroys ~60% of the transplanted cells immediately upon infusion [11], and we now recognize that inflammation generated during transplantation plays an outsized role in acute islet organoid death posttransplantation [9, 13, 22]. It was not until this past decade that bioengineering strategies enabled translatable, biomaterials-based methods to deliver islets in a way that preserved organoid viability and function [12, 15–17, 23]. Now, techniques developed for islet transplantation, such as delivery via synthetic degradable hydrogels [15], can be utilized in the emergent field of regenerative medicine, where organoids are being developed for applications in intestinal [5, 6], kidney [2, 4], and liver [2, 3] regeneration.

This degradable hydrogel delivery method has been used to deliver organoids to diverse transplant sites (e.g., subcutaneous, epididymal fat pad (EFP), omentum, small bowel mesentery). This protocol describes organoid transplantation within intraperitoneal tissue (EFP, omentum) as previous research indicates that this location results in minimal inflammatory cell infiltration and maximal vascularization [15]. However, this organoid delivery and imaging method is not limited to these sites and is versatile for

delivery to just about any tissue and location. The transplantation site should be tailored to, and optimized for, the organoid and application.

2 Materials

2.1 Vasculogenic Hydrogel Preparation

1. Hydrogel buffer solution: 1× PBS (without calcium or magnesium), 20 mM HEPES.
2. PEG component of hydrogel: 5% (w/v) 20 kDa 4-arm PEG maleimide (Laysan Bio), 1 mM adhesive ligand (RGD, sequence: GRGDSPC, Genscript), 10 μg/mL recombinant human vascular endothelial growth factor (rhVEGF, Thermo Fisher). All powders (PEG, peptides) solubilized in hydrogel buffer. VEGF is reconstituted according to manufacturer's instructions at a stock concentration of 1 mg/mL.
3. Hydrogel crosslinking solution: Degradable crosslinking peptide (VPM, sequence: GCRDVPMSMRGGDRCG, Genscript) dissolved in hydrogel buffer at concentration calculated according to Methods and Table 1.
4. COSTAR Spin-X 0.2 μm and 0.45 μm centrifuge tube filters (Cole Parmer).

2.2 Transplantation Materials

1. Prepare surgical materials: Degradable sutures, sterile gauze, sterile drapes, sterile gloves, tools (forceps, surgical scissors, hemostat/needle holders, rodent surgical staples, stapler), tips, pipettors, scale, razor, heating pad, absorbent paper, saline to moisten tissue. Appropriate personal protective equipment

Table 1
Example calculations to generate 10 gels at a volume of 15 μL each

					Final volume needed 150 μL + 15% = 172.5 μL	
		MW (g/mol)	Concentration (mM)	Maleimide remaining (mM)	Component (mg)	Buffer/component (μL)
PEG component	PEG-mal (5%)	22,000	2.27	9.09	8.625	42.26
	RGD	690.74	1	8.09	0.12	42.26
	VEGF	40,000	0.00025	8.09		1.73
Crosslinker	VPM	1697	4.045	0	1.18	86.25
					Total (μL)	172.5

To ensure adequate gel amounts for transplantation, we add a 15% buffer to our gel volume, resulting in a total required gel volume of 172.5 μL

should be used, including shoe covers, head coverings, surgical masks, surgical gowns, and sterile gloves for surgeons.

2. Prepare anesthesia: isoflurane (or alternative ketamine/xylazine cocktail), and analgesic (buprenorphine sustained release is recommended).
3. Chlorhexidine Solution: Use sterile water to dilute chlorhexidine stock solution to 4%. Cover with aluminum foil to protect from light.

2.3 Lectin Perfusion and Whole-Mount Imaging Materials

1. Assemble tools for procedure and imaging: Large-gauge needles (18–23 gauge), 10 mL syringes, insulin syringes, saline to flush recipients (10 mL per mouse, 30 mL per rat), isoflurane for anesthesia, CO_2 for euthanasia, absorbent pads, forceps, scissors, slides and coverslips, laboratory tape, and PBS.
2. 10% formalin for explanted graft fixation.
3. Tomato lectin DyLight 649 (Vector labs).
4. Confocal microscope.

3 Methods

3.1 Vasculogenic Hydrogel Preparation (Fig. 2)

1. Hydrogel Component Calculations: the concentration of PEG and PEG-bound bioactive agents (e.g., VEGF, RGD) should be decided upon first. Our standard parameters for these components are a final gel composition of 1 mM RGD, 10 μg/mL VEGF, and 5% (w/v) PEG maleimide. We first convert these to mM as shown in Table 1. From the PEG concentration in Table 1, we can calculate the moles of maleimide available (4 mol maleimide: 1 mol 4-arm PEG). To calculate the concentration of crosslinker required, we need to know the available number of maleimides after tethering RGD and VEGF. Once the moles of RGD and VEGF are subtracted as shown in column 5 of Table 1, we can calculate the needed concentration of our crosslinker VPM, keeping in mind that there are 2 mol of thiol per 1 mol VPM.
2. Prepare sterilized PEG, ligand, crosslinking peptides, and organoids (e.g., primary islets or organoids generated in-house) in advance of the surgical procedure (*see* **Note 1**). Determine the amount of PEG, VEGF, crosslinking peptide, and adhesive ligand that is needed based on total gel number and volume (*see* Table 1 for example calculations).
3. Weigh out PEG, peptide, and ligand quantities in individual 0.5–1.0 mL tubes and solubilize in hydrogel buffer at the calculated concentrations.
4. pH each component and correct using very small volumes of concentrated acid or base until pH is in the 7.0–7.5 range (*see* **Note 2**).

5. Sterilize PEG, adhesive ligand, and peptide components through individual COSTAR Spin-X 0.2 μm or 0.45 μm centrifuge tube filters by spinning at high g/rpm (≥1000 rpm) until reagents have passed through the filter (*see* **Note 3**).
6. PEG Component: Combine PEG, adhesive ligand (RGD), and VEGF volumes according to the calculator. The calculations as shown in Table 1 result in equal volume PEG and crosslinking solutions to form the final gel (i.e., for a total gel volume of 15 μL, mix 7.5 μL PEG component and 7.5 μL crosslinking solution).
7. Keep crosslinker separate from PEG mixture until gel is ready to be formed. Gel polymerizes very rapidly, on the order of seconds (*see* **Note 4**).

3.2 Organoid Transplantation (Fig. 3)

1. Organoid preparation: Organoids should be aliquoted per recipient/transplant site in conical tube (e.g., 0.5 mL Eppendorf tube in 20–30 μL of media) to allow pelleting. Just prior to delivery, excess media is removed without disturbing the pellet.
2. Prepare Surgical Area: All surgeons should scrub in and wear sterile surgical gloves. All personnel in the surgery room should wear surgical gowns, face masks, hair nets, gloves, and shoe covers. The surgical table bench is sterilized with 70% ethanol solution. Absorbent paper and a heating pad are placed in the area prepped for sterile surgery. Sterile instruments are arranged in a sterile field.
3. Weigh the animal to be operated on for a preoperative weight.
4. Anesthetize the animal with 5% isoflurane anesthesia in an induction chamber.
5. Inject one dose of sustained release buprenorphine subcutaneously (1 mg/kg) to provide 72 continuous h of pain relief (*see* **Note 5**).
6. Shave peritoneal area of animal. Shaved peritoneal area should be prepped with chlorhexidine solution or equivalent antiseptic solution.
7. Transfer the animal to the heating pad in the sterile field. Maintain anesthesia with 1.25–3% isoflurane delivered by nose cone. The animal should be unresponsive to external stimuli such as a toe pinch before and during surgery. Monitor animal breathing to ensure depth of anesthesia is not too great.
8. Place sterile drapes over animal abdominal region to isolate incision area. If using gauze as a sterile surgical drape, a liberal application of saline will aid drape adherence to the skin and prevent exteriorized tissue from sticking to the gauze (Fig. 3*i*).

9. Perform a midline incision through the skin using surgical scissors. Clear connective tissue between skin and peritoneal wall to ease the suturing process at the end of the procedure. Next create a midline incision through the peritoneal wall to access the peritoneal cavity and identify the fat pad/omentum (*see* **Note 6**), taking care not to puncture organs by lifting the peritoneal wall away from abdominal organs with a pair of forceps prior to making an incision (Fig. 3*ii*, *iii*).
10. Gently exteriorize and spread wide the fat pad/omentum via saline wash (*see* **Note 7**, Fig. 3*iv*, *v*).
11. Deliver organoids to tissue surface via the degradable hydrogel (total volume 15–30 μL depending on number of organoids and tissue area available). The PEG component of the hydrogel is mixed evenly with the organoid pellet to suspend cells and ensure maximal homogeneity. The organoid/PEG mixture is delivered to the tissue surface simultaneously with the cross-linking component (Fig. 4*i*).
12. After allowing a few seconds for gelation, excess tissue can be folded gently over the gel/organoid mixture as demonstrated in Fig. 4*ii–iv*.
13. Gently replace the fat pad/omentum and in the peritoneal cavity, either using forceps or allowing the tissue to naturally retract into the cavity when the peritoneal wall is lifted.
14. Suture incision of the muscle/fascia and close the skin with surgical staples. The staples should be close enough together to prevent the animal from reopening the wound.
15. Administer additional analgesic(s) after surgery for pain relief during recovery, where appropriate.
16. Monitor animal's weight for 3–5 days posttransplantation to verify stable recovery.
17. Remove surgical staples 10–14 days after the operation.

3.3 Lectin Injection for Vascular Labeling (Fig. 5)

1. Anesthetize the animal with isoflurane. NOTE: alternative anesthesia methods are acceptable, e.g., ketamine/xylazine cocktail.
2. Lectin solution (no dilution) is injected with an insulin syringe via tail vein or carotid artery. We recommend the carotid artery, as it is easiest to access. As this is a terminal procedure, removing a skin flap at the neck allows visualization of the carotid artery (Fig. 5a). The needle of the insulin syringe is inserted at an angle almost parallel to the artery (*see* **Note 8**). Placement in the artery should be confirmed by easy blood flow into the syringe when the plunger is extracted gently. The lectin (mouse 100–200 μL, rat 250–450 μL) is then injected and allowed to circulate for 5–15 min under anesthesia (*see* **Note 9**).

3. (OPTIONAL) Open the animal via midline incision to examine or photograph implants prior to saline flush (*see* **Note 10**).
4. Sacrifice the animal by CO_2 inhalation, and open the thoracic cavity by carefully cutting away rib cage, without cutting heart.
5. Sever the vena cava. This vessel descends from the heart and runs alongside, lateral and dorsal to the aorta, which should be readily identifiable by its dark red color. The vena cava, depleted of oxygen, will likely present as white or lighter colored as pictured in Fig. 5b.
6. Insert a large-gauge needle (18–23 gauge) with a syringe containing saline (10 mL mouse, 30 mL rat) into the apex of heart in the LEFT ventricle (*see* **Note 11**, Fig. 5c), and flush the animal's circulation with saline to eliminate blood and excess lectin (clotted blood or lectin can make vessel visualization difficult). Liver and blood vessels will "blanche" as blood drains from vena cava (Fig. 5c), stop flushing when the fluid flow becomes clearer.
7. Implants are collected in labeled vials containing 10% formalin.
8. Grafts can be processed for histology or imaged "whole mount" on a confocal microscope.

3.4 Whole-Mount Imaging (Fig. 6)

1. Rinse fixed, lectin-labeled tissue in PBS and mount on a standard microscope slide as shown in Fig. 6.
2. Using laboratory tape, secure a thin coverslip over the sample, securing it firmly to minimize tissue thickness, but without causing damage to the tissue. PBS can be applied around the sample to keep it moist (*see* **Note 12**). Refresh PBS often for long imaging periods to keep tissue hydrated.
3. For best results with dense tissue (e.g., skin, liver), compress tissue as much as possible between two glass slides and use a lectin at the farthest red that can be detected in range on your microscope (*see* **Note 13**).
4. Using a confocal microscope (*see* **Note 14**), locate clusters of blood vessels, which indicate the presence of organoids. To confirm organoid presence, a secondary stain for the tissue of interest can validate organoid presence. Example images of GFP-expressing and wild-type islets engrafted within an EFP are exhibited in Fig. 7.

4 Notes

1. Store PEG and peptides in a sealed container with desiccant. Gel components must be prepared fresh the day of the procedure but will maintain integrity and crosslinking ability up to 8 h if necessary due to length of surgical procedures.

2. pH of all gel components has a huge influence on crosslinking time, gel heterogeneity, and gel stability. Final solutions should be made including an allowance volume for pH solutions and to correct the pH to the 7–7.5 range.
3. Costar spin column sterile filtration: all components except for PEG can be sterilized using Costar filters with 0.2 μm pore size. 0.45 μm should be used with the PEG component to ensure no loss in PEG macromer.
4. If the user experiences crosslinking kinetics that are too fast or too slow: kinetics of PEG maleimide crosslinking can be studied in-depth with this valuable manuscript [24]. Briefly, stronger buffers and isotonicity of the buffer results in faster crosslinking time. Additionally, pH can be used to modulate crosslinking time, with more acidic components (e.g., pH 5–6) slowing reaction time.
5. May use institutionally approved alternative analgesic.
6. Vascularization time is transplant site-dependent. For organoids with high oxygen consumption rates, such as islets, shorter times to vascularization are preferred [15], as observed in more vascularized intraperitoneal tissue (EFP/omentum). Tissue with lower degrees of vascularization, such as the subcutaneous site, result in poor islet engraftment, but may work depending on the cell type.
7. Be careful not to induce trauma in the tissue (e.g., cause bleeds or bruising) in order to minimize localized inflammation.
8. To make carotid injection easier, place a 1-mL syringe behind the animal's neck to help expose the carotid. In mice, in particular, angling the syringe needle through the pectoral muscle can ensure correct placement of the needle within the vessel.
9. If you see a bubble forming at the site of injection, and face any resistance, the needle is no longer in the artery.
10. Do not open the thoracic cavity prior to this step, the animal will die prematurely.
11. Puncturing the right ventricle will send fluid into lungs, resulting in noticeable lung distention; simply reposition the needle into the left ventricle if this occurs.
12. Capillary action should keep fluid between the slides and sample moist, for long imaging sessions replenish with PBS occasionally to prevent sample drying.
13. Can use other fluorescent colors, but whole-mount images should ideally use a far-red dye for optimal tissue penetration.
14. Beware that the mounted sample is lower than typical slide mounts on the stage. Focal plane will be lower than typical.

Acknowledgments

The authors wish to acknowledge Alec McCall and Michael Finocchiaro for their assistance in preparing figures for this manuscript. Amy E. Emerson and Emily M. Slaby contributed equally to this work.

References

1. Clevers H (2016) Modeling development and disease with organoids. Cell 165 (7):1586–1597
2. Saito R, Ishii Y, Ito R, Nagatsuma K, Tanaka K, Saito M et al (2011) Transplantation of liver organoids in the omentum and kidney. Artif Organs 35(1):80–83
3. Nantasanti S, de Bruin A, Rothuizen J, Penning LC, Schotanus BA (2016) Concise review: organoids are a powerful tool for the study of liver disease and personalized treatment design in humans and animals. Stem Cells Transl Med 5(3):325–330
4. Schutgens F, Verhaar MC, Rookmaaker MB (2016) Pluripotent stem cell-derived kidney organoids: an in vivo-like in vitro technology. Eur J Pharmacol 790:12–20
5. Cruz-Acuña R, Quirós M, Farkas AE, Dedhia PH, Huang S, Siuda D et al (2017) Synthetic hydrogels for human intestinal organoid generation and colonic wound repair. Nat Cell Biol 19(11):1326
6. Dedhia PH, Bertaux-Skeirik N, Zavros Y, Spence JR (2016) Organoid models of human gastrointestinal development and disease. Gastroenterology 150(5):1098–1112
7. Drost J, Clevers H (2018) Organoids in cancer research. Nat Rev Cancer 18(7):407–418
8. Andersson A, Korsgren O, Jansson L (1989) Intraportally transplanted pancreatic islets revascularized from hepatic arterial system. Diabetes 38(Suppl 1):192–195
9. Barshes NR, Wyllie S, Goss JA (2005) Inflammation-mediated dysfunction and apoptosis in pancreatic islet transplantation: implications for intrahepatic grafts. J Leukoc Biol 77 (5):587–597
10. Barton FB, Rickels MR, Alejandro R, Hering BJ, Wease S, Naziruddin B et al (2012) Improvement in outcomes of clinical islet transplantation: 1999–2010. Diabetes Care 35(7):1436–1445
11. Bennet W, Groth C-G, Larsson R, Nilsson B, Korsgren O (2000) Isolated human islets trigger an instant blood mediated inflammatory reaction: implications for intraportal islet transplantation as a treatment for patients with type 1 diabetes. Ups J Med Sci 105 (2):125–133
12. Weaver JD, Headen DM, Hunckler MD, Coronel MM, Stabler CL, García AJ (2018) Design of a vascularized synthetic poly (ethylene glycol) macroencapsulation device for islet transplantation. Biomaterials 172:54–65
13. Berman DM, O'Neil JJ, Coffey LC, Chaffanjon PC, Kenyon NM, Ruiz P et al (2009) Long-term survival of nonhuman primate islets implanted in an omental pouch on a biodegradable scaffold. Am J Transplant 9 (1):91–104
14. Pedraza E, Brady A-C, Fraker CA, Molano RD, Sukert S, Berman DM et al (2013) Macroporous three dimensional PDMS scaffolds for extrahepatic islet transplantation. Cell Transplant 22(7):1123
15. Weaver JD, Headen DM, Aquart J, Johnson CT, Shea LD, Shirwan H et al (2017) Vasculogenic hydrogel enhances islet survival, engraftment, and function in leading extrahepatic sites. Sci Adv 3(6):e1700184
16. Weaver JD, Headen DM, Coronel MM, Hunckler MD, Shirwan H, Garcia AJ (2018) Synthetic poly(ethylene glycol)-based microfluidic islet encapsulation reduces graft volume for delivery to highly vascularized and retrievable transplant site. Am J Transplant 19 (5):1315–1327
17. Weaver JD, Song Y, Yang EY, Ricordi C, Pileggi A, Buchwald P et al (2015) Controlled release of dexamethasone from organosilicone constructs for local modulation of inflammation in islet transplantation. Tiss Eng Part A 21(15–16):2250–2261
18. Brady AC, Martino MM, Pedraza E, Sukert S, Pileggi A, Camillo R et al (2013) Pro-angiogenic hydrogels within macroporous scaffolds enhances islet engraftment in an extrahepatic site. Tiss Eng Part A 22 (7):1123–1135
19. Jiang K, Weaver JD, Li Y, Chen X, Liang J, Stabler CL (2017) Local release of dexamethasone from macroporous scaffolds accelerates

islet transplant engraftment by promotion of anti-inflammatory M2 macrophages. Biomaterials 114:71–81

20. Calafiore R (1997) Perspectives in pancreatic and islet cell transplantation for the therapy of IDDM. Diabetes Care 20(5):889–896
21. Kemp C, Knight M, Scharp D, Ballinger W, Lacy P (1973) Effect of transplantation site on the results of pancreatic islet isografts in diabetic rats. Diabetologia 9(6):486–491
22. Bruni A, Gala-Lopez B, Pepper AR, Abualhassan NS, Shapiro AJ (2014) Islet cell transplantation for the treatment of type 1 diabetes: recent advances and future challenges. Diab Metab Syn Obes 7:211
23. Weaver JD, Stabler CL (2015) Antioxidant cerium oxide nanoparticle hydrogels for cellular encapsulation. Acta Biomater 16:136–144
24. Jansen LE, Negrón-Piñeiro LJ, Galarza S, Peyton SR (2018) Control of thiol-maleimide reaction kinetics in PEG hydrogel networks. Acta Biomater 70:120–128

Chapter 18

High-Throughput Production of Platelet-Like Particles

Kylie M. Persson, Pauline V. Kneller, Mark W. Livingston, Lucas M. Bush, and Tara L. Deans

Abstract

The in vitro production of platelets could provide a life-saving intervention for patients that would otherwise require donor-derived platelets. Producing large numbers of platelets in vitro from their progenitor cells, megakaryocytes, remains remarkably difficult and inefficient. Here, a human megakaryoblast leukemia cell line (MEG-01) was used to assess the maturation of megakaryocytes and to develop a new methodology for producing high numbers of platelet-like particles from mature MEG-01 cells in vitro.

Key words Platelet-like particle production, Megakaryocytes, MEG-01 cell line, Proplatelet

1 Introduction

Platelets are small anucleate blood cells that circulate throughout the body and play an important role in hemostasis, wound healing, angiogenesis, inflammation, and clot formation [1]. In the bone marrow, platelets are derived from the process of hematopoiesis, the differentiation of hematopoietic stem cells (HSCs) into specialized blood and immune cells [1–4]. Platelets circulate in large numbers with an average lifespan of approximately 9–10 days. The source of this large cell population is from their progenitor cells, megakaryocytes (MKs), which are capable of producing 10^{11} platelets per day in adult humans [5, 6].

Megakaryocytes account for only 0.01% of the total bone marrow cells, making it difficult to study how they develop and mature, and how their development impacts the production of platelets [3, 7]. For this reason, MEG-01 cells, a human megakaryoblast leukemia cell line, is a popular cell line used for studying megakaryocyte maturation and platelet-like particle formation [8–11]. Similar to natural MK development and maturation, MEG-01 cells display phenotypic properties that closely resemble their natural

Mo R. Ebrahimkhani and Joshua Hislop (eds.), *Programmed Morphogenesis: Methods and Protocols*, Methods in Molecular Biology, vol. 2258, https://doi.org/10.1007/978-1-0716-1174-6_18,

counterparts as they mature including increasing in size, producing membranous extensions, increasing DNA content, and the production of functional platelet-like particles [12–16].

Studies have shown that the growth factors thrombopoietin (TPO) and phorbol myristate acetate (PMA) can independently enhance the differentiation and maturation of MEG-01 cells in vitro, increasing the production of platelet-like particles from MEG-01 cells [17–19]. Here we utilized current approaches for culturing and maturing MEG-01 cells in vitro and implemented a new method for obtaining large numbers of platelet-like particles. This approach utilizes the application of constant pressure on MEG-01 cells through a filter which enables the high-throughput production of platelet-like particles in vitro.

Here we describe a simple and efficient protocol developed in our laboratory for the high-throughput production of platelet-like particles. While this protocol was developed with MEG-01 cells, it can easily be adapted for the efficient and high-throughput production of platelets and platelet-like particles from mouse and human megakaryocytes.

2 Materials

2.1 Cell Culture for MEG-01 Cells (ATCC® CRL-2021™)

1. MEG-01 culture medium: RPMI medium (Gibco, 11875-093) contains 10% Fetal Bovine Serum (FBS) (Gibco, 10437-028).
2. MEG-01 maturing medium: Add 100 ng/mL of recombinant human thrombopoietin (TPO) (PeproTech, 300-18) and/or 5 nM phorbol myristate acetate (PMA) (Millipore Sigma, 524400) to the culture medium.
3. T25 flasks.
4. Cell scrapers.
5. 15 mL conical tubes.
6. Hemocytometer.
7. Cell culture incubator capable of regulating temperature, humidity, and carbon dioxide.
8. Centrifuge.

2.2 Flow Cytometry

1. PBS.
2. 3% BSA made in PBS.
3. Antibodies used for labeling: CD41a APC (BD Biosciences, 14-0419-80).
4. Hoechst 33342 nuclei stain (BD Biosciences, BDB561908).
5. 7-AAD cell viability staining solution (ThermoFisher, 00-6993-50).

6. Calcein AM cell viability assay (ThermoFisher, C3099).
7. Flow cytometry: Beckman Coulter Life Sciences CytoFLEX.

2.3 Imaging

1. 48-Well tissue culture-treated plates.
2. PBS.
3. 4% formaldehyde (ThermoFisher, FB002).
4. Blocking solution: 5% donkey serum, and 1% BSA in PBS.
5. Antibodies used for labeling: mouse anti-human CD41a (ThermoFisher, 14-0419-80) goat anti-mouse Alexa Fluor Plus 488 (ThermoFisher, A32723).
6. Hoechst 33342 nuclei stain (BD Biosciences, BDB561908).
7. Olympus IX73 inverted microscope with Olympus XM10 camera.

2.4 Making Platelet-Like Particles

1. PBS.
2. 5 mL syringes (BD, 309646).
3. Tubing to fit on syringe filters.
4. 5.0 μm syringe filters (Millipore Sigma, SLSV025LS).
5. KD Scientific Legato 180 syringe pump.

3 Methods

3.1 Cell Culture

1. Grow MEG-01 cells in a 37 °C, 5% CO_2 humidified incubator. Pass cells or change medium 2 or 3 times/week, ensuring that cell density does not exceed 1×10^6 cells/mL.
2. When changing the medium, care must be taken to not lose the semi-adherent cells.
   (a) Remove the medium containing the semi-adherent cells from the culture flask and place in a 15-mL conical tube.
   (b) Centrifuge the cell suspension at $300 \times g$ for 5 min, aspirate the supernatant and resuspend in 1 mL of fresh medium.
   (c) While the cell suspension is spinning, add 4 mL of growth medium to the flask of cells to prevent the adherent cells from drying out.
   (d) Return the 1 mL of semi-adherent cells to the appropriate plate of cells.
3. When passing MEG-01 cells, use a cell scraper to gently dislodge the adherent cells into the medium and transfer cell suspension to a 15-mL conical tube.
4. Take a 10-μL sample to measure the cell density using a hemocytometer.

5. Centrifuge at 300 × *g* for 5 min and discard the supernatant.
6. Resuspend the cells in culture medium to plate MEG-01 cells at 35×10^3 cells/cm^2.
7. If maturing MEG-01 cells, add TPO and/or PMA (*see* Subheading 2.1, **item 2**) and grow for 72 h before harvesting and analyzing cells. Perform medium changes every 24 h for cultures that contain PMA.

3.2 Making Platelet-Like Particles

1. Obtain 2 mL of PBS in a 5-mL syringe. Attach syringe filter and tubing.
2. Place the syringe on the syringe pump and secure the apparatus.
3. Set up conical tubes for sample and waste collection.
4. Adjust the setting of the syringe pump according to the parameters of the syringe being used.
5. To prime the filter and tubing, begin infusing 2 mL of PBS through the syringe filter and tubing at 5 mL/min, direct flow-through into the waste collection tube.
6. After culturing MEG-01 cells in growth or maturing medium for 72 h, scrape the bottom of the culture flask with a cell scraper.
7. Take a 10-μL sample to measure the cell density using a hemocytometer.
8. Collect cell suspension in a 5-mL syringe.
9. Preserving the same syringe filter and tubing from **step 5**, carefully replace the empty PBS syringe with the syringe containing the cell suspension.
10. Begin infusing the cell suspension through the syringe filter and tubing at 5 mL/min (Fig. 1). Collect flow-through containing the platelet-like particles in the sample collection tube (*see* **Note 1**).

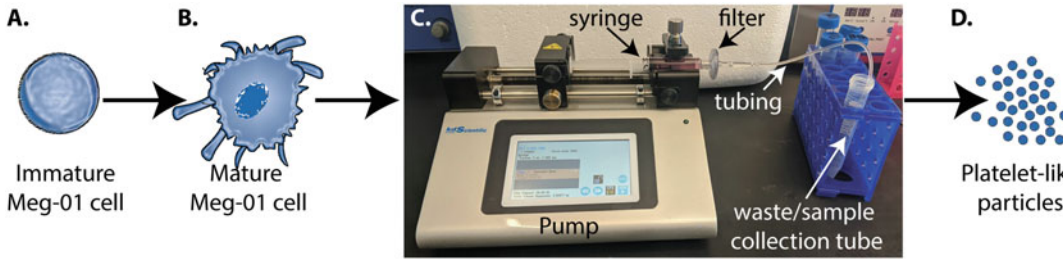

Fig. 1 Procedure for the production of platelet-like particles. MEG-01 cells are cultured in (**a**) growth medium or in (**b**) maturing medium for 72 h. (**c**) Cells are then placed in a syringe and pushed through a 5 μm filter, and the flow-through is collected in a collection tube. (**d**) Platelet-like particles are collected and analyzed

3.3 Flow Cytometry

3.3.1 Whole Cells

1. After 72-h culture in growth or maturing medium, remove flask from incubator and scrape with a cell scraper.
2. Take a 10-μL sample to measure the cell density using a hemocytometer.
3. Centrifuge cells at 300 × *g* for 5 min. Aspirate the supernatant.
4. Resuspend the cell pellet to a concentration of 1×10^6 cells in 100 μL PBS containing 3% BSA.
5. For each desired sample, aliquot 100 μL of the cell suspension into an Eppendorf tube.
6. Add 1 μL of Hoechst 33342 and 1 μL of CD41a antibody to each sample.
7. Incubate at 37 °C in a 5% CO_2 humidified incubator for 20 min (*see* **Note 2**).
8. Add 1 mL of PBS to each sample.
9. Centrifuge at 300 × *g* for 5 min and aspirate the supernatant.
10. Resuspend the cell pellet in 200 μL of PBS.
11. Add 2 μL of 7-AAD cell viability dye per 200 μL of cell suspension.
12. Analyze MEG-01 cells on the flow cytometer (Fig. 2) (*see* **Note 3**).

3.3.2 Platelet-Like Particles

1. After infusing the MEG-01 cells through the syringe filter and collecting the platelet-like particles in a 15-mL conical tube, centrifuge the sample at 800 × *g* for 15 min. Aspirate the supernatant.
2. Resuspend the pellet in 100 μL PBS containing 3% BSA per sample (*see* **Note 4**) and transfer to an Eppendorf tube.

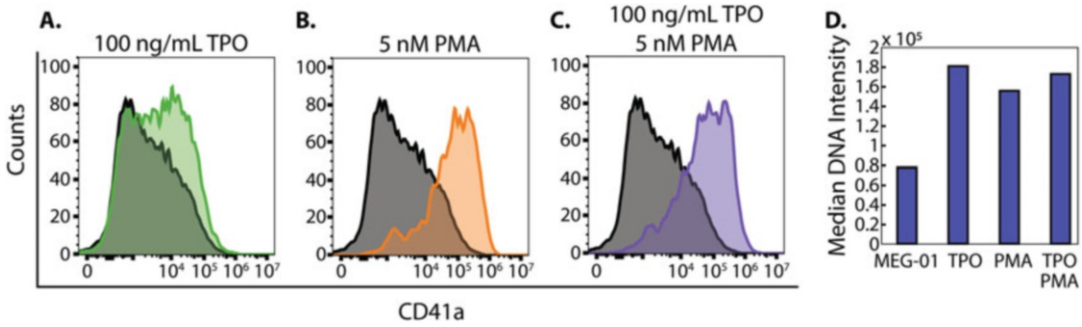

Fig. 2 MEG-01 cells grown in various media conditions. (**a**) MEG-01 cells matured with 100 ng/mL of TPO for 72 h (green) overlaid on MEG-01 cells grown in growth medium (gray). (**b**) MEG-01 cells matured with 5 nM PMA for 72 h (orange) overlaid on MEG-01 cells grown in growth medium (gray). (**c**) MEG-01 cells matured with 100 ng/mL TPO and 5 nM PMA (purple) overlaid on MEG-01 cells grown in growth medium (gray). (**d**) Median Hoechst intensity for growth and maturing conditions after 72 h. Note that the expression of CD41a and the DNA content increases when matured in either TPO or PMA

3. Add calcein AM to reach a final concentration of 2 μg/mL per sample.
4. Incubate at 37 °C in a 5% CO_2 humidified incubator for 10 min, then add 1 μL of CD41a to each sample and continue incubating at 37 °C for 20 min for a total incubation time of 30 min (*see* **Notes 5**).
5. Add 1 mL of PBS to each sample.
6. Centrifuge samples at 800 × *g* for 15 min and aspirate the supernatant.
7. Resuspend the platelet-like particles in 200 μL of PBS.
8. Analyze the samples on the flow cytometer (Fig. 3).

3.4 Imaging MEG-01 Cells from Plates

1. Plate MEG-01 cells at 35 × 10^3 cells/cm^2 (*see* **Note 6**).
2. Grow the cells in either growth or maturing medium for 72 h.
3. Carefully aspirate the medium off the cells and gently wash with 500 μL PBS (*see* **Note 7**).
4. Add 100 μL of 4% formaldehyde and incubate at room temperature for 10 min.
5. Carefully aspirate and gently wash with 500 μL PBS (*see* **Note 7**).
6. Add 100 μL of blocking solution and incubate at room temperature for 10 min.
7. Carefully aspirate the blocking solution.
8. Add 100 μL of blocking solution containing the primary antibody CD41a and incubate at room temperature for approximately one hour (*see* **Note 8**).
9. Carefully aspirate the antibody solution off of the cells and gently wash with 500 μL PBS.
10. Add 100 μL of blocking solution containing the secondary antibody and Hoechst 33342, incubate for approximately one hour (*see* **Note 9**).
11. Wash with 500 μL PBS, aspirate, then add another 500 μL PBS, so the cells do not dry out when imaging. Image immediately (*see* **Note 10**).
12. Images were acquired using an Olympus IX73 microscope and Olympus XM10 camera. Images were processed using Olympus cellSens Standard software. Figures were created with Adobe Illustrator (Fig. 4).

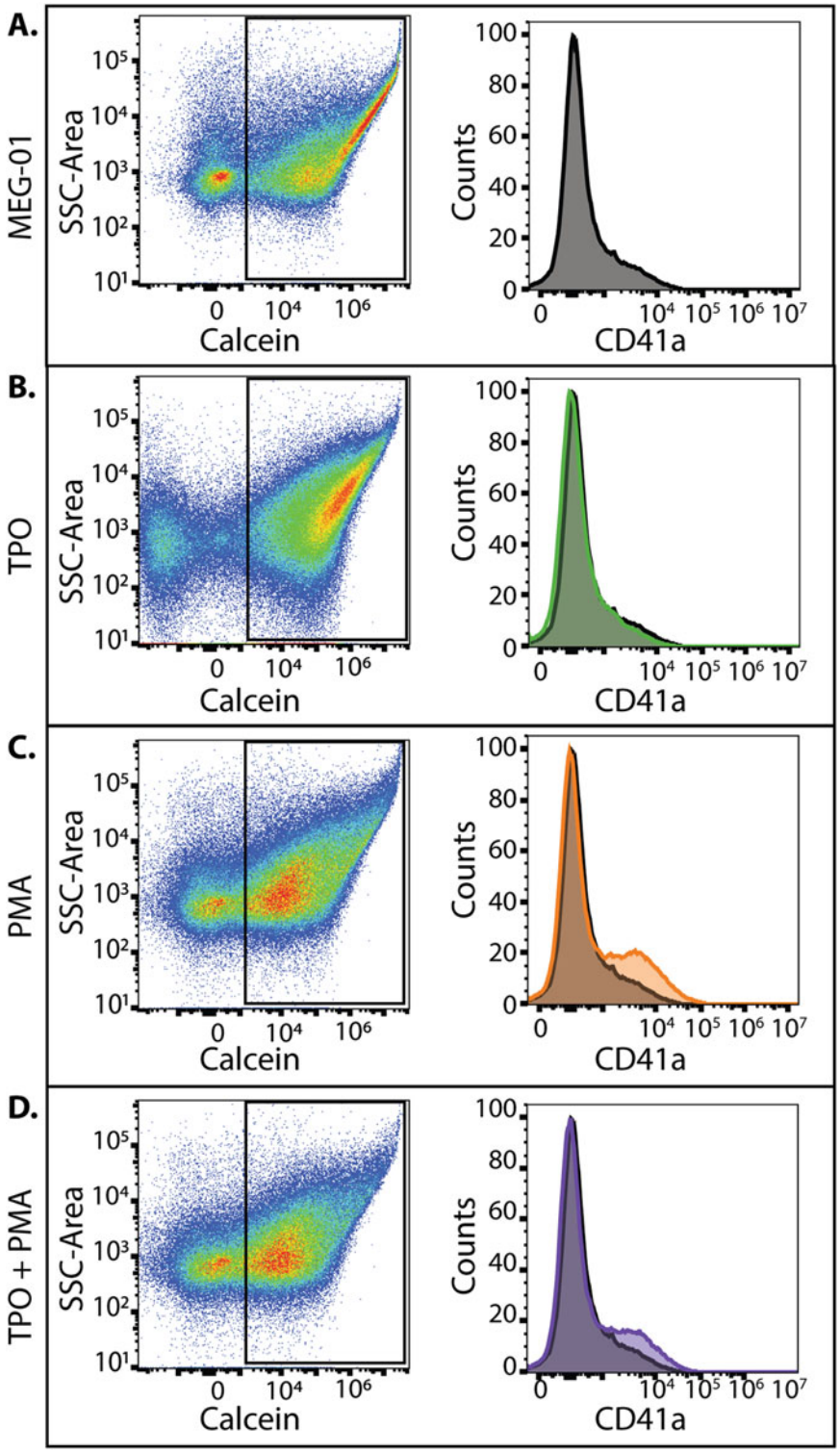

Fig. 3 Platelet-like particle viability. (**a**) Flow-through from MEG-01 cells in growth medium stained with calcein for cell viability and CD41a primary antibody. (**b**) Flow-through from MEG-01 cells matured with 100 ng/mL TPO for 72 h was stained with calcein for cell viability and CD41a primary antibody. (**c**) Flow-through from MEG-01 cells matured with 5 nM PMA for 72 h was stained with calcein for cell viability and CD41a primary antibody. (**d**) Flow-through from MEG-01 cells matured with 100 ng/mL TPO and 5 nM PMA for 72 h was stained with calcein for cell viability and CD41a primary antibody. Note that the number of CD41-positive cells increases in the viable platelet-like particles in the presence of PMA and PMA + TPO

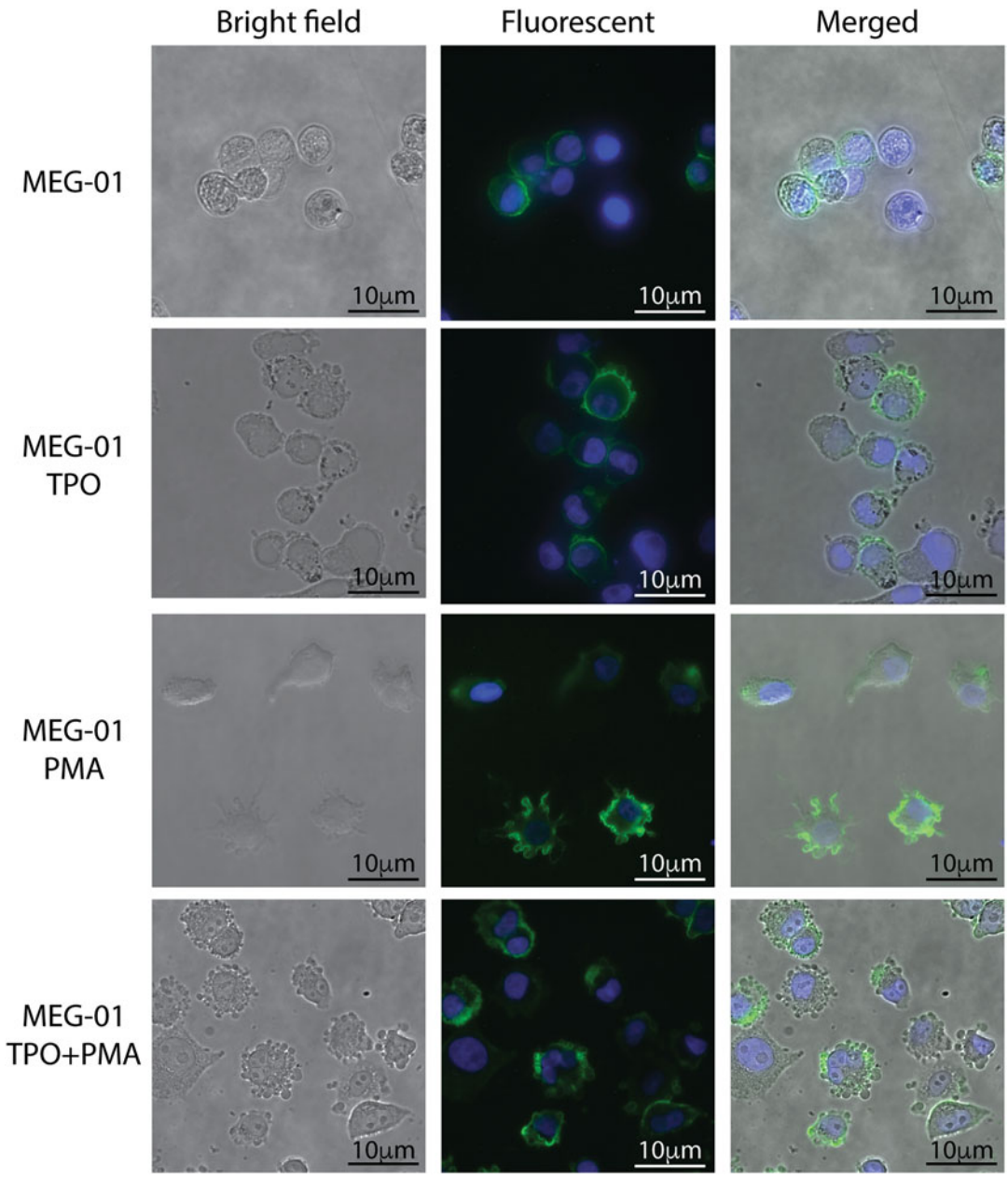

Fig. 4 Representative images of MEG-01 cells grown in various media conditions. Blue fluorescence indicates nuclei stained with Hoechst 33342, and green fluorescence indicates the presence of CD41a surface receptors. All images were taken at 10× magnification. Note that cells matured with TPO and PMA display ruffled cell membranes and cytoplasmic extensions

4 Notes

1. When finished making platelet-like particles, some cell suspension/flow-through will be left in the tube after the syringe is empty. Replace the syringe with one that contains PBS to finish flushing out the filter/tubing for optimal platelet yields.
2. When incubating the cells with antibodies, place a piece of foil over the top of the samples to protect from light.
3. When running MEG-01 cells on the flow cytometer, the following gating strategy was used: An unstained population of MEG-01 cells was run through the flow cytometer to observe the forward versus side scatter (FSC vs. SSC) plot. A gate was drawn to exclude debris. Next, the live cells were identified in the far-red spectrum, and a gate was drawn to include the live cells. From this gate, the Hoechst-positive cells were identified, and finally the CD41a APC-positive cells were analyzed. The platelet-like particles were gated based on calcein-positive particles, which were compared to an unstained sample of platelet-like particles with calcein-negative particles. From here, the calcein-positive particles were gated to analyze CD41a APC-positive platelet-like particles.
4. In the described protocol, a T25 flask of MEG-01 cells were infused through the device. The resulting platelet-like particles were spun down, and the supernatant aspirated. At this point, the pellet can be resuspended in 100 μL multiples, depending on how many samples are desired (each sample should be resuspended in 100 μL).
5. Platelet-like particles may experience activation when subjected to cold temperatures. Refrain from using ice during antibody incubation steps to reduce chances of activation.
6. When plating cells for imaging, 48-well plates were used and cells were grown for 72 h in either growth or maturation medium.
7. It is important to be gentle when washing the cells to not disturb their adherence and morphology.
8. The CD41a primary antibody was used at a 1:100 dilution in blocking solution.
9. The secondary antibody was diluted 1:1500 in blocking solution and Hoechst was added at 1 μL/mL dilution. For example, if making a 750-μL secondary antibody solution then add 0.5 μL of the secondary antibody and 0.75 μL of Hoechst to 750 μL blocking solution.

10. The cells should be imaged within a few hours after completing the antibody labeling. Over time, the cells will dislodge from the plate.

Acknowledgments

The authors gratefully acknowledge the funding sources to support this work from the National Science Foundation CAREER Program (CBET-1554017), the Office of Naval Research Young Investigator Program (N00014-16-1-3012), the National Institutes of Health Trailblazer Award (1R21EB025413-01), the National Institutes of Health Director's New Innovator Award (1DP2CA250006-01), and the Undergraduate Research Opportunity Program (awarded to KP and ML). This work was also supported by the University of Utah Flow Cytometry Facility, the University of Utah Fluorescence Microscopy Core Facility (1S10RR024761-01), the National Cancer Institute (5P30CA042014-24), and the National Center for Research of the National Institutes of Health (1S10RR026802-01).

References

1. Chang Y, Bluteau D, Debili N et al (2007) From hematopoietic stem cells to platelets. J Thromb Haemost 5(Suppl 1):318–327. https://doi.org/10.1111/j.1538-7836.2007.02472.x
2. Deutsch VR, Tomer A (2006) Megakaryocyte development and platelet production. Br J Haematol 134(5):453–466. https://doi.org/10.1111/j.1365-2141.2006.06215.x
3. Machlus KR, Italiano JE Jr (2013) The incredible journey: From megakaryocyte development to platelet formation. J Cell Biol 201(6):785–796. https://doi.org/10.1083/jcb.201304054
4. Machlus KR, Thon JN, Italiano JE Jr (2014) Interpreting the developmental dance of the megakaryocyte: a review of the cellular and molecular processes mediating platelet formation. Br J Haematol 165(2):227–236. https://doi.org/10.1111/bjh.12758
5. Brown E, Carlin LM, Nerlov C et al (2018) Multiple membrane extrusion sites drive megakaryocyte migration into bone marrow blood vessels. Life Sci Alliance 1(2):e201800061. https://doi.org/10.26508/lsa.201800061
6. Harker LA, Finch CA (1969) Thrombokinetics in man. J Clin Invest 48(6):963–974. https://doi.org/10.1172/JCI106077
7. Lambert MP, Sullivan SK, Fuentes R et al (2013) Challenges and promises for the development of donor-independent platelet transfusions. Blood 121(17):3319–3324. https://doi.org/10.1182/blood-2012-09-455428
8. Ogura M, Morishima Y, Ohno R et al (1985) Establishment of a novel human megakaryoblastic leukemia cell line, MEG-01, with positive Philadelphia chromosome. Blood 66(6):1384–1392
9. Risitano A, Beaulieu LM, Vitseva O et al (2012) Platelets and platelet-like particles mediate intercellular RNA transfer. Blood 119(26):6288–6295. https://doi.org/10.1182/blood-2011-12-396440
10. Takeuchi K, Satoh M, Kuno H et al (1998) Platelet-like particle formation in the human megakaryoblastic leukaemia cell lines, MEG-01 and MEG-01s. Br J Haematol 100(2):436–444. https://doi.org/10.1046/j.1365-2141.1998.00576.x
11. Bernard JJ, Seweryniak KE, Koniski AD et al (2009) Foxp3 regulates megakaryopoiesis and platelet function. Arterioscler Thromb Vasc Biol 29(11):1874–1882. https://doi.org/10.1161/ATVBAHA.109.193805
12. Greenberg SM, Rosenthal DS, Greeley TA et al (1988) Characterization of a new

megakaryocytic cell line: the Dami cell. Blood 72(6):1968–1977

13. Nagano T, Ohga S, Kishimoto Y et al (1992) Ultrastructural analysis of platelet-like particles from a human megakaryocytic leukemia cell line (CMK 11-5). Int J Hematol 56(1):67–78
14. Sledge GW Jr, Glant M, Jansen J et al (1986) Establishment in long term culture of megakaryocytic leukemia cells (EST-IU) from the marrow of a patient with leukemia and a mediastinal germ cell neoplasm. Cancer Res 46(4 Pt 2):2155–2159
15. Takeuchi K, Ogura M, Saito H et al (1991) Production of platelet-like particles by a human megakaryoblastic leukemia cell line (MEG-01). Exp Cell Res 193(1):223–226. https://doi.org/10.1016/0014-4827(91)90560-h
16. Tange T, Takei Y, Takaai S et al (1988) In-vitro production of human platelets. Lancet 2 (8604):218. https://doi.org/10.1016/s0140-6736(88)92318-5
17. Yang XL, Ge MK, Mao DK et al (2016) Thrombin maybe plays an important role in MK differentiation into platelets. Biomed Res Int 2016:9313269. https://doi.org/10.1155/2016/9313269
18. Isakari Y, Sogo S, Ishida T et al (2009) Gene expression analysis during platelet-like particle production in phorbol myristate acetate-treated MEG-01 cells. Biol Pharm Bull 32 (3):354–358. https://doi.org/10.1248/bpb.32.354
19. Battinelli E, Willoughby SR, Foxall T et al (2001) Induction of platelet formation from megakaryocytoid cells by nitric oxide. Proc Natl Acad Sci U S A 98(25):14458–14463. https://doi.org/10.1073/pnas.241427398

INDEX

Mo R. Ebrahimkhani and Joshua Hislop (eds.), *Programmed Morphogenesis: Methods and Protocols*, Methods in Molecular Biology, vol. 2258, https://doi.org/10.1007/978-1-0716-1174-6,

N

O

P

Q

R

S

T

V